Animal models of exercise therapy: mechanisms of activity-induced angiogenesis

Roger William Peter Kissane

Submitted in accordance with the requirements for the degree of
Doctor of Philosophy

The University of Leeds
School of Biomedical Sciences

February 2017

Intellectual property statements

The candidate confirms that the submitted work is his own and that appropriate credit has been given where reference has been made to the work of others.

This copy has been supplied on the understanding that it is copyright material and that no quotation from the thesis may be published without proper acknowledgement.

The right of Roger Kissane to be identified as Author of this work has been asserted by him in accordance with the Copyright, Designs and Patents Act 1988.

Acknowledgements

First and foremost I need to thank my supervisors Prof Stuart Egginton and Dr Graham Askew for giving me the opportunity to study under their supervision. I want to explicitly thank Stuart for all his support and advice throughout my PhD, for the surgical training, the thought provoking questions and the multiple opportunities to develop as a scientist and a person. I want to thank Graham for his training and support throughout my learning of muscle mechanic techniques and for his approachability and ever enjoyable discussions.

This thesis would not have been possible without various internal and external collaborative efforts that must be acknowledged. I first of all want to thank Dr Abdullah Al-Shammari and Dr Simon Holbek for their combined efforts in the development of the immunohistochemical analysis package Dtect and the oxygen transport modeler that has been described in chapter two. I think we have managed to develop an essential analytical data pipeline which has been long sought after. I must also thank Dr Thomas Andersen for his initial training in the muscle histology and Dr Abigail Mackey for providing the immobilization study muscle samples for use in our validation work in chapter two. I want to thank Dr Peter Tickle for his help and training in the *in-situ* preparation for the muscle blood flow and fatigue measures that have gone into chapter four. I want to thank Dr Katie Nicoll Baines for her training of the RNA extraction technique that's successfully gone forward to be used in the qPCR and microarray analysis. Chapter five was a collaboration with the motor control lab of Dr Ronaldo Ichiyama. Dr Yazi Al'Joboori, completed all the animal surgeries and animal training. Placement students Oliver Wright and Paulina Marczak should be thanked for their work on the muscle histology and initial data analysis.

The final collaborative venture with Professor Francesco Falciani and Dr Peter Davidsen facilitated the work within chapter six. I want to thank Francesco for allowing me to visit and work in his lab, and for the continuing collaborative work on the animal gene array analysis. I must also thank Dr Michela Bonomo for her training and assistance in running the microarrays. While I must thank Peter for his collaboration in developing the human angio-hub data sets and the outputs for the animal work that has facilitated the exciting novel data in chapter six.

My time in Leeds doing my PhD would not have been anywhere near as enjoyable as it has been were it not for some amazing lab friends Alex, Ellie, Laura, Tom, Yazi, Zak, Nick and Katie. The selection of coffee buddies who helped fuel most of this thesis James, Aaron, Ruth and Thomas. I want to say a personal thank you to Yazi for her help and support during my PhD, you were the first person to help me out when I needed a suture re-doing, and you've been a great colleague and friend ever since, so thank you. I can't forget my colleagues and friends at CICA Jeffrey and Andrea, thank you for all the great times we had together working and giving me the opportunity to work alongside you both.

Lastly, I have to thank all those people outside of my PhD that played a part in supporting me during this time. Firstly my mum for being such inspirational and supportive person through everything, you are an incredible role model. To my dad, who may no longer understand what I've achieved but always believed in me and spurred me onto try my best, and Ashley for his continuing support and interest in what I do. Finally, those close friends who were always there for support and a welcomed distraction outside of PhD life: James, Thomas, Little Rachel, Bethan, David and Devon.

Abstract

Skeletal muscle is spatially heterogeneous in muscle fibre type composition and microvascular supply. The capacity to quantify this heterogeneity in skeletal muscle is not routinely performed for it's a laborious and time consuming technique. We have developed a high throughput data pipeline that utilises the simultaneous immunohistochemical labelling of muscle fibre type and microvascular supply, as an input for a semi-automated analysis software package that allows for the analysis of fine morphometric indices of fibre type composition and the interactions with microvascular supply. We have successfully shown that regional variation in fibre type composition impacts the functional characteristics of a muscle. After successful characterisation of regional heterogeneity in both structure and function we sought to establish their influence in physiological (adaptive) angiogenesis.

Utilising animal angiogenic models we have shown that shear stress driven angiogenesis is principally a stochastic response that does not promote improved oxygen delivery when we analyse the spatial heterogeneity of the neovasculature. Conversely, skeletal muscle overload (abluminal stretch of microvasculature) increases the homogeneity of the oxygen supply area of the capillary bed, suggesting a tissue driven angiogenic response that is not evident in shear stress. Spinal cord injury induced rarefaction of the capillary bed attempts to maintain a homogeneous distribution of fibre size and capillary supply. The combination therapy of epidural stimulation and locomotor training can ameliorate the phenotypic change and rarefied capillary bed seen with spinal cord injury to that of intact levels.

Endurance and resistance exercise have a largely similar global genomic response following a chronic training regime, which we are able to replicate in animal models of exercise through indirect electrical stimulation. The shear stress and muscle overload driven angiogenic response have distinctly different angiogenic pathways that contain no commonly expressed networks.

Contents

List of figures

List of tables

List of abbreviations

CD	Capillary density
C:F	Capillary to fibre ratio
COPD	Chronic obstructive pulmonary disease
EC	Endothelial cell
eNOS	Endothelial nitric oxide synthase
ES	Epidural stimulation
EDL	Extensor digitorum longus
EHP	Extensor hallucis
FCSA	Fibre cross-sectional area
HIF-1α	Hypoxia inducible factor – 1 alpha
LCD	Local capillary density
LCFR	Local capillary to fibre ratio
L_0	Optimum length
MMP	Matrix metalloproteinase
MHC	Myosin heavy chain
PO_2	Oxygen partial pressure
PVD	Peripheral vascular disease
SCI	Spinal cord injury
TA	Tibialis anterior
T_{W50}	Time to 50% initial power
VEGF	Vascular endothelial growth factor
V_{MAX}	Maximum shortening velocty
VO_2	Volume of oxygen consumed
VP	Voronoi polygon
W_{MAX}	Instantaneous isotonic power

1 General introduction

This thesis will explore the physiological adaptive response of expanding the microvasculature in skeletal muscle, using an integrated approach across a variety of animal models. Angiogenesis is the process of capillary growth from pre-existing vessels, and is a complex, multifactorial process observed in a variety of pathological and physiological conditions. Capillaries form an intricate network throughout the body and supply all but avascular regions (e.g. bone and cartilage), facilitating the exchange of O_2 from blood to respiring tissue, while simultaneously exchanging nutrients and removing waste, allowing the regulated function of a given organ. One effective driving signal for targetted adaptive remodelling is exercise, which has been rigorously investigated in the field of physiological angiogenesis. Altered muscular activity drives adaptation through increases in growth factors and mechanical stimuli, which interact in a coordinated fashion to produce new functional capillaries in an expanded microvasculature. Exercise driven angiogenesis has attracted a large interest as a therapeutic tool for improving capillarity in individuals suffering with obstructed vessels, which occur in conditions like peripheral vascular disease. Despite its increased prevalence as a therapeutic resource, limitations to the prescription of endurance exercise arise with individuals suffering with cardiorespiratory and/or peripheral circulatory diseases which reduce exercise capacity. Therefore, the development of alternative treatments that may circumvent central limitations would be invaluable.

This introduction outlines how new microvasculature is formed, identifying the critical growth and mechanical factors associated with exercise. Subsequently, the various animals models used, and how the integrated response of these treatments may be investigated, is discussed. Finally, a holistic overview of animal models and exercise-induced angiogenesis is presented.

1.1 The vascular system

The vascular system comprises of three primary components, the heart, the blood vessels (Fig. 1-1) and the blood. Its fundamental function is to deliver oxygen and nutrients to cells and remove waste, which occurs predominantly *via* the capillaries by diffusion (with evidence for some oxygen exchange in arterioles and venules), and at any given time there is typically five percent of the body's total circulating blood volume in the microvasculature. The primary focus here is the capillary bed.

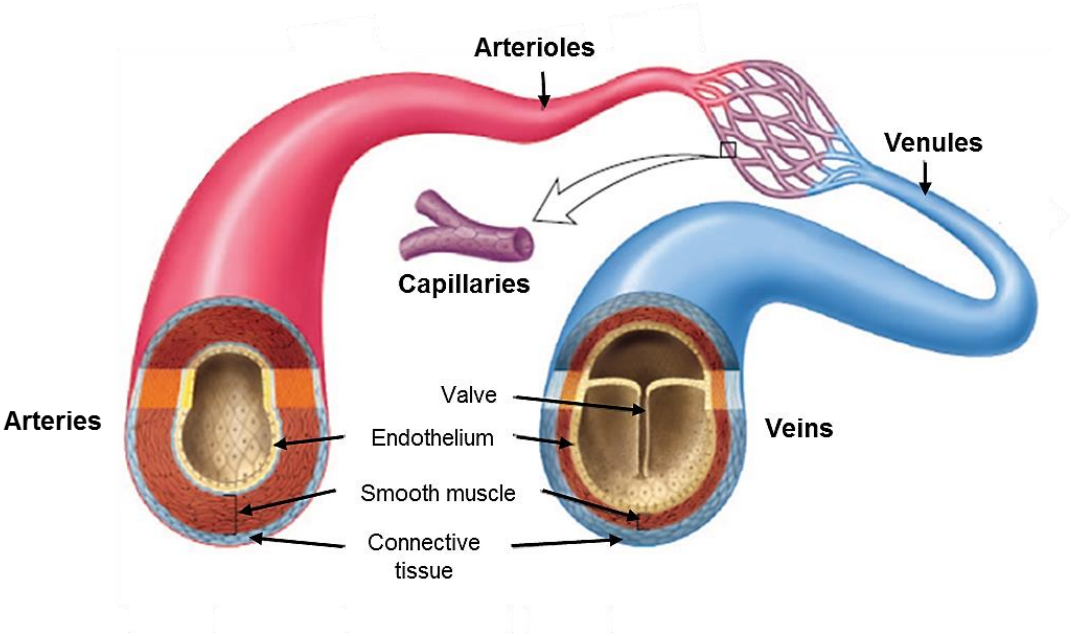

Figure 1-1. Blood vessels within the vascular system. Arteries are the largest blood vessels within the vascular system, with thick walls they act as low resistance elastic tubes that distribute the blood around the body to all of the major organs by convection (conduit vessels). The arterioles are vital in the control of organ perfusion, and play a role in the maintenance of mean systemic blood pressure (resistance vessels). The artery and arteriole branches contain smooth muscle cells that allow the vessel to contract (vasoconstriction) and relax (vasodilatation), altering the vessel radii, and subsequently pressure and flow. From the arteriole blood flows into the smallest blood vessels in the body, the capillaries (exchange vessels), where oxygen and nutrient exchange take place by diffusion, ultimately limiting the functional of a given organ. Thereafter, some nutrient and oxygen exchange occurs between the venules and interstitial fluid before flowing into the low pressure veins (capacitance vessels) and returning to the heart. Adapted from shutterstock.co.uk; stock ID: 515393440.

1.1.1 Capillaries

Capillaries are present within almost all organs (except avascular regions, above), but the fine structure may differ according to functional constraints: continuous (e.g. blood brain barrier, or effector organs like muscle), fenestrated (e.g. endocrine glands), and discontinuous (or sinusoidal, found in e.g. bone marrow and spleen). A capillary is typically around 8µm in diameter, with a vessel lumen of approximately 5µm, sufficient in size for a single erythrocyte to pass through after deformation. The capillary has a single layer basement membrane around it, providing stabilisation with the additional help of covering pericytes (Fig. 1-2).

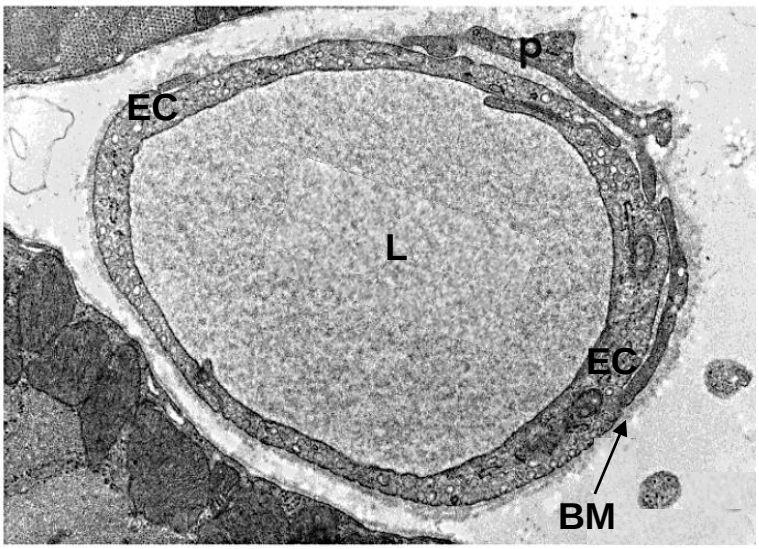

Figure 1-2. Basic structure of a capillary. Here we have a capillary formed by two quiescent endothelial cells (EC). The vessel lumen (L) is lined with a membrane bound proteoglycan, glycocalyx. The glycocalyx play an important role in the mechanotransduction of shear stress, and facilitate communication with the EC's and cellular junction molecules like PECAM-1 (platelet-endothelial cell adhesion molecule). The capillary is covered with a single layer basement membrane (BM), and a typical perivascular pericyte (a contractile cell involved in paracrine signalling, and key in angiogenesis (Gerhardt and Betsholtz, 2003)) (P) embedded within a common basement membrane. Scale bar = 1µm. Adapted from (Zhou et al., 1998b).

Capillary cross-sectional area is functionally important, with its narrow aperture it increases resistance to blood flow due to viscous drag, or shear stress. However, the large cumulative lumen surface area of capillaries actually provides less resistance to that of arterioles. This leads to a lower linear velocity compared to

that of larger vessels, which provides a sufficiently long transit time for the diffusive exchange of oxygen and nutrients (Fig. 1-3). Despite low perfusion velocity the small diameter combined therefore with low compliance means that individual capillaries may experience high levels of shear stress (below).

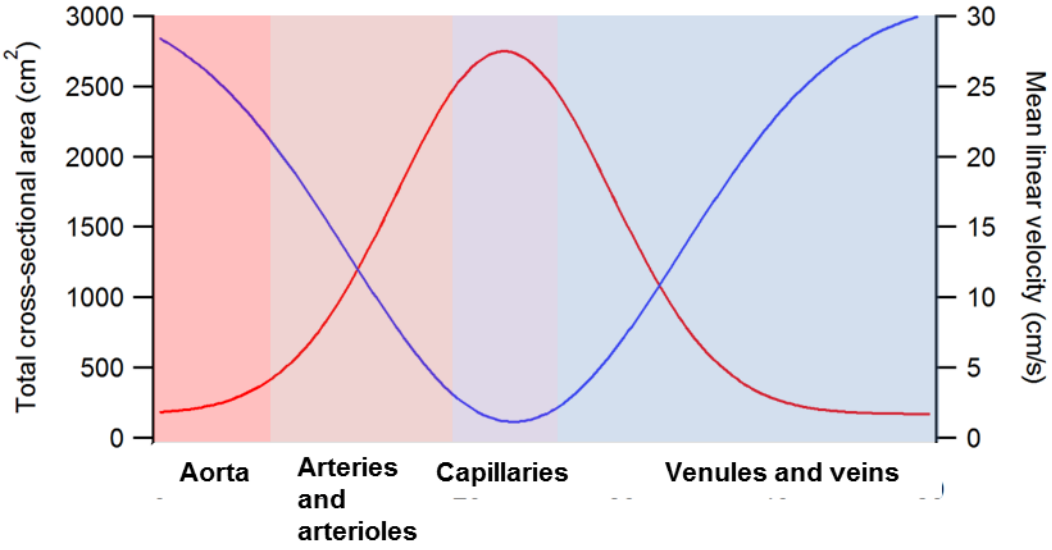

Figure 1-3. Vasculature cross-sectional area (red line) and mean linear flow (blue line). Note the large cumulative surface area in the capillary bed compensates for the slow perfusion rate to effect adequate diffusive supply of oxygen and other nutrients Adapted from EP Widmaier, H Raff, KT Strang (2006).

1.2 Angiogenesis

Angiogenesis is the process of capillary growth and remodelling initiated by an alteration in endothelial cell (EC) activity from a quiescent state, to one of active proliferation (Eelen et al., 2013). The initiation of angiogenesis is a multifactorial process dictated by a variety of metabolic, mechanical and pathological signals altering the pro- and anti-angiogenic balance of a cell (Folkman, 1971, Egginton, 2009). There are three commonly described types of angiogenesis within the literature: sprouting, longitudinal splitting and intussusception. The most commonly referred to form, sprouting, involves the proliferation and migration of EC extending away from the parent vessel, through a migrating blind-ended tube with filopodia on the leading (tip) cell sensing cytokine gradients (Risau, 1997). Longitudinal splitting and intussusception occur in already functioning capillaries, converting a single vessel lumen into two (Kurz et al., 2003, Djonov et al., 2003). The difference

between these two processes concerns involvement of perivascular cells; the former results from lamellipodia formation into the lumen without any abluminal disturbance, whereas the latter divides existing capillaries by invagination of the abluminal surface followed by mural cell invasion (Egginton, 2009).

1.2.1 Sprouting angiogenesis

The microenvironment plays a critical role in the growth of capillaries, with sprouting angiogenesis predominantly taking place in areas of poorly perfused tissue (hypoxic environment). There is typically an up-regulation in pro-angiogenic peptide growth factors, the most common being vascular endothelial growth factor (VEGF) (Kim et al., 1993, Carmeliet et al., 1999, Carmeliet and Jain, 2000, Williams et al., 2006c). The initial process includes loosening of pericyte-EC stabilizing contact, and proteolytic break down of the basement membrane by matrix metalloproteases (MMPs). The next step is the EC proliferation and elongation through tip and stalk cell interactions (Fig. 1-4). Tip cells are non-prolific in nature and guide the growth of capillaries while simultaneously modifying the extracellular matrix (ECM) with various proteolytic enzymes to increase EC traction (Carmeliet et al., 2009). The proliferating stalk cell are the main elongating component within capillary sprouting, producing a functioning lumen for the forthcoming capillary, following the successful anastomosis of tip cells and adjacent capillaries. Tip cells and stalk cells are adapted EC phenotypes associated with alterations in metabolic demand; the most commonly discussed are the VEGF-Notch signalling. The tip cells have a high density of VEGF receptor 2 (VEGFR2), ideal for the detection and directing through varying gradients of VEGF protein (Rivilis et al., 2002). Following anastomoses of sprouts, the stalk cell lumen becomes functional and oxygenated blood may now transfer through, which in turn may reduce the angiogenic (e.g. hypoxic) signalling and return VEGF to normal resting levels (under conditions promoting adaptive angiogenesis; effective negative feedback may not be present with pathological angiogenesis). Finally, the capillary requires re-stabilisation through basement membrane coverage and re-establishment of pericyte contact, returning the vessel to a near quiescent state. Paracrine signals from adjacent mural cells aid in this process, e.g. secretion of

Angiopoietin 2 will destabilise endothelial tubes, while secretion of Angiopoietin 1 will stabilise them.

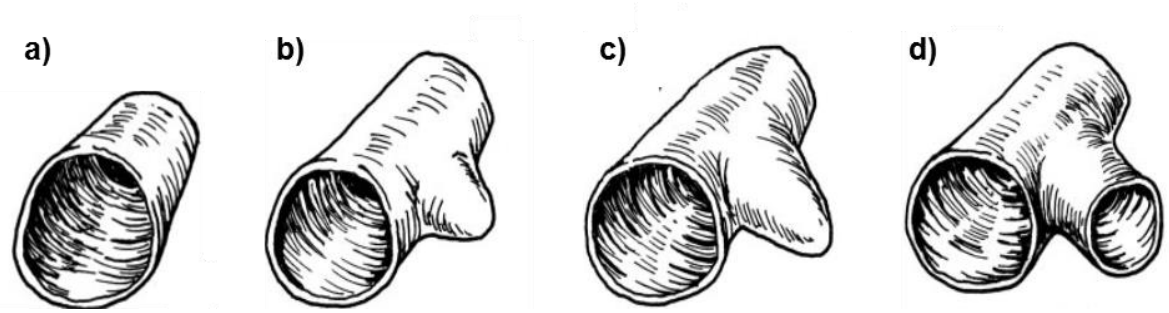

Figure 1-4 Spouting angiogenesis. Quiescent vessel lumen (a) following the pro-angiogenic switch that leads to the initiation of tip cell formation (b). Capillary sprouting with filopodia co-ordination, and beginning of elongation initiation though stalk cell proliferation (c). Functional anastomoses occur on fusion of the sprout with an adjacent capillary, and establishing a patent lumen (d). *Adapted from (Prior et al., 2004).*

1.2.2 Longitudinal (splitting) angiogenesis

Luminal division occurs through activated ECs forming luminal sheets (lamellipodia), and dividing the capillary into two separate lumen, this occurs without the breakdown of basement membrane or pericyte retraction (Deveci and Egginton, 2002b, Zhou et al., 1998a), therefore allowing the abluminal surface to remain intact. This method of angiogenesis is predominantly associated with increased shear stress, and in part mediated by nitric oxide (NO) (Amaral et al., 2001). The structural outcome is two functioning capillaries, running in parallel, requiring little proliferation or breakdown of existing EC. This low proliferative mode of angiogenesis (similar to that of intussusception) may suggest a more efficient model of angiogenesis when compared to sprouting (Egginton et al., 2001).

1.2.3 Intussusceptive angiogenesis

Intussusceptive angiogenesis is the expansion of the capillary bed while increasing surface area of pre-existing lumen, by local expansion of capillary diameter and insertion of a hole, associated with transcapillary tissue pillars - the process of intussusception (Fig.1-5) (Fulgenzi et al., 1998, Kurz et al., 2003, Djonov et al.,

2003, Burri et al., 2004, Makanya et al., 2005). The structural outcome is a capillary network with more nodes (a more dense mesh). This energy efficient mode of angiogenesis may appear similar to that of longitudinal splitting, but involvement of mural cells and modification of the abluminal surface suggests the remodelling cost may be somewhere between that of sprouting and splitting angiogenesis. Intussusception seems to take place predominantly in well oxygenated muscles, and may be an efficient mechanism of increasing capillary to fibre ratio (C:F) (Egginton et al., 2001). Vascular casts and computational models of intussusception in chick chorioallantoic membrane are available to analyse the potential mechanisms of adaptation. Recent chick chorioallantoic membrane models have suggested shear stress to be one of the main driving forces for intussusception (Schlatter et al., 1997, Baum et al., 2010).

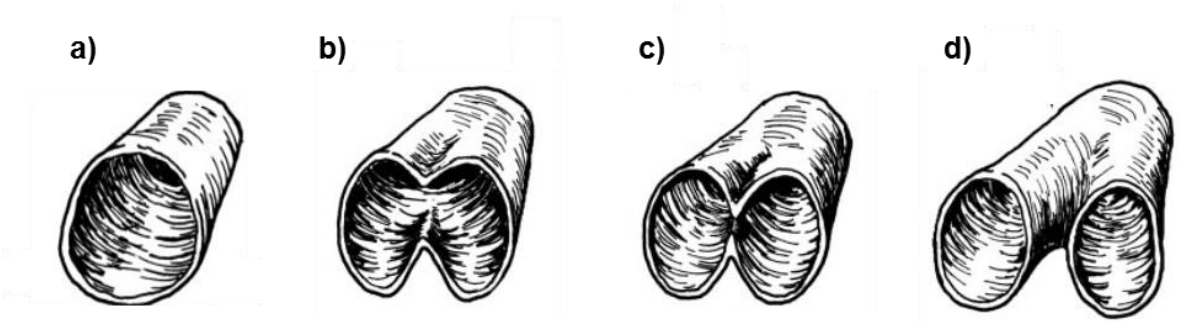

Figure 1-5 Intussusceptive angiogenesis. This is a 3D model adapted from electron micrograph images of various vascular casts, (a) and (b) show the initial 'pinching' of the capillary as the ECs protrude into the vessel lumen, prior to the local association shown at (c). Following the weak interaction between the two opposing surfaces, the supporting pericytes and BM are degraded allowing for the infiltration of perivascular cells, and generation of an interstitial pillar filled with ECM. Adapted from (Prior et al., 2004).

1.3 Exercise-induced angiogenesis

Aerobic exercise has many physiologically adaptive responses, ranging from improved cardiovascular function, reduced free fatty acid and glucose levels in blood, and increased strength and fatigue resistance of skeletal muscle (Saltin and Rowell, 1980, Saltin and Gollnick, 1983, Laughlin, 1999). The central and peripheral adaptations that occur in response to aerobic exercise each have their

own temporal response, which are briefly introduced with a focus on microvascular expansion.

The impressive plasticity of the microvasculature and the skeletal muscle it supports has been shown across a variety of species. Through the application of endurance exercise it is possible to dramatically increase microvascular supply while also improving the muscles capacity to utilise this improved fuel source, through mitochondrial biogenesis, reorganisation of fuel storage and changes in muscle fibre phenotype (Klausen et al., 1981, Ingjer, 1979a, Ingjer, 1979b, Irrcher et al., 2003, Waters et al., 2004).

The angiogenic response is a highly coordinated adaptive process, driven by changes in metabolic status of the cell and chemical signalling, in conjunction with mechanical stimuli like abluminal stretch during cyclical muscle contractions and luminal shear stress with active hyperaemia (Hoier and Hellsten, 2014). As little as four weeks cycling endurance training is sufficient to generate a significant increase in capillary content (Hoier et al., 2012), with similar adaptive responses seen after six and eight weeks (Andersen and Henriksson, 1977, Jensen et al., 2004) in humans. Four to six weeks of voluntary wheel running or treadmill training in rodents produces a significant angiogenic effect (Waters et al., 2004, Gute et al., 1994, Degens et al., 1993), with some significant increases seen at seven days (Gute et al., 1994, Waters et al., 2004). The time course of adaptation suggests that in these instances angiogenesis precedes the altered fibre type composition (Waters et al., 2004, Andersen and Henriksson, 1977), suggesting that microvascular changes are permissive for other adaptive response rather than being simply reactive.

Acute endurance exercise in untrained humans up-regulates a variety of pro-angiogenic factors; e.g. VEGF, TIE2 and MMP9 (Gavin et al., 2007, Hoier et al., 2012, Gustafsson et al., 1999), as well as some anti-angiogenic factors; e.g. endostatin, TSP-1 and TIMP1 (Olfert et al., 2006, Olenich et al., 2013, Gu et al., 2004, Dennis et al., 2008). Cross-species regulation appears to be alike, with an up-regulation of similar pro- and anti-angiogenic factors in untrained mice following

an acute bout of endurance exercise (Olenich et al., 2013) to that of humans Depression in force generation during fatigue is likely through impaired cross-bridge kinetics of myofibrils through interactions of free phosphate (generated through hydrolysis of ATP and PCr) and hydrogen ions (resulting from lactic acid accumulation), impairing calcium binding with troponin and ATPase activity (Westerblad et al., 1998, Cady et al., 1989). Subsequent training effects on mRNA of angiogenic factors at baseline suggest that there is a decrease in pro-angiogenic and an increase in anti-angiogenic compounds compared to untrained muscles. However, following an acute bout of exercise in the trained state the balance is significantly shifted into the favor of angiogenesis (Hoier et al., 2012, Olenich et al., 2013).

A large range of exercise intensities have been associated with angiogenic remodelling, from cycling training at 60-80% VO_{2MAX} (Andersen and Henriksson, 1977, Hoier et al., 2012) to intermittent knee extension exercise training at 90-150% VO_{2MAX} (Jensen et al., 2004). While animal models of treadmill training suggest low intensity exercise (20m.min^{-1}) for nine weeks is insufficient to increase capillarity, a higher velocity of 40m.min^{-1}, is capable of significantly increasing the number of capillaries (Kano et al., 1997). Differentiating the intensity and type of training during free wheel running makes it a difficult model to replicate, given inherent inter-animal behaviours two animals could run equal distances, but utilise very different durations (exercise volume) and velocities (exercise intensity) in attaining them. Hence, they may experience different drivers of angiogenesis (Rodnick et al., 1989). The proximal stimuli are likely to differ with exercise intensities (e.g. high *vs.* low-intensity endurance training and continuous *vs.* intermittent training regimes). With a varied functional outcome, caution is needed when comparing data from different training regimes.

1.4 Key angiogenic players

Angiogenesis is a remarkably complex process with a large number of potential initiation factors, such that the process of microvascular expansion *in vivo* likely requires the synergistic activation of a number of elements in different signalling pathways. *In vitro* studies are predominantly concerned with chemical signalling (growth factors) for activation and inhibition of blood vessel growth, while a substantial proportion of work has shown that mechanical stimuli play an equally important role in *in vivo* angiogenesis (Baldwin et al., 1981, Putman et al., 2004, Milkiewicz et al., 2001). Consequently, it is important to consider both mechanistic processes as it is likely to be an integrated response *in vivo*. For example in active skeletal muscle microvessels will be subject to altered haemodynamic forces, metabolic by-products, with varying levels of hypoxia and cytokines. Here, I will briefly introduce a selection of the commonly discussed angiogenic factors; it is likely that there is a balance between positive and negative regulators, and understanding this balance may be critical in understanding the ideal environment to promote angiogenesis (Folkman, 1995).

1.4.1 Chemical signalling

1.4.1.1 Vascular endothelial growth factor (VEGF)

VEGF is recognised to be a key regulator of angiogenesis during embryonic development, physiological remodelling and pathological growth. VEGF gene ablation is embryonically lethal (Ferrara et al., 1996), and is associated with improper cardiac development and death mid gestation (Carmeliet et al., 1996). VEGF is an integral signalling protein for endothelial cell proliferation, generation of functioning anastomoses and luminal sprouts, and it is essential for the two mechanotransductive forms of angiogenesis: prazosin induced shear stress and increased luminal stretch through synergist muscle ablation; discussed below (Williams et al., 2006c, Williams et al., 2006b).

VEGF-A is commonly used synonymously with ‘VEGF’ and is a member of the PDGF (platelet-derived growth factor)/VEGF family which includes VEGF-(A-D)

isoforms, PDGF, as well as placental growth factor (PlGF) (Krilleke et al., 2009). VEGF is a dimeric growth factor capable of mitogenic stimulation of EC through interactions with a variety of tyrosine kinase receptors, of particular relevance in the present context are VEGF receptor-1 (Flt-1) and receptor-2 (rodent, Flk-1; human, KDR). There are a variety of variants of VEGF-A, produced through alternative splicing of the VEGF gene (8 exons separated by 7 introns) such as $VEGF_{121}$, $VEGF_{165}$ and $VEGF_{189}$ in humans and $VEGF_{120}$, $VEGF_{164}$ and $VEGF_{188}$ in mice (Tischer et al., 1991, Shima et al., 1996). These splice variants are differentially coded through a variety of residues within exons 6 and 7, exon 7 associated with the heparin binding domain (HBD) required to bind to heparin sulphate proteoglycans within the ECM. The HBD content of VEGF alters the localisation and interaction with Flt-1 and Flk-1 (Park et al., 1993), for instance $VEGF_{121/120}$ is a freely diffusible protein due to its lack of HBD and can be readily released by a variety of cells, whereas $VEGF_{189/188}$ contains both HBDs and is mainly found on the abluminal surface or bound to the ECM (Ruhrberg et al., 2002, Ferrara et al., 2003), presumably requiring proteolytic cleavage before bioactivity is evident. The individual roles of these variants are still under debate, but it is believed that the HBD plays a critical role in the vascular branching formation, as mice expressing only the $VEGF_{120}$ died shortly after birth compared with other isoforms that lasted 1-2 weeks (Carmeliet et al., 1999). Although VEGF-A is predominantly associated with its capacity to promote EC growth it has been linked to other regulatory processes within the microvasculature, such as alterations in vascular permeability, cell survival (through expression of anti-apoptotic proteins) and vasodilatation. The VEGF-B protein has a less pronounced role within the microvasculature remodelling, but required for maintenance of the microvasculature, and typically interacts with VEGFR1 (TLT1) (Olofsson et al., 1999). VEGF-C and VEGF-D are primarily recognised for promoting lymphangiogenesis, increasing lymphatic endothelial cell proliferation and development of functioning vasculature (Jeltsch et al., 1997, Olofsson et al., 1999, Krishnan et al., 2003). VEGF-C has some VEGF-A like properties such as stimulating EC migration and altering vascular permeability (Olofsson et al., 1999, Ferrara et al., 2003).

1.4.1.2 Angiopoietins

An important mechanism for fine control of growth factor activity is the presence of ancillary or regulatory growth factors. Angiopoietins are a family of glycoprotein ligands that interact primarily with ECs, through a receptor tyrosine kinase (Tie family). EC proliferation is recruited by VEGF expression in the presence of angiopoietin-2 (Ang2), while endothelial tube integrity is promoted by angiopoietin-1 (Ang1) acting through Tie2 (Gale and Yancopoulos, 1999, Hanahan, 1997), with Tie1 potentially acting as a decoy receptor. Also, regression of supporting pericytes is thought to be predominantly regulated by the interaction of Ang1 and Ang2, acting through Tie receptor complexes. Angiopoietins predominant role is modulation of vessel development and remodelling, the latter being the emphasis of this introduction. There are four distinctive angiopoietins (Ang1-4), with Ang-1 and Ang-2 being predominantly discussed in the literature (Egginton, 2009, Singh et al., 2011). The activating ligand Ang1 interacts with Tie2 promoting the maturation and quiescence of the capillary ECs, whereas the Ang2 glycoprotein is a competitive antagonist for the same receptor and facilitates vascular remodelling. An *in vivo* measure for net effect of angiopoietins is commonly used, in the form of Ang2-to-Ang1 ratio (Ang2:Ang1) on the assumption that with a ratio >1 there is an increased pro-angiogenic (destabilising) stimuli above that of the anti-angiogenic (stabilising) effect (Lloyd et al., 2003), allowing for potential vessel remodelling.

1.4.1.3 Hypoxia inducible factor – 1 alpha (HIF-1α)

The transcription factor hypoxia-inducible factor (HIF) is most commonly associated with its reactivity to decreasing oxygen content, and comprises of two subunits HIF-1α and HIF-1β. HIF-1α has been identified as a critical subunit in changing a cells proliferative state, and has been implicated as a driving factor in angiogenesis (Carmeliet et al., 1998). HIF-1α has been shown to be largely activated in physiological ischaemia during exercise (Gustafsson et al., 1999, Wagner, 2001, Ameln et al., 2005) and pathological ischaemia, post-translational modification leading to activation of target genes offering a hypoxic defense (Lee et al., 2000, Bergeron et al., 1999, Ozaki et al., 1999). However, during mechanotransductive angiogenesis its transcriptional regulation appears to be

involved driving EC activation (Williams et al., 2006a). The two subunits, HIF-1α and HIF-1β, require dimerisation within the nucleus to effect up-regulation of hypoxia-induced VEGF expression (Forsythe et al., 1996), and their up-regulation correlates with changes in VEGF mRNA following an acute bout of exercise (Ameln et al., 2005, Lundby et al., 2006) and PGC-1α.

1.4.1.4 Matrix metalloproteinases (MMPs)

A diverse family of proteases known as matrix metalloproteinases (MMPs) is thought to be responsible for loosening or proteolytic breakdown of the basement membrane involved in tumour, inflammatory and exercise-induced angiogenesis (Haas et al., 2000). These proteins are necessary to permit sprouting angiogenesis, as the basement membrane acts as a stabilising jacket along the endothelial tube (Carmeliet and Jain, 2011), as well as providing an important interactive role with growth factors e.g. effective breakdown of the basement membrane and ECM makes for an increased angiogenic signal, as bound growth factors (*e.g.* $VEGF_{189/188}$) are released into the surrounding area. Degradation of the basement membrane and ECM are predominantly linked with increased expression of the MMP-2 and MMP-9 (Gelatinase family) proteins in response to exercise (Rivilis et al., 2002, Visse and Nagase, 2003, Yeghiazaryan et al., 2012). Using a potent angiogenic stimulus in the form of electrical stimulation, it has been shown that breakdown of the basement membrane is a critical component of physiological angiogenesis, and the inhibition of MMPs (*via* GM-6001, a broad spectrum inhibitor) diminishes any expected angiogenic response in the target muscles (Haas et al., 2000, Rivilis et al., 2002). The activity of MMPs are critical in sprouting but less so in intussusceptive and splitting angiogenesis, therefore a need for regulated control of this protease activity is important, and this is achieved though balanced activity of tissue inhibitor of metalloproteinases (TIMPs) (Carmeliet and Jain, 2011).

1.4.1.5 Tissue inhibitor of metalloproteinases (TIMPs)

As the name suggests TIMPs suppress activation of MMPs integral in the sprouting form of angiogenesis (Haas et al., 2000). There are four members of the mammalian TIMP protein family, TIMP-1, -2, -3 and -4, whose global roles are to reduce protease activity. TIMP-1 and -3 are upregulated by a variety of cytokine signalling cascades and appear to act directly on MMPs (Seo et al., 2003, Stetler-Stevenson and Seo, 2005), while TIMP-2 is able to inhibit angiogenesis through integrin-mediated interactions (Seo et al., 2003, Stetler-Stevenson and Seo, 2005, Egginton, 2009).

1.4.1.6 Thrombospondin

Thrombospondins (TSPs) are a large family of extracellular glycoproteins that are important in cell-cell and cell-matrix communication (Lawler, 2000). TSPs have a variety of functional roles involved in platelet aggregation, and cellular signalling with proteins that interact with the extracellular matrix (e.g. MMPs and integrins). The most commonly investigated family member is thrombospondin-1 (TSP-1), which has been identified as an inhibitor of angiogenesis through impairing EC proliferation and MMP activity (Bein and Simons, 2000, Lawler, 2000). More recently, a role for TSP-2 has been suggested but the *in vivo* evidence is less convincing. Other anti-angiogenic proteins are exist in the form of protein fractions derived from matrix proteins (*e.g.* endostatin, a fragment derived from collagen XVIII) which are not amenable to mRNA investigations.

1.4.2 Mechanical signalling

Exercise, a potent angiogenic signal contains a magnitude of potential angiogenic drivers, which include changes in metabolites, cytokines and oxygenation, as well as a range of mechanical signals. Passive physical activity known to increase muscle blood flow and alter muscle fascicle length (±20%) upregulate a variety of angiogenic markers in humans, however were insufficient to induce a significant angiogenic response in healthy young adults (Hellsten et al., 2008, Mortensen et al., 2012, Hoier et al., 2013). However, in a selection of animal models isolated

haemodynamic stimuli have been shown to improve capillarisation without the necessary presence of an metabolic stimulus (Williams et al., 2006c). The two most commonly referred to mechanical stimuli are localised vascular signals (shear stress and wall tension), and abluminal vessel-muscle stretch.

1.4.2.1 Shear stress

Shear stress and vessel wall tension occur in response to increased flow and perfusion pressure within a capillary, these forces act parallel and perpendicularly to the vessel lumen, respectively. The increased viscous drag on the EC and transmural pressure exerted on the vessel wall are potent angiogenic signals *ex vivo*, and *in vivo*. Shear stress result in signalling cascades that that incorporate mechanotransductive sensing by a range of molecules including the glycocalyx, integrins, PECAM-1 and VEGF2 (Urbich et al., 2000, Chiquet, 1999, Williams et al., 2006a). Shear stress responsiveness probably requires sensing by a functional complex of these molecules (Wragg et al., 2014).

Vasodilatation-induced shear stress has been shown to have great angiogenic potential (Dawson and Hudlicka, 1989, Ziada et al., 1989, Zhou et al., 1998a). This method of expanding microvasculature occurs without the formation of abluminal sprouts and breakdown of the basement membrane (Egginton et al., 2001), suggesting the shear stress induced angiogenesis is through longitudinal splitting rather than sprouting. This form of angiogenesis requires the presence of VEGF and endothelial nitric oxide synthase (eNOS) induced NO in order to produce new functioning capillaries (Williams et al., 2006c, Williams et al., 2006b).

1.4.2.2 Mechanical stretch

In vitro stretch of ECs has been shown to up-regulate VEGF and the angiopoietin signalling cascade, resulting in migration and proliferation of ECs (Zheng et al., 2001, Chang et al., 2003, Yamaguchi et al., 2002). An *in vivo* model of increased muscle overload has been explored, likely transmitting to EC stretch through surgical ablation of a muscle where the remaining synergists undergo an

overloaded stretch (an exaggerated form of the lengthening and shortening experienced during exercise duty cycle).

This abluminal stretch has been shown to have potent angiogenic response in rodent hind limb muscles (Williams et al., 2006b, Frischknecht and Vrbová, 1991, Degens et al., 1993, Zhou et al., 1998b). In contrast to shear stress driven angiogenesis, this angiogenic stimulus has been associated with increased basement membrane degradation and abluminal sprouting (Egginton et al., 2001) associated with sprouting angiogenesis (Carmeliet et al., 2009). This model of increased sprouting therefore relies on the up-regulation of proteolytic enzymes capable of breaking down ECM for the development of tip cell filopodia (Rivilis et al., 2002). This pro-angiogenic stimulus is also likely evident during exercise as an integral part of the duty cycle of locomotion.

1.5 Animal models of exercise-induced angiogenesis

Exercise involves the concomitant activation of skeletal muscle fibres that lie within different motor units, the pattern of which can be varied with different exercise intensities and allow targetted motor unit recruitment. Variation in muscle motor unit activation results in differential fuel utilisation and durations of activity, that permits manipulation of mechanical and chemical signalling for adaptive remodelling (Aagaard et al., 2010). In addition to the motor unit recruitment, the variations in exercise modality incorporate varying levels of mechanotransductive stimuli like muscle stretch and blood flow characteristics, while at the same time manipulating the metabolism and growth factor response. A selection of animal models used within the field of exercise induced angiogenic research is briefly discussed.

1.5.1 Free running

The free running model in rodents has been used extensively to replicate endurance training within humans, the principle behind its transferability is the naturally increasing distance with which animals run voluntarily, mimicking the

increasing distance expected during an endurance training regime. Free running in mice has is known to increase TA, plantaris and gastrocnemius muscle mass, following four weeks of exercise, with increasing average distance ran each week with an increased average speed (Allen et al., 2001). The combination of greater volume and intensity resulted in fibre type alteration of gastrocnemius and TA, reducing Type IIb and significantly increasing Type IIa composition by 5-10%. Accompanying this alteration in composition was an increase in Type IIa cross sectional area (CSA), although this was only apparent in the gastrocnemius (Waters et al., 2004). Four to six weeks of wheel running has increases in C:F, with significant increases as soon as seven days training (Waters et al., 2004, Gute et al., 1994). Animals selectively bred for high and low aerobic capacity are available for characterising expected adaptations to endurance exercise. High aerobically adapted rats have an improved capacity to remove fatigue associated metabolites during the recovery phase of exercise, as well as pronounced force maintenance (Torvinen et al., 2012).

As suggested previously, the primary problem with the free running model is how to characterise the exercise type, as different velocities and durations of exercise will utilise very different motor unit recruitment patterns, mechanisms of fuel utilisation, metabolic profile, and subsequent adaptive responses (Rodnick et al., 1989). Hence the need to analyse not just total distance covered, but the periodicity of that exercise bout, in order to identify potential interactions of motor unit activation. The activity pattern is susceptible to influences from external and internal stimuli. External factors like social hierarchy, food and water access, and photoperiodic conditions play an important role in behaviour (Sherwin, 1998). Similarly, internal factors like age, gender and hormone levels can also lead to changes in running intensity or duration (Mondon et al., 1985, Eikelboom and Mills, 1988).

1.5.2 Treadmill running

Motorised treadmill running has been used extensively throughout the exercise training literature as a physiological method of inducing activity linked adaptation,

incorporating alterations in duration, speed and inclination to adjust levels of training in order to ascertain differences on selected measures. Alterations in these three factors allow analysis of various exercise protocols, ranging from endurance and interval training to sprint and hill running. These protocols will alter muscle fibre recruitment patterns compared to standard endurance running, in order to alter activity of a targetted muscle group or fibre type. This section will focus on the endurance training regime designed to activate initially oxidative / intermediate motor units, recruiting predominantly Type I and Type IIa fibres.

Rat soleus, and mouse plantaris muscle have both shown significant increases in C:F following four weeks treadmill running (Waters et al., 2004, Degens et al., 1993), with some increase seen as early as seven days. This increased capillarity occurs in predominantly red and mixed muscle (Gute et al., 1994), likely associated with increased localised blood flow (Armstrong and Laughlin, 1983) and target motor unit activation. High intensity running at 40m.min^{-1} significantly increased capillarity following nine weeks of training (Kano et al., 1997), while four weeks of training at 60% of maximum running speed was sufficient to elicit a significant angiogenic response and increased oxidative enzyme activity (Ferreira et al., 2010, Dudley et al., 1982). The time course of improved capacity to deliver oxygen and the time to maximally utilise the improved capacity appears to be different, where maximal oxygen uptake took approximately eight weeks of treadmill training to become significantly increased despite a significant increase in capillary supply seen by four weeks (Kemi et al., 2002).

There is a great deal of scope for improvement in the treadmill running models, with the need for accurate training zones (intensity, volume etc.) to be determined and implemented. VO_{2max} is commonly used as an index of aerobic capacity, and correlates relatively well with endurance capacity. The majority of recent studies use previous works protocols as they have shown adaptive responses, but there are clear discrepancies with observed adaptive responses between species, gender and ages.

1.5.3 Indirect electrical stimulation

The principle of indirect electrical stimulation is to activate a muscle group *via* its respective nerve to elicit an integrated functional remodelling. The stimulus is delivered to the motor nerve with varying intensities and frequencies, recruiting a predetermined type of motor unit, or maximal contractions involving all motor units. The major focus has been on the use of supra-maximal 10Hz stimulation.

Early work by Hudlická, et al., (1982) examined the effects of 10Hz indirect electrical stimulation of the peroneal nerve on early onset capillary growth and oxidative capacity within the TA and EDL muscles. They showed that as little as 2-4 days stimulation was sufficient to significantly increase capillary content, with no change in FCSA (Hudlicka et al., 1982). Chronic (28 days) has been shown stimulation to double the capillary density of TA (Brown et al., 1976), as well as shifting the predominantly fast glycolytic fibres to a fast oxidative phenotype (Hudlicka et al., 1977). There was an increased C:F located in fast glycolytic areas of muscle, which may indicate that capillary growth precedes the fibre type alterations observed. Slow oxidative fibre content increases much later in the response, with changes only becoming significant at 18-20 days (Putman et al., 2004). This adaptation of phenotype occurs up until 24 days, at which point the fibre type shift appears to cease. The capacity of muscle to deliver and utilise oxygen only became significant after 14 days of stimulation, with further improvements at 28 days (Hudlicka et al., 1977, Simoneau et al., 1993), with a significantly improved fatigue index (i.e. greater endurance) seen at 14 days (Simoneau et al., 1993).

Other indirect electrical stimulation parameters have been explored for their angiogenic potential, for example Hudlicka et al. (1977) explored the capacity of high frequency stimulation (40Hz) to improve the oxidative capacity of a muscle. This activity pattern improved fatigability of a muscle principally through improved oxidative enzyme content rather than increased microvascular content. However, the authors suggest a temporal paradox where high frequency stimulation evoke an improved capacity to utilize oxygen before increasing supply, while low

frequency stimulation may increase capacity to supply oxygen before improving the enzymatic content/activity.

1.5.4 Overload

An *in vivo* model of increased endothelial stretch has been explored through surgical ablation of a muscle, where the remaining synergist muscles undergoing an abluminal surface stretch (an exaggerated form of the lengthening and shortening experienced during exercise), leading to compensatory remodelling. Removal of the tibialis anterior (TA) increases functional demand on the extensor digitorum longus (EDL) muscle in our rodent hind limb model (Egginton et al., 1998, Egginton et al., 2011), while other laboratories utilise a denervation of synergist muscles (soleus and gastrocnemius) to overload the plantaris (Degens et al., 1992). These models are known to induce targetted hypertrophy as well as significant stretch-induced angiogenesis, with the most pronounced stretch response achieved through complete muscle extirpation (Egginton et al., 2011).

The hypertrophic response of muscle overload has been systematically examined in the literature, with muscle mass increasing by 20-30% after just two weeks (Degens et al., 1993, Zhou et al., 1998b). This is largely a result of increased FCSA for oxidative fibres, while there is also evidence for hyperplasia (Alway et al., 1990, Rosenblatt and Parry, 1993). Muscle mass increases continually for up to four weeks, becoming significant after only three days (Rosenblatt and Parry, 1993, Egginton et al., 2011, Williams et al., 2006c).

Angiogenesis also occurs as early as three days, typically becoming evident at seven days, but with some studies only showing significant increases at 14 days (Degens et al., 1993, Zhou et al., 1998b, Williams et al., 2006c, Egginton et al., 2011). The increase in C:F occurs simultaneously with CD, despite a greater FCSA. Stretch-induced angiogenesis is predominantly associated with increased sprout formation (Egginton et al., 2001), and is independent of changes in NO (Williams et al., 2006b), but dependent on the up regulation of VEGF and Flk-1 (Williams et al., 2006c), which is significantly increased at 3-7 days (Williams et al.,

2006a). These data suggest that the overload induced sprouting requires the presence of VEGF, which plays a permissive role in angiogenesis in this model.

1.5.5 Pharmacological vasodilatation

As introduced earlier, elevated shear stress and increased wall tension are potent angiogenic stimuli. These mechanotransductive signals are common during exercise with increased cardiac output, active hyperaemia and the pump like action of contracting muscles, all contributing to changes in microvascular shear stress. Vasodilatation-induced increases in shear stress have been shown to have great angiogenic potential, typically through supplementation of the α_1-adrenoreceptor antagonist prazosin (Dawson and Hudlicka, 1989, Ziada et al., 1989, Zhou et al., 1998a), while other vasoactive supplements are available; e.g. verapamil (L-type calcium channel inhibitor) and cromakalim (K_{ATP} channel opener) (Egginton et al., 2016).

Elevated shear stress significantly increases CD and C:F independent of changes in muscular activity. Prazosin treated rats and mice show a significant alteration by 14 days, with further improvements up to 28 days (Egginton et al., 2001, Williams et al., 2006b, Egginton et al., 2016). This mechanism of increasing capillarisation occurs without the formation of abluminal sprouts and breakdown of the basement membrane (Egginton et al., 2001), suggesting the shear stress induced angiogenesis is through longitudinal splitting. This angiotype requires the presence of VEGF and endothelial nitric oxide synthase (eNOS) induced NO release in order to produce increased functioning capillaries (Williams et al., 2006c, Williams et al., 2006b). After 14 days of prazosin supplementation, despite a significant increase in capillary content, there were no change in fatigue resistance (George, 2012).

1.6 Integrated analysis

It is important to be aware of the limitations surrounding any experimental designs, and the techniques used to draw conclusions in experimental biology (Fig. 1-6). The remaining portion of this introduction will introduce some of the methods and

rational for their use in generating the overview of mechanisms underlying *in vivo* angiogenesis.

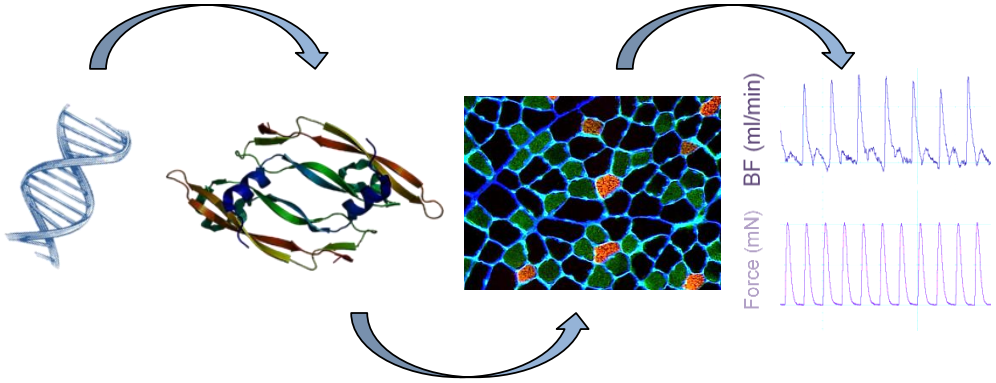

Figure 1-6. Holistic overview to experimental biology. An adequate understanding of any biological process requires integration of information from many levels of organisation. For example, gene expression quantification by its self only provides information on the regulation of a signal, this signal still requires translation into functional proteins, which in turn invoke a modified phenotype that finally translates into different functional capacity.

1.6.1 Molecular interpretations

Identification of differentially expressed pathways in response to exercise and disease has become a major analytical tool in recent years. Individual genes do not function in an isolated manner, they are integrated in networks of signalling cascades, and picking out single genes for quantification only provides insight into one element of the potential interactions. This cannot sufficiently represent a physiological process (Emmert-Streib and Glazko, 2011, Keller et al., 2011). Microarray experiments allows for large gene coverage, often at the expense of sensitivity, and may not detect changes of an individual gene within a pathway but will allow for analysis of interactions among networks and families of genes that are sufficiently represented. The systems biology approach is focused on development of functionally relevant analysis pipelines that allow for generating and testing of novel hypotheses.

1.6.2 Morphometric analysis of angiogenesis

There are a handful of practical considerations to be made before undertaking any form of histological assessment of skeletal muscle. These have been discussed in detail previously (Egginton, 1990a) of which the most relevant are summarised here.

1.6.2.1 Capillary markers

Histochemical staining has become the most common method of identifying capillaries, where previously injection of dyes into the microvasculature was used (Krogh, 1919). Early identification of capillaries utilised a stain for the enzyme alkaline phosphatase, an enzyme with high activity in the microvasculature (Klingmuller, 1958). There are uncertainties about reproducibility among different alkaline phosphatase staining methods, and its validity as a comparable marker have been questioned (Egginton, 1990a). With the development of immunohistochemistry there are an array of antibodies designed to probe for various endothelial targets, such as CD31 commonly known as platelet endothelial cell adhesion molecule-1 (PECAM-1), and Flk-1. An increasingly common marker used to visualise capillary location is *Griffonia simplicifolia* lectin-1, a polysaccharide that binds to the glycocalyx of capillaries, due to the relative simplicity of staining. We have unpublished data to show that with alternative markers for endothelial cells, there is a disparity among results when used to stain the same muscle sections (Fig. 1-7) (Williams, 2005). Therefore, it is important to be aware of the markers used to identify capillaries when comparing data in the literature.

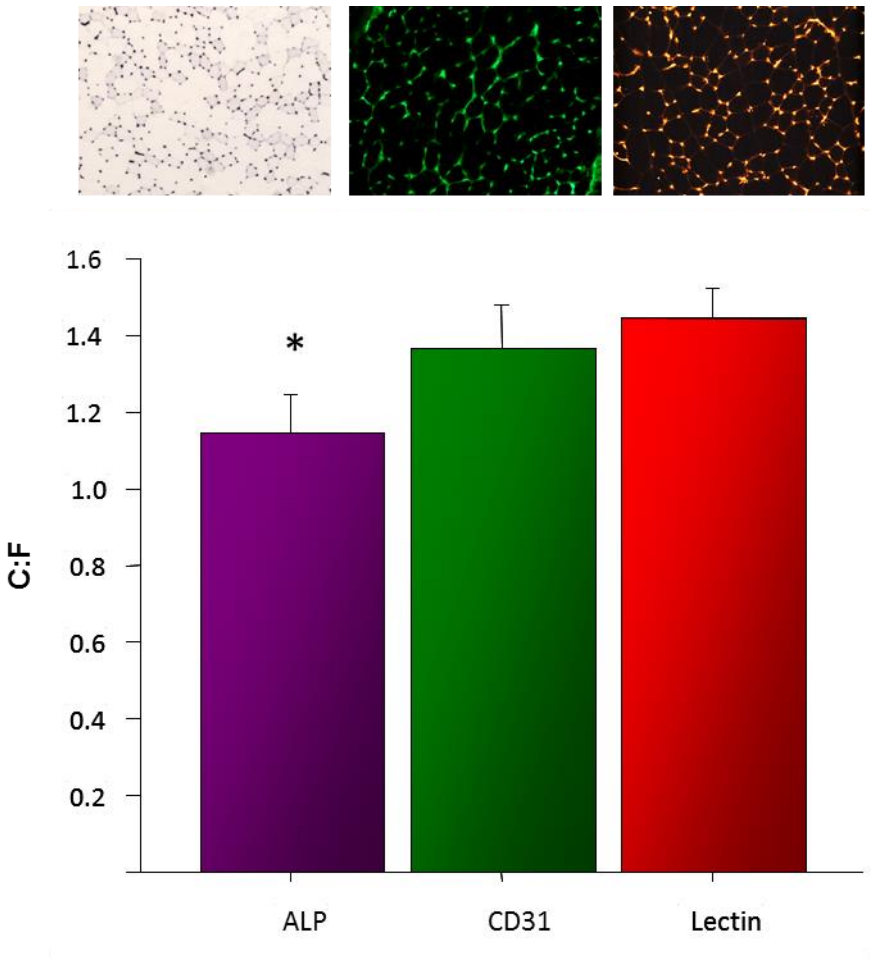

Figure 1-7. C:F of the mouse EDL using multiple markers for capillary location. Adapted from Williams (2005), * *P*<0.05 from Lectin (n=6). There may also be a species effect, as the discrepancy among markers in rat EDL is less pronounced (*unpublished data*).

1.6.2.2 Unbiased sampling

Acquiring a reliable estimate of tissue morphometric indices requires an understanding of morphological impact on quantitative outcomes, and a structured sampling routine that provides reproducible and representative data (Egginton, 1990a). The heterogeneous distribution of muscle fibre types, if simply counted for numerical density, would bias counts towards smaller objects (Type I fibres) within any field of view. As such the use of quadrats with inclusion and exclusion boundaries has been well established as an appropriate method of reducing sampling bias (Fig. 1-8) (Egginton, 1990a, Egginton, 1990b). It has been suggested that to efficiently generate a representative measure of global means, at least 20% of the total fibres should be included in the analysis, in rat muscles this

is typically upwards of 150 fibres (Ceglia et al., 2013). Such empirical observations, however, may over-estimate the effort required for a robust outcome if a systematic-random sampling design is followed (Egginton and Johnston, 1983).

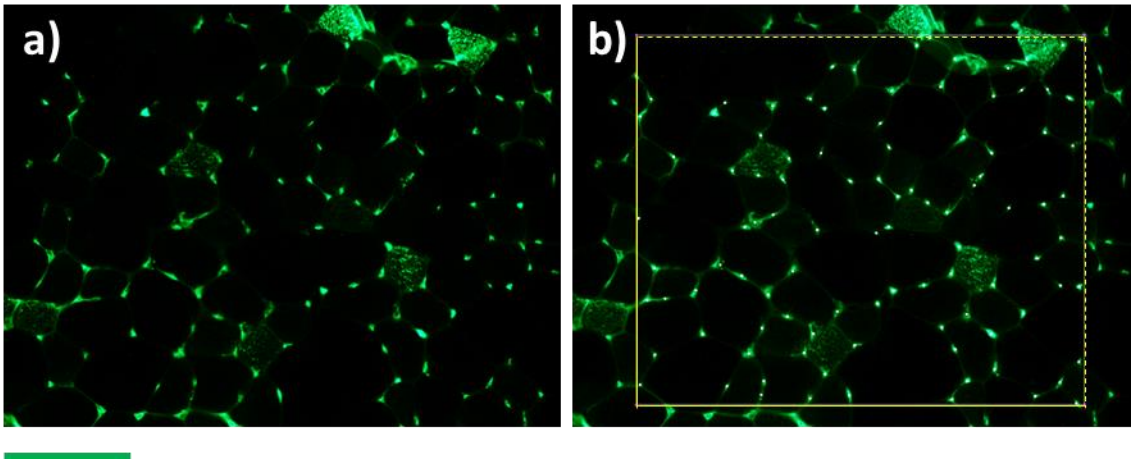

Figure 1-8. Unbiased sampling. A counting frame is placed over the histological section, with strict inclusion (dotted lines) and exclusion (solid lines) boundaries for the region of interest. Lectin (*Griffonia simplicifolia* lectin-1) labelled capillaries with Type IIa fibres labelled with SC-71 antibody. Scale bar = 100µm.

1.6.2.3 Morphometric indices

There are well over a dozen different indices used in the literature to describe the changing characteristics of the microvasculature, measures that typically fall into the bracket of either global or local indices. Global measures generally involve simple counting procedures that inform gross changes across a whole muscle section, while local indices look to describe the anatomical distribution of capillaries and their interaction with muscle fibres, and facilitate incorporation of realistic data into theoretical models, e.g. to estimate the maximal capacity of microvasculature to supply oxygen (Egginton and Ross, 1989, Egginton, 1990a, Egginton and Ross, 1992, Egginton and Gaffney, 2010, Al-Shammari et al., 2014b, Al-Shammari et al., 2014a). The most common indices used throughout this thesis will be briefly outlined, however for more detailed guidance on the global and local indices see Egginton's (1990) review on morphometric analysis of tissue capillary supply.

1.6.2.3.1 Global indices

The two most commonly reported indices of global capillary content are CD and C:F. These scalar measures are scale-dependent, and as such are affected by alterations in muscle fibre size (Fig. 1-9). This property has important implications for published descriptions of angiogenesis in skeletal muscle, as this is almost always accompanied by changes in FCSA.

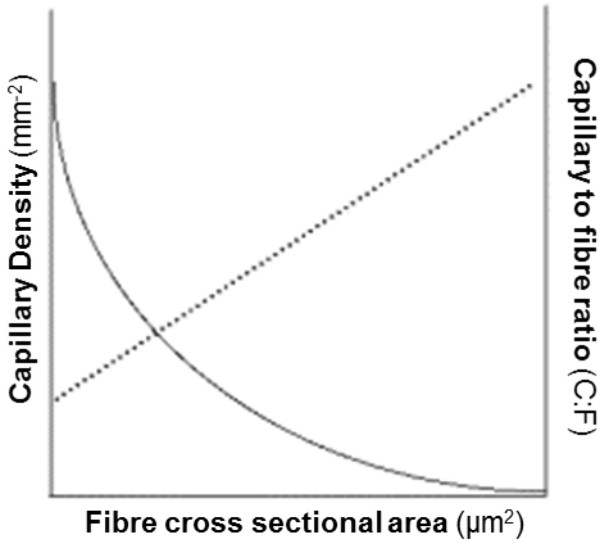

Figure 1-9. Influence of fibre cross-sectional area on CD and C:F. There is a positive linear relationship between FCSA and C:F (dotted line), while CD has a negative non-linear relationship with FCSA (solid line). This may reflect a mismatch in rate of angiogenesis and fibre hypertrophy. *Adapted from (Egginton, 1998).*

1.6.2.3.1.1 Capillary density (CD)

This is the most common capillary supply measure reported in the literature, and typically is presented per unit area of tissue (mm^{-2}). Capillary density is highly sensitive to changes in muscle fibre size, including elevated fibre size due to oblique sectioning, and other structural anomalies that may occur in physiological and pathological adaptation and tissue processing (e.g. fibrosis, or other increase in interstitial space, will lower CD; excessive fixing during histochemistry, leading to shrinkage of tissue and fibre size, will raise CD). CD cannot account for changes in

local geometry of the capillary distribution (Fig. 1-10), but does provide a simple, first-pass index of tissue oxygen delivery, reflecting the functional capacity of supply (Egginton, 1990a), and is most appropriate when neovascularisation occurs alongside minimal changes in muscle fibre area.

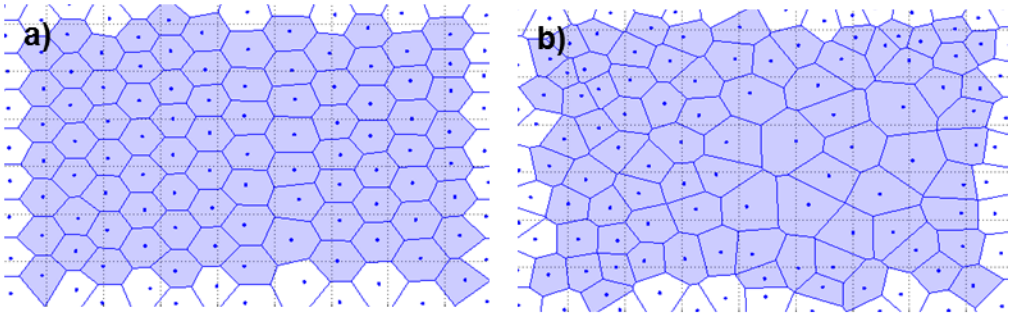

Figure 1-10. Limited descriptive capacity of capillary density. Here we have two example capillary distributions with identical capillary densities. While they both contain the same number of capillaries the spatial distribution are evidently different, with a highly homogeneous distribution (a) and highly heterogeneous distribution provided (b). Scale bar = 100µm.

1.6.2.3.1.2 Capillary to fibre ratio (C:F)

C:F is typically a robust measure for multiple muscle comparisons, as it shows a less sensitive effect of fibre size. C:F is typically higher in more oxidative muscle phenotypes (e.g. soleus), and classically higher in wild type animals compared to domesticated equivalents. Although C:F is indirectly affected by changes in fibre area (as a fibre grows the greater perimeter accommodates a higher number of capillaries), It provides a ready check on the numerical capillary content (e.g. whether or not angiogenesis has taken place), and has the advantage of being relatively insensitive to tissue section angle.

1.6.2.3.2 Fibre type composition

Clearly the capillary bed is there to serve the needs of the host tissue, and within this thesis the host tissue will primarily focus on skeletal muscle. Skeletal muscle typically comprises of multiple fibre types: Type I, oxidative; Type IIa oxidative-glycolytic and Type IIB/X fast-glycolytic. These fibre types comprise of different

intra-cellular proteins that alter the oxygen demand and will impact the flux of oxygen across the tissue.

1.6.2.3.3 Local indices

These measures enable the identification of more subtle changes in distribution of capillaries, and allow analysis of microvascular supply capacities relative to the cells of host tissue. Local capillary indices may differ from global indices by being scale-independent, if they take into account the changes in cell area and capillary content.

1.6.2.3.3.1 Capillary domains

Capillary domains, based on Voronoi polygons, are tessellated areas of tissue space that predict regions of supply for an individual capillary in a 2D plane. Capillary domains are made up of all the points nearest to an individual capillary, with the boundary situated equidistant between the target capillary and that adjacent to it (Fig. 1-11). The initial aim was to provide a measure of capillary spacing (Hoofd et al., 1985), which has since been used to derive a measure of capillary supply heterogeneity (Egginton et al., 1988, Degens et al., 1992, Egginton, 1990a, Egginton and Ross, 1992). The overlap of capillary supply areas (domains) with muscle fibre profiles has pathed the way for functional analysis of local capillary supply, and provided a framework for the modelling of oxygen supply and consumption (Egginton, 1990a, Egginton and Gaffney, 2010, Al-Shammari et al., 2012, Al-Shammari et al., 2014b, Al-Shammari et al., 2014a).

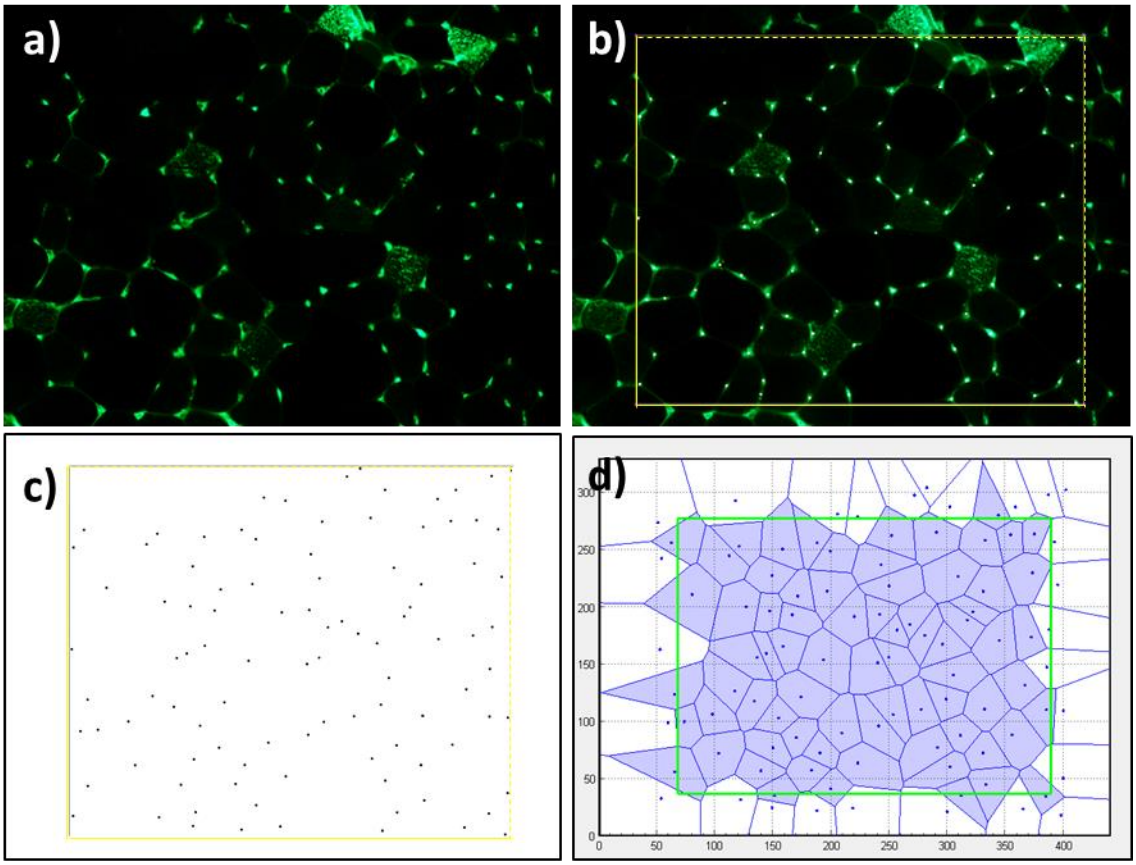

Figure 1-11. Example of capillary domain calculation. These areas are generated from histological images (a). Utilising the capillary locations identified in (b) the image can be digitised through colour thresholding, with the remaining point representative of the centroid of capillary lumen (c). Boundaries (navy boarders) are placed equidistant between the target and adjacent capillaries to form the capillary domain (blue filled polygons), which tessellate to form individual regions of capillary supply (d). Scale bar = 100µm.

1.6.2.3.3.2 Local capillary to fibre ratio (LCFR)

An individual capillary domain typically overlaps two or more fibres, and the proportion of a supply area that overlaps a fibre can be quantified. Summation of the cumulative fractions of capillary domain areas that overlap an individual fibre provides a measure of local capillary supply (LCFR). LCFR can be approximated by the ratio of mean fibre cross sectional area (FCSA) and mean capillary domain area. However, for a more accurate measure this requires capability for computational analysis of fibre area (Fig. 1-12b), capillary location (Fig. 1-12c) and domain area (Fig. 1-12d). This depth of analysis is currently a laborious and time-

consuming technique that is rarely employed in experimental physiological research.

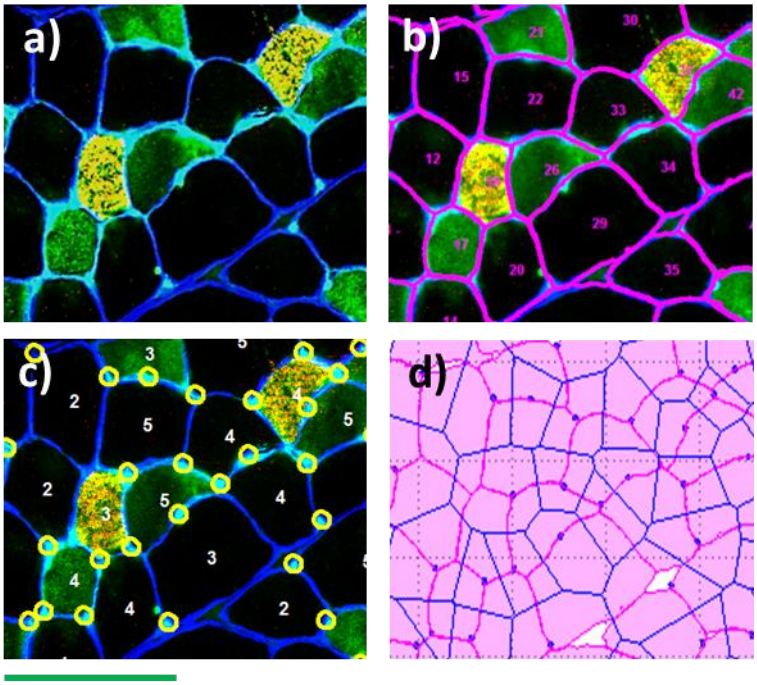

Figure 1-12. Generation of local capillary to fibre ratio. A transverse muscle section requires simultaneous identification of fibre boundaries and capillary location, and if possible a differentiating marker for fibre type (a). This information allows for a fibre skeleton to be generated (magenta outline) (b) and capillary location to be associated with individual fibres (yellow circles) (c). The capillary domains (light pink) tessellate across the fibre skeleton (magenta outline) and the summed fraction of individual capillary domain areas is generated for each fibre. Scale bar = 100µm.

1.6.2.3.3.3 Local capillary density (LCD)

LCFR plotted against FCSA shows a typically positive linear trend (Egginton, 1990a, Egginton and Ross, 1992, Ahmed et al., 1997), suggesting a positive allometric response of capillary supply in a growing muscle. In an effort to provide a scale-independent measure of capillary supply, LCFR can be normalised by dividing by FCSA, generating LCD for individual fibres of known phenotype. However, LCD in the main appears to be negatively correlated to FCSA to a minor extent, possibly reflecting adjustments in fibre size during section preparation (Egginton and Ross, 1992).

1.6.2.3.4 Tissue PO_2

The importance of altered microvascular content on the PO_2 of a tissue is not commonly reported. CD is considered to be a good index of tissue oxygen status in homogenous and cardiac tissue, however, the heterogeneous distribution of capillaries and fibre type composition of skeletal makes CD an insufficient representative of tissue PO_2. LCFR has been utilised to inform mathematical modelling by providing an anatomically correct input for oxygen diffusion.

1.6.3 Functional readouts

1.6.3.1 Muscle blood flow

To elucidate the functional relevance of structural adaptations identified through histological sampling an *in situ* preparation is typically used that allows the simultaneous assessment of muscle/limb blood flow, and measures of muscle fatigability. Blood flow previously had been calculated using microsphere injection through a central line running into the ventricles, and distributed throughout the body. Injecting a known number of microspheres allows for the proportion of total injected that lodge in arterioles to be calculated, and converted into blood flow for muscles activated during locomotion or for an isolated muscle procedure (Hawker and Egginton, 1999, Marsh et al., 2004, Armstrong, 1988). This technique is limited in the number of independent variables (frequency of stimulation) that can be tested, requiring multiple fluorescent coloured microspheres. There is also limited capacity to monitor functional and reactive hyperaemia. However, this technique does allow the analysis of blood flow kinetics *in situ* and *in vivo.* Finally, there has been recent evident to suggest that some commercial microspheres are suspended in preservatives that have vasoactive properties which may impact the vascular response centrally, and must be considered when interpreting data and repeating previous experiments. More recently the use of vascular flow probes has allowed real time measures of functional and reactive hyperaemia during an *in situ* preparation (Ray and Marshall, 2009). This method allows for multiple vessels to be analysed across a range of stimulation parameters, however this is not feasible during *in vivo* locomotion.

1.6.3.2 Muscle contractile properties

The most common functional measure derived during *in situ* experimentation is fatigue index (FI), generated through prolonged tetanic muscle contractions, where the ratio of initial and final tension is used to represent the capacity to maintain force (Hawker and Egginton, 1999, Ray and Marshall, 2009). The functional relevance and descriptive capacity of a tetanic muscle fatigue run has been brought into question, for its lack of translatability to regular muscle function in locomotion and its limited capacity to describe changes in many functional fatigue responses (e.g. changes in relaxation capacity and force-velocity relationship shifts) (Askew et al., 1997).

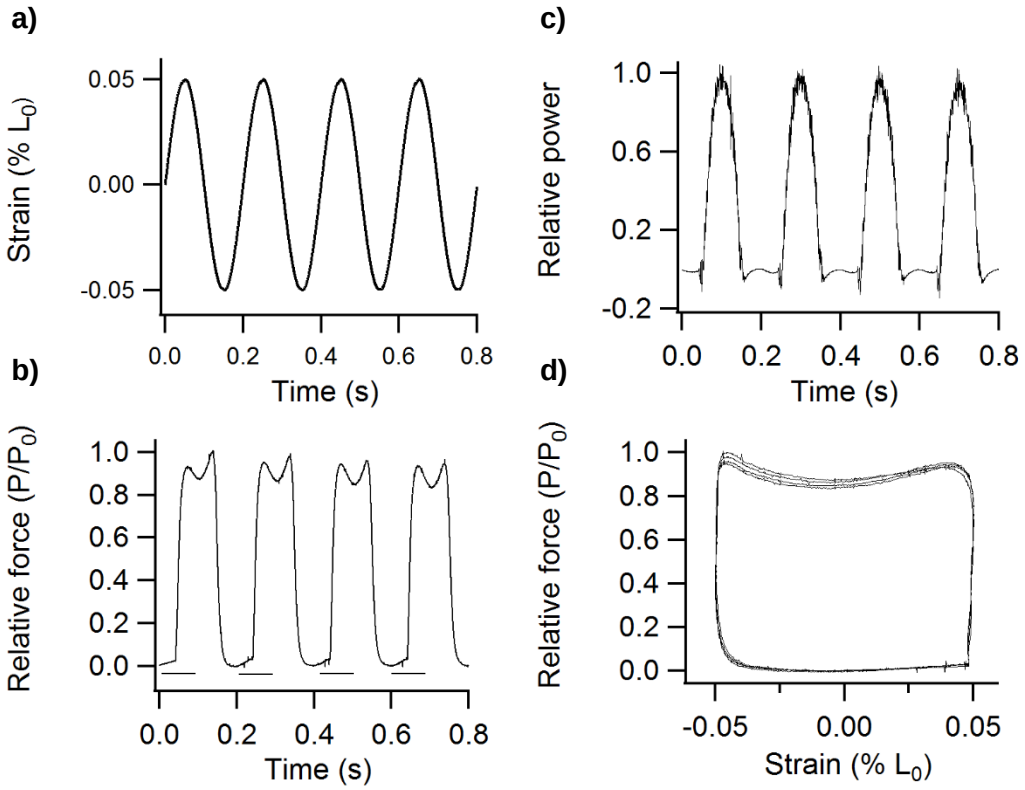

Figure 1-13. The method for measuring work output. A rat EDL was subjected to a 5% sinusoidal length change (a) and stimulated for 88ms using a, 0.2ms pulse width (black lines indicate stimulation duration) to generate force during shortening (b). The power generated during each cycle is displayed (c), while force and strain are plot to form the traditional 'work loop' where the area encompassed in the loop is the net work done per cycle (d) (Josephson, 1985).

Subsequently, the use of the work loop technique (Josephson, 1985) has pioneered the measurement of muscle function through simulation of behaviors seen during locomotion (Askew et al., 1997, Ahn, 2012, James et al., 1995). Usually during locomotion muscles undergo rhythmic length changes with pulsatile activation, predominantly during the shortening phase of the duty cycle. This is the underpinning principle of the work loop technique where a muscle is subjected to a repetitive strain trajectory (Fig. 1-13a) (symmetrical sinusoidal length trajectories, or asymmetrical saw-toothed length changes (Askew and Marsh, 1997)). Phasic activation of the muscle generates force (Fig. 1-13b), which permits the calculation of net work produced during a full cycle (Fig. 1-13d). The work loop technique allows for comparative length and activation parameters to be tested across the same muscle following various interventions, or the more functionally relevant method involving the replaying of length trajectories recorded during locomotion and activating the muscle in synchrony with EMG recordings.

1.7 Aims and objectives

The aim of this thesis is to further characterise the mechanisms of exercise-induced angiogenesis, utilising animal models of altered muscle activity. The research conducted set out to generate a high throughput data pipeline that provides a more comprehensible overview of capillary content in exercise/pathological striated muscle than currently available. This level of analysis will be applied to various exercise models described in the introduction to uncover differences in oxygen diffusion capacity and adaptive remodelling induced by the training regimes. To further our understanding and generate a holistic overview of exercise-induced angiogenesis we set out to utilise publically available exercise gene array data to explore the transcriptional response of key angiogenic networks. These networks will then be correlated with the angiogenic animal models to further elucidate the signalling networks involved in mechanotransductive driven remodelling.

We hypothesized that regional variation in fibre type composition within a muscle would result in differential contractile properties that would relate to the recruitment pattern of the muscle. Having characterized the structural and functional composition of the rat EDL we expect to be able to detect the local capillary changes in response to shear stress and muscle stretch induced angiogenesis that global analysis has yet to describe. Utilising the more spatially resolved data we believe it will be possible to predict the potential functional benefits of a given angiogenic intervention and postulate potential clinical application, following characterization of various pathological models. Finally we hypothesise that the commonly used angiogenic animal models would have largely similar global genotypic responses to human exercise training regimes that evoke an angiogenic response (e.g. endurance exercise). While there would be some differential angiogenic signalling among the animal models associated with differences in mechanotransductive origins of angiogenesis.

2 An integrated method for quantitative morphometry and oxygen transport modelling in striated muscle

This work has been completed in collaboration with Simon Holbek (Technical University of Denmark) and Abdullah Al-Shammari (University of Kuwait). Simon Holbek wrote the MATLAB script (Dtect) to process the immunofluorescent muscle images and generate a digital skeleton and representative overlay while Abdullah generated the MATLAB script to compute the local capillary distribution and model tissue O_2 tension. Roger Kissane completed all immunohistochemistry method development, data collection and analysis, software functionality and usability.

2.1 Abstract

Understanding structural characteristics underpinning pathological dysregulation in tissue O_2 transport is primarily restricted by the methods employed to characterise physiological remodelling. In turn this has failed to develop effective therapeutic strategies. Understanding O_2 transport within striated muscle faces major challenges, most notably the difficulty in quantifying how well fibres are served with O_2, which has necessitated exploring O_2 transport in tissue using theoretical modelling. Having identified capillary domains as a suitable model for the description of O_2 supply with less intensive computational demand than trapping regions, we sought to design a high throughput method for histological analysis.

This chapter describes the development of an image analysis system for skeletal and cardiac muscle research that incorporates both global and local morphometric indices, using a semi-automated software package. We have designed a robust immunohistochemical protocol allowing the parallel quantification of fibre type composition and microvascular distribution. This permits analysis of both rodent and human muscle composition at a high spatial resolution, with closer integration of data and greater flexibility of analysis than previously reported. In addition, an optional routine is incorporated for exploring the functional capacity of capillary distribution, by calculating effects of structural remodelling on local variation in tissue O_2 tension. Worked examples are provided to illustrate the process, and experimental data included to illustrate utility of this approach.

2.2 Introduction

Striated muscle is characteristically plastic, with a dynamic capacity to remodel in response to varying physiological, pharmacological and pathological stimuli. Microvascular remodelling (e.g. angiogenesis) in striated muscle has been identified as a highly coordinated physiological process (Williams et al., 2006a, Williams et al., 2006b, Egginton, 2009), and being able to explore the functional importance of targetted interventions or the consequential effect of pathology on the microvascular O_2 transport would be a valuable technique. In a muscle with uniform phenotype, typically cardiac or to a first approximation the soleus muscle, this presents a relatively straightforward problem that may be solved using an approximately point source supply location (capillaries) and homogenous O_2 demand (fibre MO_2) in modelling the outcome (Al-Shammari et al., 2012, Hoofd et al., 1985). While in most skeletal muscles, it is necessary to accommodate varying fibre type and size, and the relationship with the extent of microvascular supply and its distribution.

The earliest attempt to model O_2 diffusion across a muscle was by the Noble prize winner August Krogh in 1919. Krogh postulated a model where each capillary within a muscle ran parallel with muscle fibres and supplied O_2 in a cylindrical fashion, and the area encompassed within the cylinder is the functional supply area for that individual capillary (Fig 1a, b)(Krogh, 1919). This model relied on a variety of assumptions, for instance; that O_2 consumption was uniform across fibres, that capillaries were parallel and equally spaced, and that the average tissue PO_2 equaled that of the average capillary PO_2 at the capillary wall (Kreuzer, 1982).

The use of cylindrical supply regions is clearly an unlikely physiological system for O_2 delivery, given the inherent difficulty in close packing of cylinders (*i.e.* circles when represented as 2D tissue sections). Cylindrical supply regions would suggest that there are areas where no O_2 will diffuse (Fig. 2-1b, anoxic regions between), and instances of overlapping supply areas that involve intercapillary interactions and excess delivery (Kreuzer, 1982). The excluded regions of tissue O_2 supply within Krogh's cylinder method lead to the testing of tessellating (space filling)

polygons to remove these voids, moving towards the establishment of the capillary domain area as a useful quantitative index of capillary supply (Fig 2-1d).

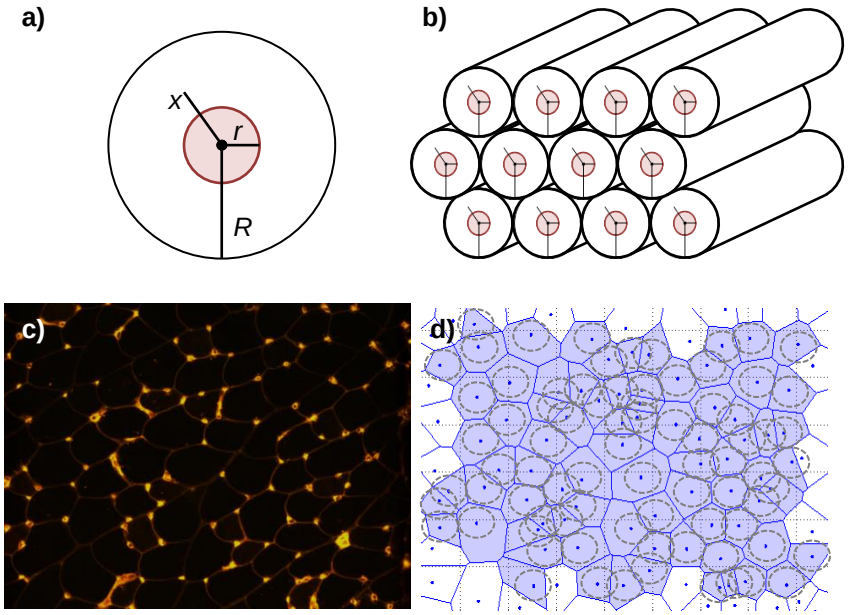

Figure 2-1. Krogh's original hypothesis of tissue oxygenation with a histological example. Krogh's circle cylinder supply area (black circle) around the capillary (red circle), where R denotes the radius of this cylinder, r the capillary radius, and x the distance from the capillary of which the equation predicts the PO_2 (a). The stacking of supply cylinders described by Krogh which inevitably comprise of anoxic voids (b). Rat EDL muscle stained for capillary location with *Griffonia simplicifolia* lectin (c). A digitised composite of the histological sample with Krogh's cylinders (grey circles) around the capillaries (blue dot), in addition to capillary domain areas (navy polygons) (d). Scale bar = 200µm.

Capillary domains describe the area of tissue supplied by an individual capillary that incorporates tissue closest to its centroid than any other, with the domain boundary placed equidistant to the nearest capillary (Fig 2-1d). This tessellation of domains within a tissue cross section allows analysis of the functional relevance of the geometric capillary distribution, within both homogeneous and heterogeneous tissue (Egginton et al., 1988, Hoofd et al., 1985). The distribution of domain areas allows the quantification of capillary heterogeneity, and the functionally relevant effect of fibre area to be incorporated into the analysis of local capillary supply (Egginton and Ross, 1992).

The capacity of capillary domains to model O_2 flux has been explored using striated muscle with uniform O_2 uptake (cardiac tissue) (Hoofd et al., 1985) and tissue with asymmetrical capillary supply and heterogeneous O_2 demand (Al-Shammari et al., 2014b), and compared with the more physiologically relevant trapping region model (a numerical solution for O_2 transport that builds the biophysical properties of O_2 delivery into a geometrical skeleton generated from histological images). Comparative simulations of capillary domains and trapping regions have been shown to be highly correlated in muscles with both uniform O_2 uptake, and to some extent those with heterogeneous demand (Al-Shammari et al., 2014b). The dissociation between capillary domains and trapping regions becomes apparent around larger fibres, regions of tissue with highly heterogeneous oxidative capacities, and in instances of significant capillary rarefaction (Al-Shammari et al., 2014b, Al-Shammari et al., 2014a).

Structural changes in muscle are most commonly analysed using immuno/histochemical staining and laborious manual image processing techniques. Current quantification of anatomical composition from histological samples predominantly utilise global indices (C: F, CD), due to the time-consuming manner of acquiring finer scale morphometric indices, and the computational difficulty in modelling of O_2 transport. Standard operating procedures have been devised to allow unbiased and reproducible morphometric analysis (Egginton, 1990b, Ceglia et al., 2013), with some attempts to produce semi-automated (Smith and Barton, 2014) and fully automated analyses (Mula et al., 2013) (Miazaki et al., 2015) for global morphometric indices. In principle, algorithms reduce operator bias to a minimum (reproducibility from independent runs with fully automatic algorithms are close to 100%) and all fibres in an image can be classified much more quickly than traditional, manual approaches. This does, however, rely on unambiguous staining profiles (e.g. fibre boundaries must be detectable with an algorithm that produces a realistic outline, and individual muscle fibres assigned to a specific fibre type), which is rarely achievable, and no current method provides the necessary flexibility for both delineating fibres at a single pixel resolution, nor associating individual capillaries to neighbouring fibres.

Therefore, the aim of this study was to provide an integrative method for muscle biopsy analysis that provides a more comprehensive analytical approach than currently available. This necessitated developing a semi-automated image processing data pipeline, with improved throughput, but maintaining interactive capabilities for non-standard applications. The task was divided into sub-packages, which could be used independently or combined to provide a comprehensive description of muscle phenotype. First, a multi-purpose immuno/histochemical staining protocol was formulated to identify key components within rodent and human muscle samples. From digitised images a comprehensive data file was produced describing morphometric indices of muscle composition, with the capacity for semi-automated detection of individual structures, using an unbiased sampling protocol within selected regions of interest. Along with this digitised skeleton we incorporated microvascular locations to generate fibre type-specific indices, in addition to commonly reported global values for capillary supply. The data file containing muscle fibre boundaries, fibre type, and capillary location may then be incorporated into a model of O_2 diffusion to generate a PO_2 profile across the biopsy sample. This chapter illustrates the analytical approach using worked examples, and the utility is demonstrated using experimental data. The codes will be available from collaborators (see acknowledgments).

2.3 Material and methods

Rodent sampling was conducted in accordance with guidelines set by the UK Home Office (HO) by competent HO personal licence holders, and in accordance with the 1986 ASPA. Both rats and mice were culled by schedule one methods (concussion to the brain and cervical dislocation) and the *extensor digitorum longus (EDL) and tibialis anterior* (TA) muscle was carefully removed, trimmed of proximal and distal tendons, and the mid-portion coated with OCT on cork discs, and snap frozen in isopentane cooled in liquid nitrogen. All participants for the human muscle biopsy protocol gave written informed consent to be included in the study, which conformed to the standards set by the Declaration of Helsinki, and in accordance with local ethics committee approval. Muscle samples from *vastus lateralis* (VL) were taken using a 5mm Bergström needle (Bergström 1975) with

suction. Samples were snap frozen in liquid nitrogen. All samples were stored at -80°C for later analysis.

2.3.1 Immunohistochemistry

Muscle samples were warmed to -20°C for cryosectioning, serial sections cut at 10µm, and fixed to polysine adhesion slides (VWR International). Slides were stored at -20°C until staining.

2.3.2 Fibre type validation

A selection of monoclonal antibodies have now made it possible to detect the three major fibre types within rodent and human tissue, as well as allow for detection of hybrid muscle fibres (Smerdu and Soukup, 2009) (Bloemberg and Quadrilatero, 2012). Figure 2-2 shows the availability of three monoclonal antibodies available from the Developmental Studies Hybridoma Bank (DSHB, University of Iowa, USA) to identify the most commonly reported fibre types. Serial sections were used to compare the monoclonal antibodies BAD5, SC-71 and BF-F3 (Developmental Studies Hybridoma Bank (DSHB, University of Iowa, USA) with the commonly used ATPase method of fibre type differentiation (Fig. 2-3). This was to simplify the protocols that differentiate hybrid muscle fibres (Smerdu and Soukup, 2009, Bloemberg and Quadrilatero, 2012), and retain the differentiation of the three major fibre types: Type I, Type IIa and Type IIb.

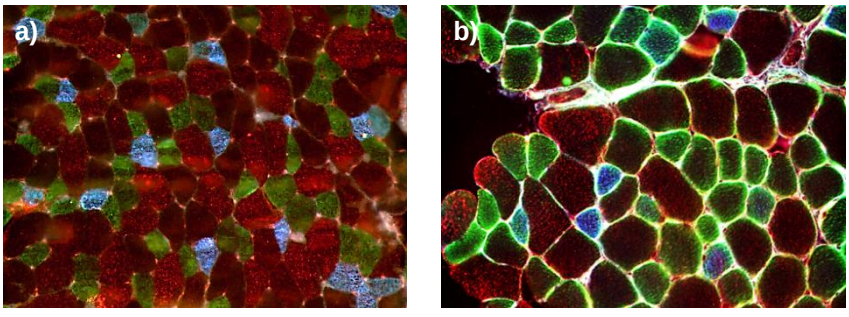

Figure 2-2 Major fibre type identification using monoclonal antibodies. Rat EDL (a) and mouse TA (b) stained for muscle fibre type identification using similar protocols to Smerdu & Soukup (2009) and Bloemberg & Quadrilatero (2012). Type I fibres labelled with BA-D5 (blue), Type IIa/x with SC-71 (green) and Type IIb with BF-F3 (red). Scale bar 200µm.

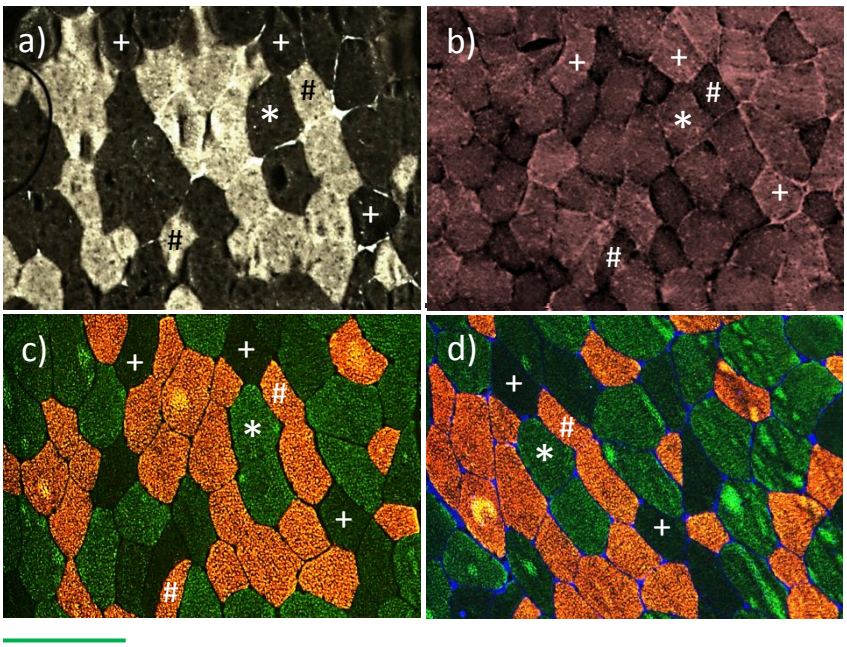

Figure 2-3 Immuno/histochemical analysis of fibre type in human VL muscle. (a) Muscle phenotype differentiated by myosin ATPase activity following alkaline pre-incubation; light stain identifies Type I (slow) fibres and dark fibres are Type II (fast) fibres. (b) Succinate dehydrogenase activity used to differentiate fibres based on their oxidative capacity; unstained/white fibres correspond to Type IIx while darkly stained fibres identify Type I and IIa. (c) Anti-mouse monoclonal antibodies for myosin-heavy chain isoforms identify Type I in red, Type IIa in bright green, and Type IIb dark green/unstained. (d) Combination of myosin heavy-chain antibodies and laminin basement membrane marker (blue), allowing automatic detection of fibre boundaries. *, Type I. #, Type IIa. +, Type IIx. Scale bar 200µm

2.3.3 *Integrated fibre type and capillary composition*

Following multiple pairwise comparisons of antibody staining for individual fibre types, a validated simplified protocol was adopted (Appendix 1). Monoclonal-myosin heavy chain (MHC) antibodies were used to simultaneously label two of the three main fibre types; BA-D5 (1:1000 dilution) for Type I fibres (slow MHC) labelled with Alexa Fluor 555 Goat Anti-Mouse IgG (1:1000 dilution) (Life Technology, A21422) and SC-71 (1:500 dilution) for Type IIa (fast oxidative, glycolytic) labelled with Alexa Fluor 488 Rabbit Anti-Mouse IgG (1:1000 dilution) (Life Technology, A11059). leaving Type IIb unstained. Fibre boundaries were identified by applying a fluorescent probe to the extracellular matrix protein, laminin (Sigma, L9393), using an optimised protocol (Fig. 2-4). Finally, capillaries were labelled with a carbohydrate-binding protein (lectin) specific to the species of

interest: for rodent endothelial cells *Griffonia simplicifolia* lectin I (GSL I, Vector Labs, FL-1101) (1:250 dilutions) and human endothelial cells *Ulex europaeus* agglutinin I (UEA I, Vector Labs, FL-1061) (1:250 dilutions). This combination of markers allows for differentiation of the three main MHC isoforms and fibre boundary localisation, allowing fibre-specific interaction with individual capillaries to be quantified, in a protocol shown to be robust for both rodent and human samples (Fig. 2-5).

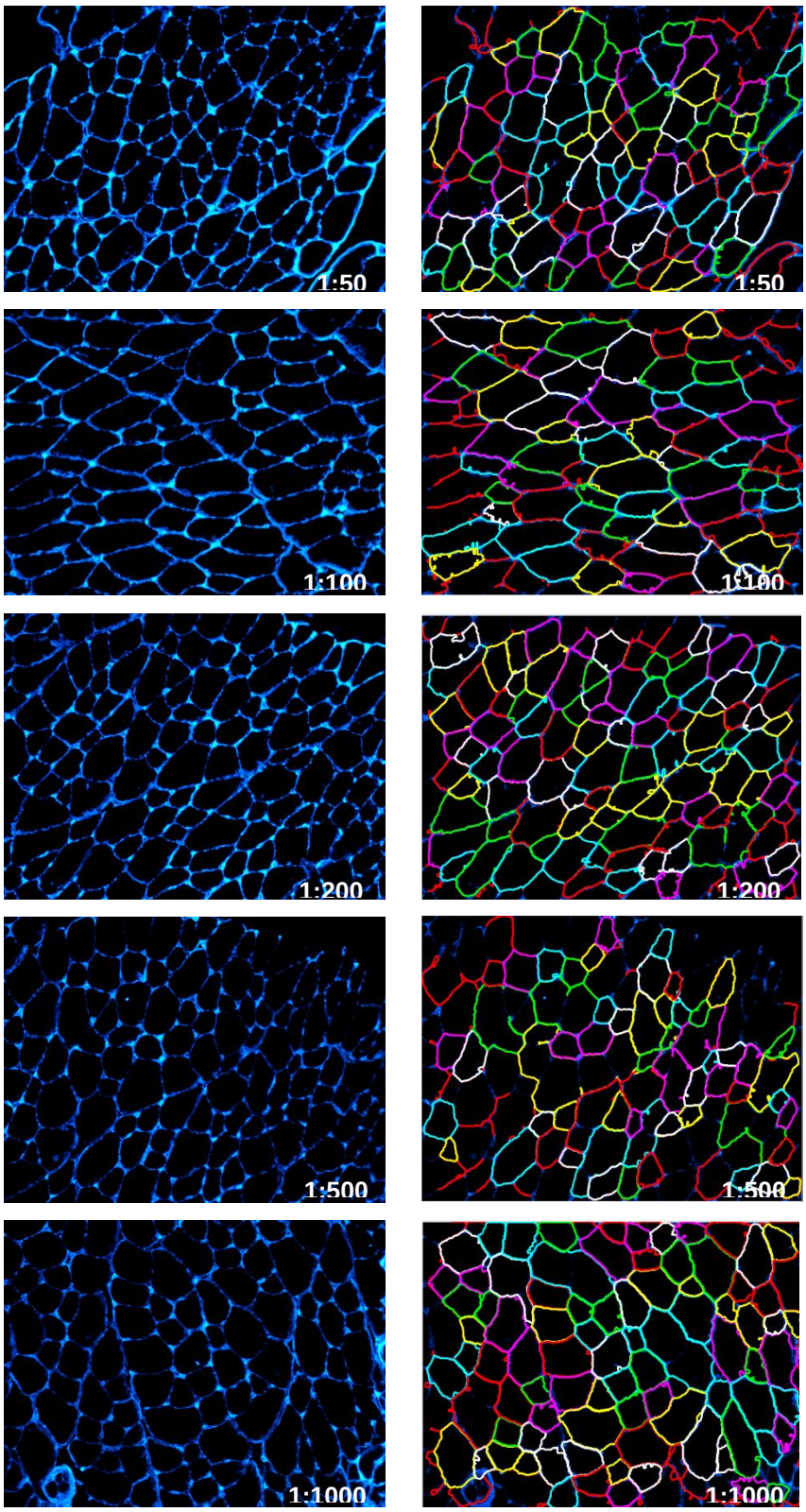

Figure 2-4. Laminin boundary optimisation. Serial dilutions made for fibre boundary marker (laminin, blue composites) using segmentation algorithm to calculate fibre boarder (multicolour overlay). 1:200 dilutions generated similar levels of accuracy to 1:50 and 1:100, and subsequently is used throughout histological staining. Scale bar 200µm.

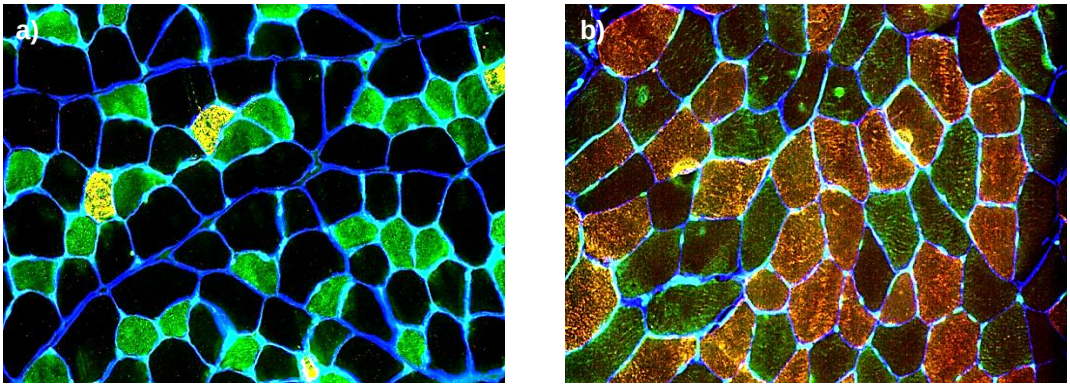

Figure 2-5. Combination of immunohistochemical staining of muscle samples. Rat *extensor digitorum longus* (a), human *vastus lateralis (b)*. Blue fibre borders labelled with laminin, red stained Type I MHC, green labelled Type IIa MHC and unstained/negative fibres are Type IIb (rodent)/Type IIx (human). Scale bars 200µm.

2.3.4 Fibre type segmentation

A stand-alone graphical user interface, Dtect, was coded in MATLAB for semi-automatic fibre segmentation. Step I detects fibre boundaries based on an immunostained basal lamina image, and offers the user the possibility to edit the image (add indistinct and remove artefact lamina segments) to improve delineation accuracy. In step II, automated classification into different fibre types is attempted, but with the opportunity to correct classification of individual fibres to accommodate problems with sample preparation or age, that may give rise to indistinct threshold classification. An output file with fibre type morphometric statistics is produced at this point, with the option to proceed. Step III is used to manually mark capillary location on the image (based on vessel centre of gravity), and link their position with adjacent fibres. Global indices of muscle capillary supply are then generated. Step IV generates an output file containing capillary and fibre boundary coordinates, with fibre type annotation, and is used as input for tissue oxygen tension calculations (see below).

2.3.5 Muscle fibre boundary identification

The goal is to create a binary image of the basal lamina where noise is filtered and a skeleton is preserved. An RGB image file (.jpg, .png, or .tif.) from the

immuno/histochemical method above is imported and the scaling factor recorded (pixels.mm^{-1}). In this study, blue fluorescence was used for lamina coding and a default threshold value used to create a binary image, with the aim of segmenting out the lamina in the image; further user refinement of the threshold value is possible to improve segmentation accuracy. Subsequently, all isolated pixels are cleared (a cleaning process whereby the number of pixels in objects to be deleted can be user-defined) from the image, and a bridging operation ensures that gaps between unconnected pixels are treated as contiguous lamina segments, if they have two nonzero pixels that are connected. Morphological opening (dilation) operation is applied to the image to fill holes of single pixel size, and finally a closing (erosion) operation is performed to shrink the binary image into a lamina skeleton of one pixel width, producing a connected line halfway between the inner and the outer lamina boundaries. An optional user-specified, uniform lamina width could subsequently be obtained through a morphological dilation operation with a symmetric circular structuring element. Inherent limitations in designing the structuring element means the diameter can only be of uneven pixels size, which translates to a resulting uniform lamina of uneven pixel width in the binary image.

With the preferred configuration of the binary image, a boundary detection algorithm (Gonzalez, 2004 digital image processing) was applied, allowing the area of all objects present in the image to be calculated (Fig. 2-6). Only objects within the user specified area (region of interest, ROI) were classified as fibres and identified onscreen.

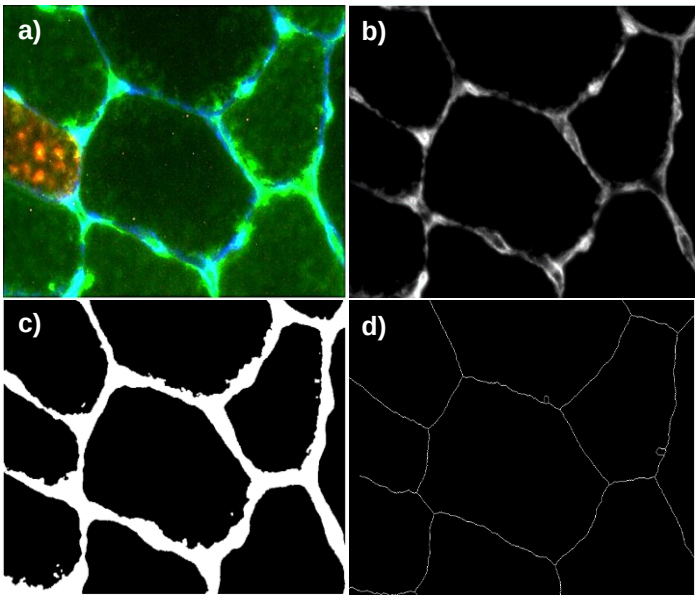

Figure 2-6. Processing scheme for skeletonising the RGB image. Zoomed region of Rat EDL muscle, RGB formatted image (a). First the image is transformed to a gray scale image of the blue channel, representing lamina staining (b). A binary threshold is then applied (c), followed by cleaning, bridging, dilation and filling operations, that result in a shrinking of the fibre boarder to single pixel width (d).

2.3.6 Muscle fibre type allocation

Following detection of the fibre boundary skeleton the program allows different fibre types to be classified in a user-defined manner, allowing for tailored analysis. For the purpose of this study we defined fibres according to the three major phenotypes (Type I, IIa and IIb/x). The mean red and green colour saturation levels were calculated for all fibres based on the RGB pixel values inside their respective detected boundary. A k-means clustering algorithm was applied to divide all identified fibres into three types, based on their red and green colour saturation combination (Fig. 2-7). As automated classification is not infallible, the user can manually re-allocate individual fibres to a different type. As an additional option, the user can specify any of the detected fibres to be excluded in the statistics, e.g. due to structural abnormalities or staining artefacts. Once the fibre type classification is accepted data are saved as a .txt file containing muscle fibre statistics, with an accompanying .mat file that contains all the morphometric information (lamina position, fibre boundaries, fibre type classification).

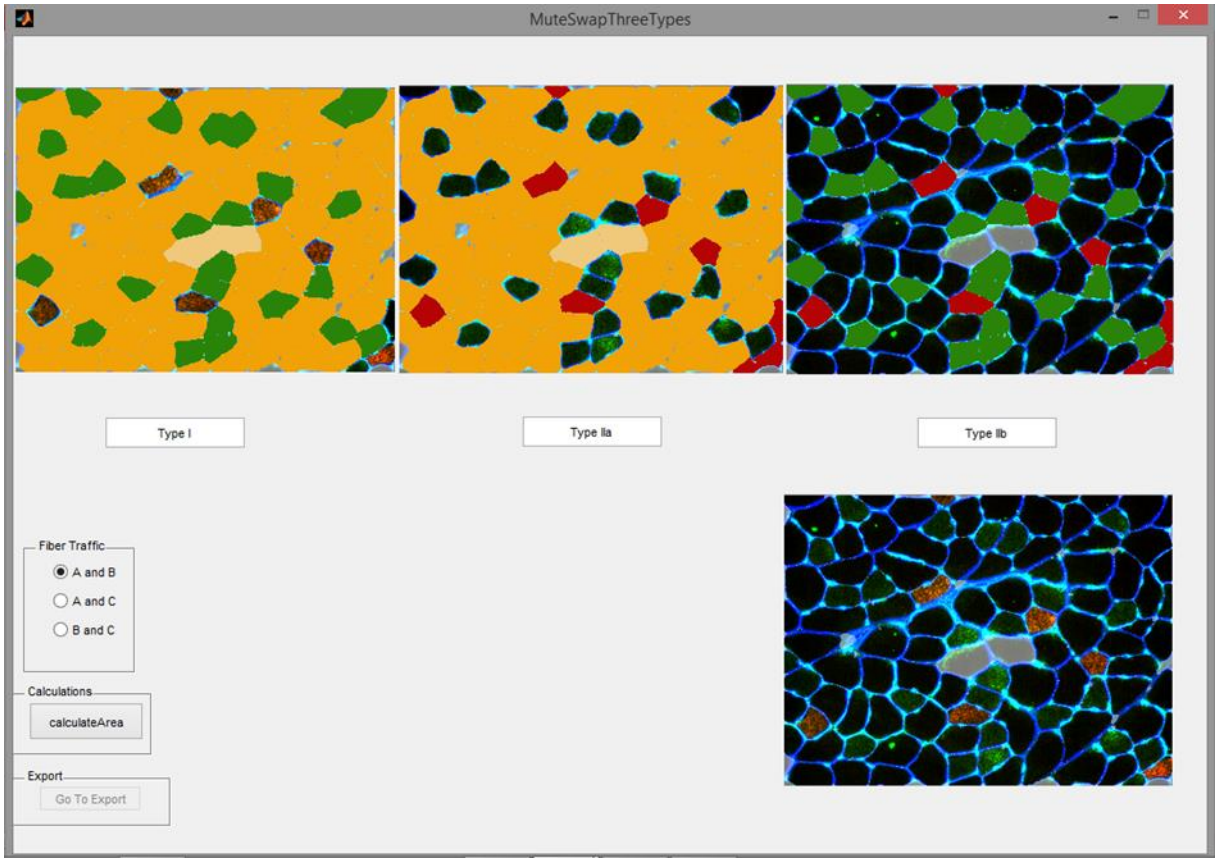

Figure 2-7. Muscle fibre type allocation. Screenshot showing how Dtect samples saturation levels within an object boundary, and automatically assigns a fibre type based on pre-set threshold levels. Dtect differentiates fibres based on their colour fill, red fill – Type I, green fill – Type IIa and unstained – Type IIb. If the saturation of stain is under the pre-assigned threshold fibres may be incorrectly assigned, but the built in user capabilities allows the relabeling of fibres using the Fibre Traffic function. Fibres can also be excluded from analysis by 'muting' those clicked in the bottom right window (opaque fibres).

2.3.7 Capillary positioning

This optional step allows users to input capillary location around the lamina boundary, and subsequently define interaction with individual fibres. The .mat project file generated previously is loaded into the capillary identification package, where capillaries are manually identified one by one on the image with a mouse click. Coordinates in the image (x,y position) are extracted from each mouse click, such that the exact location of all the identified capillaries is defined. If the shortest distance between the recorded location of a capillary and the boundary of a fibre is less than the default threshold, an association to local fibres is established (Fig. 2-

8). Thus, the established association both keeps track of which fibres / fibre types are connected to individual capillaries, and vice versa. This interaction allows analysis of fibre type-specific indices of capillary supply. Following the identification of all capillaries a .mat file is generated with the additional information for capillary location, to be used in the oxygen tension analysis.

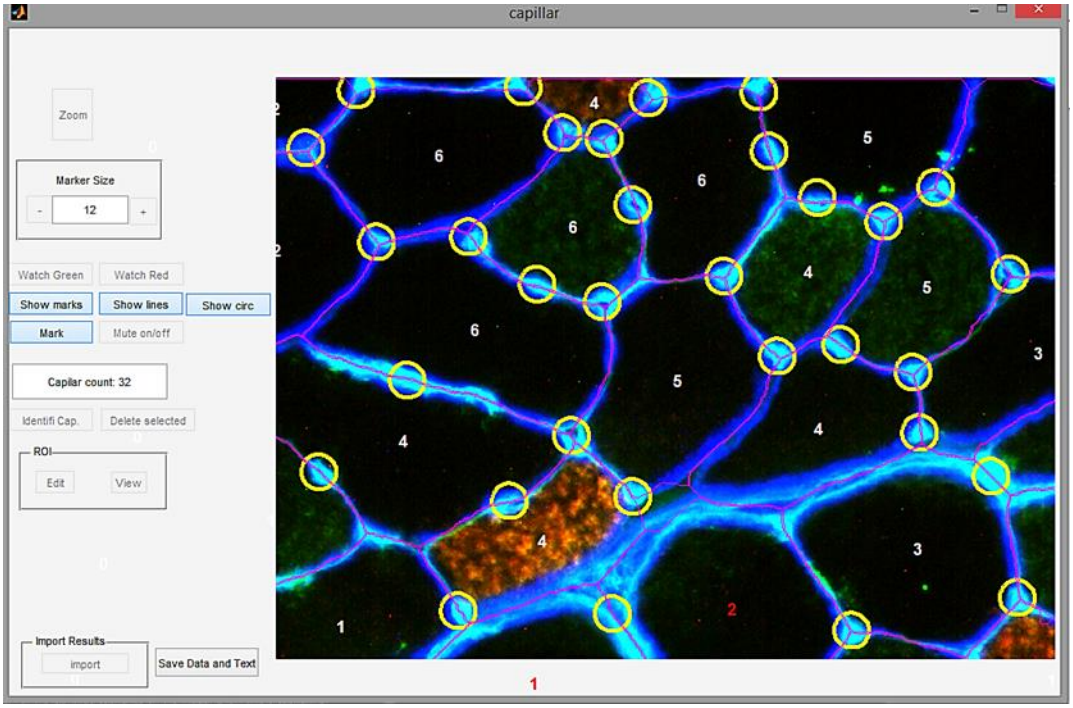

Figure 2-8. Screenshot showing microvascular identification and location within the interstitium. Each capillary is labelled by a yellow marker with the centre of the circle corresponding to the centroid of the microvessel. The capillary is then 'associated' with the bordering fibres (number in fibre centre represents the number of capillaries in contact with it), which can be manually edited if an incorrect association is made.

2.3.8 Calculating morphometric indices

The user is required to provide information about the type of tissue geometry to be processed. The current image segmentation algorithms can process three types of image: (1) capillary location only, (2) capillary location and fibre outlines, and (3) capillary location with boundary outlines and defined fibre type (Fig. 2-9).

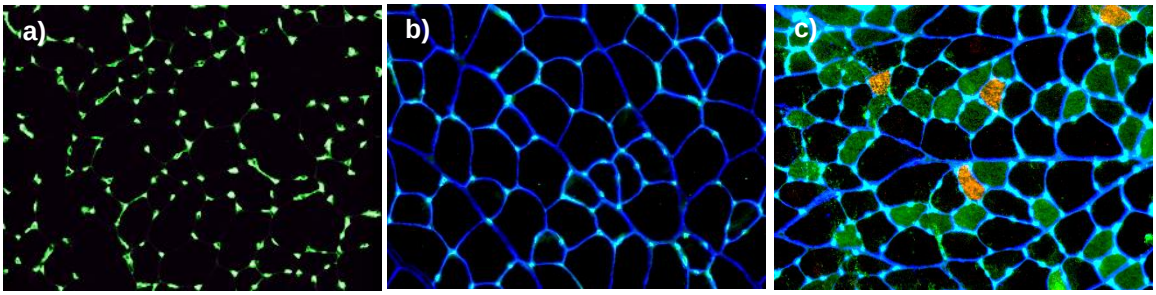

Figure 2-9. Versatility of image input for capillary indices calculations. Individual capillary location labelled with *Griffonia simplicifolia* lectin-1 staining (a). Capillary location with fibre boundary coordinates is optional, used primarily for homogeneous tissue phenotypes (b). Finally, capillary location built onto muscle fibre boundaries with fibre type composition, allowing differential tissue oxygen consumption modelling.

Capillary location alone (Fig. 2-9a) allows for global morphometric indices like capillary density (CD) and inter capillary distances (ICD) to be quantified, as well as the calculation of capillary domains and the beginning of capillary heterogeneity analysis (Egginton, 1990a). Capillary location with fibre boundaries (Fig. 2-9b) gives rise to the generation of local non-integer based indices, and allows for the modelling of capillary supply regions assuming homogeneous oxygen consumption, such as found in cardiac tissue (Al-Shammari et al., 2012). Incorporating the additional heterogeneities in oxygen uptake *via* fibre type allocation (Fig. 2-9c) allows the generation of fibre type specific, local capillary indices and subsequently model tissue PO_2 (Al-Shammari et al., 2014b). Examples of data output of global and local capillary indices (Fig. 2-10) and individual fibre-capillary indices (Fig. 2-11) are provided.

Number of Capillaries	144.5	**NCAF/fibre perimeter**	
Capillary Density	996	**All fibres**	15.095
X Length Scale	439.86	Type I	18.685
Y Length Scale	329.9	Type IIA	15.135
		Type IIB	14.61
Total number of fibre	79		
Number of included fibre	34	**LCFR**	
C:F	2.765	**All fibres**	1.72
		Type I	1.71
Mean fibre area		Type IIA	1.59
All fibres	2020.81	Type IIB	1.81
Type I	1290.98		
Type IIA	1432.715	**LCD**	
Type IIB	2547.66	**All fibres**	1021
		Type I	1320.235
Fibre numerical density		Type IIA	1098.7
Type I	0.07	Type IIB	666
Type IIA	0.4		
Type IIB	0.53	**Number of Voronoi Cells**	144.5
		Included Voronoi Cells	70.5
Fibre area density		**Mean[Voronoi Cell Area]**	973.615
Type I	0.05	**STD[Voronoi Cell Area]**	352.93
Type IIA	0.28	**SEM[Voronoi Cell Area]**	41.97
Type IIB	0.67	**LogSD[Voronoi Cell Area]**	0.15155
NCAF		**Mean[Domain Eq. Diameter]**	34.67
All fibres	6.155	**STD[Domain Eq. Diameter]**	6.145
Type I	6.125	**SEM[Domain Eq. Diameter]**	0.73
Type IIA	5.16	**LogSD[Domain Eq. Diameter]**	0.0758
Type IIB	6.88		
		Mean[Mean NN Distance]	34.395
		STD[Mean NN Distance]	6.245
		SEM[Mean NN Distance]	0.745
		Mean[STD NN Distance]	10.765
		Mean[SEM NN Distance]	4.51

Figure 2-10. Example data output presenting mean values for global and local capillary indices.

Domain Areas (um^2)	Min NN (um)	Unique Min NN (um)	Mean NN (um)	Rand NN (um)	FDR
1202.62	24.73	28.14	38.49	47.81	4
1352.94	24.73	24.73	41.15	34.71	4
1221.8	16.57	16.57	39.59	34.71	3
780.75	16.57	16.57	34.92	20.87	4
1120.07	20.87	31.17	39	20.87	3
1559.08	31.17	31.17	44.38	71.34	5
2119.66	23.28	23.28	50.55	23.28	5
1045.88	18.79	18.79	38.02	47.81	3
1179.71	27.46	28.36	38.07	28.36	5
959.06	17.86	23.28	35.26	17.86	3
864.46	17.86	19.59	34.2	17.86	4
1592.23	21.46	21.46	47.66	57.28	4

Fibre Type	Fibre Area (um^2)	DFR	LCFR	LCD ($1/mm^2$)	NCAF	NCAF/Perimeter (1/mm)
21	826.61	3	0.57	692.58	3	11.57
22	2031.27	5	1.49	731.76	5	12.5
22	1246.57	5	0.98	788.76	5	15.62
21	1104.14	3	0.94	851.06	3	9.93
22	2239.53	6	1.8	805.83	6	14.09
22	1463.53	4	1.13	770.27	4	11.42
22	1614.18	5	1.17	724.77	5	12.5
1	399.98	3	0.43	1076.26	3	16.18
22	2413.85	7	2.09	867.38	7	15.4
21	829.95	3	0.68	817.28	3	11.41
22	1778.37	5	1.33	748.43	5	12.82
22	1536.42	5	1.37	894.33	5	13.99

Figure 2-11. Example data output providing individual fibre-capillary indices, for collation of data in instances where numerous regions of interest are taken.

Using the geometric mesh generated from the histological image, a direct exploration of the oxygen transport capacity of the tissue can be made using a mathematical modelling framework with physiological parameters applied to structural objects. Oxygen transport is considered to be a 2D process, and completed through three exchange pathways, free O_2 diffusion, facilitated diffusion *via* myoglobin, and within muscle fibres primarily by Michaelis-Menten O_2 consumption. Intravascular boundary conditions (e.g. O_2 exchange with interstitial fluid or fibre boundaries) are accounted for and built into the model through a

Robin boundary condition at the capillary wall (Al-Shammari, 2014). The primary regions of O_2 demand are the interstitial space (low) and muscle fibres (variable) that are accommodated with the assumption that the interstitial space diffusivity and solubility of O_2 are equal those of the neighbouring fibres, and different fibre types are assigned individual physiologically informed values for oxygen uptake (Table 2-1).

The tissue domains oxygen tension (PO_2) is calculated as follows:

$$\nabla \cdot [\underbrace{D(x)\nabla(\alpha(x)p)}_{\text{free diffusive flux}} + \underbrace{C^{Mb}(x)D^{Mb}(x)\left(\frac{dS_{Mb}}{dp}\nabla p\right)}_{\text{myoglobin-facilitate flux}}] = \underbrace{M(x,p), x \in \Omega,}_{\text{tissue consumption}} \quad (1)$$

$$n_i \cdot [a(x)D(x)\nabla p] = k\left(p_{cap} - p\right), x \in d\Omega_i, \quad (2)$$

$$n_{tissue} \cdot [a(x)D(x)\nabla p]|_{d\Omega=0,} \quad (3)$$

$$S_{Mb}(p) = \frac{p}{p + p_{50,Mb}}, M(x,p) = \frac{M_0(x)p}{p + p_c}, \quad (4)$$

Ω denotes the global tissue domain, exclusive of capillaries (Ω_i) with the external boundary $\partial\Omega$

S_{Mb} is the equilibrium saturation of myoglobin, while $p_{50,Mb}$ is the tissue oxygen partial pressure at half myoglobin saturation.

p_c describes the tissue PO_2 reflective of the partial pressure scale where mitochondria are no longer able to extract oxygen at maximal rate. M is the rate of oxygen consumption within the tissue, and M_0 is $VO_{2\,max}$ (Al-Shammari, 2014). All remaining physiological parameters are detailed in Table 1.

Table 2-1. Physiological parameters for homogenous and mixed muscle oxygen modelling.

Parameter	Symbol	Uniform phenotype	Fibre Type			Units
			I	IIa	IIb	
O_2 demand	M_0	15.7	15.7	13.82	7.85	10^{-5}ml O_2/ml s
Mb concentration	C^{Mb}	10.2	10.2	4.98	1.55	10^{-3}ml O_2/ml
O_2 solubility	α	3.89 x 10^{-5}	3.89 x 10^{-5}			ml O_2/ml mmHg
O_2 diffusivity	D	2.41 x 10^{-5}	2.41 x 10^{-5}			cm^2/s
Mb diffusivity	D^{Mb}	1.73 x 10^{-7}	1.73 x 10^{-7}			cm^2/s
Mass transfer coefficient	k	4.0 x 10^{-6}	4.0 x 10^{-6}			ml O_2/cm^2 mmHg s
Intracapillary PO_2	p_{cap}	30	30			mmHg
Mb half-saturated PO_2	$P_{50\ Mb}$	5.3	5.3			mmHg
PO_2 at half demand	p_c	0.5	0.5			mmHg
Capillary radius		1.8-2.5 x 10-4	1.8-2.5 x 10^{-4}			cm

Default biophysical parameters within oxygen transport modeller, with user versatility to amend parameters. Table adapted from (Al-Shammari et al., 2014b)

Capillary to fibre ratio [C:F; N_N (c,f)]. The most commonly reported global average of capillary content describing the numerical ratio of capillaries to fibres:

$$N_N\,(c,f) = \frac{N(c)}{N(f)}$$

Mean fibre area [MFA; ā(f)]. The average fibre area generated using a unbiased lattice counting frame. The output also generated fibre type specific MFA:

$$\bar{a} = \frac{n_1\bar{a}_1 + n_{21}\bar{a}_{21} + n_{22}\bar{a}_{22}}{n_1 + n_{21} + n_{22}}$$

Capillary density [CD; N_A(c,f)]. The density of capillaries within a unit of tissue area, typically expressed mm^{-2}:

$$N_A(c,f) = \frac{N(c)}{n \cdot a(f)}$$

Fibre numerical density [N_N(i)]. Relative number of fibre type (*i*), where n_1, n_{21}, and n_{22} correspond to the number of Type I, IIa and IIb, respectively:

$$\frac{n_i}{n_1 + n_{21} + n_{22}}$$

Fibre area density [$A_{\bar{a}}$(*i*)]. Relative areal composition of muscle that is made up of a particular fibre type (i), where $\bar{a}_1$, $\bar{a}_{21}$, and $\bar{a}_{22}$ correspond to the area of tissue comprised of Type I, IIa and IIb fibres, respectively:

$$\frac{\bar{a}_i}{\bar{a}_1 + \bar{a}_{21} + \bar{a}_{22}}$$

Number of capillaries around a fibre [NCAF; $\dot{N}$(c,f)]. The mean number of capillaries in contact with a fibre:

$$\dot{N}(c,f) = \sum_{i=1}^{i=n} \frac{N(c)i}{N_f}$$

Mean Voronoi cell/capillary domain area [ā(domain)]. The area of a polygon (V_i) associated with the ith capillary. Polygon boundaries are formed by perpendicular bisectors of lines equidistant between the capillary of interest and all neighbouring capillaries. N_c denotes the number of capillaries and x_i the position of the centroid of the ith capillary:

$$V_i = \{\boldsymbol{x} | \boldsymbol{x} A \Omega;\ \ j\boldsymbol{x} - \boldsymbol{x}_i J r\ J\boldsymbol{x} - \boldsymbol{x}_k\ \ J; k a\ i\}$$

Local capillary to fibre ratio [LCFR]. The mean cumulative fraction of capillary domain areas that overlap each fibre that allows contribution of non-contiguous capillary supply to be estimated. Ω_j denotes the region of the ith fibre and $A(\cdot)$ the area:

$$LCFR_j^{VP} = \sum_i \frac{A(\Omega_j \cap V_i}{A(V_i)}$$

Local capillary density [LCD]. A normalised value of capillary density to accommodate allometric scaling, where LCFR is divided by that individual fibre area:

$$LCD_j^{VP} = \frac{1}{A(\Omega_j)} \sum_i \frac{A(\Omega_j \cap V_i}{A(V_i)}$$

2.4 Implementation

2.4.1 Heterogeneity of skeletal muscle composition

Tibialis anterior (TA) is the predominant ankle flexor muscle in the peroneal compartment with two distinguishable regions, a deep oxidative core and anterior glycolytic cortex (Fig. 2-12). The global composition of rat TA are presented, using numerical indices based on integer values (Table 2-2).

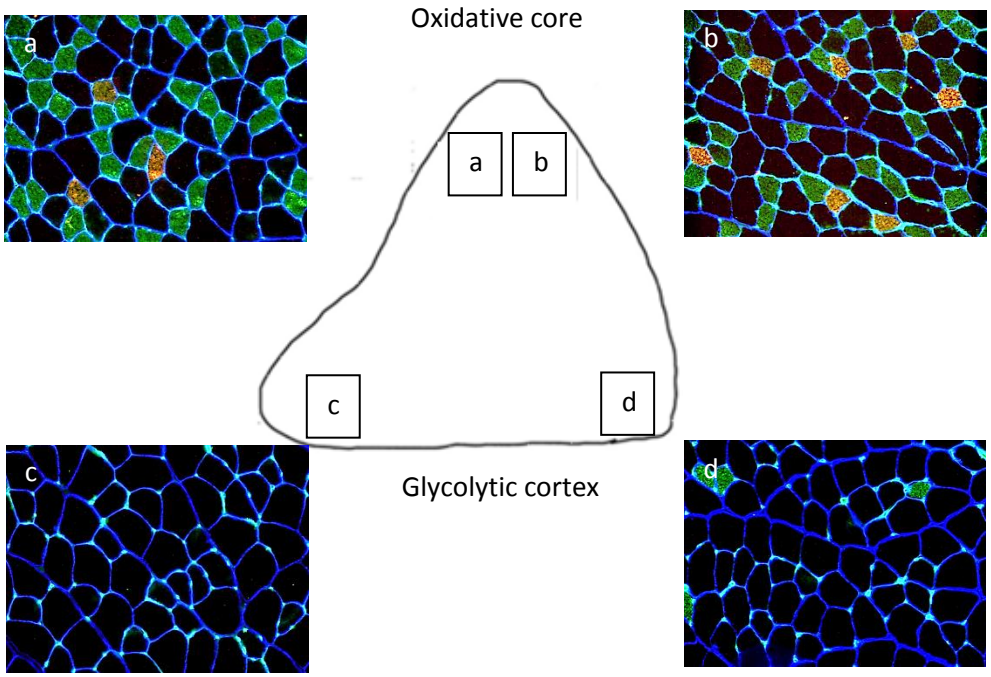

Figure 2-12. Cross section of rat TA with representative immunohistochemical inserts from the deep core (a,b) and superficial cortex (c,d). There is a prevalent oxidative gradient (Type I – red fibres and Type IIa – green fibres) increasing content from the lateral cortex towards the medial core.

Moving to an area-based analysis, we define the capillary supply area as the volume of tissue closest to an individual vessel than any other. The resultant boundary, calculated by bisecting intercapillary distances for nearest neighbour vessels, identifies the capillary domain (Hoofd, 1985; Egginton, planar, 1992). The frequency distribution of these domains shows a distinct difference between the two regions of the TA (Fig. 2-13).

Table 2-2. Morphometric analysis of Wistar rat TA

	Core	Cortex
C:F	1.95 ± 0.12	1.40 ± 0.07 *
CD (mm^2)	953 ± 59	579 ± 47 *
MFA (μm^2)	2387 ± 92	1777 ± 92 *
Type I (%)	4.7 ± 0.02	0 *
Type IIa (%)	41.8 ± 0.05	3.0 ± 0.03 *
Type IIb (%)	53.5 ± 0.05	97.0 ± 0.03 *

Data generated by Dtect. C:F, capillary to fibre ratio; CD, capillary density; areal fraction of fibre type given as a proportion of total muscle cross sectional area. Mean ± S.E.M. (n=4); * $P < 0.05$ core *vs.* cortex

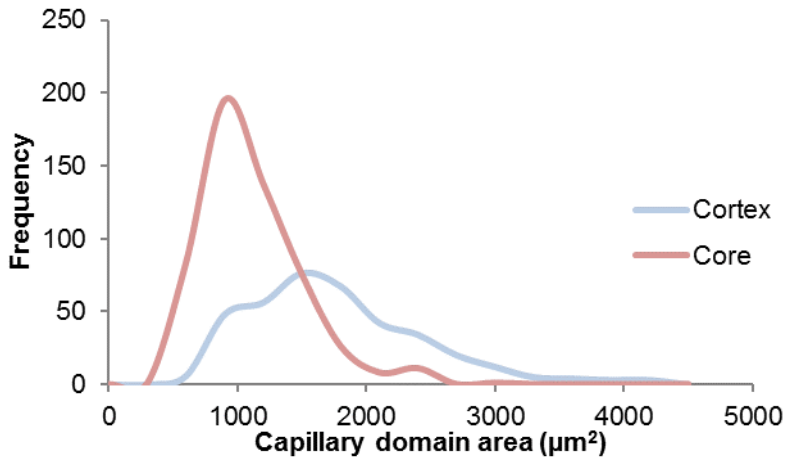

Figure 2-13. Local capillary supply area for the oxidative core (mean domain area 874 μm^2) and glycolytic cortex (mean domain area 1505 μm^2). Heterogeneity of the logarithmic normal distribution, calculated by the standard deviation of log-transformed area (logSD), indicates a more homogeneously distributed capillary supply in the core compared to the cortex; logSD = 0.151 ± 0.008 and 0.166 ± 0.004 μm^2, respectively. Mean ± S.E.M, (n=4).

Having identified capillary locations and adjacent fibre type of varying size, the local capillary supply can be calculated. Through the non-integer index of local capillary to fibre ratio (LCFR = cumulative fraction of individual domains

overlapping a fibre) it is possible to calculate the average supply of a fibre relative to capillary domain area (Egginton and Ross, 1992), which globally is approximated by the ratio of mean fibre and domain areas. Normalising this index (dividing LCFR by fibre area) provides a local scale-independent measure of capillarity, giving a local capillary density (capillary supply equivalent per unit area of fibre) specific to individual fibres. These values of supply can be partitioned according to fibre type (Table 2-3). Such data illustrate the manner by which microvascular delivery of oxygen and other substrates, and removal of metabolites, is partitioned among both regions and fibre types. Of note is the extent to which global values even out local differences in functional capillary supply, and hence are less sensitive to tissue remodelling during adaptation or pathology.

Table 2-3. Scale-independent measures for the core and cortex of the rat TA

	Core	Cortex
Global		
LCFR	1.80 ± 0.20	1.34 ± 0.10
LCD (μm^2)	1058 ± 98	602 ± 61 *
Type I		
LCFR	1.34 ± 0.32	-
LCD (μm^2)	1144 ± 82	-
Type IIa		
LCFR	1.37 ± 0.20	1.12 ± 0.04
LCD (μm^2)	1095 ± 94	875 ± 82 *
Type IIx		
LCFR	2.23 ± 0.26	1.36 ± 0.10 *
LCD (μm^2)	1014 ± 93	592 ± 58 *

Mean ± S.E.M. (n=4); * $P < 0.05$ core *vs.* cortex. LCFR, local capillary to fibre ratio; LCD, local capillary density.

2.4.2 Two weeks immobilisation – a worked example

Understanding not only the physiological response to adaptive remodelling but that of pathological remodelling is critical in the development and prescription of therapeutic exercise. Prolonged bed rest is a potent stimulus for reduction in muscle mass, force generating capacity and fatigability, and of which these effects are amplified in the elderly (Harper and Lyles, 1988, Morley et al., 2001, Partridge et al., 2012). We utilised a unilateral limb immobilisation cast to mimic bed-rest for two weeks to investigate the effect on muscle phenotype and oxygen delivery kinetics (Boesen et al., 2013, Suetta et al., 2013).

Four healthy untrained males (age 71 ± 6.5 years, BMI 25.6 ± 2.7) were recruited to take part in this study. The participants consented to two weeks unilateral lower limb immobilisation. Immobilisation was performed using a lightweight fibre cast running from the malleoli to bellow the groin, with the knee positioned flexed and held at 50°. Participants were instructed to use crutches throughout the two week casting. Muscle biopsies from the vastus lateralis were taken at day 0 and 14 (Boesen et al., 2013), and sections were treated as above, and images processed for analysis (Fig. 2-14).

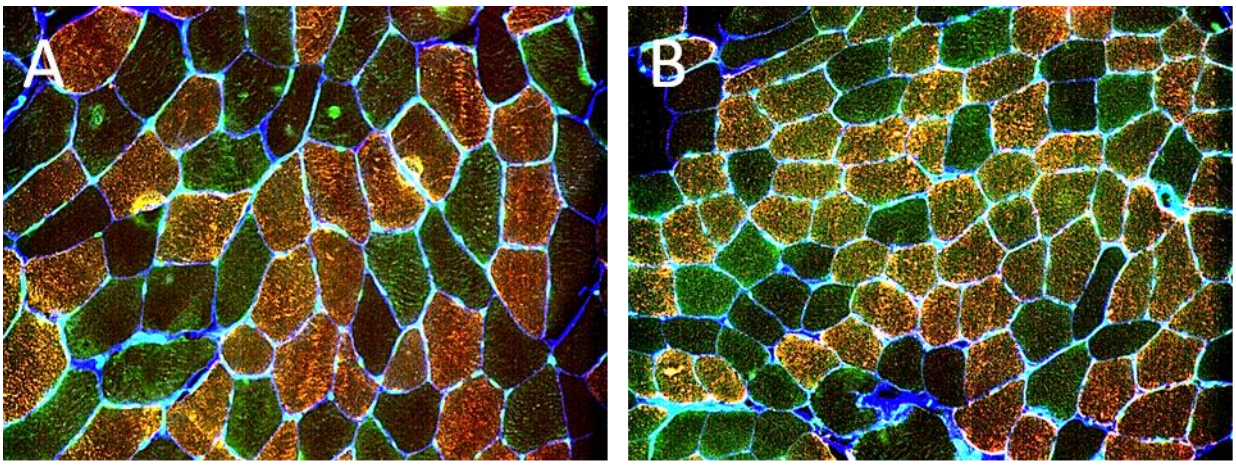

Figure 2-14. Vastus lateralis cross-section. Baseline (A) and two-weeks post leg casting (B) for the same individual. Immuno/histochemical staining for fibre type, boundaries and capillary location. Note the evident atrophy following immobilisation. Red – Type I fibres, Green – Type IIa, scale bar 200µm.

Although somewhat underpowered for diagnostic purposes, the expected trend for muscle atrophy is evident; as there was no change in C:F then the functionally relevant CD consequently increased (Fig. 2-15). Note this increase in apparent capillarity is entirely explained by the muscle, rather than microvascular response to immobilisation. The numerical proportion of fibres was adjusted in favour of Type IIa, whereas the greatest change in areal composition was found for Type IIb fibres (Supplementary Table 1). Given these changes, it is impossible to ascertain from global values whether or not local compensatory mechanisms have been evoked.

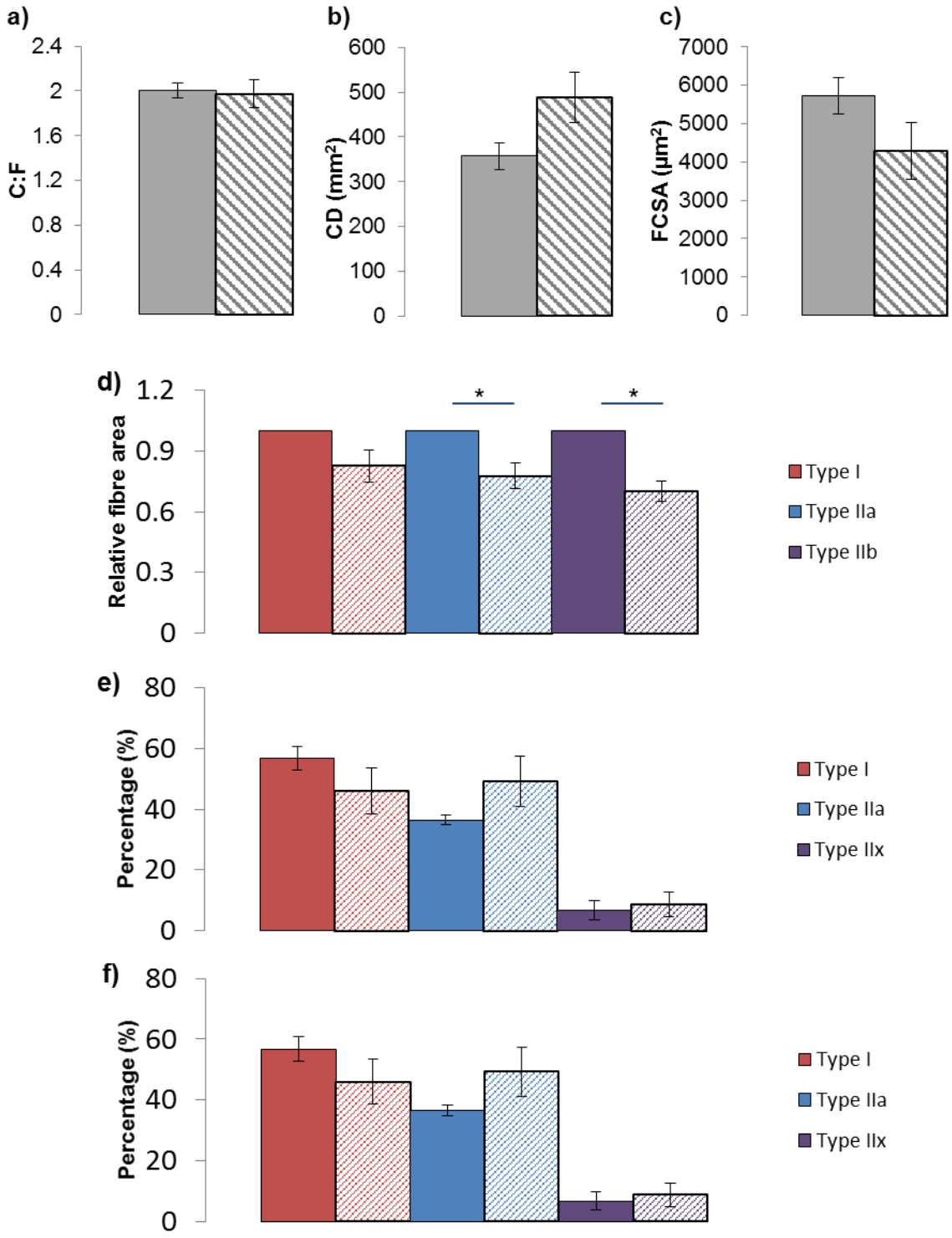

Figure 2-15. Global microvascular and muscle morphometric indices at baseline (solid bars) and following 14 days immobilisation (hatched bars). Capillary to fibre ratio (a), capillary density (b), mean fibre area (c), relative fibre type specific area change (d), % numerical fibre type composition (e) and % fibre area composition (f). Mean ± S.E.M. (n=4); * *P*<0.05 baseline *vs.* immobilized.

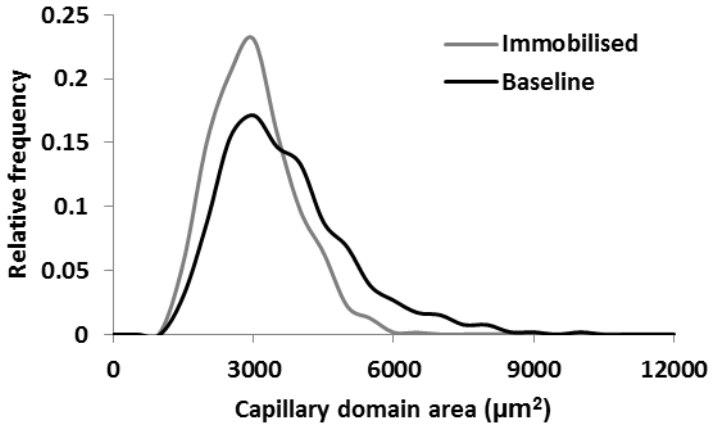

Figure 2-16. Local capillary supply area for vastus lateralis muscle at baseline and following two weeks of immobilisation. Mean domain area decreased from 3428.3µm to 2767.6 µm, while heterogeneity also decreased (LogSD) from 0.167 to 0.143. Data presented from pooled samples, Baseline domains (*n = 524*) and immoblised (*n = 723*).

Indeed, for Type I fibres both LCFR and LCD were increased, while for Type IIa fibres LCFR was unchanged while LCD increased, and for Type IIb fibres there were reciprocal changes in the indices of local capillary supply (Fig. 2-16, Table 2-4).

2.4.3 Muscle oxygenation

Oxygen tension across muscle is dependent on both capillary supply and fibre demand, and influenced by spatial distribution of both elements. Using estimates of capacity for supply and demand, an estimate of the integrative response to low and high oxygen consumption can be modelled (Fig. 2-17). Note that fibre atrophy following immobilisation tends to ameliorate the apparent supply deficit under conditions of simulated muscle activity (Table 2-4).

Table 2-4. Baseline vs. 14 days immobilisation

	Baseline	Immobilised
Global		
LCFR	1.69 ± 0.04	1.73 ± 0.03
LCD (μm^{-2})	281 ± 30	362 ± 25
Type I		
LCFR	1.72 ± 0.11	1.84 ±0.08
LCD (μm^{-2})	285 ± 34	376 ± 25
Type IIa		
LCFR	1.71 ± 0.12	1.70 ± 0.11
LCD (μm^{-2})	278 ± 32	359 ± 27
Type IIx		
LCFR	1.54 ± 0.21	1.35 ± 0.02
LCD (μm^{-2})	240 ± 13	307 ± 28

Mean ± S.E.M. (n=4). LCFR, local capillary to fibre ratio; LCD, local capillary density.

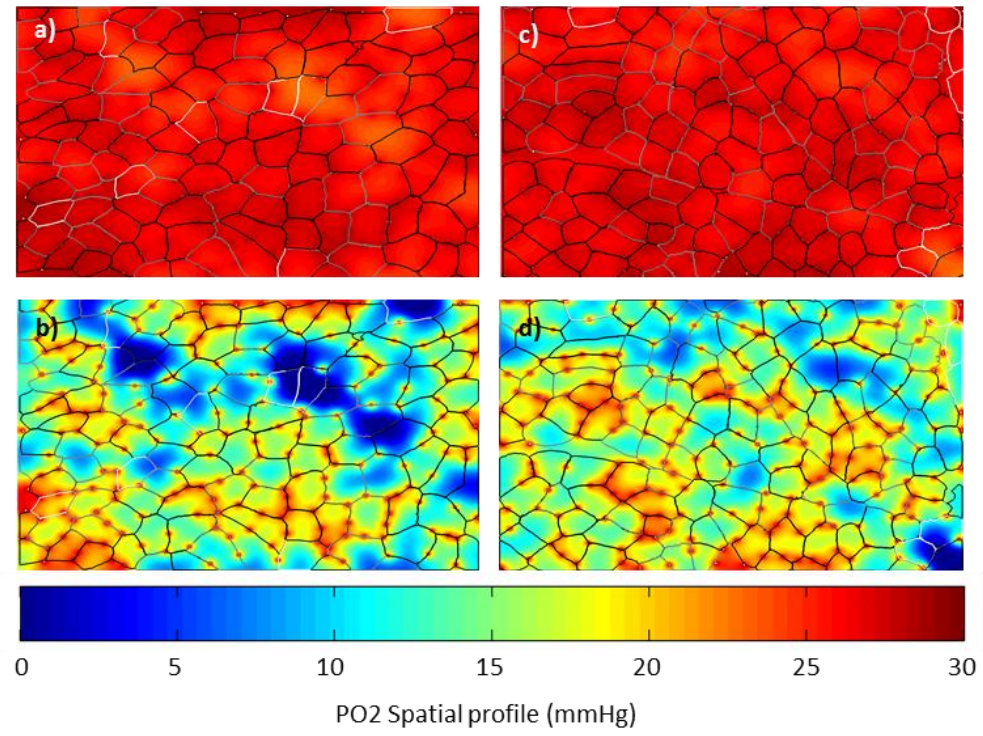

Figure 2-17. Oxygen modelling – simulation of muscle PO2 at rest (a baseline, c immobilised), and at MO2max (b baseline, d immobilised). Note the regions of tissue hypoxia, highlighted in blue, in this model hypoxia was considered to have a PO2 of < 0.5mmHg. See Table 2-5 for fibre type-specific values.

The optimisation of oxygen supply and demand by integration of capillary and fibre distributions is evident from a similar oxygen tension for each fibre type at rest, a good example of structure-function homeostasis (Table 2-5). Interestingly, the differential atrophy among fibre types is reflected in the extent to which fibre PO_2 is calculated to change on exercise after 14 days immobilisation (Table 2-5), thereby identifying local sites of likely dysfunction that may be specifically targetted by subsequent therapies.

Table 2-5. PO_2 predictions for one individual at baseline *vs.* 14 days immobilisation

Simulation	Baseline	Immobilised
Resting O_2 consumption		
Tissue PO_2 (mmHg)	26.27 ± 1.19	25.82 ± 0.93
Type I PO_2 (mmHg)	26.36 ± 1.06	26.95 ±0.91
Type IIa PO_2 (mmHg)	26.11 ± 1.12	26.58 ± 0.83
Type IIx PO_2 (mmHg)	25.33 ± 1.57	25.98 ± 1.03
% Hypoxic tissue	0	0
Maximum O_2 consumption		
Tissue PO_2 (mmHg)	14.58 ± 5.78	15.90 ± 4.58
Type I PO_2 (mmHg)	15.21 ± 5.13	16.03 ± 4.44
Type IIa PO_2 (mmHg)	13.40 ± 5.44	15.62 ± 4.13
Type IIx PO_2 (mmHg)	9.63 ± 7.19	12.13 ± 4.94
% Hypoxic tissue	2.43	0.51

Mean ± SD. Hypoxia is user defined, and describes the percentage of tissue area that has a PO_2 below that value, in this case < 0.5mmHg O_2.

2.5 Experimental data discussion

Bed rest has been shown to have a pronounced debilitative effect on skeletal muscle mass and aerobic capacity (Harper and Lyles, 1988, Berg et al., 1997, Topp et al., 2002, Gallagher et al., 2005). The inactivity results in atrophy of muscle fibres, alteration in blood flow kinetics and reduced oxidative capacity, which subsequently affect a muscles capacity to perform as normal, especially in the case of the elderly (Harper and Lyles, 1988). We utilised a unilateral limb immobilisation cast to mimic bed-rest for two weeks to investigate the effect on muscle phenotype and oxygen delivery kinetics (Boesen et al., 2013, Suetta et al., 2013).

Following two weeks of lower-limb casting the vastus lateralis atrophied, with a 31% decrease in mean fibre area, with Type II fibres showing the largest degree of atrophy. These data are in line with those reported by (Suetta et al., 2013) however others have reported over longer durations of two weeks a larger atrophy response in Type I fibres (Appell, 1990, Tomanek and Lund, 1974, Hortobágyi et al., 2000). There was no evident rarefaction of the capillary bed, however the global atrophy of muscle fibres resulted in an improved CD. A similar response has been shown in cold acclimated hamsters, that manage to reduce oxygen diffusion distance, through reduction in FCSA and increasing CD (Deveci and Egginton, 2002a). Mean capillary domain area decreased, with an improved homogeneity of capillary supply that improved LCD across all three major fibre types. The reduced diffusion distance and subsequent improved local capillary supply area when modelled at high intensity exercise levels showed a better PO_2 status across the tissue, and reduced proportion of the tissue considered to be hypoxic (in this model hypoxia was considered to have a PO_2 of < 0.5mmHg). This adaptive remodelling appears to preserve the capacity of the tissue to be supplied with oxygen, possibly as a compensatory mechanism. As the tissue has a reduced capacity to utilise because of decreased oxidative enzyme content and mitochondria (Booth and Kelso, 1973, Jansson et al., 1988) this greater PO_2 and flux will help maintain the drive in those mitochondria remaining and allow them to work optimally (Bosutti et al., 2015).

2.6 Methodological discussion

There is an increasing body of experimental data that is derived from muscle histology, where a variety of labelling methods contribute to variability in results and image processing is unacceptably laborious thereby reducing the scope for comparative analyses. We have developed a robust histological stain for the identification of tissue fibre phenotype and microvascular content within rodent and human tissue. Recent progress in computational modules have seen the development of semi-automatic muscle analysis code; however the breadth of measurements and output has been limited. In conjunction with the histological labelling we have developed semi-automated detection software for the identification of fibre boundaries and fibre types that allows the co-localisation of capillaries onto the anatomical skeleton. Subsequently, a digitised mesh representative of the tissue geometry is created, and provides the framework for improved spatially resolved data acquisition, and the possibility of oxygen tension modelling.

2.6.1 Fibre type composition

Accurate quantification of skeletal muscle composition is labour intensive, and sometimes difficult to reconcile results from different studies. The literature has become dominated by concerns about pure and hybrid phenotypes (a single fibre expressing more than one MHC isoform; (Bloemberg and Quadrilatero, 2012)). There are a variety of monoclonal antibodies developed to probe for various configurations of these phenotypes, which allow muscle fibre type compositions to be determined (Gregorevic et al., 2008, Bloemberg and Quadrilatero, 2012). However, the functional capacity of these scarce hybrid fibres is still to be determined, and the relevance to overall phenotype is debatable. A more broadly applicable method would be to use an oxidative continuum to classify fibres, e.g. using data from succinate dehydrogenase and α-glycerophosphate dehydrogenase activity in conjunction with the various MHC monoclonal antibodies (Bloemberg and Quadrilatero, 2012).

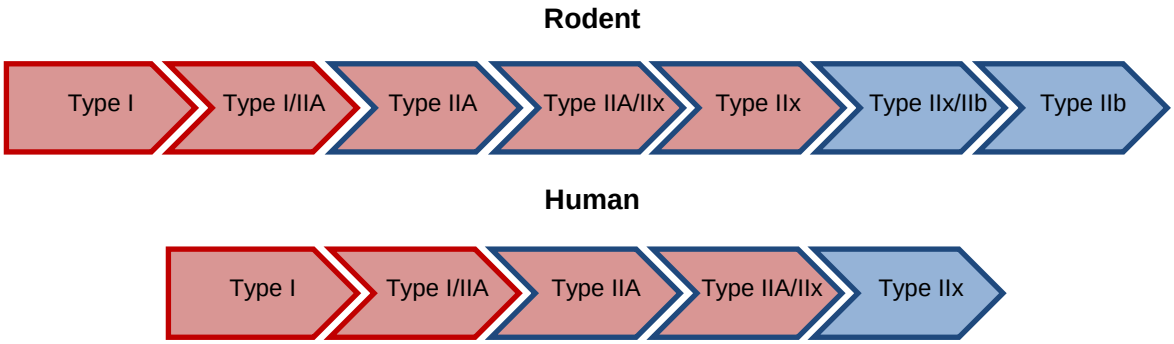

Figure 2-18. Dynamic spectrum of skeletal muscle myosin heavy chain phenotypes, accommodating both pure and hybrid fibres.

Using this continuum (left most oxidative, moving to entirely glycolytic, Fig. 2-18) it is possible to accommodate the categorisation of three major fibre types. The flexibility of the programme to allow user-defined classifications will permit groupings for undifferentiated hybrid fibres if required. Accordingly, the purpose of the immuno/histochemical protocol is to provide a high throughput method of fibre type differentiation, in combination with our automated detection system, analysis and modelling package.

2.6.2 Adaptability of the analysis package

As discussed above, some longitudinal studies seek to identify transient changes as part of an adaptive response, and so we have incorporated the possibility to utilise either serial sections and a corresponding monoclonal label for hybrid fibre types (or other molecule of interest), or an additional fluorophore may be used for four colour immunofluorescence, which may then be incorporated into the morphometric analysis.

The primary limitation with the semi-automated detection software relates to the quality of images, with variability in specificity or intensity of stains (especially in older cut tissue). There is an apparent reduced reactivity/affinity of monoclonal antibodies to tissue that have been cut and stored for extended periods of time

(over 12 months). Tissue that has been exposed to numerous freeze thaw cycles also showed poorer staining of fibre boarders with laminin, making the automatic detection of fibre boundaries ineffective and difficult to define. This can lead to artefacts like gaps within the laminin which may result in automated shrinking and removal of lamina and joining of two adjacent fibres. This will require the user to adjust the threshold or manually define those boundaries through pruning of incorrect boundaries and addition of missing segments. Initially, the laminin threshold should be explored before any manipulations of fibre lamina. Using a low threshold allows noise to pass that can result in erroneous detected fibres, whereas a high threshold creates gaps and unites fibres; only once the optimal threshold has been defined should manual correction be attempted.

To unambiguously define a fibre type three critical pieces of information are required: fibre size, shape and colour fill. At present there is a user-defined minimum and maximum fibre area size that establishes boundary conditions for identified fibres and infers whether to include them in the statistics or not. While differentiation between types is primarily based on colour fill of that fibre, future implementations could allow incorporation of fibre type criteria based on size and staining intensity, or to avoid fibre boundary artefacts by implementing morphometry algorithms, for instance include only convex and smooth objects.

One of the more flexible components of this project was the development of a fibre skeleton that allowed the incorporation of physical objects (i.e. capillaries) to then be positioned and analysed at an individual fibre type level, allowing for more sensitive geometric analysis. The versatility of the capillary identification software should be of wider interest, given the interest in the co-localisation of other structures. Our software allows the geometric distribution and interactions with specific fibre types to be generated for structures like location of myosatellite cells, infiltration of macrophages, or specificity of proteins, like the transcription factor PGC-1 α (Selsby et al., 2012).

The packages are assembled in such a way that output files are generated at each stage: fibre type composition and morphometric details, capillary and fibre global indices, fine-scale non-integer local capillary indices, and finally tissue PO_2 modelling. This allows flexibility in extraction of morphometric data at the level desired for a particular study design. However, given the ease of data acquisition and speed of the data pipeline it is plausible to generate the full range of morphometric indices at no extra cost, thereby allowing observation- rather than hypothesis-driven explorations. The local indices of capillary supply are able to identify the onset of fine-scale changes that occur during physiological adaptation (training response) and pathological remodelling, usually prior to differences in global indices becoming apparent. The ability to effortlessly generate these data could provide the potential for the discovery of unknown abnormal pathological responses, and aid development of targetted therapeutic treatments.

In conclusion, we have designed a robust histological protocol and analysis package (based on MATLAB code) that will be free to download and use. The data pipeline allows for flexibility in morphometric indices acquired, and provides a more comprehensive overview of microvascular and skeletal muscle phenotype than is currently available. The potential for more spatially resolved data may have an impact on requirements for statistical power within a study, and as such an impact on the reduction of animals required for experiments (supporting consideration of 3R's in ethical approvals). As such the development of this image processing methodology will likely prove to be valuable, impacting studies at a scientific, economic and ethical level.

This methodology provide to be very useful in subsequent analysis in Chapters 3, 4 5.

3 Regional variation in the mechanical properties and fibre type composition of the rat extensor digitorum longus muscle

3.1 Abstract

Many muscles are heterogeneous in fibre type distribution. However, the distribution of these fibre types often varies spatially indicating that there may be regional variation in recruitment and mechanical output. The rat extensor digitorum longus muscle (EDL) is composed of predominantly fast-twitch fibres, but exhibits a gradient in oxidative capacity ranging from an oxidative medial compartment to a glycolytic lateral compartment. Here, we utilised this regional variation in fibre type composition between the medial and lateral compartments of the EDL to investigate the consequences for regional differences in mechanical performance. The isometric tetanic stress and force-velocity relationships were similar in both muscle compartments, but the isometric twitch kinetics were slower in the medial compartment compared to the lateral compartment. The medial compartment had a lower optimum frequency for maximum power generation compared to the lateral compartment (11 Hz in medial compartment vs. 15Hz in lateral compartment). This difference is due to the slower contractile kinetics in the medial compartment resulting in a lower level of activation and reduced work generation at increasing cycle frequencies, compared to the lateral compartment. The more oxidative, medial compartment had a significantly higher resistance to fatigue, and developed more cumulative work over 30 cycles compared to that of the glycolytic, lateral compartment, 99.79 ± 12.67 J kg^{-1} *vs*. 92.37 ± 12.63 J kg^{-1}, respectively. The regional variation in mechanical performance suggests a differential recruitment pattern during locomotion, with the medial compartment being utilised during slow speed locomotion and the lateral compartment during burst activities.

3.2 Introduction

The force developed by a muscle and the duration for which it can be sustained depends on the number of motor units recruited and the type(s) of muscle fibre that the motor neurons innervate. Muscle fibre contractile properties vary in the rates of force development and their shortening velocity, as well as on the metabolic pathways (aerobic or anaerobic) that supply the high-energy phosphates. Motor unit recruitment often follows a pattern that depends on motor neuron excitability (size principle), however, it may alternatively follow mechanical demands (Wakeling et al., 2006, Hodson-Tole and Wakeling, 2007). Many muscles are composed of a mixture of muscle fibre types in proportions that relate to the mechanical function of the muscle during motion. However, the distribution of these fibre types often varies regionally indicating that there may be regional variation in recruitment and mechanical output. Much of our knowledge about muscle contractile properties has been obtained using supramaximally activated whole muscle preparations. Measurements of this type yield information on the average mechanical performance of the muscle, but potentially obscure regional variations in mechanical output.

The extensor digitorum longus (EDL) muscle has been used as an example of a 'fast' muscle in many contractile studies (Close, 1964, Luff, 1981, James et al., 1995, Askew and Marsh, 1997). The rat EDL contains approximately 5% Type I, 53% Type IIa and 42% Type IIb (Schiaffino et al., 1970, Pullen, 1977, Windisch et al., 1998) while in mice the proportions are 46% Type IIa and 54% Type IIb (Askew and Marsh, 1997). In both of these species, the fibre type of the EDL is predominantly fast, with a similar number of both oxidative and glycolytic fibre types. The fibre type distribution within the EDL is non-uniform: there is a transverse gradient in aerobic capacity, with decreased oxidative and increased glycolytic fibre proportion across the medial-lateral axis of the muscle (Pullen, 1977, Egginton, 1990b). In addition to regional variation in fibre type, an additional indicator that there may be regional variation in EDL function comes from the fact that the peroneal nerve diverges into two extramuscular branches (K and F branches), which innervate the medial and lateral compartments of the muscle,

respectively (Balice-Gordon and Thompson, 1988). A differential activation pattern of the muscle compartments has been confirmed by glycogen depletion histology (Balice-Gordon and Thompson, 1988, Deveci et al., 2001).

It is expected, that regional differences in fibre type composition result in regional differences in contractile characteristics and susceptibility to fatigue within the same muscle. The aim of this study was to characterise regional variation in muscle mechanics in relation to fibre type distribution of rat EDL. We quantified isometric twitch kinetics and isotonic contractile properties from the force-velocity relationship, while power output and fatigability of the muscle were determined using the work loop technique (Josephson, 1985). We hypothesised that the isometric, isotonic and cyclical properties of the muscle would not differ between the muscle compartments (Josephson and Edman, 1988), reflecting the predominance of 'fast' fibre types. However, given the gradient in fibre oxidative capacity across the muscle, we reasoned that fatigue resistance would be higher in the medial compartment compared with the lateral compartment.

3.3 Material and methods

3.3.1 Animals and ethical approval

Twenty in-house bred male Wistar rats, aged 6-8 weeks and weighing 249 ± 2g were used in this study. Animals were culled under terminal anaesthesia with cervical dislocation. All animal experimentation was approved by the University of Leeds Animal Welfare and Ethics Committee, and was conducted in accordance with UK Animals (Scientific Procedures) Act 1986.

3.3.2 Muscle preparation

Animals were anaesthetised with Isoflurane: 5% IsoFlo® in O_2 (0.4 L min kg^{-1}) induction, and 0.28 L min kg^{-1} during dissection. The fusiform EDL comprises a single proximal tendon originating on the lateral epicondyle of the distal femur; the distal portion subdivides into four tendons that insert onto the distal phalanx of

digits 2-5. The extensor muscle tendons were exposed, released by transecting the retaniculum ligament in the ankle, allowing the tibialis anterior muscle to be reflected, exposing the EDL. A ligature (4-0 Mersilk, Ethicon) was attached to the proximal tendon of the EDL to enable the muscle to be manoeuvred, allowing it to be freed from connective fascia. Following its removal, the EDL was immediately placed in chilled (4°C), oxygenated (95% O_2, 5% CO_2) Krebs-Henseleit Ringer's solution [117 NaCl, 4.7 KCl, 2.5 $CaCl_2$, 1.2 $MgSO_4$, 24.8 $NaHCO_3$, 1.2 KH_2PO_4 and 11.1 glucose; concentrations in mmol l^{-1} (Burton, 1975)]. The whole EDL was pinned out in a Petri dish (Fig. 3-1a), and the medial and lateral compartments were separated from the intermediate compartments, and pinned out at approximately their resting length (Fig. 3-1b) in the animal until required for contractile measurements.

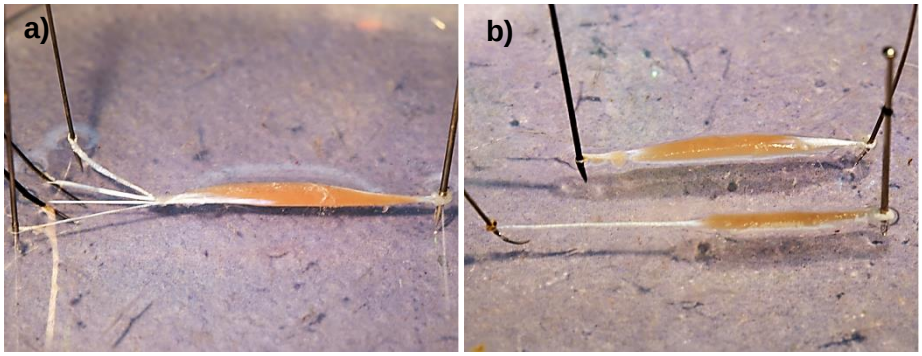

Figure 3-1. Multi distal tendon arrangement and compartments of the EDL. Whole right EDL pinned out by the proximal tendon and multiple distal tendons (a). The most lateral (top muscle) and medial (bottom muscle) compartment dissected from whole EDL (b).

One of the muscle compartments (randomised order of lateral or medial) was transferred to a Perspex flow-through muscle chamber, through which oxygenated Ringer's solution at 37°C was circulated. The distal tendon of the muscle was secured to the base of the chamber using stainless steel clips, and the proximal tendon was attached to an ergometer (series 300B-LR, Aurora Scientific Inc., Ontario, Canada) that controlled muscle strain trajectory *via* a light-weight (100mg) stainless steel rod. Muscle resting length was controlled using a moveable stage on which the ergometer was mounted. Following mounting, the muscle

compartment was allowed 30 minutes recovery in fresh, oxygenated Ringer's solution before measurements were taken.

3.3.3 Mechanical properties of EDL

Isometric and cyclical contractions were controlled using custom written software (CEC Tespoint version 7, Norton, MA, USA) *via* a D/A board (DAS1801AO, Keithley Instruments, Theale, UK), and the computer generated wave was converted into an analogue signal by a 16-bit A/D converter that was used to control the ergometer (series 300B-LR, Aurora Scientific Inc., Ontario, Canada).

Data were sampled at 10kHz during isometric twitch kinetics, and at 1000× cycle frequency during the work loop experiments.

3.3.4 Isometric contractile properties

Optimal muscle length (L_0, defined as the muscle length that generated maximal isometric twitch force) was determined using a series of isometric twitches performed at a range of muscle lengths varied incrementally by 0.5mm. The muscle was activated using a supramaximal stimulus with a 0.2ms pulse width (Askew and Marsh, 2001) delivered using platinum electrodes. L_0 was used as the mean length in all subsequent experiments. An isometric tetanus was performed using a train of stimuli delivered at 200Hz for 200 ms; the maximum isometric tetanic force was defined as P_0.

3.3.5 Force-velocity characteristics

The force-velocity relationship was determined using a series of afterloaded isotonic contractions (*ca.* 5-80% P_0). Force and velocity were plotted and a hyperbolic-linear function was fitted to the data (Marsh and Bennett, 1986). Maximum shortening velocity (V_{max}) was determined from the force-velocity relationship by extrapolating to zero force, and expressed relative to muscle fibre length ($L_{0\text{-}F}$; see below for methodological details). Peak instantaneous isotonic

power (W_{max}) and the curvature of the force-velocity relationship (defined as a power ratio calculated as the ratio of W_{max} to the product of V_{max} and P_0) were also determined. The condition of the muscle preparation was determined by performing control isometric tetanic contractions every fourth isotonic contraction, to allow correction for any decline in force generating capacity. Data were excluded if the predicted P_0 fell below 70% of the initial P_0.

3.3.6 Muscle mechanical power output during cyclical contractions

The work loop technique (Josephson, 1985) was used to quantify the net power output of each muscle compartment over a range of cycle frequencies (3-25 Hz) using a sinusoidal length trajectory and a strain amplitude of ± 5% of fibre length ($L_{0\text{-}F}$). At each frequency the timing and duration of stimulation were optimised to yield maximum net power output. Five cycles were performed at each cycle frequency and the average of the two highest net power outputs was calculated. Control work loop cycles were performed at 7Hz every fourth run, to assess the condition of the preparation and to allow for correction of any decline in net power (assuming a linear decline in force generation). Data were excluded once predicted control net power had declined below 70% of the initial net power. A fatigue run of 30 cycles at 7 Hz was performed to analyse the rate of decline in net power. Net power was normalised to the net power output of the first cycle, and an index of fatigue was determined as time taken for net power to drop below 50% of initial net power (T_{W50}).

3.3.7 Muscle fibre type composition

Mid-portions of each muscle segment were mounted on cork discs and snap frozen in isopentane cooled in liquid nitrogen, and stored at -80°C. Serial cryostat sections (10µm) were cut at -20°C and attached to polysine coated slides (VWR International), and stored at -20°C until staining. Muscle fibre types were distinguished using two monoclonal anti-MHC antibodies (Appendix 1) (Developmental Studies Hybridoma Bank, University of Iowa): BA-D5 (1:1000

dilution) for Type I fibres (slow MHC) labelled with Alexa Fluor 555 Goat Anti-Mouse IgG (1:1000 dilution) (Life Technology, A21422) and SC-71 (1:500 dilution) for Type IIa (fast oxidative, glycolytic) labelled with Alexa Fluor 488 Rabbit Anti-Mouse IgG (1:1000 dilution) (Life Technology, A11059). The remaining unstained fibres are considered to be Type IIb (fast glycolytic), validated by use of BFF3 antibody (Developmental Studies Hybridoma Bank, University of Iowa) (Andersen et al., 2014, Soukup et al., 2002). Muscle fibre boundaries were labelled with an anti-laminin antibody (1:250 dilution) (Sigma, L9393), a glycoprotein integrated in the basement membrane. Biotinylated against with Anti-Rabbit IgG (1:250 dilution) (Vector Labs, BA1000) and Streptavidin, Pacific Blue Conjugate (1:250 dilution) (Life Technology, S11222).

3.3.8 Relative muscle fibre length

Muscle fibre length was determined following fixation in 10% neutrally buffered formalin for 24 hours at L_0. Once fixed, individual muscle fibres were freed from any connective tissue following a 48 hour digestion in 30% nitric acid, and separated in a 50% glycerol solution; 10-20 fibres were measured from five medial and lateral compartment, and mean muscle fibre length ($L_{0\text{-}F}$) determined relative to L_0.

3.3.9 Statistical analysis

All data are expressed as mean ± S.E.M. (*n*). Differences between the medial and lateral muscle compartments were analysed using an Independent-sample *t*-test, with statistical significance defined as $P<0.05$.

3.4 Results

3.4.1 Muscle morphology

The morphological characteristics of the medial and lateral compartment of the rat EDL are presented in Table 3-1. Relative fibre length was not significantly different in the medial compartment compared to that of the lateral, 0.66 ± 0.03 and 0.60 ±

0.01 (t_8 = -2.016, P=0.079) of L_0, respectively. The medial compartment had a significantly higher numerical and areal composition of oxidative fibres compared to the lateral compartment (Fig. 3-2), comprising both Type I and Type IIa fibres, while the lateral compartments oxidative fraction comprised only Type IIa fibres (Fig. 3-2). The Type IIb fibre area was significantly smaller within the medial compartment, compared to the lateral compartment (t_8 = 4.487, P=0.002) with the Type IIa fibres also tending towards a smaller fibre area within the lateral compartment.

Table 3-1. Morphometric characteristics of medial and lateral compartment of rat EDL

	Medial	Lateral	t	P
Mass (mg)	22.23 ± 1.23 *(12)*	63.12 ± 1.91 *(13)*	18.027	<0.001
Optimal muscle length, L_0 (mm)	19.35 ± 0.22 *(12)*	25.05 ± 0.36 *(13)*	13.117	<0.001
Relative fibre length ($L_{0\text{-}F}$ /L_0)	0.66 ± 0.03 *(5)*	0.60 ± 0.01 *(5)*	-2.016	=0.079
Mean Type I fibre area (μm^2)	921.80 ± 38.02 *(5)*	0.00 ± 0.00 (*5*)	-24.246	<0.001
Mean Type IIa fibre area (μm^2)	1049.20 ± 57.21 *(5)*	1212.60 ± 50.84 *(5)*	2.135	=0.065
Mean Type IIb fibre area (μm^2)	1572.00 ± 23.94 *(5)*	2218.20 ± 142.00 *(5)*	4.487	=0.002
Numerical composition Type I fibre area (%)	7.48 ± 0.93 *(5)*	0.00 ± 0.00 *(5)*	-8.073	<0.001
Numerical composition Type IIa fibre area (%)	25.54 ± 1.77 *(5)*	13.07 ± 1.05 *(5)*	-6.061	<0.001
Numerical composition Type IIb fibre area (%)	66.98 ± 1.54 *(5)*	86.93 ± 1.05 *(5)*	-6.061	<0.001
Area composition Type I fibre area (%)	4.90 ± 0.57 *(5)*	0.00 ± 0.00 *(5)*	10.719	<0.001
Area composition Type IIa fibre area (%)	19.38 ± 2.00 *(5)*	7.56 ± 0.53 *(5)*	10.719	<0.003
Area composition Type IIb fibre area (%)	75.72 ± 1.94 *(5)*	92.44 ± 0.53 *(5)*	-8.676	<0.001

Values are means ± S.E.M. (n)

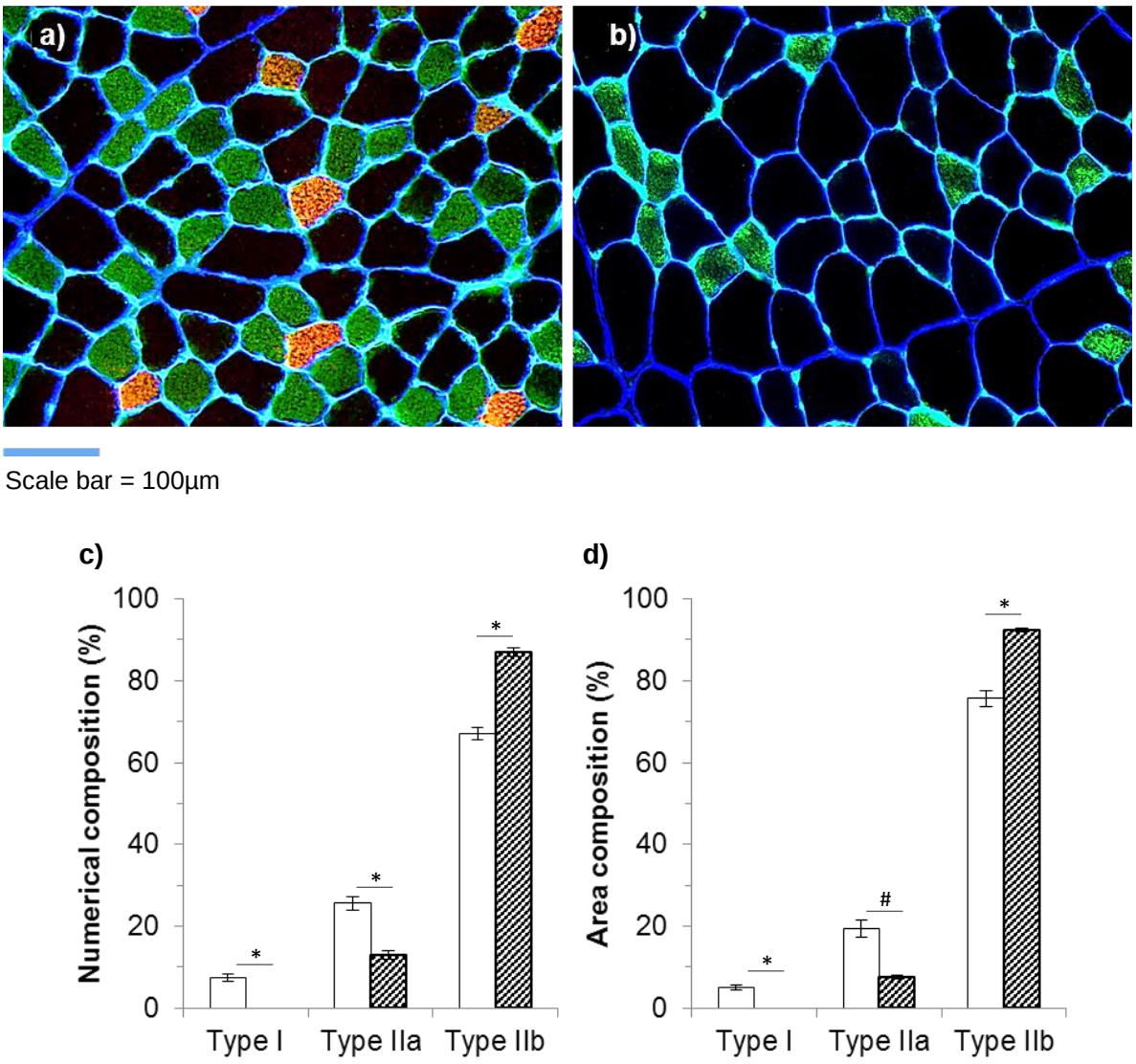

Figure 3-2. Fibre type composition of rat EDL using immunohistochemical markers for myosin heavy chain isoforms. Type I fibres – Red, Type IIa fibres – Green, Type IIb fibres – Unstained. Transverse cross section cut 10µm thick for the medial (a) and lateral (b) compartments. Numerical fibre type composition (c), and areal fibre type composition (d) for the medial (open bars) and lateral compartment (hatched bars). Data presented as means ± S.E.M. *(n=5)*. * *P*<0.001, # *P*=0.003.

3.4.2 Isometric properties

The medial and lateral compartments both generated comparable maximal isometric tetanic stresses, 280.08 ± 14.30 kN m^{-2} and 300.19 ± 15.04 kN m^{-2},

respectively (t_{23}, P=0.345), with similar twitch:tetanus ratio (0.24 ± 0.01 *vs.* 0.24 ± 0.01, respectively, t_{15} = -0.519, P=0.611) but had distinct isometric twitch characteristics. The medial compartment had both a slower twitch rise time (10.21 ± 0.31 ms compared to 9.14 ms ± 0.21, t_{15} = -2.865, P=0.012), and slower rate of relaxation when compared to that of the lateral portion, with half-relaxation times of 11.93 ± 0.57 ms *vs.* 8.55 ± 0.29 ms, respectively (t_{15} = -5.421, P<0.001).

3.4.3 Force-velocity relationship

W_{max} was not significantly different between the medial and lateral compartments, generating 364.29 ± 25.71 W kg^{-1} and 347.32 ± 20.73 W kg^{-1}, respectively (t_6 = -0.459, P=0.662). The force-velocity relationships for both muscle compartments studied were similar, with no significant differences in V_{max} or curvature, as characterised by the power ratio (Table 3-2; Fig. 3-3). Consequently, both the medial and lateral compartments have equivalent V/V_{max} and P/P_0 values at which maximum isotonic power was generated (Table 3-2).

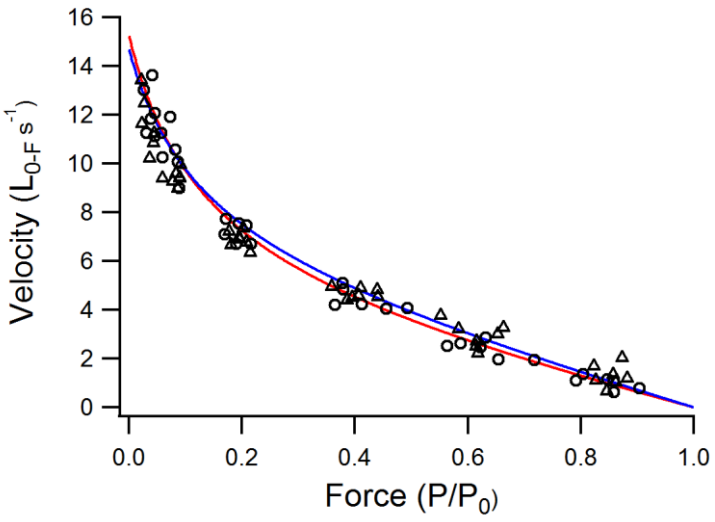

Figure 3-3. Force-velocity relationship for the medial (circles, red line) and lateral (triangle, blue line) muscle compartments. All data points are displayed, with the force-velocity curve plotted using the coefficients of a hyperbola-linear equation generated and averaged across the four animals (Marsh and Bennett, 1986).

Table 2. Isotonic properties of the medial and lateral muscle segments of rat EDL

	Medial	Lateral	t	P
W_{max} (W kg^{-1})	364.3 ± 25.7 *(4)*	347.3 ± 20.7 *(4)*	-0.459	= 0.662
V_{max} ($L_{0\text{-}F}$ s^{-1})	15.3 ± 0.7 *(4)*	14.8 ± 1.1 *(4)*	-0.353	= 0.736
V/V_{max} at max power	0.28 ± 0.01*(4)*	0.29 ± 0.02 *(4)*	0.259	= 0.805
P/P_0 at max power	0.43 ± 0.01 (*4*)	0.46 ± 0.02 (*4*)	1.536	= 0.176
Power ratio	0.12 ± 0.01 *(4)*	0.13 ± 0.01 *(4)*	0.999	= 0.356

Values are means ± S.E.M. (*n*)

V/V_{max}, ratio defining the velocity that generates maximum isotonic power compared to V_{max}; P/P_0, ratio defining the force that generated maximum isotonic power divided by maximum isometric force; Power ratio, (W_{max}/P_0V_{max}).

3.4.4 Cyclical muscle contractions

The power-frequency relationship is presented for both absolute net power (Fig. 3-4a) and as relative power (Fig. 3-4b; where net power, W, was normalised to net power at a cycle frequency of 7 Hz, W_{7Hz}). The frequency yielding maximum relative power was significantly different between the two compartments, with maximum relative power generated at 11 Hz for the medial compartment, and 15 Hz for the lateral compartment (1.11 W/W_{7Hz} ± 0.03 *vs. 1.26* W/W_{7Hz} ± *0.02,* P<0.05) (Fig. 3-4). These frequencies correspond to maximum absolute net powers of 64.19 W kg^{-1} ± 2.52 and 85.29 W kg^{-1} ± 11.89, respectively (t_5=-1.342, P=0.237). The maximum net power for the medial compartment was not significantly different across 7-19 Hz, while they were not significantly different across 9-19 Hz in the lateral compartment.

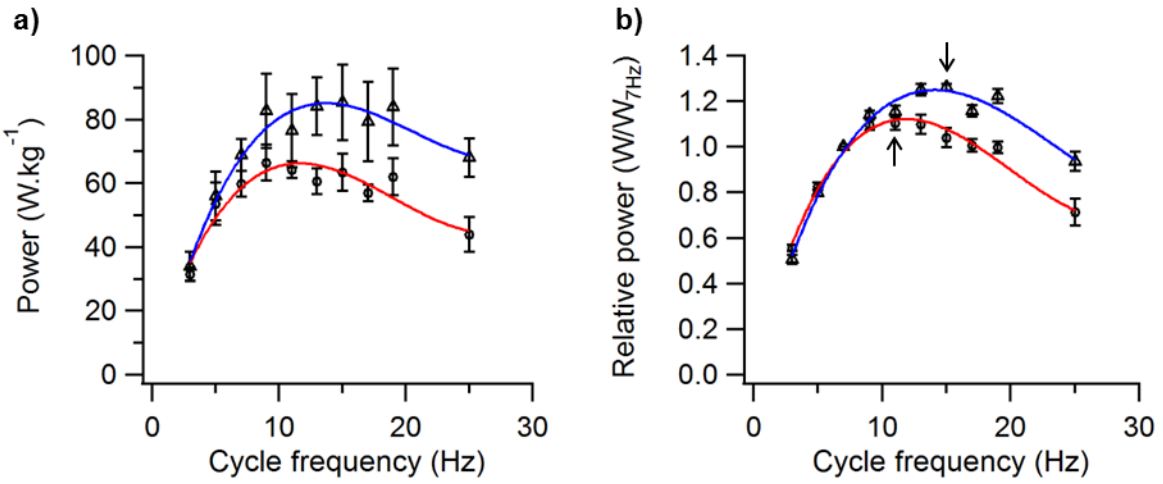

Figure 3-4. Power-frequency relationship for the medial and lateral compartments of the EDL. The absolute power-frequency relationship is presented (a) and the relative power-frequency relationship normalised to 7Hz (b). Medial (circles, red line) and lateral (triangles, blue line) data are presented as mean ± S.E.M with a forth-order polynomial fitted. Arrows depict optimum frequency for the medial compartment (11Hz) and the lateral compartment, (15Hz).

3.4.5 Muscle fatigability

T_{W50} for the medial compartment was 2.95 ± 0.13 s, maintaining power significantly longer than the lateral portion, where T_{W50} = 2.34 ± 0.12 s (t_{15} =-3.440, P = 0.004; Fig. 3-6a). Over the 30 cycle fatigue run the medial compartment produced more cumulative work 101.97 ± 11.88 J kg^{-1} compared to the lateral 93.69 ± 11.88 J kg^{-1} (t_{15} = -0.49, P = 0.631, Fig. 3-5b).

The work loop shapes for the medial and lateral compartment changed differently over the 30 cycles (Fig. 3-6c, d), with the medial compartment having a greater capacity to maintain force during shortening as the muscle fatigued, compared to the lateral compartment (Fig. 3-6e, f). Conversely, the medial compartment showed an impaired capacity to relax during shortening, resulting in force generation continuing into lengthening, thus requiring an increased amount of work to re-lengthen the muscle (i.e. negative work; Fig. 3-6g). This phenomenon was less apparent in the lateral compartment (Fig. 3-6h).

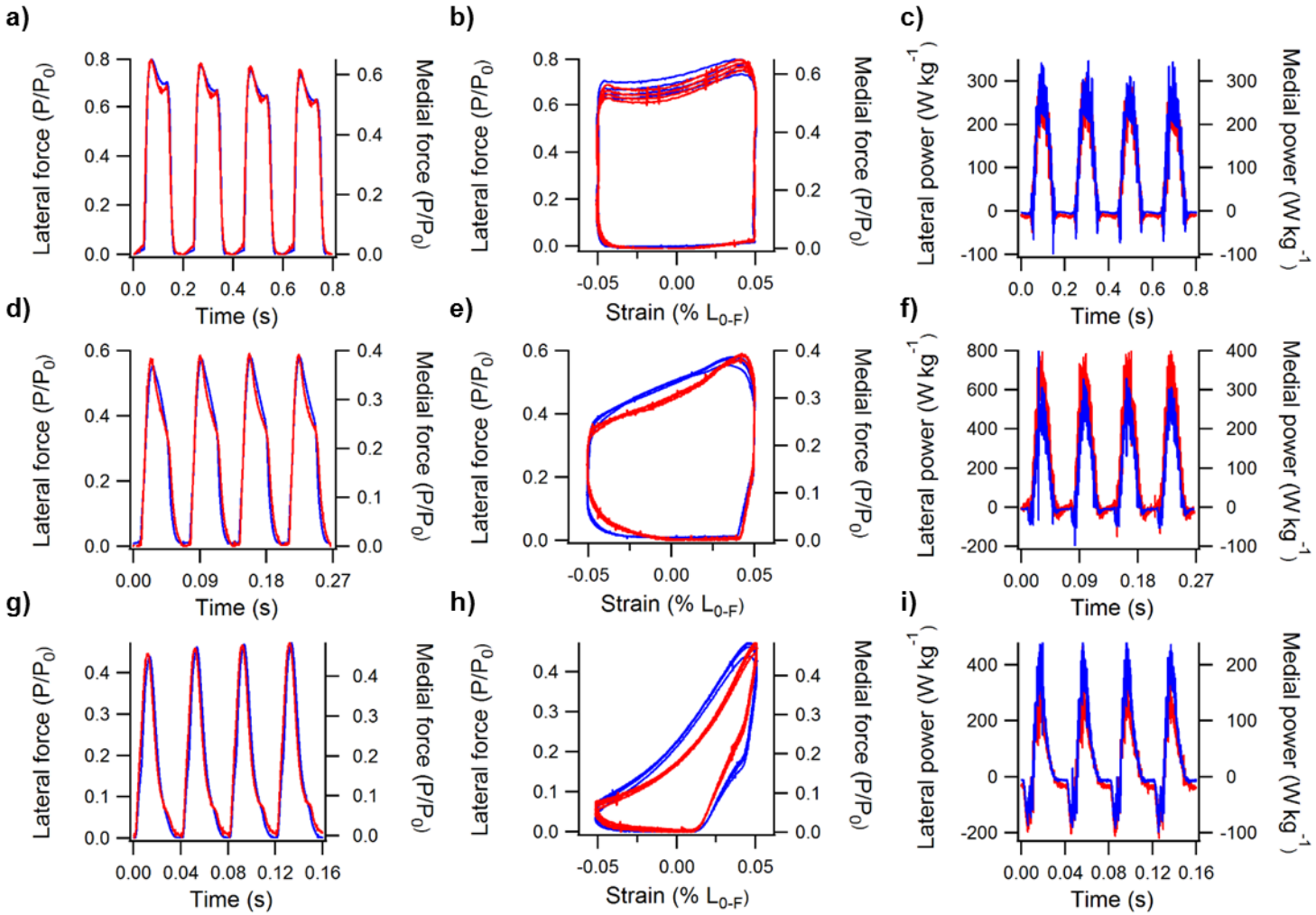

Figure 3-5. Representative work loop traces (b, e, h) with force- (a, d, g) and power-time (c, f, i) plots for at 5Hz (a, b, c), 15Hz (d, e, f) and 25Hz (g, h, i) for both the medial (red line) and the lateral compartment (blue line).

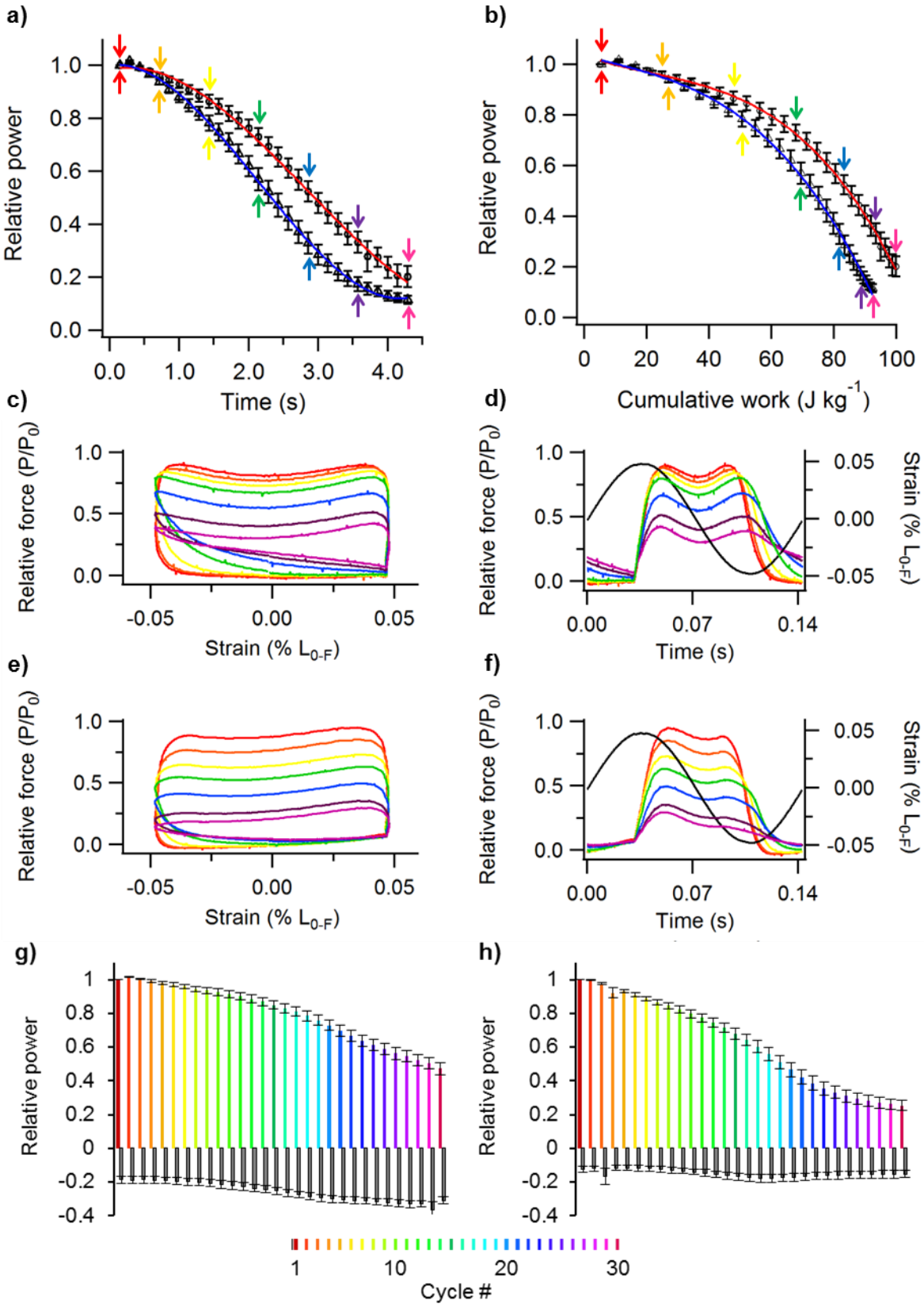
a)
Relative power
Time (s)
b)
Relative power
Cumulative work (J kg-1)
c)
Relative force (P/P0)
Strain (% L0-F)
d)
Relative force (P/P0)
Strain (% L0-F)
Time (s)
e)
Relative force (P/P0)
Strain (% L0-F)
f)
Relative force (P/P0)
Strain (% L0-F)
Time (s)
g)
Relative power
h)
Relative power
Cycle #

Figure 3-6. Relative power output during a 7Hz fatigue run and its effect on work loop shape and force-time characteristics. Relative power output against time (a) and cumulative work (b) for the medial (circles, solid line) (*n*=8) and lateral (triangles, dashed line) (*n*=9) compartments. Work loop shape and force-time characteristics displayed for medial (c) and (d), and the lateral compartments (e) and (g), respectively. Overlaid on the relative force trace is the sinusoidal length change (black line). Net work broken down into positive (coloured fill) and negative (grey fill) composites during the fatigue work loop cycles for the medial (g) and lateral compartment (h). Data are presented as mean ± S.E.M with a fourth-order polynomial fit.

3.5 Discussion

The main aim of this study was to investigate the effect of spatial fibre type heterogeneity on the mechanical properties of a skeletal muscle, utilising the transverse heterogeneity in fibre type composition and compartmental differences in innervation in the extensor digitorum longus muscle. It was hypothesised that the predominance of fast-twitch fibres in both the lateral and medial EDL compartments would result in minimal differences in the contractile characteristics under isometric and dynamic conditions, but that the presence of type I fibres in the medial compartment would result in a higher resistance to fatigue. Regional variation in fibre type had no bearing on the force-velocity properties between the medial and lateral compartments of the EDL. However, the oxidative fibre type composition in the medial compartment resulted in slower isometric twitch kinetics and a significantly higher fatigue resistance compared to that of the lateral compartment.

3.5.1 Regional variation in fibre type distribution

In this study, as in previous studies (Pullen, 1977, Deveci et al., 2001), it was found that the medial compartment contains all three major fibre types (Type I, IIa and IIb), whereas the lateral compartment only contains fast phenotypes (Type IIa and IIb). It was also found that there was a higher proportion of oxidative fibre types (Type I and IIa) in the medial compartment of the EDL compared to the lateral compartment.

Unlike previous studies that have reported fibre type composition by fibre number, we additionally determined regional variation in fibre type composition by fibre area. Fibre type composition by area provides a better index of muscle functional capacity than fibre type composition by number since force generation is proportional to myofibrillar cross-sectional area, which varies between different fibre types. The importance of reporting areal histological fibre type composition data is emphasised by our finding that the size of the type IIb fibres varied regionally, with those in the medial compartment being 29.2% smaller than those within the lateral compartment. The proportion of oxidative fibres based on fibre number is 13.07% in the lateral compartment compared with 33.02% in the medial compartment whereas the comparable proportions by fibre area are 7.56% and 24.28%, respectively. The spatial heterogeneity of fibre type composition within the EDL enabled the functional relevance of different fibre composition to be investigated.

3.5.2 Regional variation in isometric and isotonic contractile properties in EDL

The medial and lateral compartments both generated comparable isometric tetanic stresses, and had similar twitch:tetanus ratios to that previously reported ranging from 0.19 to 0.26, in whole rat EDL (Close, 1964, Close, 1967, Frischknecht and Vrbová, 1991, Buffelli et al., 1997). The major differences in the isometric twitch contractile characteristics between the two compartments of the EDL were in the twitch-rise and twitch half-relaxation times. Isometric twitch rise time for the medial compartment was 11.7% longer than that of the lateral, with a 39.5% longer twitch half-relaxation time. The slower twitch kinetics are likely the result of differences in myosin heavy chain isoforms composition which determine cross bridge cycling rates, together with differences in the magnitude and time-course of the myoplasmic [Ca^{2+}] (Baylor and Hollingworth, 2012, Bottinelli et al., 1996). There were no regional differences in the isotonic force-velocity properties detected between the two compartments of the EDL (as assessed by V_{max}, W_{max}, power ratio, optimal P/P_0 and optimal V/V_{max}) and the maximum shortening velocities of the lateral and medial compartments were comparable to the values reported for

the whole EDL muscle (Ranatunga, 1984). There is a dependence of force-velocity characteristics on myosin heavy-chain isoform (Bottinelli et al., 1991, Ranatunga, 1984). However, within each muscle fibre type there is a broad distribution in the maximum shortening velocity, that can overlap between the different fibre types (Bottinelli et al., 1991). Clearly, V_{max} of the maximally activated muscle compartments is dictated by the fastest fibre type (Josephson & Edman, 1988). Given the predominance of type II fibres in both EDL compartments the absence of any significant differences in the force-velocity characteristics between the two compartments is perhaps not surprising. *In vivo*, motor units can be differentially recruited and is therefore possible to recruit just slow motor units (with a slower V_{max}) as well as faster motor units (generating a higher V_{max}). Under such circumstances there could be regional differences in the mechanical performance of the EDL.

3.5.3 Regional variation in net power output during cyclical contractions

The absence of a difference in the maximum net power output between the lateral and medial EDL compartments, is consistent with the lack of any differences in their force-velocity characteristics. However, there was a shift in the optimum cycle frequency for maximum net power to a lower frequency in the medial compartment, compared to the lateral compartment. This is likely to result from the slower activation and deactivation kinetics of the medial compartment, as indicated by the slower twitch rise and half-relaxation times. For a given cycle frequency, slower contractile kinetics result in a muscle spending a greater proportion of the cycle submaximally activated than one with faster twitch kinetics. In addition, the slower contractile kinetics mean that the muscle has to be activated with an earlier phase and stimulation duration compared to that of the fast twitch muscle to ensure sufficient relaxation occurs. At all cycle frequencies, stimulating the medial compartment with an earlier phase avoided increasing the negative work done on the muscle, however, at the higher cycle frequencies the slower activation kinetics meant that the muscle was less completely activated and this reduced the positive work generated by the muscle in comparison to the lateral compartment. It is

likely that a lower level of activation in the medial compartment and a concomitant reduction in positive work generation is the primary reason for the lower mass-specific power at high cycle frequencies and the shift in the optimal frequency for maximum power output to lower cycle frequencies in the medial compartment compared to the lateral compartment (Fig. 4a). Despite the shift in optimal cycle frequency between the lateral and medial compartments, both muscle compartments generate in excess of 90% of the maximum power across a broad range of cycle frequencies (Supplementary Table 1; details).

3.5.4 Fatigability of intramuscular compartments

Muscle fatigue results in a reduced capacity to generate power during sustained activity, underpinned by changes in mechanical components such as a decline in force generating capacity, changes in the force-velocity properties and a slowing of relaxation (Curtin and Edman, 1994, Barclay, 1996, Edman and Mattiazzi, 1981). Many investigations into muscular fatigue induce and quantify fatigue using multiple isometric tetanic contractions (Cady et al., 1989, Lännergren and Westerblad, 1991), which only allows the quantification of decline in force-generating capacity. This gives an incomplete insight into the decline in muscle performance during fatigue as many muscles during locomotion undergo repetitive cyclical contractions, during which changes in the force-velocity and relaxation characteristics will impact on muscle performance. Therefore in this study, we utilised a fatigue model that induced fatigue and assessed changing performance during cyclical contractions (Josephson, 1985, Askew et al., 1997). The rate of decline in power output was significantly lower in the medial compartment, as assessed by T_{W50}, which resulted in a larger cumulative amount of work done during the 30 cycles of work, compared to the lateral compartment. A distinct change in the pattern of force generation over time (Fig. 6d, f) and the relative size and shape of the work loop during the sequence of 30 cycles reflects the underlying changes in the physiological properties of the muscle with the onset of fatigue (Fig. 6c, e). These are a reduction in force during shortening and an increase in force during lengthening, particularly at the onset of lengthening. This

reflects a reduction in the force generating capacity of the muscle and a slowing of relaxation. Depression of force generation during fatigue is likely through impaired cross-bridge cycling resulting from interactions of free phosphate (generated through hydrolysis of ATP and PCr) and hydrogen ions (resulting from lactic acid accumulation), which impairs calcium binding with troponin and ATPase activity (Westerblad et al., 1998, Cady et al., 1989). While mechanisms contributing to the slowing of relaxation in the oxidative compartment of the EDL are impaired excitation-contraction coupling and calcium re-uptake (Holloway et al., 2006, Allen et al., 2008). The consequence of the reduction in force and slowing of relaxation as a result of fatigue is a reduction in the work generated during shortening and an increase in the work that must be done on the muscle to re-lengthen it: overall the net work generated decreases (Fig. 3-6g, h). The effects of fatigue are more pronounced in the lateral compartment of the EDL, due to the glycolytic fibre type composition, whereas the more oxidative, medial compartment is more resistant to fatigue. Differential fatigue resistance within two compartments of the same muscle undergoing the same fatigue protocol have not been reported previously.

3.5.5 Fibre type heterogeneity and EDL function

Characterising the regional variation in the contractile properties of a muscle, as we have done in this study in the rat EDL, can help interpret task dependent regional variation in recruitment. Currently there are rather limited data available on *in vivo* activity patterns in rat EDL in relation to limb kinematics and none in relation to specific regions of the muscle. The EDL in rats is active throughout the swing phase of the hindlimb during walking (Nicolopoulos-Stournaras and Iles, 1984). This activity coincides with a decrease in the joint angle of the ankle (Thota et al., 2005, Wilson et al., 1997, Gruner et al., 1980), suggesting that the EDL could play a role in ankle dorsiflexion during walking. This has been similarly shown in cats (Abraham and Loeb, 1985, Goslow et al., 1973, Goslow et al., 1977), (Perret and Cabelguen, 1980) and dogs (Tokuriki, 1973a), where it has also been shown that the EDL plays a similar role in swing at higher speeds of locomotion also (Abraham

and Loeb, 1985, Tokuriki, 1973b). It is currently unknown how regional variation in recruitment of the EDL varies with speed during locomotion.

The fatigue resistance of the medial compartment of the EDL indicates a role during sustained, sub-maximal activation, e.g. during low speed locomotion. Whereas the glycolytic compartment of the EDL is more likely to be recruited during burst activities, such as high speed locomotion. Goslow et al (1973) identified a bimodal fatigue response in the cat EDL, and suggested that this was an adaptive mechanism due to the differences in duty cycle between walking and high speed galloping. Therefore, the fatigue resistant compartment of the EDL is likely to be active during the slower duty cycle (walking) and the more fatigable compartment would be used during pursuit of flight activities (together with the medial compartment if the size principle is followed). The utilisation of predominantly Type I and IIa fibres during walking has been shown in cats and rats (Armstrong et al., 1977, Sullivan and Armstrong, 1978, Smith et al., 1977) with an increasing prevalence of Type IIb recruitment as the speed of locomotion increases. Further data on muscle length change and recruitment are required to test these hypotheses.

In conclusion, mammalian muscle is typically heterogeneous in fibre type distribution, with regional variation in composition, which can affect the mechanical performance of the muscle. We have quantified fibre type composition of the rat extensor digitorum longus (EDL) muscle, and identified a largely oxidative medial compartment and a predominantly glycolytic lateral compartment. The contractile properties varied regionally within the EDL, suggesting that the two compartments of the EDL will have differential activation during locomotion. Having characterized regional heterogeneity in both structure and function we now sought to establish their influence in physiological (adaptive) angiogenesis.

4 Differential expansion of the capillary bed through physiological angiogenesis in skeletal muscle

4.1 Abstract

Angiogenesis is a complex, multifactorial process that is initiated and driven by a variety of mechanical and chemical signals. These differential signalling pathways result in various means of microvessel growth, involving either proliferation and migration of endothelial cells, or differentiation from pre-existing capillaries. Understanding the different driving mechanisms and subsequent patterns of microvascular expansion is a major step towards developing effective angiotherapies (including situations of inadequate capillary supply or capillary rarefaction, but also identifying targets to ameliorate excessive angiogenesis). We explored the effectiveness of low and high frequency indirect electrical stimulation on the capacity to evoke an angiogenic response, while examining the effect of differential angiogenic models on their capacity to improve oxygen supply. Angiogenic models utilising miniaturised implantable stimulators, running for seven days at 4Hz, 10Hz and 40Hz for eight hours/day were used, and ran in parallel with a model of capillary longitudinal splitting (prazosin supplementation) and endothelial sprouting (muscle overload). Angiogenesis was characterised through global capillary counts, and local capillary distribution explored through the analysis of capillary domains. Stimulation at 4Hz, 10Hz and 40Hz all significantly increased C:F by 46%, 49% and 37%, respectively, while prazosin and overload both resulted in a 16% increase in C:F relative to their controls ($P<0.05$). Distributions of capillary supply area were not significantly different among the three stimulation protocols. However, despite prazosin and overload inducing similar levels of angiogenic responsiveness, their distribution of new capillaries differed greatly. Longitudinal splitting angiogenesis without the presence of additional muscle activity appears to maintain the inherent heterogeneity of capillary distribution, which suggests a stochastic form of microvascular expansion. Conversely, muscle overload and indirect electrical stimulation, known drivers of sprouting angiogenesis, appear to have refined control of new capillary location suggesting control at a more local level.

4.2 Introduction

The capacity of a muscle to deliver and utilise oxygen is an important regulatory factor in its capacity to perform work. Oxygen is delivered to muscle through convection within the cardiovascular system, then by diffusion at the tortuous capillary network distributed among muscle fibres in a typically heterogeneous distribution (Egginton and Ross, 1992, Al-Shammari et al., 2012, Al-Shammari et al., 2014b, Bosutti et al., 2015). Both the density of microvascular supply as well as heterogeneity of this supply distribution will affect tissue oxygenation, and subsequently impact function (Degens et al., 2006, Goldman et al., 2006, Egginton and Gaffney, 2010). Therefore, an effective angiogenic therapy needs not only to improve the density of capillaries, but be directed by tissue demand and optimised for oxygen delivery (see chapter 2).

A number of *in vivo* angiogenic models have been identified derived from component stimuli present during aerobic exercise (Williams et al., 2006b, Egginton et al., 2011, Hellsten and Hoier, 2014). A highly reproducible and controlled animal model of selected muscle activity through indirect electrical stimulation has shown to have a potent angiogenic potential across a number of species (Pette et al., 1973, Hudlicka et al., 1994, James et al., 1997, Egginton and Hudlicka, 1999, Egginton and Hudlicka, 2000, Amaral et al., 2001, Tsutaki et al., 2013). The targetted recruitment of muscle at 10Hz is the most commonly utilised frequency, given it is the inherent firing rate of slow muscles (Eccles et al., 1958), with few other variations in stimulation frequency having been explored for angiogenic potential (Ebina et al., 2002, Egginton and Hudlicka, 2000).

Two isolated stimuli; vascular shear stress and longitudinal muscle stretch have been shown to expand the microvascular bed through differential angiogenic signalling pathways, resulting in longitudinal vessel splitting or endothelial sprouting, respectively (Zhou et al., 1998b, Zhou et al., 1998a, Egginton et al., 2001, Williams et al., 2006b). Increased microvascular shear stress is typically induced through the administration of prazosin, a α_1-adrenergic antagonist (Ziada

et al., 1989, Fulgenzi et al., 1998, Egginton et al., 2001, Williams et al., 2006b). However, the level of increased blood flow, and subsequently microvascular shear stress by the administration of prazosin are potentially supra-physiological when compared to levels and durations of hyperaemia achieved during exercise (Williams et al., 2006b). A physiologically appropriate model of increased shear stress may be achievable through indirect electrical stimulation to evoke maximal (functional) hyperaemia. Acute stimulation at 4Hz has been shown to evoke maximal hyperaemia in the *tibialis anterior* (TA) and *extensor digitorum longus* (EDL) muscles (Hawker and Egginton, 1999), and to have angiogenic potential in a 24h a day stimulation protocol (Ebina et al., 2002).

Longitudinal stretch of a muscle and its microvasculature is typically performed through ablation of a dominant agonist muscle, overloading a smaller but functionally similar muscle. Extirpation of the TA leads to a 20% increase in stretch of the EDL muscle, while hind limb blood flow remains unchanged; this drives an angiogenic response accompanying the hypertrophic remodelling (Ziada et al., 1989, Williams et al., 2006b, Egginton et al., 2011). The adaptive genetic response of longitudinal stretch (overload) incorporates the up-regulation of various extracellular matrix remodelling proteins, with matrix metalloproteinases-2 (MMP-2) playing an integral role in the adaptive remodelling (Williams et al., 2006a, Olenich et al., 2013, Haas et al., 2000, Stetler-Stevenson, 1999).

Within this model there are elements of supra-physiological signalling (a chronic 20% increase in longitudinal stretch); however, Egginton et al (2011) showed that a reduced degree of stretch is capable of also eliciting an angiogenic response, suggesting that physiological angiogenesis is a graded, not threshold response. Therefore, to mimic the angiogenic potential developed by the overload model, a hypoxic environment with reduced blood flow may stimulate a similar response. This could be achieved through tetanic muscular activation increasing oxygen consumption while impeding muscle blood flow (Hudlicka et al., 1977, Molé et al., 1999). This physiologically relatable model may be achieved through high frequency indirect electrical stimulation with the pattern of firing occurring in fast

nerves (Eccles et al., 1958), eliciting an unfused tetani, allowing for targetted recruitment and better defined duration of stimulus than that currently available with the overload model. This may be achieved through 40Hz stimulation, a protocol which has shown to improve fatigability through increased oxidative enzyme content and microvascular content (Hudlicka et al. 1980).

We hypothesise that 4Hz indirect electrical stimulation will comprise of a largely hyperaemia driving angiogenic signal which will overlap with the prazosin treated animals. Conversely, the 40Hz stimulated muscles would comprise predominantly of a stretch and metabolically driven angiogenic response that would be closer to that of the muscle overload model. Figure 4-1 outlines the hypothesised overlap between variations in stimulation frequency and known mechanical and chemical stimuli. The aim of this study was to validate the hyperaemia response across a range of stimulation frequencies, and to determine their capacity as translatable models of longitudinal splitting and sprouting angiogenesis. Furthermore, we sought to characterise the angiogenic response of these patterns of activation, while better defining the local capillary response of the two established angiogenic models, prazosin and overload, further characterising their oxygen delivery potential.

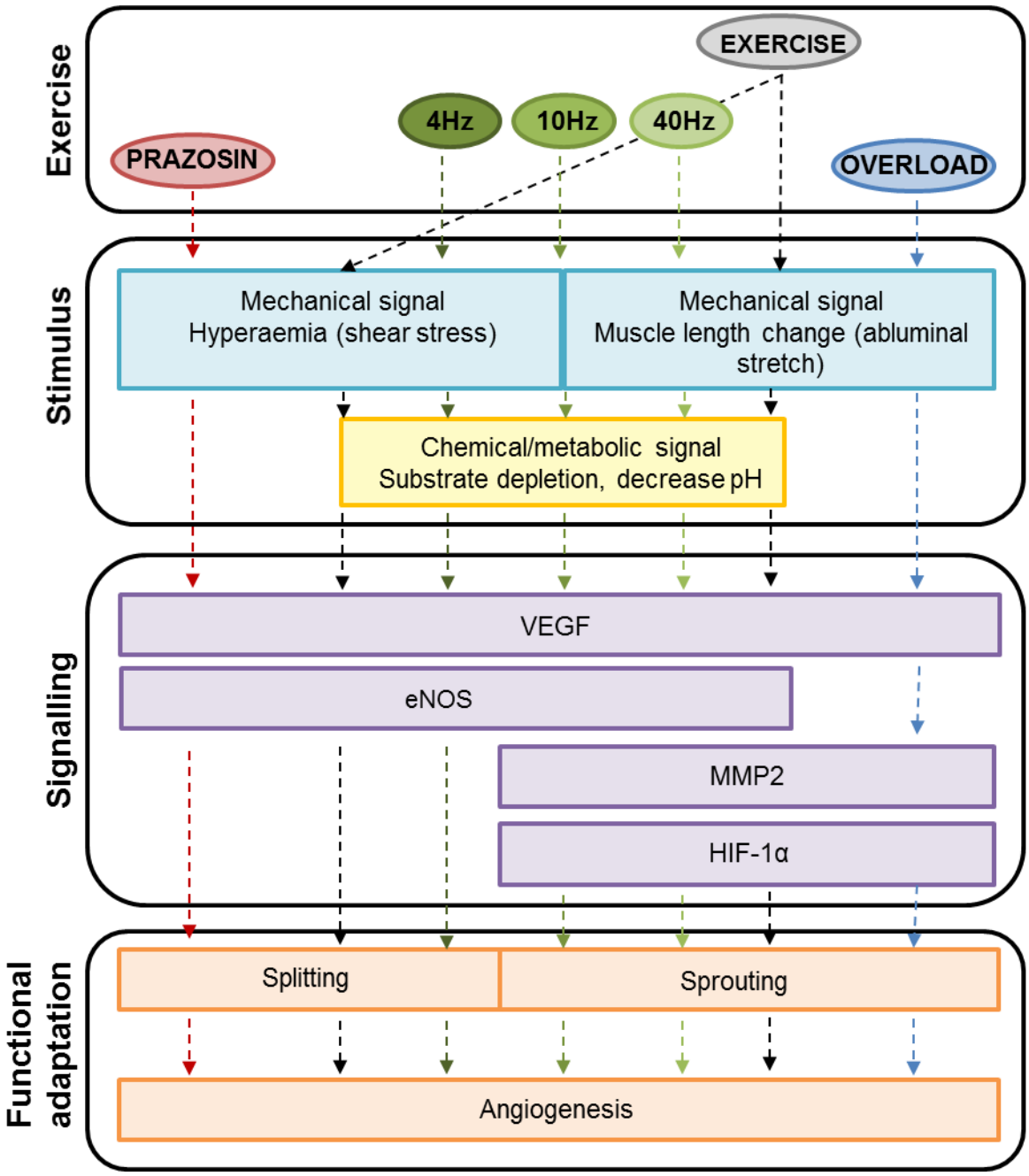

Figure 4-1. Hypothesised microvascular expansion in skeletal muscle. Exercise induces a multitude of mechanical and chemical signaling cascades that interact to induce angiogenesis. Prazosin and overload have been established as two distinct angiogenic models that act through differential signaling cascades and result in longitudinal splitting and sprouting angiogenesis, respectively. Utilising the indirect electrical stimulation method as a way of controlling for duration and pattern of activity, we explored the potential of three stimulation parameters on the selective manipulation of identified mechanical and chemical signals. Based on (Hoier and Hellsten, 2014).

4.3 Material and methods

4.3.1 Ethical approval

All rodent work was carried out in accordance with the Animals (Scientific Procedures) Act 1986 (ASPA, 1986). Animals were sourced in-house, and housed on a 12 hour light-dark cycle at 21 °C with *ad libitum* access to food and water.

4.3.2 Blood flow dynamics

To validate our hypothesis of the differential response in hind limb blood flow to supramaximal stimulation at different frequencies, we utilised a terminal *in situ* preparation of bilateral peroneal nerve stimulation while recording femoral artery blood flow (similar to Hawker and Egginton, 1999). Briefly, five control animals (257 ±7g) were induced into an anaesthetic plane using 5% Isoflurane (IsoFlo ®) with 2 $L.min^{-1}$ O_2 flow, and maintained on a face mask at 2.5% isoflurane. A jugular vein catheter was placed for infusion of Alfaxan (Jurox), maintaining anaesthesia through a 10mg/hour infusion rate, the trachea was intubated to support spontaneous ventilation, and a carotid artery line was placed to record systemic blood pressure. In both hind limbs the *tibialis anterior* muscle was extirpated, allowing isolation of the EDL tendons and attachment to corresponding ergometers (series 305C-LR, Aurora Scientific Inc., Ontario, Canada). The femoral arteries were isolated for blood flow measures using the Transonic Perivascular Flow Module (TS420, Transonic, Ithaca, NY) with 0.7mm probes (MA0.7PSB: Transonic, Ithaca, NY) and the peroneal nerve was exposed at the knee for indirect supramaximal stimulation. Muscle length was optimised to generate peak force, and randomised fatigue protocols were run, with 30 minute recovery time between each. Fatigue stimulation protocols ran for three minutes at 1 (*4*), 4 (*4*), 10 (*5*) or 40Hz (*4*) with a pulse width of 0.3ms (number of animals in parentheses). Fatigue index (FI) was calculated as the percentage of peak tension (FI (%) = (final tension/peak tension) * 100). EDL conductance (C) was normalised to pre-stimulation values (C_0) at time -30 s, where stimulation was initiated at time 0s. Force (F) was also normalised to pre-stimulation values, also at time -30s (F_0).

4.3.3 Angiogenic regimes

The following surgical and pharmacological angiogenic protocols were carried out over a seven day period. Electrical stimulation groups received eight hours of their respected stimulation frequency that consisted of 4Hz (frequency that generates the largest functional hyperaemia), 10Hz (natural firing rate of nerve nerve fibres) and 40Hz (natural firing rate of fast muscle fibres). Unstimulated contralateral sides were used as an internal control (STCT), as well as a SHAM stimulation group that underwent the full stimulator implantation surgery but received no stimulation. Muscle overload (OV) animals underwent unilateral TA extirpation, while the contralateral side was used as an internal control (OVCT). The vasoactive compound prazosin (PR) works as a systemic vasodilator, and as such does not allow for internal controls, and data were compared with untreated sedentary animals (CT).

4.3.4 Surgical interventions

Animal surgery was conducted under aseptic conditions with inhalation anaesthetic (Isoflurane, IsoFlo®). Anaesthetic induction was conducted with 5% Isoflurane with a 2 $L.min^{-1}$ O_2 flow, and maintenance during surgery set at 2.5% with a 2 $L.min^{-1}$ flow rate. Surgery only began after confirmation of anaesthetic plane (no withdrawal reflex).

4.3.5 Electrical stimulation

Animals underwent indirect electrical stimulation of the hind limb extensors (peroneal muscle group), through stimulation of the deep lateral peroneal nerve. Miniaturised, battery-powered electrical stimulators were coated with hypo-allergenic beeswax and placed in a subcutaneous pouch in the mid-thoracic region of the back (Linderman et al., 2000). The stimulator was inserted through a two centimetre incision, and sutured into place to contain the stimulator on the animals back. The stimulator is operated through a superficial magnetic reed-switch, allowing the stimulator to be activated 24h following surgery. Teflon coated seven-

strand braided stainless steel wires (A-M Systems) were tunnelled distally towards the right hind limb under the skin, and a loose wire loop sutured into place on the *rectus femoris* to provide flexibility in the wire during the animals locomotion. The deep peroneal nerve is located in the groove between the *biceps femoris* and the *tibialis anterior*, which requires no cutting of covering muscle. Following localisation of the nerve, a suture was placed proximally and distally to the nerve to act as a guide for the placing of the wire coils, as well as anchoring them in place (Fig. 4-2). A 23G needle was used to pull the wires through the vastus lateralis towards the nerve, ensuring close proximity of the coils, as well as providing some stability for wire placement. Once the wires were within close proximity of the nerve, a 4-6 loop coil was made and sutured into place, followed by the re-covering of fascia across the superficial muscles to ensure localisation of the coils adjacent to the nerve. The animals were given 24 hours to recover before the stimulators were activated, allowing sufficient time for surgical trauma/inflammation to subside as well as normal locomotion to resume. Initial gait was impaired for 24-36 hours.

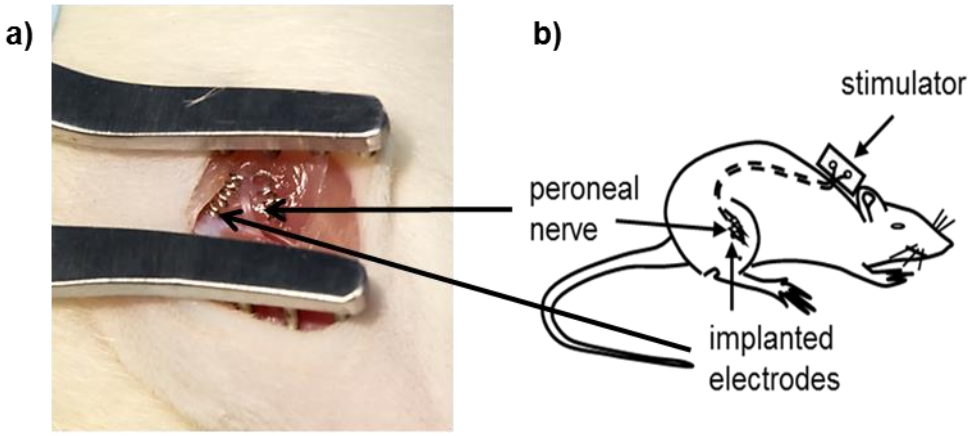

Figure 4-2. Implanted stimulation device, with stainless steel coils parallel to peroneal nerve. Note, the stimulator is implanted subcutaneously for chronic studies.

4.3.6 Muscle overload

The target leg for extirpation was examined through flexing the knee and ankle to identify muscle ridges (lateral boarder of *tibialis anterior*). An incision was made two thirds up the length of the TA, towards the lateral side of the muscle. The covering fascia was cleared exposing the *tibialis anterior* muscle, allowing the release of its tendon and dissection from the lateral surface of the tibia. Ablation of the TA, with a residual muscle stump attached to the tibia (Fig. 4-3), resulted in minimal blood loss and good wound healing within 48h.

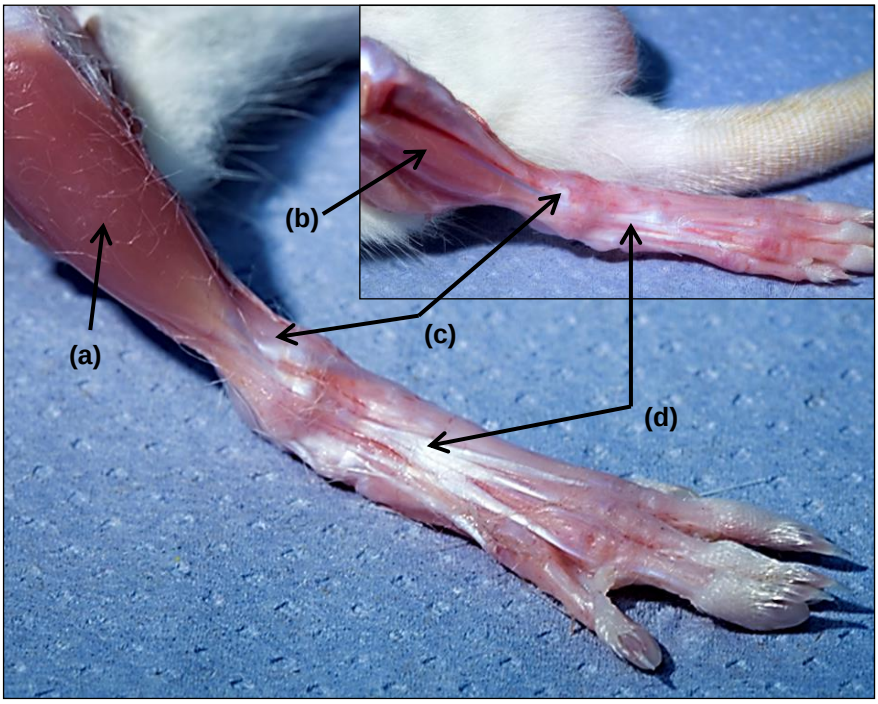

Figure 4-3. Extirpation surgery in rat hind limb. Overload surgery involves the removal of the tibialis anterior (a) increasing the basal stretch of the extensor digitorum longus (b), while being sure not to release the ligament (c). Extensor digitorum longus multi-tendon arrangement (d).

4.3.7 Administration of vasoactive compound

Drinking water was supplemented with prazosin (Cambridge Bioscience), dissolved at 40°C with a working concentration of 50mg per litre. Palatability was improved using sugar, and the drug was provided *ad libitum* in water (Fig. 4-4).

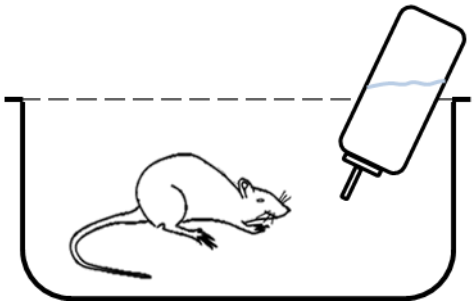

Figure 4-4. Prazosin supplementation through their drinking water.

4.3.8 Muscle sampling

Animals were culled by a competent Home Office personal license holder through Schedule 1 approved techniques. Whole muscles were carefully dissected from the hind limb of the animal and weighed. Muscle samples were split into three equal portions with the proximal and distal portions frozen in liquid nitrogen for qPCR analysis and Chapter 6's gene array, while the mid portions were used for histology. EDL muscle mid-portions were used for muscle histology as this is best representative of the muscle phenotype, avoiding excessive influence of anchoring tendons. Muscles were mounted perpendicularly to cork discs in OCT, snap frozen in isopentane cooled in liquid nitrogen, and stored at -80°C until further use.

4.3.9 Immunohistochemistry

Serial cryostat sections (10µm) were cut at -20°C and fixed to polysine adhesion slides (VWR international), and left to air dry for 30 minutes before being store at -20°C for later staining.

4.3.10 Capillary localisation

Griffonia simplicifolia lectin-1 (Vector Laboratories, UK) was used as a marker for capillaries, due to its known binding affinity to proteoglycans in the glycocalyx of microvessels. We used a rhodamine-labelled lectin that produces a red fluorescence. Samples were fixed with 2% paraformaldehyde solution for two minutes. *Griffonia simplicifolia* lectin-1 was diluted with phosphate buffered saline

(1:250), and sections incubated for one hour at room temperature. Slides were mounted in VectaShield (Vector, H-1400) to minimise photo bleaching of the fluorochrome.

4.3.11 Morphometric analysis

Four regions of interest (0.145 mm^2) were used across the transverse section of the EDL (Fig. 4-5). Global morphometric indices for capillary (C:F, CD) were generated with local geometric tissue supply regions (capillary domain area) using the oxygen transport modelling software (Chapter 2).

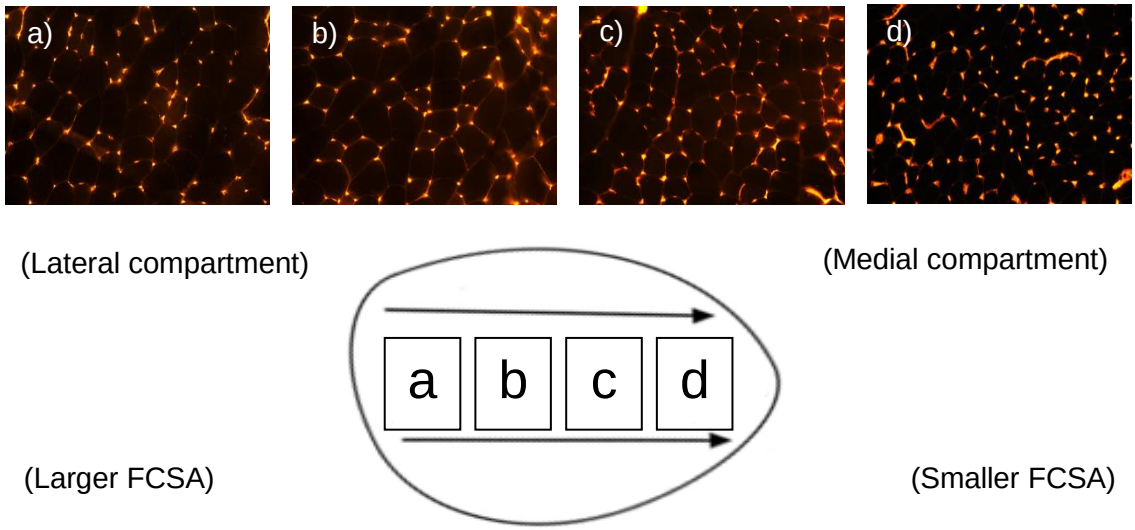

Figure 4-5. Transverse cross-section of the EDL illustrating sampling regions for histological and domains analysis. Moving medially from the lateral compartment (a-d) there is an increase in capillary density, and decrease in fibre cross sectional area.

4.3.12 RNA extraction

All equipment was autoclaved where appropriate and cleaned with RNAse Zap (Ambion, Inc.), RNase free tips were used throughout. Tissue was homogenised in Tryzol using a bead mill (TissueLyser LT, Qiagen) with 5mm stainless steel beads. Following complete homogenisation chloroform was added and spun at 13000 rpm at 4°C for 10 minutes, to separate the solution into two portions the aqueous (top) and organic (bottom) phase. The aqueous phase contains the RNA; which was

aspired and put through the RNeasy Mini Kit (Qiagen) and suspended in 50µl of RNase free molecular biology grade water. Quality control of the samples were quantified using a nanodrop, and RNA integrity checked on the Bioanalyser 2100 (Agilent).

4.3.13 Reverse transcription

500ng of RNA was reverse transcribed using the Quantitect reverse transcription kit (Qiagen) in a 10µl reaction according to manufacturer's details. This kit has a gDNA wipe out kit that was used to remove potential contaminating gDNA carried over during RNA extraction, this was carried out according to manufacturer's details. A random 10% of the samples were run in duplicate to check accuracy of the normalisation. The completed reverse transcription were diluted 10-fold with 0.5µg/mL tRNA in water.

4.3.14 qPCR

Two microlitres of each diluted cDNA were amplified in a 10 µL reaction using Quantifast SYBR green master mix (Qiagen) with each primer (Table. 4-1) at a final concentration of 500nmol/L. No-template controls were also run using 2ul of tRNA 0.5µg/mL. DNA standards for each gene of interest and reference genes were run at serial dilutions of 10^7-10^1 for each reaction. PCR amplification parameters: 95oC for 5 min followed by 40 cycles of 95oC for 10 sec, 60oC for 20 sec using a Rotor-Gene Q PCR machine (Qiagen). Copy numbers/reaction were derived from the standard curves using the Rotor-Gene Q software. The three reference genes (GAPDH, ACTB and TBP) were used to calculate the normalisation factor and GOI copy numbers were normalised. Primers span regions of the gene similar to the probes used in the SurePrint G3 Rat Gene Expression v2 Microarray Kit, 8x60K, Agilent. Two VEGF genes were used to identify potential differences in expression level of those isoforms containing heparin domain binding sites (spanning exon 7) and all isoforms of VEGF (spanning exon 4).

Table 4-1. Forward and reverse primers for qPCR.

Gene		Primer
VEGFA	Forward	ctcaccaaagccagcacatagg
	Reverse	tctttctttggtctgcattcacatc
VEGFA	Forward	tttgtttgtccaagatccgcagac
	Reverse	ccttggcttgtcacatctgcaag
MMP2	Forward	atcgcagactcctggaatgc
	Reverse	agccagtccgatttgatgct
eNOS	Forward	tgtcactatggcaaccagcgt
	Reverse	gtggtagcgttgctgatccc
GAPDH	Forward	tggtgaaggtcggtgtgaacggat
	Reverse	tccatggtggtgaagacgccagta
ACTB	Forward	acggtcaggtcatcactatcg
	Reverse	agccaccaatccacacaga
TBP	Forward	cccaccagcagttcagtagc
	Reverse	caattctgggtttgatcattctg

Primers based on regions probes designed on the microarray in Chapter 5.

4.3.15 Statistical analysis

All data are expressed as mean ± S.E.M. (*n*) with figures generated in Igor Pro 6.22 (WaveMetrics). A one-way analysis of variance (ANOVA) was used to determine differences between groups, using LSD post-hoc testing for individual comparison when there were significant differences, set at $P<0.05$. Group sizes were: CT (*6*), STCT (*7*), 4Hz (*6*), 10Hz (*5*), 40Hz (*4*), SHAM (*4*), PR (*5*), OV (5), and OVCT (6).

4.4 Results

4.4.1 Muscle fatigability and blood flow

There was a significantly different fatigue response to the four frequencies of indirect electrical stimulation (Fig. 4-6). The end tension of the three minute fatigue protocol varied directly with the frequency of stimulation. 1Hz showed little to no fatigue response (104.8 ± 5.3% of F_0), while 40Hz showed the largest decrease in force over the three minute stimulation (16.4 ± 1.9% of F_0).

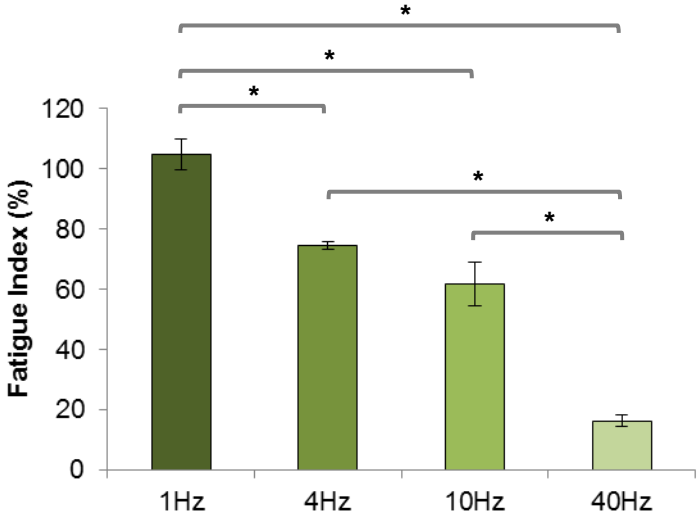

Figure 4-6. Fatigue index of the EDL following three minutes of stimulation. 1Hz (4), 4Hz (4), 10Hz (5) and 40Hz (4), * P<0.05.

Similarly, the EDL blood flow kinetics differed substantially between the four stimulation protocols. 1Hz showed little increase in conductance during stimulation with a rapid return to baseline after one minute (Fig. 4-7a). 4Hz showed a large hyperaemia response during stimulation, reaching a peak after two and a half minutes (1.63±0.20 C/C_0), and decreased dramatically following cessation of stimulation (Fig 4-7b). The 10Hz stimulation showed a more dramatic rise in conductance, after just one minute (1.70±0.36 C/C_0) and plateaued over the subsequent minute. There was a noticeable hyperaemia response maintained upon completion of the fatigue protocol, but flow returned to baseline after three minutes (Fig. 4-7c). 40Hz stimulation increased conductance during stimulation,

while peak flow (1.75±0.28 C/C_0) was seen 30 seconds following the completion of the fatigue protocol (Fig. 4-7d).

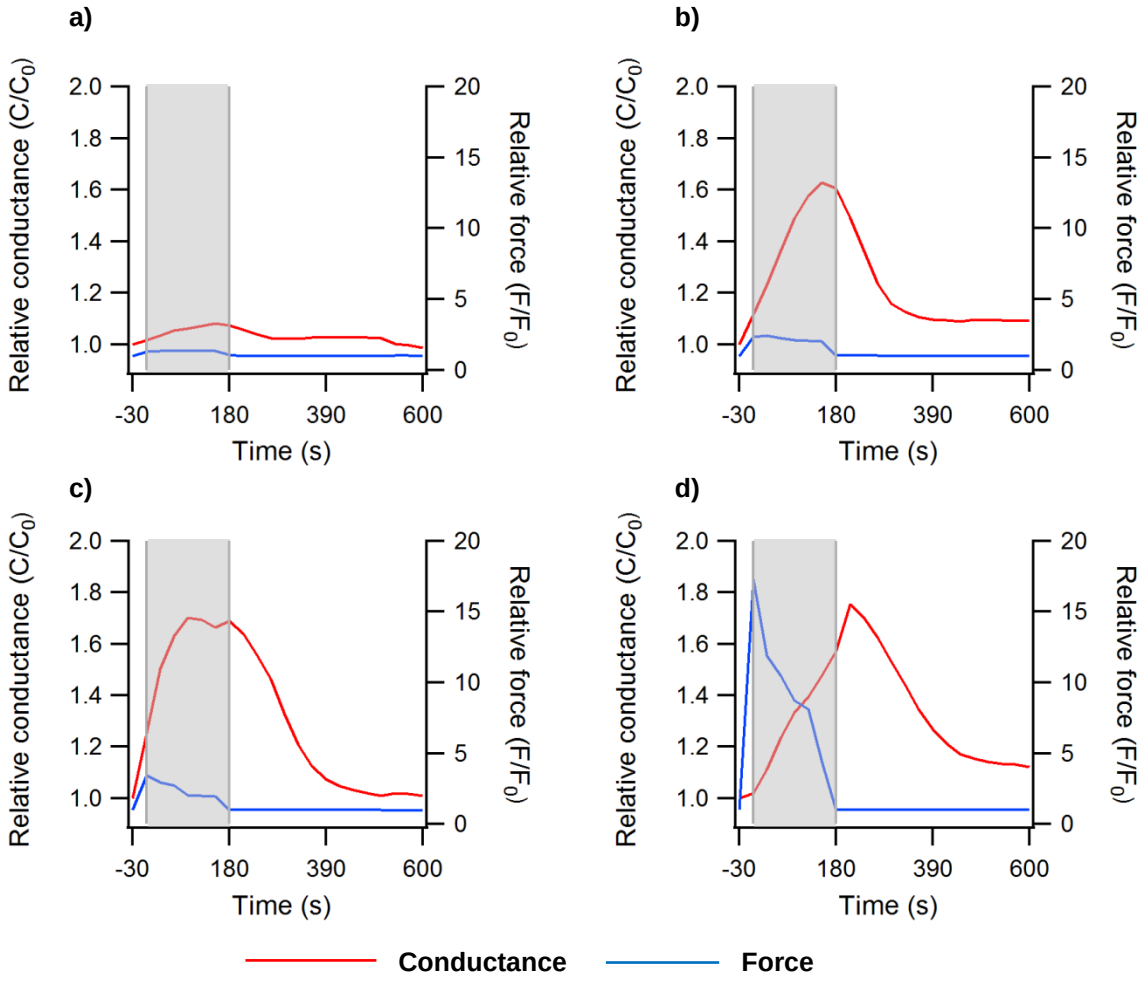

Figure 4-7. Relative EDL blood flow and force kinetics during indirect electrical stimulation. Indirect electrical stimulation was completed at 1Hz (a), 4Hz (b), 10Hz (c) and 40Hz (d). Functional hyperaemia shown through changes in relative conductance (red line) within the shaded box, and reactive hyperaemia in the successive white area. Grey area depicts duration of stimulation.

4.4.2 Relative muscle mass

Following seven days of indirect electrical stimulation, relative EDL mass was not significantly different from control or contralateral muscles, across any of the different stimulation frequencies (Fig. 4-8). Seven day supplementation with prazosin did not alter the relative mass of the EDL (n.s.), while overload resulted in

a significant increase in relative mass compared to CT (*P*=0.008) and OVCT (*P*=0.03).

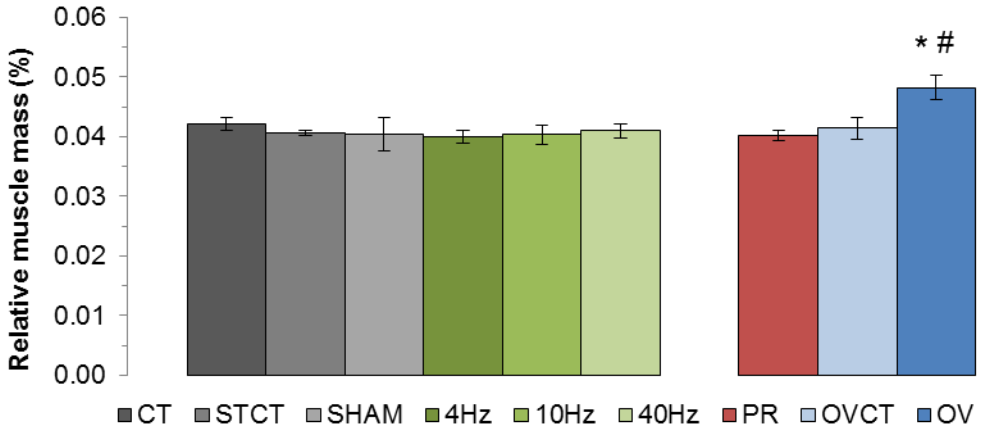

Figure 4-8. EDL muscle mass relative to body weight. * *P*<0.05 *vs.* CT, # *P*<0.05 *vs.* OVCT

4.4.3 Global angiogenic response

Global angiogenic indices are presented in Figure 4-9. Briefly; CT, STCT and SHAM did not significantly differ from one another, with a C:F of 1.42±0.04, 1.43±0.02 and 1.43±0.02, respectively (n.s.). Stimulation at 4Hz, 10Hz and 40Hz significantly increased C:F compared to control, 2.09±0.07 (*P*<0.001), 2.14±0.13 (*P*<0.001) and 1.96±0.10 (*P*<0.001), respectively. Prazosin supplementation significantly increased C:F to 1.66±0.05 (*P*=0.012) *vs*. CT. Seven days of muscle overload significant increased C:F to1.87±0.07 when compared to CT (*P*<0.001) and OVCT (1.60±0.06, *P*=0.001). CD followed similar trends in changes to that of C:F (Fig. 4-9) in all but that of PR, where there was no significant change in CD compared to CT (*P*=0.827). Mean fibre cross sectional area (FCSA) was not significantly different across the stimulation or overload groups, while prazosin was significantly higher when compared to control (*P*=0.029).

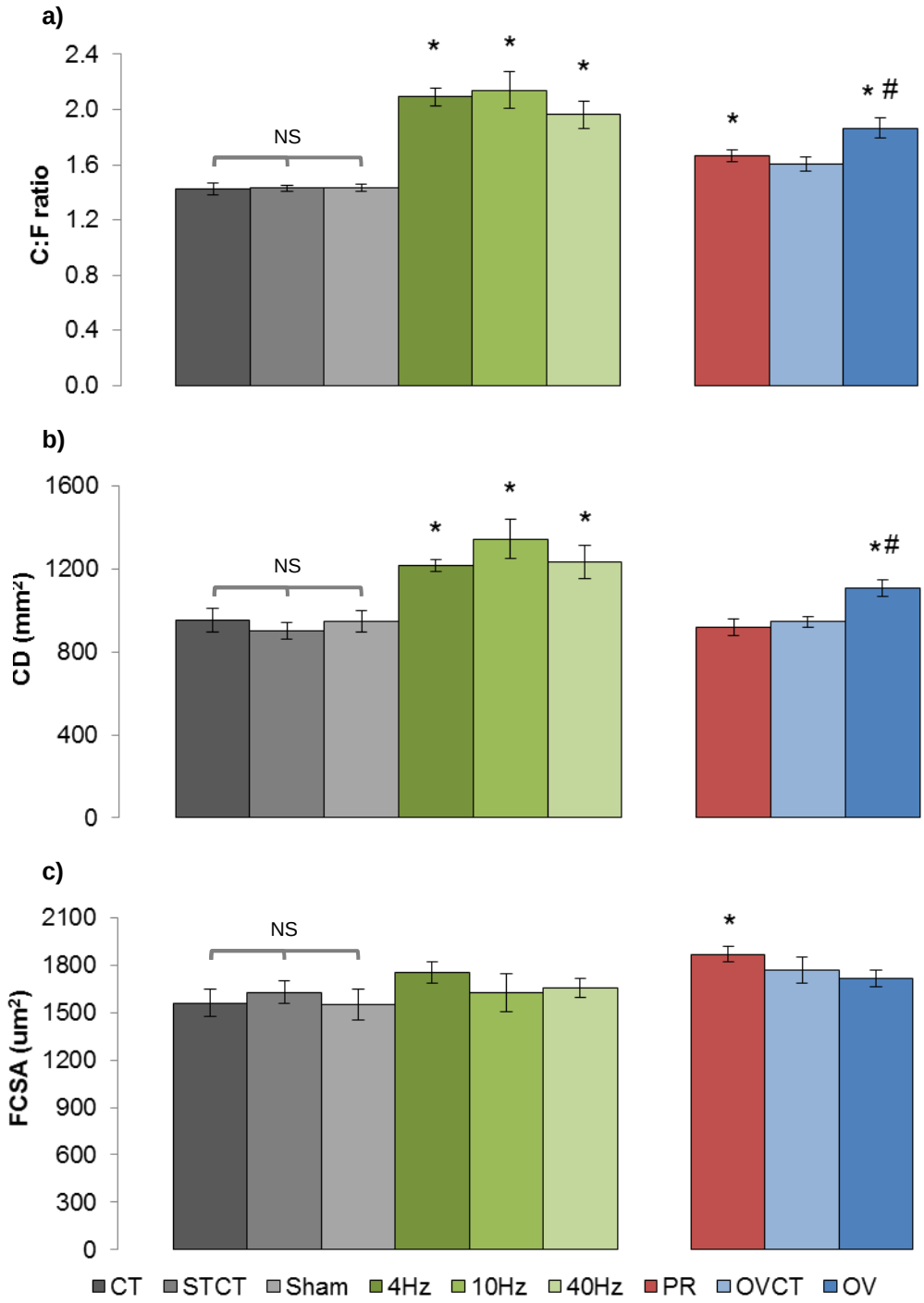

Figure 4-9. Global angiogenic response in the EDL. Changes in capillary to fibre ratio (a), capillary density (b) and fibre cross sectional area (c) following seven days of intervention.

* $P < 0.05$ *vs.* CT, # $P < 0.05$ *vs.* OVCT.

4.4.4 Capillary domains

The relative frequency distributions for capillary domain area are presented for all pooled group data in Figure 4-10, with parametric and non-parametric data in Table 4-2. Distributions for the three control groups: CT, STCT and SHAM were similar, with comparable mean domain areas 1049.6 ± 186.7 μm^2, 1130.0 ± 199.5 μm^2 and 1015.0 ± 203.9 μm^2 (n.s.) The differential electrical stimulation treatments resulted in a large leftward shift in the distributions for 4Hz, 10Hz and 40Hz (Fig. 4-10a) with comparable changes in median frequency. In addition to the leftward shifts in distribution there was a significant decrease in capillary domain heterogeneity (LogSD) across 4Hz (0.145 ± 0.005, $P < 0.001$), 10Hz (0.144 ± 0.005, $P < 0.001$) and 40Hz (0.150 ± 0.002, $P < 0.001$), compared to CT. The administration of prazosin showed no noticeable shift in capillary domain distribution or significant change in capillary spatial heterogeneity ($P = 0.152$). Whereas, seven days of muscle overload showed a dramatic leftward shift in median frequency compared to control (Fig. 4-10b), with a significant decrease in tissue heterogeneity compared to CT ($P < 0.001$) and OVCT ($P = 0.001$).

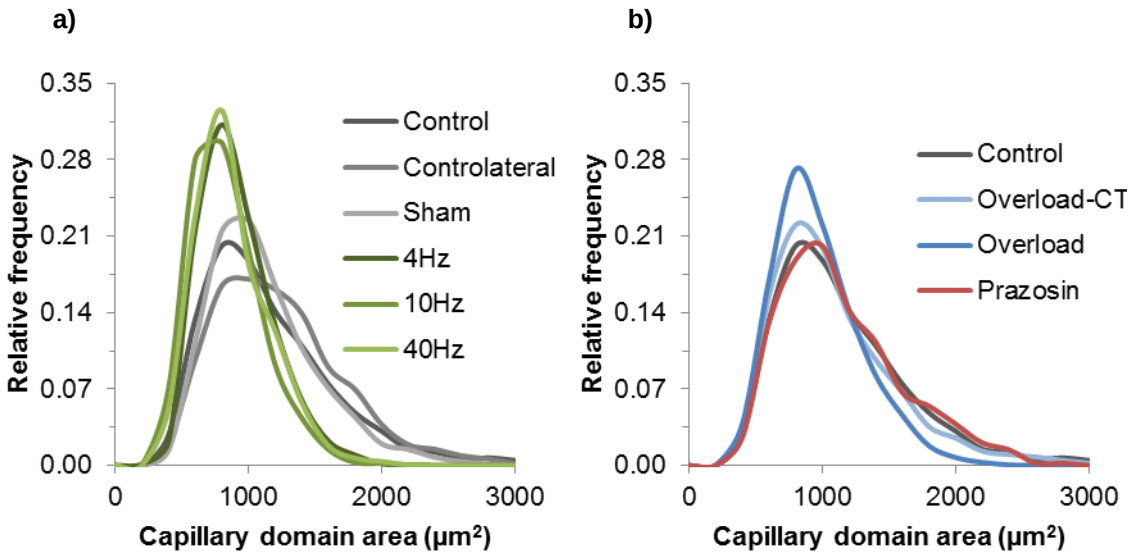

Figure 4-10. Capillary domain area distribution in the EDL. Relative frequency distribution for differential stimulation parameters, with corresponding controls (a), and prazosin and overload models (b).

Table 1. Capillary domain distribution indices

		Pooled domain data			
Group	**LogSD**	***n***	**Mean (μm^2)**	**Median (μm^2)**	**LogSD**
CT	0.193 ± 0.005	*2137*	1049.6 ± 186.7	945.11	0.198
STCT	0.182 ± 0.008	*1682*	1130.0 ± 199.5	1047.31	0.190
SHAM	0.166 ± 0.003 **	*1359*	1015.0 ± 203.9	932.195	0.171
4Hz	0.145 ± 0.005 ***	*2423*	811.0 ± 112.7	768.3	0.147
10Hz	0.144 ± 0.005 ***	*2210*	735.9 ± 119.8	693.46	0.157
40Hz	0.150 ± 0.002 ***	*1655*	779.2 ± 141.7	724.33	0.157
PR	0.181 ± 0.009	*1453*	1039.4 ± 203.8	951.14	0.192
OVCT	0.191 ± 0.005	*1915*	997.9 ± 133.4	885.395	0.192
OV	0.162 ± 0.005 *** ##	*1787*	869.1 ± 146.1	814.06	0.165

* $P < 0.05$ *vs.* CT, ** $P < 0.01$ *vs.* CT, *** $P < 0.001$ *vs.* CT, ## $P < 0.01$ *vs.* OVCT

4.4.5 qPCR

qPCR data for the animal models of angiogenesis are presented in Figure 4-11. Following seven days of prazosin treatment there was a significant decrease in MMP2 mRNA (P=0.013), and no change in eNOS (P=0.597) and VEGF (P=0.582 and P=0.101, Fig. 11c-d). MMP2 was significantly up-regulated in the overload model *vs.* overload contralateral (P=0.001), while eNOS and VEGF differentially were down-regulated. Conversely there was a significant increase in MMP2 (P=0.02), eNOS (P=0.001) and VEGF (P=0.049) in the 10Hz stimulated muscle. 4Hz stimulated muscle showed no noticeable increase in MMP2 (P=0.636) but increased eNOS (P=0.096), while 40Hz showed a large increase in MMP2 (P=0.107) and little change in eNOS (P=0.174).

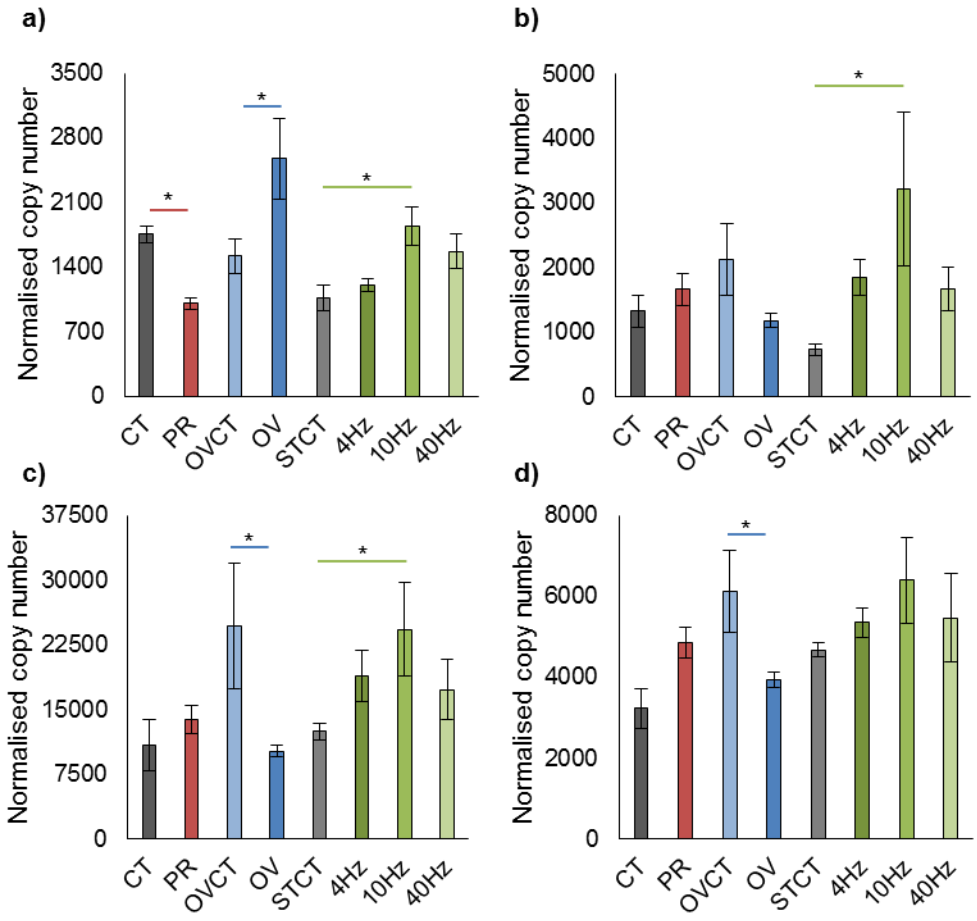

Figure 4-11. Normalised copy number for qPCR data. Absolute quantity of RNA for angiogenic genes: MMP2 (a), eNOS (b) VEGFA (c-d). Primers span regions of the gene similar to the probes used in the SurePrint G3 Rat Gene Expression v2 Microarray Kit, 8x60K, Agilent. Paired analysis for contralateral muscles, CT *vs.* PR, OV *vs.* OVCT, STCT *vs.* 4Hz, STCT *vs.* 10Hz and STCT *vs.* 40Hz. * $P<0.05$

4.5 Discussion

Physiological angiogenesis can be elicited through a variety of surgical and pharmacological interventions that target distinct signalling and morphological pathways (Egginton et al., 2001, Williams et al., 2006a, Williams et al., 2006b). The efficacy of the differential expansion in the microvascular network for local tissue demand has yet to be explored, with predominantly global indices of capillary content reported. We sought to explore the effectiveness of different muscle recruitment patterns on microvascular expansion, as well as determine changes in

oxygen supply heterogeneity following two distinct forms of angiogenesis, longitudinal splitting and capillary sprouting.

4.5.1 Blood flow kinematics

Indirect electrical stimulation allows the selective activation of different motor unit populations as well as the manipulation of muscle recruitment patterns during supramaximal stimulation. We hypothesised that 4Hz stimulation would generate peak blood flow, while 40Hz would impede flow during stimulation through vascular compression that may result in a large post-stimulation (reactive) hyperaemia response. To validate the hypothesis for use of our differential stimulation frequencies we determined muscle blood flow through an *in situ* preparation utilising a fatigue test protocol similar to Hawker & Egginton (1999). The primary difference between our protocol and that of Hawker & Egginton (1999) was their use of microspheres to measure individual hind limb flow, whereas ours used the Transonic flow probes, which provides quantitatively incomparable values, but qualitatively similar.

Fatigue index decreased with increasing stimulation frequency, while blood flow increased, with a positive linear trend in blood flow (functional hyperaemia) during stimulation at 1Hz, 4Hz and 10 Hz. Conversely, 40Hz demonstrated a modest increase in blood flow during stimulation, with a large reactive hyperaemia response following cessation of stimulus. Similar results were reported by Hawker & Egginton (1999), supporting the notion that muscle blood flow increase is primarily dependent on vasodilator metabolites that are released in proportion to muscle work (Brown, 1995, Kjellmer, 1964), to a point where the force exerted (40Hz generation of an unfused tetanus) impedes muscle blood flow through changes in intramuscular pressure or vessel stenosis. Interestingly, 10Hz stimulation demonstrated a decrease in conductance towards the latter end of stimulation, with a small reactive hyperaemia response following cessation of stimulation, suggesting some potential arterial stenosis at this frequency also.

4.5.2 Relative muscle mass

The EDL contributes approximately one fifth of the mass of the anterior hind limb compartment. Following seven days of indirect electrical stimulation there was no change in relative muscle mass across any of the stimulation frequencies. 10Hz stimulation has been shown to reduce muscle mass following protocols longer than 21-28 days (Hudlická et al., 1980, Hang et al., 1995); however, at this early stage in the remodelling our data are consistent with findings of others (Hang et al., 1995). Prazosin supplementation also showed no effect on relative muscle mass of the EDL, consistent with findings in rat (Fulgenzi et al., 1998, Ziada et al., 1989) and mice (Williams et al., 2006b). Overload training for seven days evoked a 16% increase in mass compared to the contralateral muscle, indicative of a hypertrophic response. This increase in muscle mass is comparable to similar studies of this duration (Egginton et al., 2011), where peak relative muscle mass was typically seen at 14 days.

4.5.3 Global angiogenic response

Seven days of indirect electrical stimulation at 4Hz, 10Hz and 40Hz increased C:F 46%, 49% and 37%, respectively. These increases were mimicked by changes in CD (34%, 48% and 36%, respectively), and demonstrate a robust angiogenic response independent of any changes in FCSA. 10Hz has been previously shown to induce an angiogenic response at seven days (Brown et al., 1976, Hansen-Smith et al., 1996), while 4Hz and 40Hz have not previously been tested in rodent models with supramaximal stimulation. A 24 hour stimulation protocol at 4Hz was used by Ebina et al. (2000) to match the number of stimuli delivered during an 7 hour 10Hz protocol that has been shown to have a positive angiogenic response (Hudlicka et al., 1977). In our initial development of stimulation parameters we also utilised a 4Hz protocol with an equivalent number of stimuli to that of 10Hz. These experiments resulted in a 29% increase in C:F (Fig. 4-12b), a 55% increase in CD (Fig. 4-12c), but a 17% decrease in FCSA (Fig. 4-12d) and a 10% decrease in relative muscle mass (Fig. 4-12a). Only C:F and CD were reported by Ebina et al. (2000), therefore it is difficult to establish the degree to which the angiogenic

response is physiological, or amplified by a potentially pathogenic atrophy and damage to the muscle. Therefore, we utilised a 4Hz protocol duration matched to that of 10Hz and 40Hz.

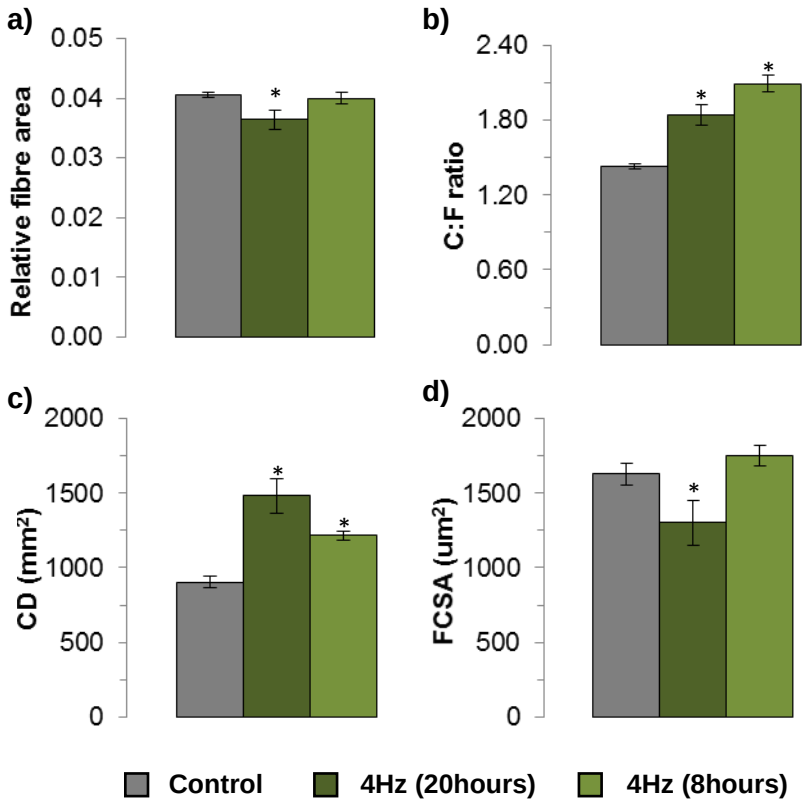

Figure 4-12. Global morphometric data for 4Hz stimulation at 20 and 8 hours duration. Relative fibre area (a), capillary to fibre ratio (b), capillary density (c) and fibre cross sectional area (d) for 7 day stimulation at 4Hz for 20 and 8 hour protocols. * $P < 0.05$ *vs.* control.

Supplementation of the vasoactive compound prazosin resulted in a 16% increase in C:F compared to control animals, however there was no significant increase in CD. This was due to the significantly higher FCSA in the prazosin-treated animals compared to control, which likely reflects the unequal animal mass between these two groups, given the prazosin group were 15% heavier than the controls. Nonetheless, there was an angiogenic response identified through the capillary to fibre ratio. The relative increase in C:F with prazosin treatment was similar to that of the overloaded animals, which also increased C:F by 16% when compared to contralateral limbs. Overload compared to control animals had a 31% higher C:F,

however the acknowledged contralateral effect within the overload model (Egginton et al., 2011) makes it appropriate to utilise the internal control for comparisons.

4.5.4 Capillary heterogeneity

All five of the tested models demonstrated a positive angiogenic response after seven days of treatment; however, there were no clear differences between the three stimulation treatments, or the shear-stress and muscle stretch model, using comparison of global indices. Utilising the area-based approach of capillary domains we analysed the heterogeneity of capillary supply, using the analysis package described in Chapter 2.

Indirect electrical stimulation, regardless of frequency, generated a similar distribution in capillaries with a leftward shift in median domain area, and reduced mean area, compared to control. The narrowing of the domain area distributions, by reducing the right hand tail, increased the proportion of capillary supply areas around the mean, becoming more Gaussian in shape, and hence more homogenous in distribution. The two differential angiogenic models, prazosin and overload, responded substantially differently. Prazosin showed no dramatic alteration in median or mean capillary domain area, with a similar distribution of capillaries to that of the control tissue, suggesting a stochastic angiogenic response underlying the positive C:F change. Conversely, overloaded muscles showed a reduced median and mean domain area, and an increasingly homogenous distribution. The decreased spatial heterogeneity seen in the stimulation and overload models suggest a functionally directed angiogenic response, with the site of neovascularisation controlled at a local level within the muscle. An improved homogeneity of capillary supply would support a more efficient diffusive exchange, hence an improved oxygen delivery capacity to the working muscle (i.e. reducing the individual capillary supply area, increasing the partial pressure difference across the supply area and the drive of oxygen to the working tissue) (Egginton, 1990a, Egginton and Ross, 1992, Egginton and Gaffney, 2010).

4.5.5 Key angiogenic markers

We have recapitulated the importance of MMP2 in the overload model of angiogenesis that is not required for prazosin driven angiogenesis (Rivilis et al., 2002, Williams et al., 2006a) and while the eNOS derived data was not significant its direction was in line with previous findings (Williams et al., 2006a, Williams et al., 2006b). The most interesting trend within the data was the increasing MMP2 mRNA content in the higher stimulation frequencies (10Hz and 40Hz) compared to 4Hz, with the inverse relationship for eNOS. These data may suggest a larger proportion of the microvascular expansion in 4Hz is through longitudinal splitting while 40Hz is through extra-cellular matrix remodelling driven by sprouting microvasculature (Williams et al., 2006a, Egginton et al., 2001). The up-regulation of VEGF across all the angiogenic models is consistent with previous findings and supports its integral role in physiological angiogenesis (Williams et al., 2006c).

4.5.6 Differential angiogenic response

We have demonstrated that three distinctly different stimulation parameters all evoke a large angiogenic response, irrespective of their blood flow kinetics and tension generation fatigue response. The local capillary distribution appears to suggest a similar response across the three frequencies, inferring an equally improved capacity to deliver oxygen. High frequency stimulation at threshold for glycolytic fibre recruitment has shown to evoke an angiogenic response without changes in capacity of oxidative metabolism (Brown et al., 1976, Egginton and Hudlicka, 2000). This may serve to improve metabolic by-product removal rather than substrate delivery. While low frequencies of stimulation demonstrated a modest increase in citrate synthase after just 7 days of stimulation, alongside the pronounced angiogenic response and improved resistance to fatigue (Brown et al., 1976, Hudlicka et al., 1982, Simoneau et al., 1993). In this case, the early increase in fatigue resistance arising independent of changes in oxidative enzyme activity may be as a result of directed vascular growth in regions of high mitochondria density (typically regions with small domains), suggesting adaptation driven by local oxidative capacity (Bosutti et al., 2015).

Angiogenesis induced by prazosin is nitric oxide dependent and driven by an increase in vascular shear stress (Williams et al., 2006b). The fine structure changes in capillaries have shown longitudinal divisions of vessel lumen to produce new functioning capillaries, with an orientation of daughter vessels in the same direction as existing vessels (Egginton et al., 2001). Given the low mitotic drive of this form of angiogenesis, having a low cellular turnover rate, it has been suggested to be an efficient form of microvascular expansion that is also highly reversible (Egginton et al., 2001, Egginton et al., 2016). Pharmacologically-induced vasodilatation has been suggested as a potential short-acting angiotherapy, but the efficacy of the new microvasculature has yet to be explored (Egginton et al., 2016). It could be argued that the angiogenic potential has not been exhausted, as it typically takes 14 days to reach peak C:F. The 'completed' angiogenic response may result in an overall more homogenous distribution of capillaries and capacity to supply oxygen (Egginton et al., 2016, Williams et al., 2006b, Egginton et al., 2001), however, gene responses and mitotic activity associated with capillaries declines within a few days, suggesting induction of a stereotypic cascade of events following angiogenic stimulation. This would imply that while neovascularisation may continue between 7 and 14 days, however this is unlikely to change the domain area and distribution of the new microvessels enough to improve the functional capacity of the muscle.

Conversely, microvascular expansion through muscle stretch (overload) results in proliferation of endothelial cells and basement membrane degradation, allowing sprouting filopodia to direct vessel formation (Rivilis et al., 2002, Egginton et al., 2001, Egginton et al., 2011). The increased homogeneity of microvascular distribution within our overload model appears to have preceded increases in FCSA. The overload response is typically maximised at 14 days, along with muscle hypertrophy (Baldwin et al., 1981, Frischknecht and Vrbová, 1991, Degens et al., 1993, Egginton et al., 2011), however at 14 days the overloaded EDL does have an improved fatigue resistance compared to control and prazosin supplemented

animals (George, 2012). This may in part be explained by more homogeneous distribution of capillary supply, improving oxygen or other substrate delivery.

4.5.7 Conclusions

The different forms of angiogenesis, shear stress induced longitudinal splitting *vs.* lumen stretch induced sprouting, have further distinctive features through their spatial distribution of the expanded microvasculature. Shear stress-induced angiogenesis suggests a stochastic response, not reliant on local tissue feedback, while sprouting angiogenesis appears to be controlled at the local tissue level, likely improving global oxygen delivery capacity through reduced capillary supply areas. Utilising indirect electrical stimulation at a supramaximal level, as a model of differential muscle activity patterns, is able to generate similar levels of angiogenesis, while simultaneously improving the local capillary density and oxygen delivery status of the tissue. Given the dissimilar force and hyperaemia responses of the three stimulation parameters, we believe that the angiogenic driving stimuli differ, particularly between the high and low frequencies.

As we have developed morphometric analysis that accommodates both global and local changes in capillarity with respect to fibre type, we explored the skeletal muscle response to an extreme locomotory challenge, in the form of spinal cord injury.

5 Combined epidural stimulation and locomotor training improves skeletal muscle microvascular remodelling in rats with spinal cord injury

5.1 Abstract

The morphological characteristics of skeletal muscle distal to a spinal cord injury (SCI) undergo dramatic phenotypic and microvascular changes, which vary with location and degree of trauma. Here we utilise a contusion model of SCI at T9-10 in adult female Sprague Dawley rats. SCI animals received eight weeks intervention: cage-control SCI (CGCT), epidural stimulation (ES), locomotor training (TR) or combination of the two (CB). Muscle fibre phenotype and local capillary supply area were determined for the *tibialis anter*ior muscle (TA). SCI induced a significant shift in Type II fibre phenotype from oxidative to glycolytic ($P<0.05$) as well as rarefaction of the capillary bed within both the oxidative core and glycolytic cortex, compared to intact weight matched controls (decreased C:F and CD, $P<0.05$). Microvascular pruning reduced capillary spatial heterogeneity, while increasing mean domain area, with a normalising of local capillary supply per fibre area (LCD) across all three fibre types. ES and TR showed no angiogenic response across the TA, while their capillary rarefaction and hypertrophic remodelling further reduced local capillary supply to glycolytic fibres, further decreasing oxygen supply capacity of the muscle. Conversely, CB treatment increased C:F in the core and cortex, by 31% and 18%, respectively (CB *vs.* CGCT, $P<0.05$). The angiogenic response improved capillary homogeneity in the core and cortex, while decreasing the mean capillary domain area in both compartments. This suggests targetted angiogenesis around glycolytic fibres, as local capillary to fibre ratios (LCFR) increased significantly in Type IIa and IIb fibres, compared to CGCT animals. There appears to be an important role for weight bearing locomotor training in maintaining oxidative fibre composition, and in combination with ES there is a better maintenance of glycolytic capillary supply area than in standalone treatments.

5.2 Introduction

Spinal cord injury (SCI) is a traumatic life changing injury, associated with neurological impairment and paralysis of skeletal muscles that are innervated caudal to the lesion site. Following spinal cord injury there is a dramatic atrophying of skeletal muscle in both animals (Durozard et al., 2000, Hiraizumi et al., 1990, Landry et al., 2004) and humans (Lotta et al., 1991, Castro et al., 1999, Round et al., 1993). This reduction in muscle mass is accompanied by a phenotypic shift from an oxidative, fatigue resistant muscle to a highly glycolytic, fatigable muscle (Otis et al., 2004, Hutchinson et al., 2001, Huey et al., 2001). In addition, rarefaction of the microvascular bed within the muscle reduces its capacity to deliver oxygen and fuel, and is correlated with reduced fatigue resistance (Borisov et al., 2000, Crameri et al., 2002). These morphometric and functional outcomes are consistent across a variety of animal models and SCI in humans. However, the time course and severity of these changes appear to differ according to the animal model used (Biering-Sørensen et al., 2009), which may have important implications for the translational potential of these data.

The categories for human SCI comprise of solid cord injury, contusion injury, laceration and massive compression (Bunge et al., 1993, Norenberg et al., 2004). Solid cord injury involves the degradation of internal architecture and demyelination while no evidence of trauma is visible on the dura. Contusion, similarly shows no damage to the surface but there are large areas of cord haemorrhage and necrosis. Contusion injuries are the most common type of SCI in humans and the second most commonly used animal model. Lacerations are typically cuts to the surface, while complete spinal transections are the most commonly used animal models but are rarely seen in human cases. Finally, massive compression injury is typically generated through traumatic crush of the cord that results in large maceration of the centre, which is replaced with large volumes of scar tissue. Efforts are being made to design strategies to improve recovery of voluntary control of movement, and preserving the functional capacity of locomotory muscle.

Locomotor training has been shown to evoke neural plasticity and ameliorate the loss in muscle mass and function in SCI humans (Crameri et al., 2002, Giangregorio et al., 2006) and animals (Dupont-Versteegden et al., 2000, Roy et al., 1999, Roy et al., 1998). Treadmill locomotor training also has been shown to improve microvascular supply in denervated skeletal muscle of animals (Jakubiec-Puka et al., 2008) suggesting an additional, potentially beneficial adaptation for physical activity during treadmill training in SCI. Functional electrical stimulation involves the direct stimulation of skeletal muscle, which has been shown to reverse changes in the muscle phenotype shift seen in SCI and restore microvascular supply (Rochester et al., 1995). However, this method has limited benefit in the recovery of spinal circuits involved in locomotion. An alternative approach is direct stimulation of the spinal cord surface, epidural stimulation (ES). This has been shown to elicit hind limb stepping in a rhythmic, locomotor fashion, in both animals (Gerasimenko et al., 2003, Ichiyama et al., 2005, Iwahara et al., 1991) (Iwahara et al., 1991) and humans (Minassian et al., 2004). An advantage of ES compared with direct muscle stimulation is that it allows a more natural, coordinated recruitment of synergistic muscle groups, thus inducing less muscle fatigue (Bamford et al., 2005). Although ES can effectively improve locomotor function, its ability to modulate skeletal muscle phenotype and microvascular supply has not been determined.

These strategies as standalone treatments have their own distinct adaptive benefits, and therefore pose a strong argument for the use as a combination therapy to utilise the different adaptive mechanisms. Patients given the combination of ES and voluntary movement were able to recover intentional movement and fine movement control in paralysed muscles (Angeli et al., 2014). The combination of ES with locomotor training can synergistically reinforce specific sensorimotor pathways, resulting in a more selective and stable network of neurons that control locomotion. This may provide an enhanced neural stimulus to improve locomotor function, and thus increase the mechanical loading on skeletal muscles. Local feedback mechanisms may then potentiate the modulatory effects

on phenotype and microvascular supply, helping to restore the oxidative capacity of skeletal muscles.

The morphometric, contractile and functional capacity of muscle in SCI has been well characterised in both humans and animal models, however, the variety of experimental treatments have yet to be similarly examined. In this study we determined the phenotypic transformation of skeletal muscle in response to epidural stimulation and treadmill locomotor training, individually and in combination. In addition, we quantified muscle capillary content, as atrophy within SCI likely produces microvascular rarefaction but the need to induce angiogenesis during treatment has been overlooked. As commonly used measures are scale-dependent, we applied local capillary analysis to incorporate fibre area and quantify the supply area of individual capillaries. We hypothesised that the application of a single training stimulus would reduce the degree of fibre atrophy, and alleviate the decrease in global and local capillary supply. We reasoned the combination of both treatments would have an additive response, and hence improve capacity for routine physical activity that is fundamental to quality of life.

5.3 Material and methods

5.3.1 Ethical approval

Twenty out-sourced (Charles River) female adult Sprague Dawley rats were used, with body mass at experimentation ranging from 210-240g. Animals were individually housed on a 12 hour light/dark cycle with *ad libitum* access to food and water. All animal procedures were approved by the University of Leeds Animal Welfare and Ethics Committee, in accordance with UK Animals (Scientific Procedures) Act 1986.

5.3.2 Overview of experimental timeline

All animal surgery, training and husbandry were completed by Dr Yazi Al'Joboori and followed the experimental timeline in Fig. 5-1. Briefly, animals received a

severe contusion injury and implantation of epidural electrodes during week one. Animals were then randomly assigned to experimental treatment groups; cage control (CG), training only (TR), epidural stimulation only (ES) or a combination of both TR and ES (CB). Training was initiated one week following SCI and continued for eight weeks. Following the allotted training, various kinematic and electrophysiological measures were made over a three week period, followed by animal sampling. Intact weight matched controls (CT) were also used to compare the effect of SCI on baseline physiological factors.

Figure 5-1. Experimental timeline for SCI and locomotor training.

5.3.3 Spinal cord injury

Animals were anaesthetised with Isoflurane: 5% IsoFlo® at 2 $L.min^{-1}$ O_2 flow (0.4 $L.min.Kg^{-1}$) induction, and maintained with 2.5% (0.20 $L.min.Kg^{-1}$) throughout surgery. An incision was made from ~T4 to ~S5 and cleared of fascia and muscle around the laminectomy site. Partial laminectomies were performed at vertebral levels of the contusion (T10), and epidural implant sites (T12/13 and L2). A severe midline contusion injury was made at T9/10 (Scheff et al., 2003) using the Infinite Horizon impactor at 250kdyn (Precision Systems & Instrumentation, Lexington, KY, USA). This imitates the type of crush injury seen in e.g. road traffic accidents. All SCI animals within this study received a microinjection of lentiviral chondroitinase immediately after contusion, an enzyme designed to break down extracellular matrix molecules that inhibit axon growth.

5.3.4 Epidural stimulation

Stimulation was delivered *via* stainless steel wires (AS632, Cooner Wire, Chatsworth, CA, USA) implanted in the midline of the spinal cord facing the dorsal aspect over segments L2 and S1. The wires were secured with sutures (Ethilon 9.0, Ethicon) either side of the notch to the spinal dura, and a common ground wire inserted into paravertebral muscle and also sutured into place. The implanted wires were connected to a skull mounted head plug, and stimulation was delivered *via* a stimulation (S88X stimulator; Astro-Med®, Inc. Grass instruments, Middleton, WA, USA) and isolation unit (SIU-V Isolation unite; Astro-Med®, Inc. Grass instruments, Middleton, WA, USA). Continuous rectangular pulses (200 μs in duration at 40 Hz, with no delay) were used (Ichiyama et al., 2005, Ichiyama et al., 2008a, Ichiyama et al., 2008b) with a sub-threshold voltage sufficient to stimulate a full range of motion.

5.3.5 Locomotor training

All animals undergoing locomotor training on a small animal treadmill were secured to a custom-made jacket to provide body weight support, and allow for manipulation of training from a bipedal-to-quadrupedal stepping. Bipedal-to-quadrupedal training was used based on findings from pilot research in the Ichiyama laboratory (*unpublished.*) showing rats trained in the quadrupedal position attempt fewer steps (reaching speeds of 5-9 $cm.s^{-1}$) with their hind limbs compared to rats trained in the bipedal-to-quadrupedal regime where they could reach speeds of 14-16cm/s. Training in both orientations maximises the use of hind limbs during the session. Training took place for 20 minutes a day (10 minutes stepping, 10 minutes rest, 10 minutes stepping) five days a week for eight weeks.

5.3.6 Muscle sampling

Spinal cord injury animals were sacrificed using a terminal dose of pentobarbital by intra-peritoneum injection, while control intact animals received cerebral concussion and cervical dislocation. The tibialis anterior (TA) were dissected from

the anterior hind limb compartment and the muscle mid-belly snap frozen in liquid nitrogen cooled isopentane. Tissue blocks were stored at -80°C until cryosectioning.

5.3.7 Muscle preparation and immunohistochemistry

Serial cryostat sections (10µm) were cut at -20°C and attached to polysine coated slides (VWR international), and stored at -20°C until staining. Muscle fibre types were distinguished using two monoclonal anti-MHC antibodies (Appendix 1) (Developmental Studies Hybridoma Bank, University of Iowa): BA-D5 (1:1000 dilution) for Type I fibres (slow MHC) labelled with Alexa Fluor 555 Goat Anti-Mouse IgG (1:1000 dilution) (Life Technology, A21422) and SC-71 (1:500 dilution) for Type IIa (fast oxidative, glycolytic) labelled with Alexa Fluor 488 Rabbit Anti-Mouse IgG (1:1000 dilution) (Life Technology, A11059). The remaining unstained fibres are considered to be Type IIb (fast glycolytic), validated by use of BFF3 antibody (Developmental Studies Hybridoma Bank, University of Iowa) (Andersen et al., 2014, Soukup et al., 2002). Muscle fibre boundaries were labelled with an anti-laminin antibody (1:250 dilution) (Sigma, L9393), a glycoprotein integrated in the basement membrane. Biotinylated against with Anti-Rabbit IgG (1:250 dilution) (Vector Labs, BA1000) and Streptavidin, Pacific Blue Conjugate (1:250 dilution) (Life Technology, S11222). Capillaries were simultaneously identified using *Griffonia simplicifolia* lectin-1 (1:250 dilution) (Vector Laboratories, UK) due to its binding affinity to proteoglycans in the glycocalyx of microvessels.

5.3.8 Morphometric analysis

Two metabolically distinct regions within the TA were studied, the oxidative core and the glycolytic cortex, utilising five fields of interest each 0.145 mm^2 (Fig. 5-2). Utilising the immunohistochemical protocol developed in Chapter 2, global morphometric indices for capillary (C:F, CD) and fibre type composition (FCSA, numerical and areal composition) were generated. Subsequently, the local

geometric tissue supply regions (capillary domain area) and fibre-specific supply area were generated using the oxygen transport modelling software (Chapter 2).

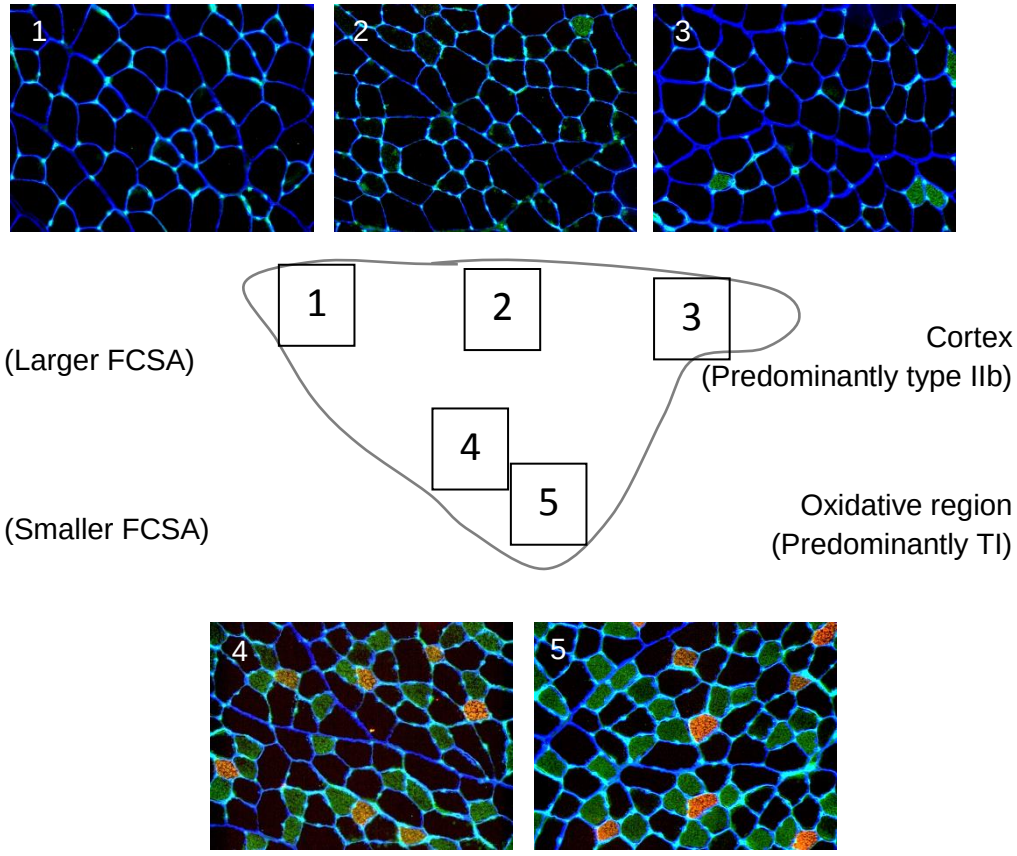

Figure 5-2. Transverse cross-section of the TA illustrating location of the systematic sampling regions used for histological analysis. The heterogeneous fibre type and capillary supply allows for regional analysis of two metabolically distinct areas where regions 1-3 are contained within a glycolytic cortex, and 4-5 are in a highly oxidative core. Heterogeneity of fibre composition is illustrated by representative immunohistological images. FCSA, fibre cross sectional area.

5.3.9 Statistical analysis

All data are expressed as mean ± S.E.M. (*n*) with figures generated in Igor Pro 6.22A (WaveMetrics). A one-way analysis of variance (ANOVA) was used to determine differences between groups, using Tukey post-hoc testing for individual

comparison when there were significant differences, set at $P < 0.05$. Least-squares regression slopes showing the relationships between; LCFR *vs.* FCSA and LCD vs. FCSA, were determined for pooled data, and the significance of these slopes were calculate as described by (McFarlane et al., 2016). Group numbers are distributed accordingly: CT (*4*), CG (*4*), CB (*4*), TR (*5*) and ES (*3*).

5.4 Results

5.4.1 Global angiogenic response to spinal cord injury

Twelve weeks of SCI resulted in a significant decrease in C:F in both the core (1.54 ± 0.04 *vs.* 2.14 ± 0.07, $P<0.001$) and cortex (1.27 ± 0.06 *vs.* 1.57 ± 0.02, $P=0.001$), for CG *vs.* CT (Fig. 5-3a,d). CD was also significantly decreased in the two regions of the TA, with no significant difference in FCSA (Fig. 5-3). TR and ES had significantly decreased C:F compared to CT in the core, while only TR remained significantly lower in the cortex ($P=0.032$); CD was significantly decreased in both the core and cortex following TR and ES (Fig. 5-3b,e). CB treatment showed a significant angiogenic response, with a C:F close to that of CT, significantly increasing in the core (2.03 ± 0.04, $P=0.002$) and cortex (1.50 ± 0.06, $P=0.01$) *vs.* CG. The increase in C:F was not mirrored by a change in CD, while MFA showed a modest but not significant increase in both the core (*P=0.510)* and cortex (*P=0.157)*, *vs.* CT (Fig. 5-3c,f).

5.4.2 Fibre type composition following SCI

Numerical fibre type composition in the CG core showed a significant decrease in Type IIa fibres (0.20 ± 0.02 *vs.* 0.40 ± 0.03, $P=0.002$) and increase in Type IIb (0.75 ± 0.03 *vs.* 0.57 ± 0.04, $P=0.038$), compared to CT (Fig. 5-4). This shift in numerical composition was mirrored in the changes in relative fibre area, while there were no significant changes in mean fibre size. TR and ES both showed significant decreases in core numerical Type IIa fibre composition, with slight increases in Type I and IIb when compared with intact animals. CB therapy displayed similar significant decreases in Type IIa numerical composition

compared to CT, however there was a significant increase in numerical and areal density for Type I compared to CT and CG (Fig. 5-4b, c).

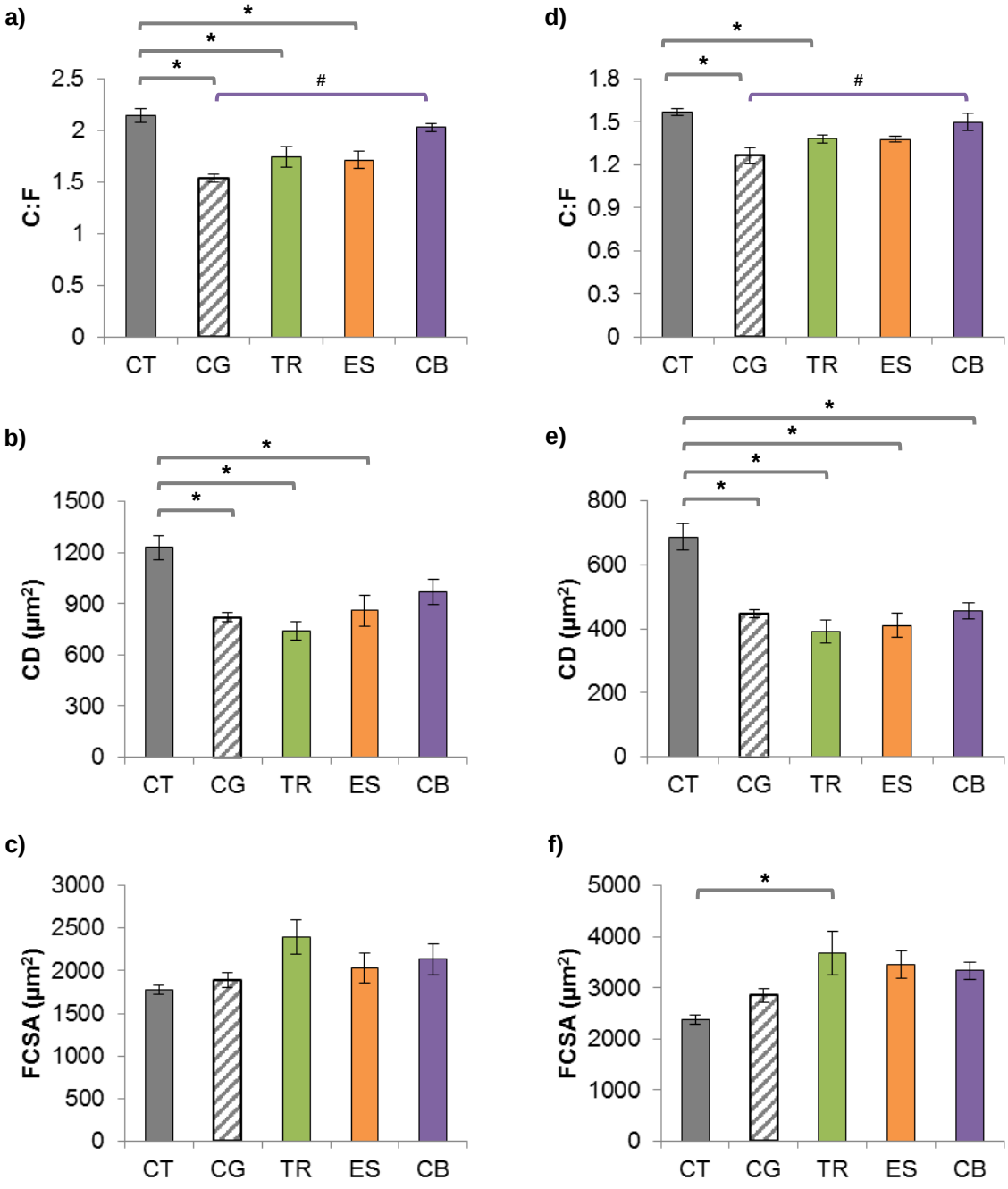

Figure 5-3. Global angiogenic response to SCI and locomotor treatment in the TA core and cortex. Capillary to fibre ratio, capillary density and fibre cross sectional area are provided for the core (a, b, and c) and the cortex (d, e, and f), respectively. * $P<0.05$ *vs.* CT, # $P<0.05$ *vs.* CG

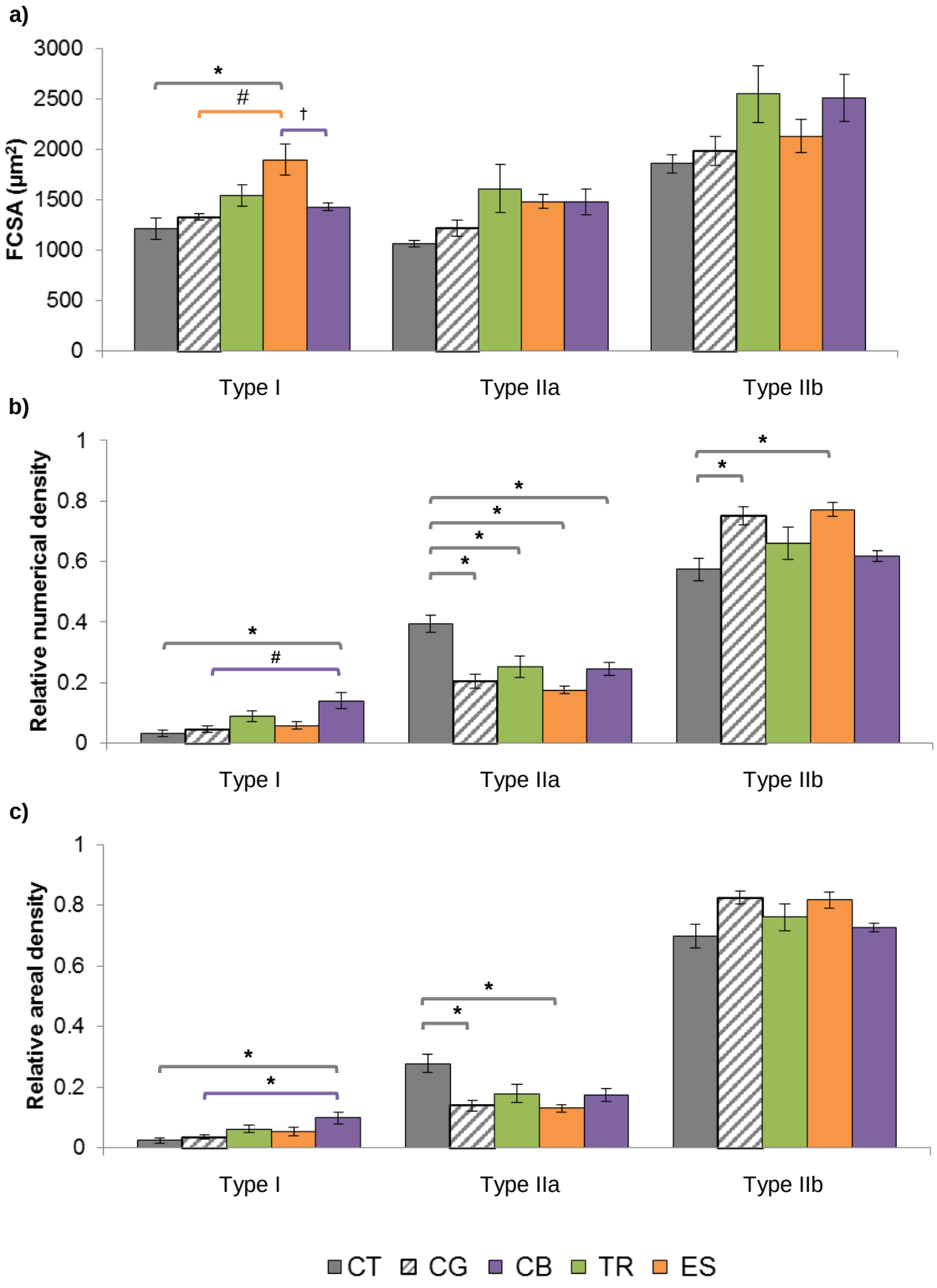

Figure 5-4. Fibre type composition of the TA core. Fibre type specific changes for average area (a), relative numerical density (b) and relative areal density (c). * P<0.05 vs. CT, # P<0.05 vs. CG, † P<0.05 vs. CB.

5.4.3 Capillary domains

The frequency distribution displays a large right shift in median capillary domain area for CG animals compared with CT, 1146.1μm^2 *vs.* 712.3 μm^2 and 2110.5 *vs.* 1203.0 μm^2, for the core and cortex, respectively (Fig. 5-5). The shift in distribution corresponds with a significant reduction in the LogSD for the core (0.13 ± 0.004 *vs.* 0.15 ± 0.01, *P*=0.034) and cortex (0.13 ± 0.01 *vs.* 0.20 ± 0.01, *P*<0.001) (Fig. 5-5). Neither individual treatment (TR or ES) altered the capillary domain distribution in relation to CG, with equivalent median capillary domain areas across both core and cortex (Fig. 5-5a,b). Capillary heterogeneity in the TR group significantly increased in the core relative to CG (0.16 ± 0.004 *vs.* 0.13 ± 0.004, *P*=0.001; Fig. 5-5c,d), while in the cortex both TR and ES were not significantly different from CG. The CB group demonstrated a leftward shift towards CT, with an intermediate median capillary domain area situated between CB and CG (Fig. 5-5a,b). The heterogeneity of the CB group was significantly reduced in the core when compared to CT, TR and ES, while only maintaining a significantly reduced LogSD in the cortex compared with CT (Fig. 5-5c,d).

5.4.4 Local capillary supply

LCFR and LCD for the major fibre type compositions in the core and cortex of the TA are presented in Table 5-1, with correlative representations presented in Figure 6-6. Local capillary supply was significantly reduced in CG compared to CT, with lower LCFR and LCD across the three fibre types within the core (all, *P*<0.02*),* and in the cortex Type IIb LCFR decreased (*P*=0.344) with LCD (*P*<0.001). Following TR, the LCFR and LCD remained significantly decreased for the three major fibre types in the core, as well as the Type IIb fibres in the cortex, when compared to CT with no significant improvement relative to CG. The ES training attenuated some of the reductions in LCFR across Type I and IIa fibres, while LCD remained significantly reduced across the core and cortex, compared to CT. The CB treatment group showed re-establishment of local capillary supply compared to CG, with similar LCFR values for Type IIa fibres in the core (1.57 ± 0.08 *vs.* 1.54 ± 0.04, *P*=0.999), Type IIb in the core (2.36 ± 0.07 *vs.* 2.34 ± 0.02, *P*=0.919) and

Type IIb fibres within the cortex (1.67 ± 0.04 *vs.* 1.42 ± 0.06, *P*=0.107) to that of CT.

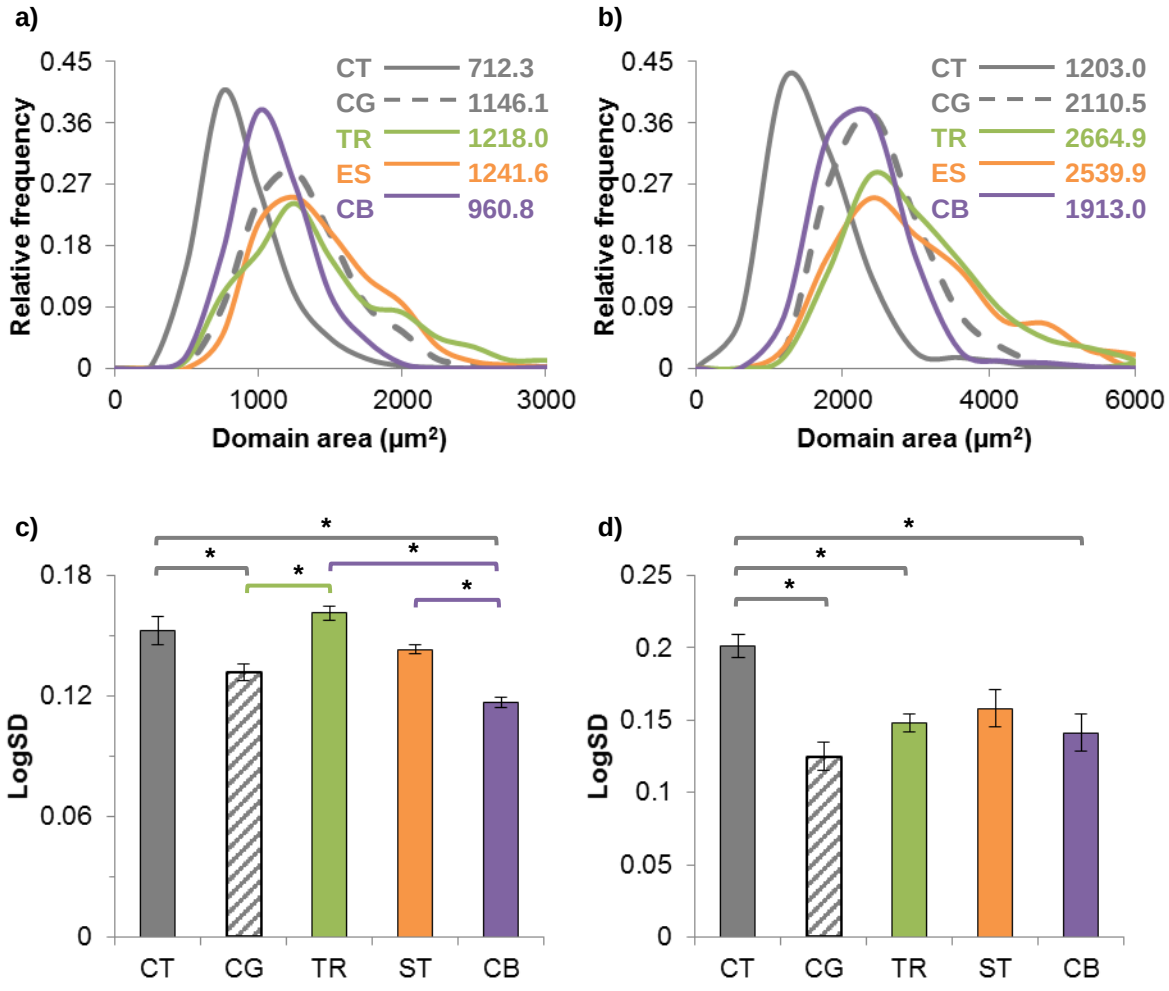

Figure 5-5. Capillary domain distribution and heterogeneity for TA core and cortex. Frequency distribution for capillary domain areas and capillary heterogeneity presented as LogSD for the core (a, c) and cortex (b, d), respectively. Inset values are median capillary domain area. * *P*<0.05 *vs.* CT, # *P*<0.05 *vs.* CG, † *P*<0.05 *vs.* CB.

The correlative data for local capillary supply (LCFR and LCD) relative to FCSA showed significant shifts across all fibres types following SCI (all, *P*<0.05). ES alone was unable to returning the correlation of LCFR and LCD to levels in intact animal, while TR further disjointed the typical relationship between capillary supply area and FCSA (Fig. 5-6, Table 5-2). The CB treatment rectified the relationship across Type IIa fibres, but while Type IIb LCFR was normalised (*P* = n.s., *vs.* CT and *vs.* CGCT), LCD was not (*P*<0.05, *vs.* CT and *vs.* CGCT).

Table 5-1. Comparison of local capillary data for individual fibre types within the TA core and cortex

	Core						Cortex	
	Type I LCFR	**Type IIa LCFR**	**Type IIb LCFR**	**Type I LCD**	**Type IIa LCD**	**Type IIb LCD**	**Type IIb LCFR**	**Type IIb LCD**
CT	1.85 ± 0.24	1.54 ± 0.04	2.34 ± 0.02	1540.2 ± 111.7	1456.4 ± 50.7	1244.9 ± 54.2	1.42 ± 0.06	802.9 ± 44.2
CG	1.15 ± 0.05 *	1.03 ± 0.08 *	1.65 ± 0.12 *	868.0 ± 65.1 *	858.6 ± 28.0 *	844.8 ± 30.3 *	1.24 ± 0.08	452.5 ± 9.9 *
TR	1.08 ± 0.11*	1.11 ± 0.13 * †	1.61 ± 0.12 * †	714.0 ± 81.8 *	752.6 ± 126.3 *	690.9 ± 96.0 *	1.07 ± 0.07 * †	338.8 ± 38.5 * †
ES	1.54 ± 0.09	1.12 ± 0.08 †	1.57 ± 0.12 * †	820.0 ± 20.5 *	752.8 ± 29.3 *	749.5 ± 46.8 *	1.11 ± 0.05 * †	364.4 ± 60.1 *
CB	1.42 ± 0.10	1.57 ± 0.08 #	2.36 ± 0.07 #	993.5 ± 70.8 *	1073.8 ± 71.1 *	959.6 ± 60.4	1.67 ± 0.04 #	525.74 ± 31.8 *

* $P < 0.05$ *vs.* CT, # $P < 0.05$ *vs.* CG, † $P < 0.05$ *vs.* CB.

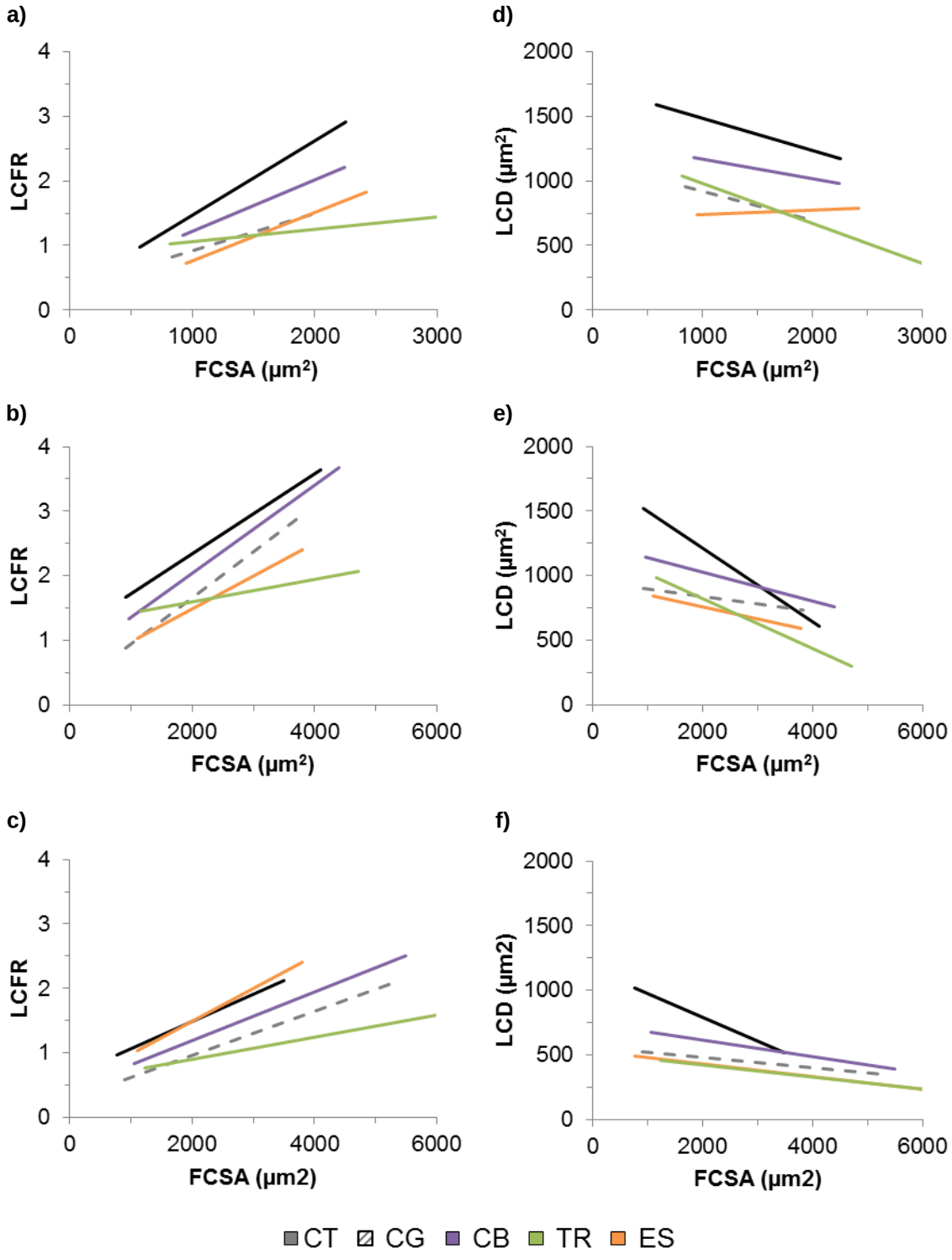

Figure 5-6. Local capillary supply differentiated by fibre type. LCFR and LCD presented for Type IIa fibres in the core (a, d), Type IIb fibres in the core (b, e) and Type IIb in the cortex (c, f). Lines represent least-squares regression fitted to all data points; note the deviation from normal allometric scaling with TR.

Table 5-2. Correlation coefficients for local capillary supply data presented in Figure 6.

		Core				Cortex	
		Type IIa LCFR	**Type IIb LCFR**	**Type IIa LCD**	**Type IIb LCD**	**Type IIb LCFR**	**Type IIb LCD**
CT	b	0.0012	0.0006	- 0.2478	- 0.2854	0.0004	- 0.1854
	a	0.3193	1.0929	1731.8	1780.1	0.6403	1161.7
	R^2	0.399	0.303	0.033	0.228	0.276	0.199
CG	b	0.0006 *	0.0007	- 0.2257	- 0.0578 *	0.0003 *	- 0.0402 *
	a	0.3463	0.2424	1141.9	957.2	0.2844	564.2
	R^2	0.288	0.526	0.0842	0.035	0.525	0.096
TR	b	0.0002 * # †	0.0002 * # †	- 0.3065	- 0.1912 * # †	0.0002 * # †	- 0.0454 *
	a	0.8586	1.2439	1284.8	1202.3	0.5578	511.0
	R^2	0.053	0.070	0.249	0.321	0.260	0.217
ES	b	0.0007 *	0.0005 # †	- 0.0334	- 0.0931 *	0.0005 * # †	- 0.0494 *
	a	0.0105	0.4784	703.4	946.7	0.4784	531.0
	R^2	0.353	0.406	0.002	0.088	0.406	0.156
CB	b	0.0008	0.0007	- 0.1522	- 0.1118 *	0.0004	- 0.0634 * #
	a	0.4294	0.6671	1323.1	1250.5	0.4331	738.5
	R^2	0.323	0.595	0.033	0.140	0.580	0.229

b, slope coefficient; a, y-axis intersect; R^2, Coefficient of determination. LCFR, local capillary to fibre ratio; LCD, local capillary density. * $P < 0.05$ *vs.* CT, # $P < 0.05$ *vs.* CG, † $P < 0.05$ *vs.* CB.

5.5 Discussion

This study sought to characterise the phenotypic change in skeletal muscle fibre type composition and microvascular supply following SCI, and how to optimise the use of potential therapeutic interventions to ameliorate these changes. We examined the TA muscle due to its importance in hind limb locomotion, as well as its distinct metabolic regions defined by the oxidative core and glycolytic cortex. CB treatment restored microvascular supply near to that of intact animals, while individual treatments alone did not. Locomotor training appears to have a greater effect on FCSA, resulting in a shift in allometric scaling of local capillary supply. Overall, CB treatment best improved microvascular supply, shifting capillary distribution back towards intact levels, and best maintained the oxidative phenotype of the muscle, compared to individual treatments alone.

5.5.1 Global microvascular morphometrics

Regional comparisons within the TA muscle have shown rarefaction of capillaries following a 250kdyn contusion injury; this reduced number of capillaries combined with a well maintained FCSA resulted in a 35% decrease in CD across the muscle, and suggests an impaired functional aerobic capacity of the TA. Standalone treatments of ES or locomotor training showed no observable changes in capillary content, while the hypertrophic response within the core and cortex further reduced CD. However, the combination of these training modalities was sufficient to evoke an angiogenic response within both the oxidative and glycolytic compartments of the TA, although the global hypertrophic response reduced the functionally relevant CD. It is important to be aware of potentially conflicting inferences made depending on the global measures examined (C:F *vs.* CD, as discussed in the Chapter 1). The combination of treatments appears to ameliorate the capillary rarefaction that result from SCI, but understanding the functional relevance of the angiogenic response cannot be inferred from the CD alone (Egginton, 1990a).

5.5.2 Muscle phenotype

Muscles typically begin to atrophy a few days after SCI, and vary in atrophying response dependent on initial muscle phenotype, and injury type (Biering-Sørensen et al., 2009). The time course and degree of atrophy within SCI models differs greatly, with complete transections generating the greatest level of atrophy, followed by contusion (Biering-Sørensen et al., 2009). Oxidative fibres typically atrophy prior to glycolytic muscle fibres, and normalise at different times (Durozard et al., 2000, Landry et al., 2004), with some returning back to control levels after 6-8 weeks (Durozard et al., 2000). This highlights a benefit of using the TA muscle and its two distinct compartments for histological analysis, as we are able to characterise metabolically distinct fibre regions and their response within one functionally integrated muscle.

Following 11 weeks of recovery the average fibre cross sectional area in our study did not differ from weight matched intact animals. There was a clear shift in core phenotype to an increasingly glycolytic form, through a reduction in Type IIa fibres, and increased Type IIb. All three treatment groups showed a global hypertrophic response within the two portions of the TA. ES showed a transformation of Type IIa fibres to Type IIb, with Type I numerical composition being maintained. This decrease in number dramatically reduced the overall oxidative proportion of the TA core. Conversely, locomotor training and the combination therapy better maintained oxidative composition with higher numerical and areal densities of Type I and IIa fibres. This may suggest an integral role for weight bearing training and afferent stimulation of normal locomotion in order to maintain oxidative phenotype. Interestingly, no fibre type clustering was observed across any of the SCI groups, as typically seen in muscle re-innervation following motor nerve damage and aging (Holloszy and Larsson, 1995), this is due to maintained neural activation during paralysis through the incomplete contusion injury (Hutchinson et al., 2001).

5.5.3 Local capillary supply

Heterogeneity in capillary spacing differs greatly between the two portion of the TA, with the core having a lower average capillary domain area and narrower distribution (Egginton, 1990a) as also demonstrated in Chapter 2, conditions known to optimise oxygen diffusion (Egginton and Gaffney, 2010). The summed proportion of capillary domains normalised to fibre area (LCD) demonstrate that capillary supply is higher in oxidative fibres than glycolytic (Gray and Renkin, 1978) irrespective of fibre size (Gray and Renkin, 1978, Egginton and Ross, 1989, Degens et al., 1992) in the intact control animals. Capillary rarefaction induced by SCI decreases capillary heterogeneity, and appears to predominantly target glycolytic fibres, generating an overall lower LCD to that seen in intact mixed muscle phenotypes (Egginton and Ross, 1989, Degens et al., 1992).

The apparent rarefaction of capillaries within the core of epidural stimulated animals was not accompanied by any decrease in capillary heterogeneity, despite an increase in average domain area, likely due to an increase in fibre area within the core. Conversely, capillary rarefaction in the cortex produced a more homogenous distribution, despite the increase in capillary domain area and FCSA. The universal effect of ES across the TA was a further reduced LCD for glycolytic fibres. Locomotor training increased capillary domain area across both the core and cortex, and maintained a normal level of heterogeneity of capillary distribution within the core, despite a severe rarefaction. Maintaining the heterogeneity retained the intact relationship of LCD within oxidative fibres, but the predominant hypertrophy effect across glycolytic fibres further reduced the proportion of oxygen supply by capillaries to levels below that of SCI animals. It is interesting to note that the increase in FCSA in the cortex occurred in conjunction with a more homogeneous distribution of capillaries, which is likely due to a normalisation of glycolytic fibre area.

The simultaneous application of epidural stimulation and locomotor training proved to be the most promising in improving oxygen transport kinetics. Through maintenance of oxidative phenotype and targetted angiogenesis the combination

therapy was sufficient to shift the distribution of capillary domains closer towards intact levels, reducing both average domain area and heterogeneity of supply. The increased LCFR across all fibre types compared to SCI animals supports the presence of angiogenesis, and might suggest a feedback drive to improve oxidative capacity across the muscle in response to impaired locomotor capacity.

5.5.4 Conclusions

There are very few data on the angiogenic response of SCI and that of therapeutic interventions within skeletal muscle. This is in part because the primary driving outcomes for the SCI research are looking at the potential for neuronal sprouting and connectivity of spinal circuitry, and the reestablishment of locomotory function, not necessarily the functional capacity of the muscles. To this point I have not discussed any issues with the experimental design of this study. Exercise training was completed at week nine, followed by three weeks of kinematic, electrophysiological and behavioral testing. During this time no further training intervention was delivered, and it's very likely that there is a detraining/reverting of training effects within the plastic skeletal muscle. Therefore it is likely we are underestimating the effectiveness of the various interventions, nevertheless there were some maintained adaptive remodelling worth discussing.

There are clear differences in adaptations with the two standalone treatments. Epidural stimulation does not rectify the glycolytic shift seen with SCI, whereas locomotor training appears to alleviate it. Neither ES nor TR were sufficient to evoke an angiogenic response, and fibre hypertrophy further reduced CD across the muscle. The individual treatments increased the heterogeneity of capillary supply across the TA compared to that in SCI muscle, which suggests a further reduced efficiency in delivery of oxygen to muscle compared to that of SCI animals. This is the first example of such a dramatic uncoupling between fibre area and local capillary supply, and we have yet to explore its influence on the fibres capacity to utilise oxygen. Overall the combination therapy showed the most promising adaptive remodelling, improving the capacity to deliver oxygen through

reorganisation of capillary distribution, increasing homogeneity of supply, rather than increasing the density of the microvascular network. It may be the case that during pathological remodelling and rarefaction in the case of SCI the local capillary supply becomes tightly related to oxidative capacity, matching supply to demand, opposing that relationship seen in intact muscle (Bosutti et al., 2015). This is consistent with the principle of symmorphosis, which assumes that structures are matched to the functional demand.

Given the multitude of potential angiogenic regulators, combined with the different physiological challenges (chemical and mechanical stimuli) it is essential to avoid a simplistic analysis of underlying signalling processes. To this end, we have utilised a systems biology approach to investigate this complex problem.

6 A systems biology approach to exercise induced angiogenesis

This work has been completed in collaboration with Peter Davidsen (University of Copenhagen) and Francesco Falciani (University of Liverpool). Peter Davidsen completed the normalization of the gene array data, KEGG and GOBP processing and the nearest neighbor analysis for hub genes. Roger Kissane completed all animal experiments, RNA extraction, microarray chip processing, hub gene list compiling and data analysis.

6.1 Abstract

The molecular networks involved in physiological (exercise-induced) angiogenesis are not well understood. There are a large number of 'key' angiogenic factors discussed within the literature that we believe to be important in the regulation of angiogenesis, but are yet to distinguish a link between these key-regulators and the phenotypic response of exercise. Therefore, we utilised a systems biology approach, that utilised chronic human exercise data to derive angiogenic networks for commonly reported 'key' angiogenic proteins. These human derived angiogenic gene sets were then used to characterise known angiogenic animal models to establish their viability for translational angiogenic research and to further explore the unique angiogenic pathways involved in mechanotransduction driven remodelling.

Endurance and resistance training have a largely similar global phenotype with increased extra-cellular matrix remodelling proteins and inflammatory mediated signalling. Prazosin induced shear stress showed no commonality with overload driven angiogenesis and no evident overlap with endurance or resistance derived angiogenic networks. Indirect electrical stimulation has a largely similar angiogenic genotype to endurance and resistance exercise, with little differentiation between frequencies. The P53 pathway plays an important role in the inhibition of angiogenesis, inhibition of mTOR/IGF-a pathway, and mitochondrial biogenesis and shows some promise in unpicking the fine control elements of these adaptive responses. The animal model of angiogenesis has suggested a potential role for the histone deacetylase (HDAC's) in shear stress driven angiogenesis, while overload induced adaptation appears to be largely cytokine driven.

6.2 Introduction

Endurance exercise is a potent adaptive stimulant, capable of central and peripheral adaptations that are integral predictors of longevity and quality of life (Wisløff et al., 2005). Regular endurance training has been shown to be a remarkable driver for adaptive remodelling of skeletal muscle, improving the capacity to deliver and utilise oxygen, through increased microvascular content (Andersen and Henriksson, 1977, Gustafsson et al., 1999, Waters et al., 2004, Ingjer, 1979a) and increased oxidative enzymes and fuel transport proteins (Saltin and Rowell, 1980, Saltin and Gollnick, 1983, Rodnick et al., 1989). These adaptive responses are known to occur following endurance training, but the potential of resistance exercise for angiogenic and oxidative remodelling has largely been overlooked (McCall et al., 1996, Green et al., 1999, Campos et al., 2002).

Angiogenesis is a complex multifactorial adaptive process that involves the differential regulation of pro- and anti-angiogenic factors (Egginton, 2009, Olenich et al., 2013, Hoier and Hellsten, 2014). The most prevalent pro-angiogenic growth factor is vascular endothelial growth factor (VEGF), known for its proliferative effect on endothelial cells. Animal models of mechanotransduction-driven angiogenesis have shown VEGF to be essential for successful microvascular expansion (Williams et al., 2006c), and as such an integral component in physiological adaptive remodelling. Other notable pro-angiogenic factors include matrix metalloproteinases (MMPs), VEGF-receptor 1 (FLT1) and VEGF-receptor 2 (Rodent, Flk-1; Human, KDR) (Haas et al., 2000, Gustafsson et al., 2005). Anti-angiogenic factors of particular interest in exercise-induced angiogenesis include thrombospondin-1 (TSP-1), tissue inhibitors of matrix metalloproteinases (TIMPs) and endostatin. Thrombospondin acts through multiple inhibitory process, reducing the proliferative status of endothelial cells and inhibiting MMP activity (Lawler, 2000). Similarly, TIMPs inhibit extracellular matrix (ECM) remodelling through inhibition of MMPs, while endostatin is a fragment derived from collagen XVIII that is generated through the degradation of plasminogen, through MMP activity, which subsequently inhibits endothelial cell proliferation (O'Reilly et al., 1997).

Acute endurance and resistance exercise have been shown to upregulate a variety of key pro-angiogenic factors and receptors; VEGF, TIE2, MMP9, NRP1 (Gavin et al., 2007, Hoier et al., 2012), as well as anti-angiogenic factors; endostatin, TSP-1 and TIMP1 (Olfert et al., 2006, Olenich et al., 2013, Gu et al., 2004, Dennis et al., 2008). This acute response differentially changes with training. Following four weeks of endurance training in humans, VEGF RNA is no longer elevated significantly following an acute bout of exercise, while MMP9 and TIMP1 maintain a significantly elevated state following acute endurance exercise (Hoier et al., 2012). Similar changes have been seen in a longitudinal study in mice, trained for four weeks, where baseline VEGF decreased compared to control and the acute mRNA response was no longer significantly elevated compared to baseline (Olenich et al., 2013). However, in the mouse training study the baseline TSP-1 had significantly increased, but dropped back to acute levels following an acute bout of exercise.

There is evidently a fine control over the composition of pro- and anti-angiogenic factors following exercise training. To date the molecular regulation of physiological angiogenesis lacks convincing evidence for any differential molecular driving signals in response to exercise. This may reflect the lack of temporal resolution of such experiments, and/or the use of individual gene targets that provide only a snapshot of the regulatory effects within a given signaling pathway. Genes do not function in isolation, and looking at individual 'key players' may not sufficiently characterise a molecular signature associated with a single stimulus/adaptive phenotype. Therefore, we sought to use a systems biology approach to identify discrete networks that may be differentially expressed in endurance exercise (a typically high angiogenic training regime) compared to that of resistance exercise (a relatively angiostatic stimulus). Moreover, we have developed a variety of animal models isolating mechanotransductive signaling and manipulating muscle activity patterns, and have started to characterise the highly coordinated adaptive process. We set out to identify differential angiogenic molecular signaling cascades following endurance or resistance exercise in humans. Subsequently, using the networks generated by the two human training regimes, we profiled existing

angiogenic animal models, and compared their genetic signature to those of the human responses to validate their efficacy as translatable models of physiological angiogenesis.

Given the overlapping adaptive responses of both endurance and resistance exercise training we hypothesis that their global genomic response will not differ greatly, while their angiogenic signaling and interactions will be substantially different. Given the large hyperaemia response of indirect 4Hz stimulation (Chapter 4) we hypothesise that 4Hz indirectly stimulated muscle and prazosin treated animals will have overlapping driving signalling. While, indirect stimulated muscle at 40Hz will comprise of overlapping signaling networks to that of the overloaded muscle. Key signaling networks within the electrically stimulated muscles not evident in the prazosin treated animals may be important in the directed angiogenic response seen in Chapter 4.

6.3 Material and methods

6.3.1 Ethical approval

This chapter utilises data from the HERITAGE (Bouchard et al., 1995) and DERBY (Phillips et al., 2013) data sets, with ethical approval carried out at the respective institutions. Both the HERITAGE and DERBY genome data are publically available within the Gene Expression Omnibus (links provided below).

HERITAGE: https://www.ncbi.nlm.nih.gov/geo/query/acc.cgi?acc=GSE47874
DERBY: https://www.ncbi.nlm.nih.gov/geo/query/acc.cgi?acc=GSE47881

All rodent work was carried out in accordance with the Animals (Scientific Procedures) Act 1986 (ASPA, 1986) at Leeds. Animals were sourced in-house, and housed on a 12 hour light-dark cycle at 21 °C with *ad libitum* access to food and water.

6.3.2 HERITAGE training regime

The HERITAGE family study collated participant information from five institutions across North America and Canada, collecting data from 652 participants (294 men and 358 women; BMI, 26.6 ± 5.2 $kg.m^{-2;}$ $VO_{2MAX,}$ 31.1 ± 8.8 $mL.kg^{-1}.min^{-1}$). Participant variables are available for age, sex and race (Skinner et al., 2001). Participants completed 20 weeks of aerobic exercise on a cycle ergometer in a labotratory, where exercise intensity was customised for each participant based on the heart rate-VO_2 relationship measured at baseline. Training was conducted 3 times a week, and duration and intensity were increased fortnightly for 14 weeks, starting at 55% VO_{2MAX} for 30 minutes, working up towards 50 minute long sessions at 75% VO_{2MAX}. Vastus lateralis muscle biopsies were used for Affymetrix microarray analysis (Human Genome U133 Plus 2.0 Array, Affymetrix). Biopsies were taken in a rested state 24 hours after the last training bout.

6.3.3 DERBY training regime

The DERBY training study consisted of 44 participants across a range of young and old participants (18-75 years old, all participants were normotensive with blood pressures less than 140/90) (Phillips et al., 2012). Participants underwent a 20 week resistance exercise training program. Training involved three sessions a week of 60 minute, the first four weeks were completed at an 'induction' level, working at 40-60% one-rep max, with the following 16 weeks at 70%, with 12 repetitive sets. Monthly assessments of one-rep max were taken to adjust for any improvements, and maintain a 70% work intensity. Samples (~150 mg) were taken from the participant's vastus lateralis muscle under local anaesthesia (2% lidocaine) in a fasted and non-exercised "basal" state (Phillips et al., 2013) and examined using the Affymetrix Human Genome U133 Plus 2.0 Array (Affymetrix)

6.3.4 Rodent angiogenic regimes

Surgical and pharmacological angiogenic protocols were carried out over a seven day period targetting the peroneal muscle group, with the *extensor digitorum*

longus (EDL) muscle used for microarray analysis. Indirect electrical stimulation groups received eight hours of their respected stimulation frequency per day, which consisted of 4Hz, 10Hz or 40Hz. Unstimulated contralateral muscles were used as an internal control (STCT). Animal overload (OV) models received a unilateral muscle extirpation of the tibialis anterior, overloading the extensor digitorum longus, while the contralateral side was used as an internal control (OVCT). The vasoactive compound prazosin (PR) works as a global vasodilator, and as such does not allow for internal controls. All surgical descriptions and supplement dosages are detailed in Chapter 4 *Methods*.

6.3.5 Muscle sampling

Animals were culled by competent Home Office personal license holders, using Schedule 1 approved techniques (concussion with cervical dislocation). Whole muscles were carefully dissected from the hind limb of the animal and weighed. Muscle samples were split into three equal portions, with the proximal and distal portions frozen in liquid nitrogen for gene array and qPCR analysis.

6.3.6 RNA extraction

All equipment was autoclaved where appropriate and cleaned with RNAse Zap (Ambion, Inc.); RNase free tips were used throughout. Tissue was homogenised in 1ml of Tryzol using a bead mill (TissueLyser LT, Qiagen) with 5mm stainless steel beads. Following complete homogenisation 0.2ml of chloroform was added and spun at 13000 rpm at 4°C for 10 minutes, to separate the solution into two portions the aqueous (top) and organic (bottom) phase. The aqueous phase contains RNA, which was aspired and cleaned using the RNeasy Mini Kit (Qiagen) and suspended in 50µl of RNase free molecular biology grade water. Quality control of the samples were quantified using a nanodrop (Nanodrop 2000, Thermo Scientific), and RNA integrity checked on the Bioanalyser 2100 (Agilent).

6.3.7 Microarray analysis

The microarrays were completed by myself with the help of Michela Bonomo (University of Liverpool), while the bioinformatics analysis was assisted by Dr Peter Davidsen (University of Liverpool). Whole genome arrays (SurePrint G3 Rat Gene Expression v2 Microarray Kit, 8x60K, Agilent) were performed on the three largest angiogenic responders from groups: Control (CT), 4Hz, 10Hz, 40Hz, Stimulation-CT (STCT), Prazosin (PR), Overload (OV) and Overload-CT (OVCT). Samples were labelled using the LowInput QuickAmp Labeling Kit One-Color (Agilent) to generate a fluorescent complimentary RNA for hybridisation to the gene array chips for scanning. Probes with a lower intensity than background were removed from analysis, and across the three biological replicates two out of three needed to be significantly higher than background to be carried forward. Probes carried forward were normalised using quantile normalisation (Bolstad et al., 2003).

We utilised the Kyoto Encyclopaedia of Genes and Genomes (KEGG) and Gene Ontology Biological Process (GOBP) to build a functional profile of the various interventions.

The HERITAGE data set was used to generate an endurance induced angiogenic network for comparison with resistance-trained individuals (DERBY) and the subsequent animal models. The global response of endurance training was restricted to angiogenic-specific functions and associated biological pathways using the nearest neighbour networks approach (Huttenhower et al., 2007). Briefly, a 240 item library of functionally relevant angiogenic genes (in physiological and pathological angiogenesis) (Appendix 1) was mapped onto the global response of endurance training. These pre-defined hub genes were then associated with neighbouring genes of similar response, generating gene-sets of functional pathways associated with that hub gene. The endurance angiogenic networks were overlapped across the remaining models of exercise to investigate their coherence with endurance-induced angiogenesis. A similar gene hub data set was generated for the DERBY data.

To evaluate significance of the various hub gene networks we utilised the Gene Set Enrichment Analysis (GSEA) method (Subramanian et al., 2005). GSEA utilises a pre-determined set of genes, in this case those generated from the endurance-training regime. Each gene within the set is ranked based on its importance/prevalence within that set (a continuum from up-regulated to down-regulated), and GSEA determines upon comparison whether the gene distributions are random, or whether there are clearly defined genes associated with the top or bottom of that list (Subramanian et al., 2005). Figure 6-1 displays the enrichment plot for the VEGF associated gene set. An enrichment score reflects the over-representation at the top/bottom of the gene ranking list, each time a gene within the VEFG list is found the enrichment score increases and for each gene not in the list it decreases (Fig. 6-1a). The *P* value is calculated from the enrichment score. Within this study we utilised the familywise-error rate (FWER) with $P<0.05$ as statistically significant; this method corrects for multiple hypothesis testing, and is considered to be quite a conservative method (Subramanian et al., 2005). Individual genes of interest identified from the HERITAGE and DERBY data may be presented as Log transformed fold changes (Log(FC)), where a negative Log(FC) denotes an up-regulation (and will be represented with solid filled bars), and a positive Log(FC) denotes down-regulation (and will be represented with hashed filled bars).

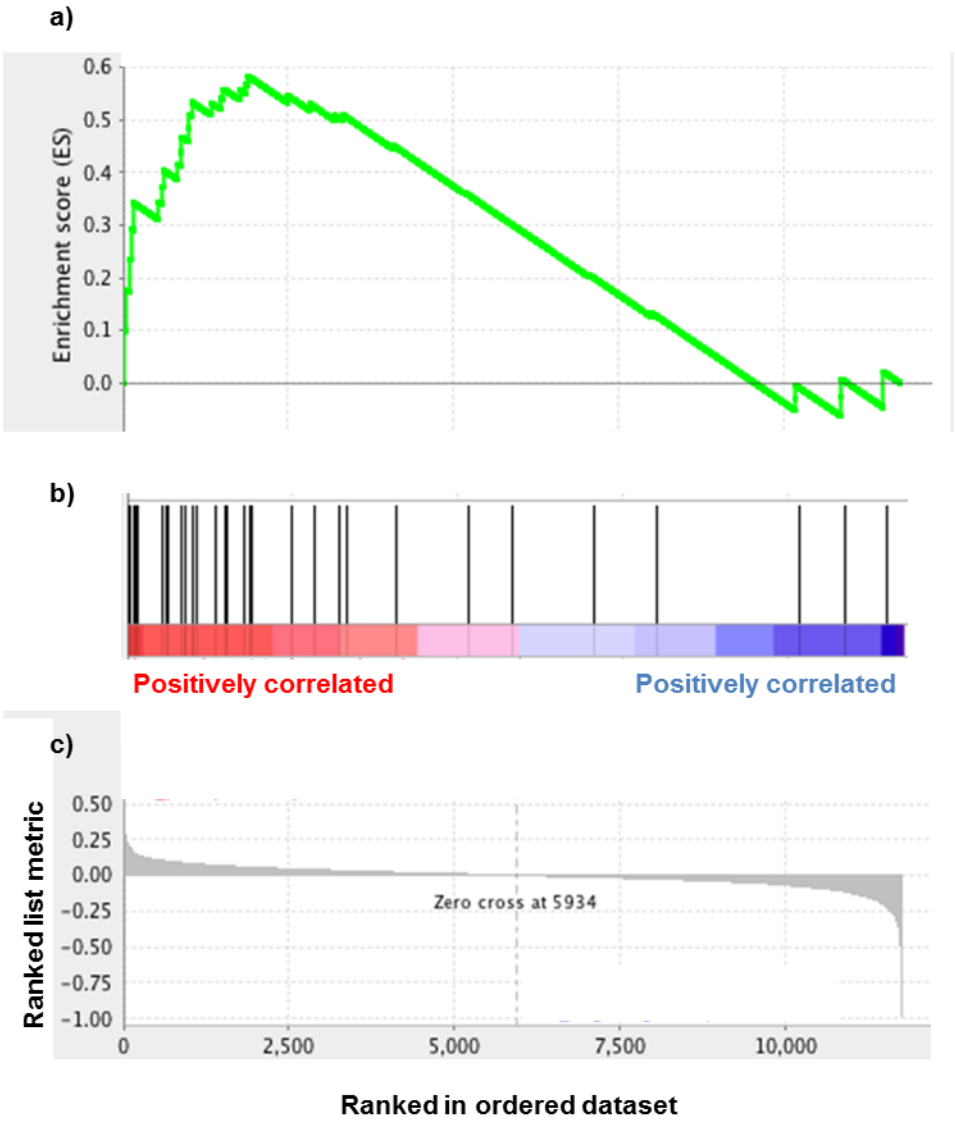

Figure 6-1. Example enrichment plot for a gene set (DERBY *vs.* HERITAGE). The enrichment plot for VEGF gene set with a running plot for enrichment score which in this example is 0.5834 (a). Hits within the gene list, in this case there are 34 hits and their location within the gene list are displayed as an individual black line (b) which are compared against the global distributed of genes from the largest up-regulated to largest down-regulated genes (c).

6.4 Results

6.4.1 Endurance (HERITAGE) vs. resistance (DERBY) training

The expression profile following 20 weeks of endurance exercise or resistance training identified commonality in significantly up-regulated KEGG pathways (Fig. 6-2) with cell adhesion molecules, ECM-receptor interaction, and protein digestion and absorption (all $P<0.001$). Overlapping down-regulated pathways include the spliceosome and RNA transport pathways (all $P<0.01$). There was noticeable up-regulation across a selection of energy metabolism pathways following resistance training (oxidative phosphorylation, citrate cycle and beta-alanine metabolism) that were not evident in endurance-trained networks. The major differentially expressed KEGG pathways were significantly up-regulated inflammatory pathways chemokine signalling (FWER, $P=0.038$), small cell lung cancer (FWER, $P=0.049$) and the P53 signalling pathway (FWER, $P=0.028$) following resistance training. The commonly up-regulated KEGG pathways showed a large number of overlapping candidates, where the top ten enriched genes from the cell adhesion molecules and ECM-receptor interaction pathways are presented in Figure 6-3, along with the two differentially expressed pathways (chemokine signalling and P53 signally pathways).

The angiogenic networks generated from the HERITAGE and DERBY data sets demonstrate a large number of overlapping up- and down-regulated hub gene sets with similar nearest neighbour counts (LAMA4, THBS2, CTGF, FOXO4, PPARGC1A, TGFB3, VEGFA, ACVR2B, FLT4, FGF2). Some hub gene sets had higher nearest neighbour counts when generated from the endurance training data (MMP2, SPARC, PGF, TIE1, ESM1, EGFR, CXCL14, ECM1, ANG and HIF1AN). Conversely, a proportion of hub genes had increased neighbour counts when generated using the resistance training data (IFITM1, ERG, VEGFC, EGLN3, SERPINF1, PTN, BTG1, HDAC5, IL33 and AGGF1) (Fig. 6-4). However, the number of nearest neighbours does not fully discriminate similarities/differences between the two generated hub gene sets. Table 5-1 shows hub genes with a similar number of nearest neighbours that have overlapping index's (OI) of 0.

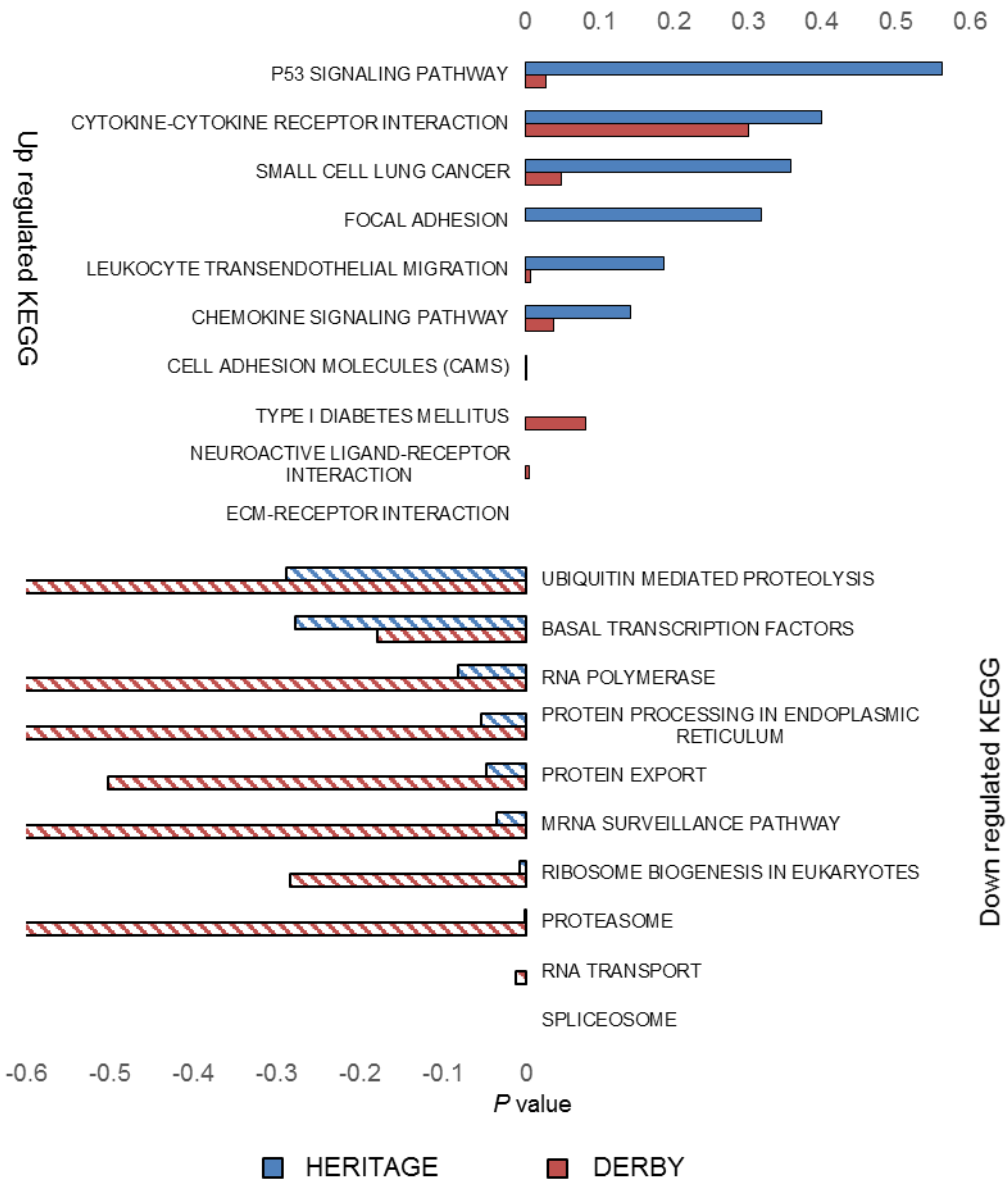

Figure 6-2. KEGG pathway enrichment following endurance and resistance training. Up-regulated (filled bars) and down-regulated (hashed bars) KEGG pathways following endurance (HERITAGE) and resistance (DERBY) training.

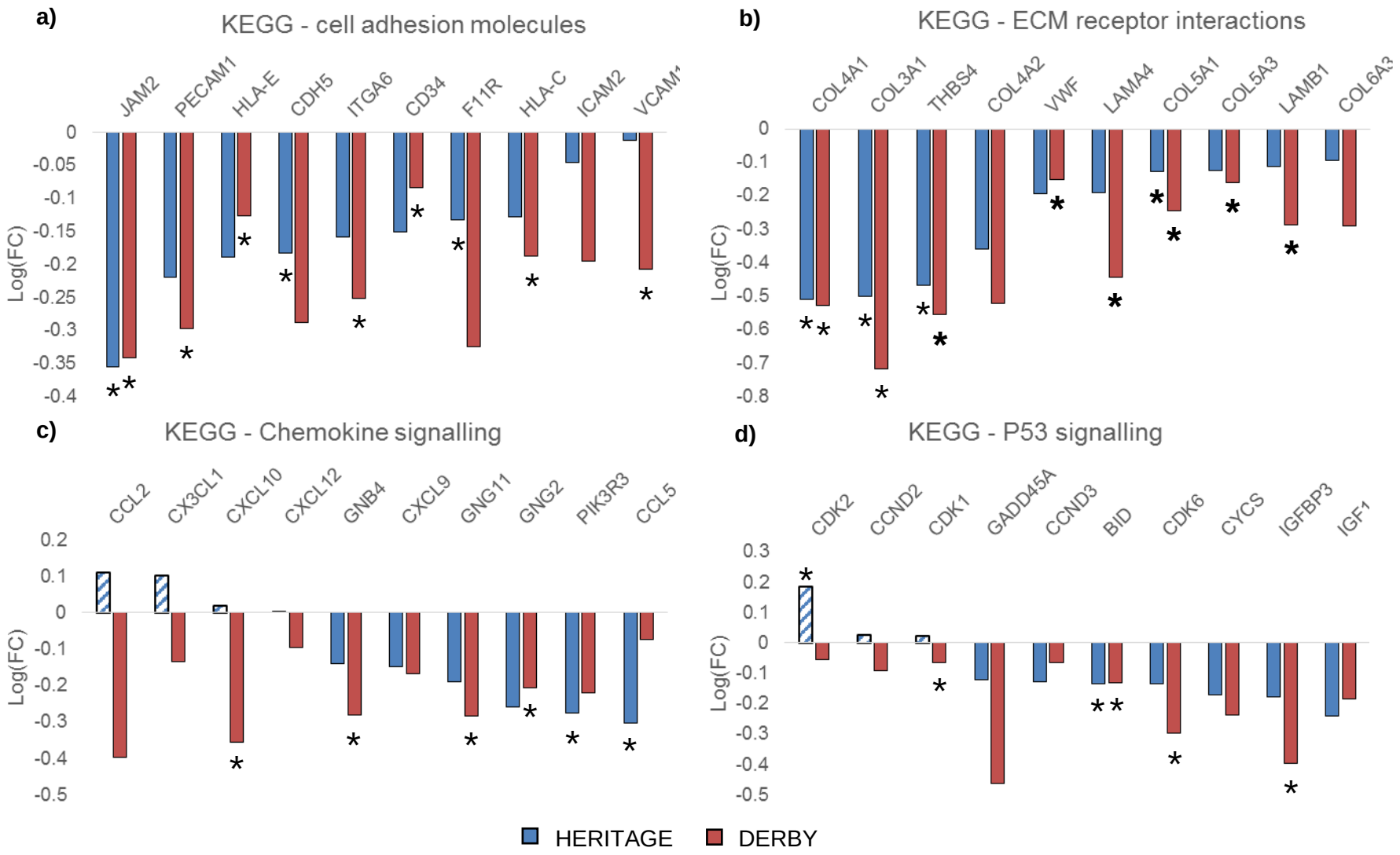

Figure 6-3 Enriched genes from KEGG pathway analysis. Top ten enriched genes for endurance and resistance training in the significantly up-regulated cell adhesion molecules (a) and ECM receptor interaction (b) KEGG pathways. Top ten enriched genes in chemokine signalling (c) and P53 signalling pathway (d) for significantly up-regulated KEGG pathways following resistance training. * *P*<0.05 post training *vs.* baseline.

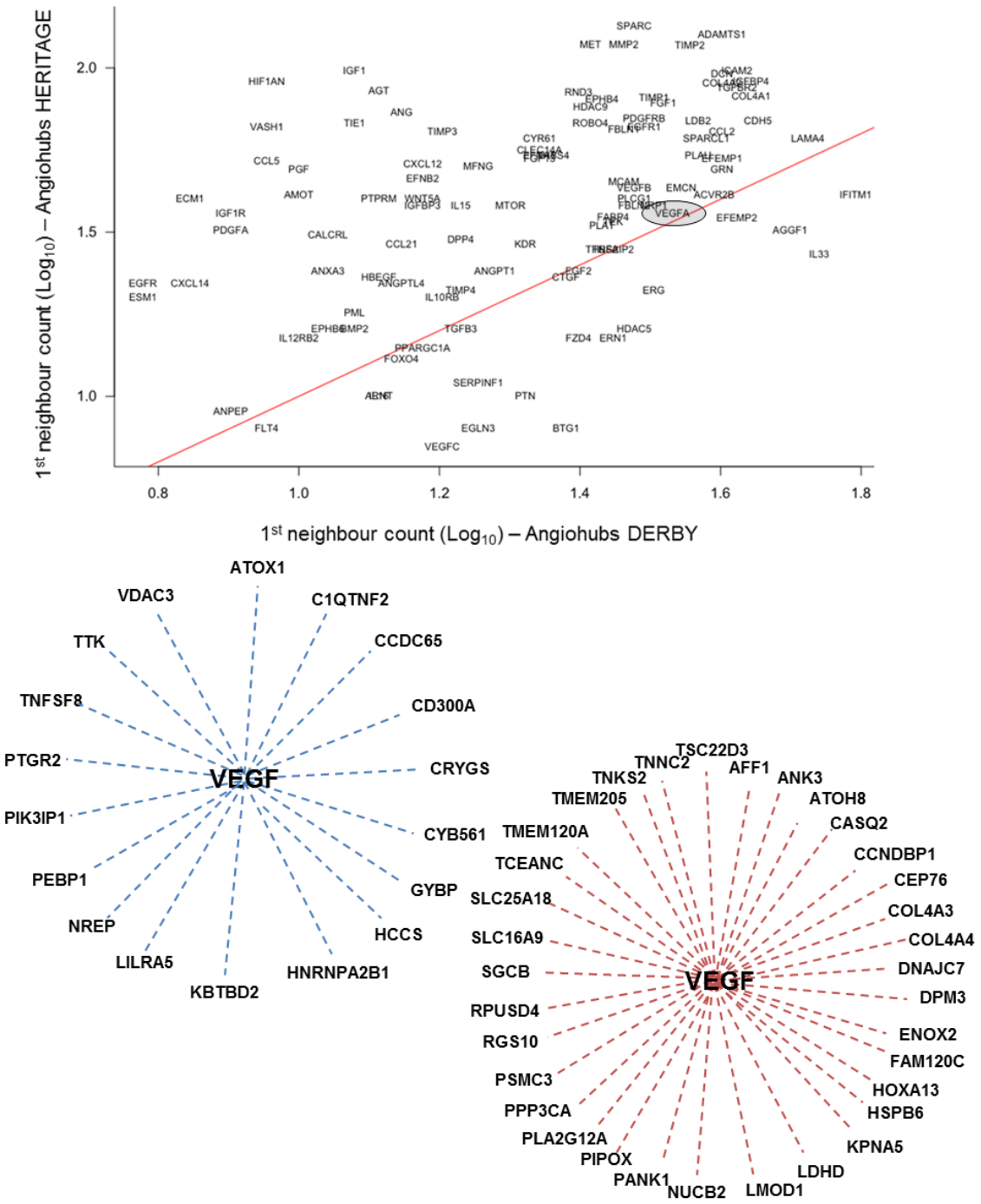

Figure 6-4. Number of nearest neighbour genes for individual hubs generated by the HERITAGE and DERBY data sets. Line fit for y = x (red) describes an equal number of nearest neighbours for the gene sets derived from the HERITAGE and DERBY data. This does not necessarily describe the commonality of those genes. For example inserted below the graph are VEGF gene sets generated by the HERITAGE (blue) and DERBY (red) data. In contrast to expectation based on prior literature detailing individual gene expression data there are no common genes within these sets.

Table 6-1. First neighbour count with overlapping index. Gene sets derived from both data sets are compared and an index of the common genes between both derived lists is generated. They have been categorised based on the number of genes within their list.

HERITAGE > DERBY		HERITAGE = DERBY		HERITAGE < DERBY	
Hub Gene	**OI**	**Hub Gene**	**OI**	**Hub Gene**	**OI**
MMP2	0.207	LAMA4	0.151	IFITM1	0.098
SPARC	0.2	THBS2	0.074	ERG	0
PGF	0	CTGF	0.043	VEGFC	0
TIE1	0	FOXO4	0	EGLN3	0
ESM1	0	PPARGC1A	0	SERPINF1	0
EGFR	0	TGFB3	0	PTN	0
CXCL14	0	VEGFA	0	BTG1	0
ECM1	0	ACVR2B	0	HDAC5	0
ANG	0	FLT4	0	IL33	0
HIF1AN	0	FGF2	0	AGGF1	0

OI, overlapping index

Endurance and resistance training significantly up-regulated a number of individual genes from baseline, including COL4A1, THBS4, COL4A2 and SPARC (FWER, P<0.05) (Fig. 6-5). While resistance training significantly up-regulated KDR and NRP1, there was a down-regulation following endurance training (Fig 6-5b). These significantly up- and down-regulated individual genes corresponded with significantly enriched hub gene pathways for the resistance-trained individuals. A selection of non-significantly regulated individual genes in the resistance-trained cohort showed significant pathway enrichment (VEGFA, HIF-1α, VEGFB, HDAC5 and IGF2R, FWER *P>0.05*), with a selection of them having differentially enriched pathways when compared to the individual gene (HIF-1α, HDAC5 and VEGFA) regulation (Fig. 6-5c).

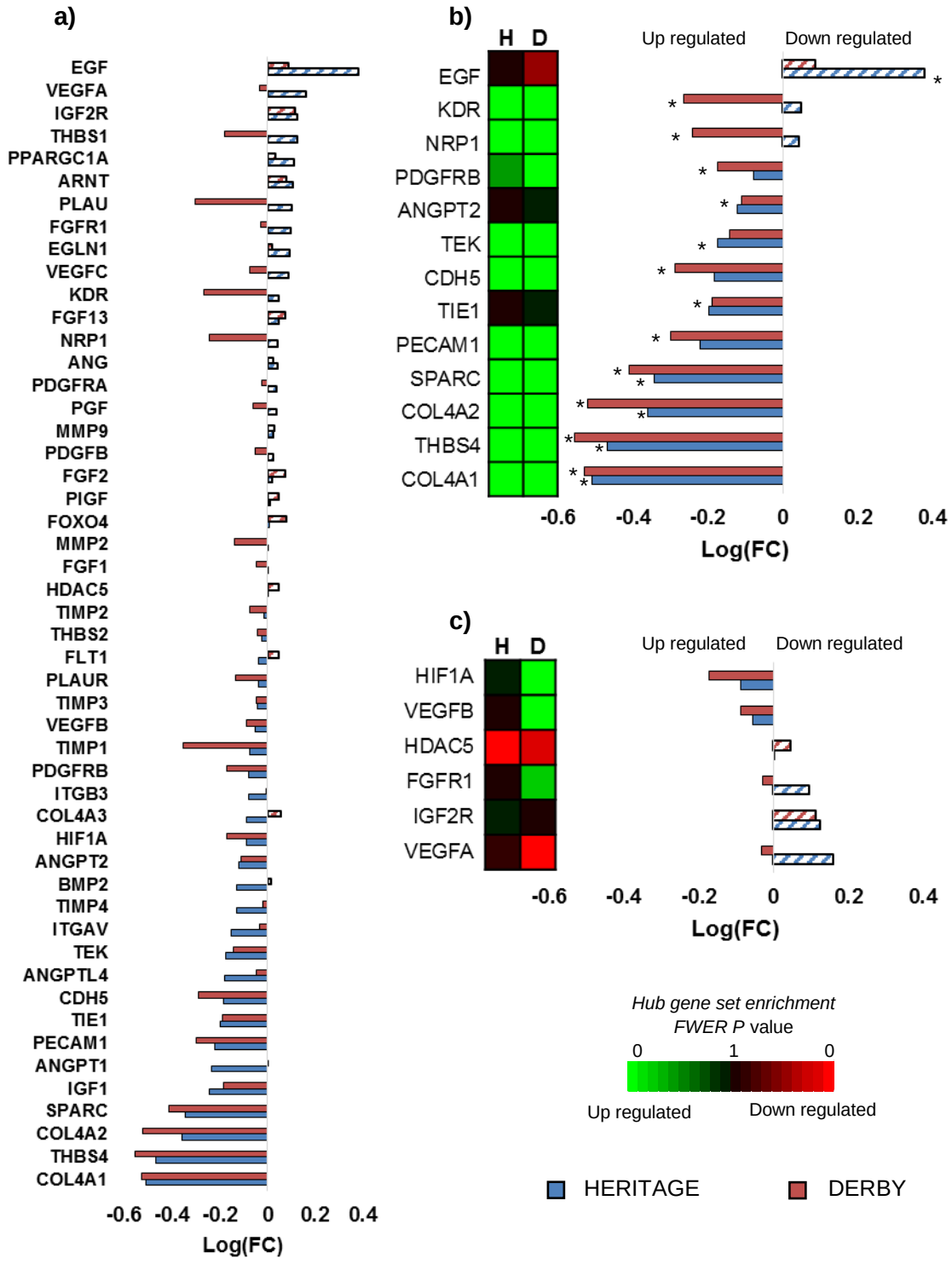

Figure 6-5. Angiogenic key-players response to exercise training. Top 50 ranked individual genes from the 240 selected angiogenic genes of interest (Appendix 1) and their Log(FC) (a). Selection of significantly altered genes, with reciprocal changes in the individual gene and the pathway analysis (b), with a selection of individual genes that showed significantly opposing pathway responses independent of the individual gene response (c).

6.4.2 Animal models of angiogenesis

The global transcriptional response differed markedly between the eight experimental treatments, with defined groupings among the principal component analysis (Fig. 6-6).

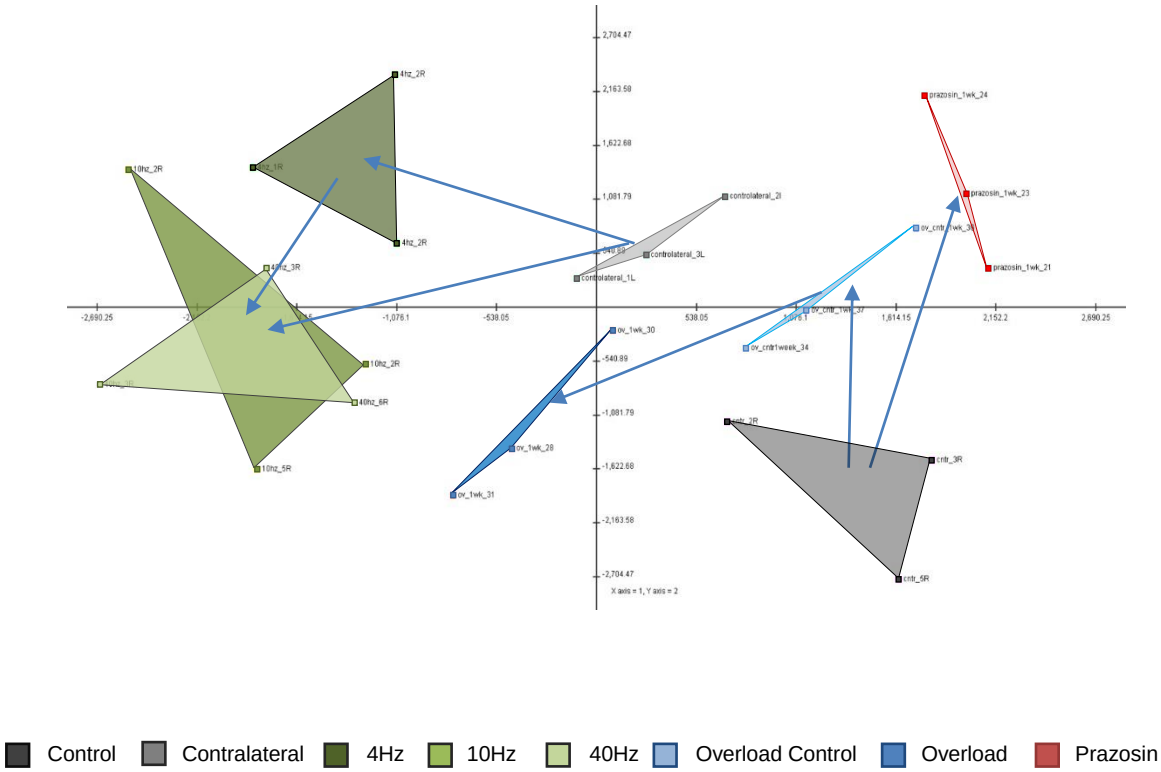

Figure 6-6. Principal component analysis for rodent angiogenic models. Global transcriptional response across each group (*n* = 3). Principal component 1 (x-axis) accounts for 24% of the variation seen among the groups, while principal component 2 (y-axis) accounts for 13%.

Prazosin treated rats showed significant up-regulation in the pyruvate (FWER, *P*=0.032) and tryptophan (FWER, *P*=0.0185) metabolism KEGG pathways compared to CT while there was significant down-regulation of focal adhesion (FWER, *P*<0.001), ECM-receptor interaction (FWER, *P*<0.001) and TGF-β signalling (FWER, *P*<0.001) KEGG pathways. A large number of immunological pathways were up-regulated in OV compared to OVCT,

including KEGG pathways: chemokine signaling (FWER, *P*=0.02), leukocyte transendothelial migration (FWER, *P*=0.0185), cytokine-cytokine receptor interaction (FWER, *P*<0.001) and antigen processing and presentation (FWER, *P*=0.034) and GOBP pathways: response to interferon-gamma (FWER, *P*<0.001), innate immune response (FWER, *P*<0.001), leukocyte migration (FWER, *P*<0.001), inflammatory response (FWER, *P*=0.001). The direct comparison of prazosin and overload are described in Table 5-2.

The significant up-regulated pathways in 4Hz *vs*. STCT were oxidative metabolism oriented, with oxidative phosphorylation (FWER, *P*<0.001), citrate cycle (TCA cycle) (FWER, *P*<0.001) and fatty acid metabolism (FWER, *P*<0.001) KEGG pathway enrichment. Up-regulation in GOBP metabolic pathways were also evident: electron transport chain (FWER, *P*<0.001), ATP synthesis coupled electron transport (FWER, *P*<0.001) and mitochondrial respiratory chain complex I biogenesis (FWER, *P*=0.016). Conversely, 40Hz had fewer oxidative metabolism pathways up-regulated while having similar trends in immunological pathways to that of OV, cytokine-cytokine receptor interaction (FWER, *P*=0.34) and antigen processing and presentation (FWER, *P*=0.34). The 10Hz stimulation resulted in significant up-regulation of ECM-receptor interaction (FWER, *P*=0.004) and oxidative phosphorylation (FWER, *P*=0.007) KEGG pathways. A variety of GOBP pathways were also up-regulated following 10Hz stimulation including: extracellular matrix organisation (FWER, *P*=0.001), cell-substrate adhesion (FWER, *P*=0.002), angiogenesis (FWER, *P*=0.016) and regulation of leukocyte migration (FWER, *P*=0.039). A selection of enriched individual genes from the up-regulated ECM-receptor interactions and fatty acid metabolism KEGG pathways are presented in Figure 6-7.

Table 6-2. Differential changes in KEGG and GOBP pathways between animal models

Category	TERM	Interaction	Up-regulated	FWER (*P*)
KEGG	ECM-RECEPTOR INTERACTION	OV *vs.*PR	OV	< 0.001
KEGG	PROTEIN DIGESTION AND ABSORPTION	OV *vs.*PR	OV	0.007
KEGG	PROPANOATE METABOLISM	OV *vs.*PR	PR	0.014
GOBP	EXTRACELLULAR MATRIX ORGANIZATION	OV *vs.*PR	OV	< 0.001
GOBP	EXTRACELLULAR STRUCTURE ORGANIZATION	OV *vs.*PR	OV	< 0.001
GOBP	COLLAGEN METABOLIC PROCESS	OV *vs.*PR	OV	< 0.001
KEGG	VALINE, LEUCINE AND ISOLEUCINE DEGRADATION	4Hz *vs.*40Hz	4Hz	< 0.001
KEGG	CITRATE CYCLE (TCA CYCLE)	4Hz *vs.*40Hz	4Hz	< 0.001
KEGG	FATTY ACID METABOLISM	4Hz *vs.*40Hz	4Hz	0.021
KEGG	TRYPTOPHAN METABOLISM	4Hz *vs.*40Hz	4Hz	0.04
KEGG	PYRUVATE METABOLISM	4Hz *vs.*40Hz	4Hz	0.083
KEGG	RIBOSOME	4Hz *vs.*40Hz	40Hz	0.02
KEGG	ECM-RECEPTOR INTERACTION	4Hz *vs.* PR	4Hz	< 0.001
KEGG	PROTEIN DIGESTION AND ABSORPTION	4Hz *vs.* PR	4Hz	< 0.001
KEGG	OXIDATIVE PHOSPHORYLATION	4Hz *vs.* PR	4Hz	< 0.001
KEGG	FOCAL ADHESION	4Hz *vs.* PR	4Hz	0.009
KEGG	CARBOHYDRATE DIGESTION AND ABSORPTION	4Hz *vs.* PR	PR	0.008
KEGG	RIBOSOME BIOGENESIS IN EUKARYOTES	4Hz *vs.* PR	PR	0.021
GOBP	EXTRACELLULAR STRUCTURE ORGANIZATION	4Hz *vs.* PR	4Hz	< 0.001
GOBP	EXTRACELLULAR MATRIX ORGANIZATION	4Hz *vs.* PR	4Hz	< 0.001
GOBP	ATP SYNTHESIS COUPLED ELECTRON TRANSPORT	4Hz *vs.* PR	4Hz	0.009
GOBP	EXTRACELLULAR MATRIX DISASSEMBLY	4Hz *vs.* PR	4Hz	0.029
GOBP	MITOCHONDRIAL ELECTRON TRANSPORT	4Hz *vs.* PR	4Hz	0.029
KEGG	ECM-RECEPTOR INTERACTION	40Hz *vs.* OV	40Hz	0.003
GOBP	CELLULAR RESPONSE TO INTERFERON-GAMMA	40Hz *vs.* OV	40Hz	0.02
GOBP	PROTEIN ACTIVATION CASCADE	40Hz *vs.* OV	40Hz	0.054
KEGG	ECM-RECEPTOR INTERACTION	10Hz *vs.* PR	10Hz	< 0.001
KEGG	FOCAL ADHESION	10Hz *vs.* PR	10Hz	0.009
KEGG	CELL ADHESION MOLECULES (CAMS)	10Hz *vs.* PR	10Hz	0.237
GOBP	EXTRACELLULAR MATRIX ORGANIZATION	10Hz *vs.* PR	10Hz	< 0.001
GOBP	EXTRACELLULAR STRUCTURE ORGANIZATION	10Hz *vs.* PR	10Hz	< 0.001
GOBP	EXTRACELLULAR MATRIX DISASSEMBLY	10Hz *vs.* PR	10Hz	< 0.001
KEGG	ECM-RECEPTOR INTERACTION	10Hz *vs.* OV	10Hz	0.002
KEGG	FOCAL ADHESION	10Hz *vs.* OV	10Hz	0.111
GOBP	CELLULAR RESPONSE TO INTERFERON-GAMMA	10Hz *vs.* OV	10Hz	0.032
GOBP	LYMPHOCYTE MEDIATED IMMUNITY	10Hz *vs.* OV	10Hz	0.034
GOBP	IMMUNOGLOBULIN MEDIATED IMMUNE RESPONSE	10Hz *vs.* OV	10Hz	0.043

Alternate shading to differentiate pairwise interactions in the order: OV *vs.* PR, 4Hz *vs.*40Hz, 4Hz *vs.* PR, 40Hz *vs.* OV, 10Hz *vs.* PR and 10Hz *vs.* OV.

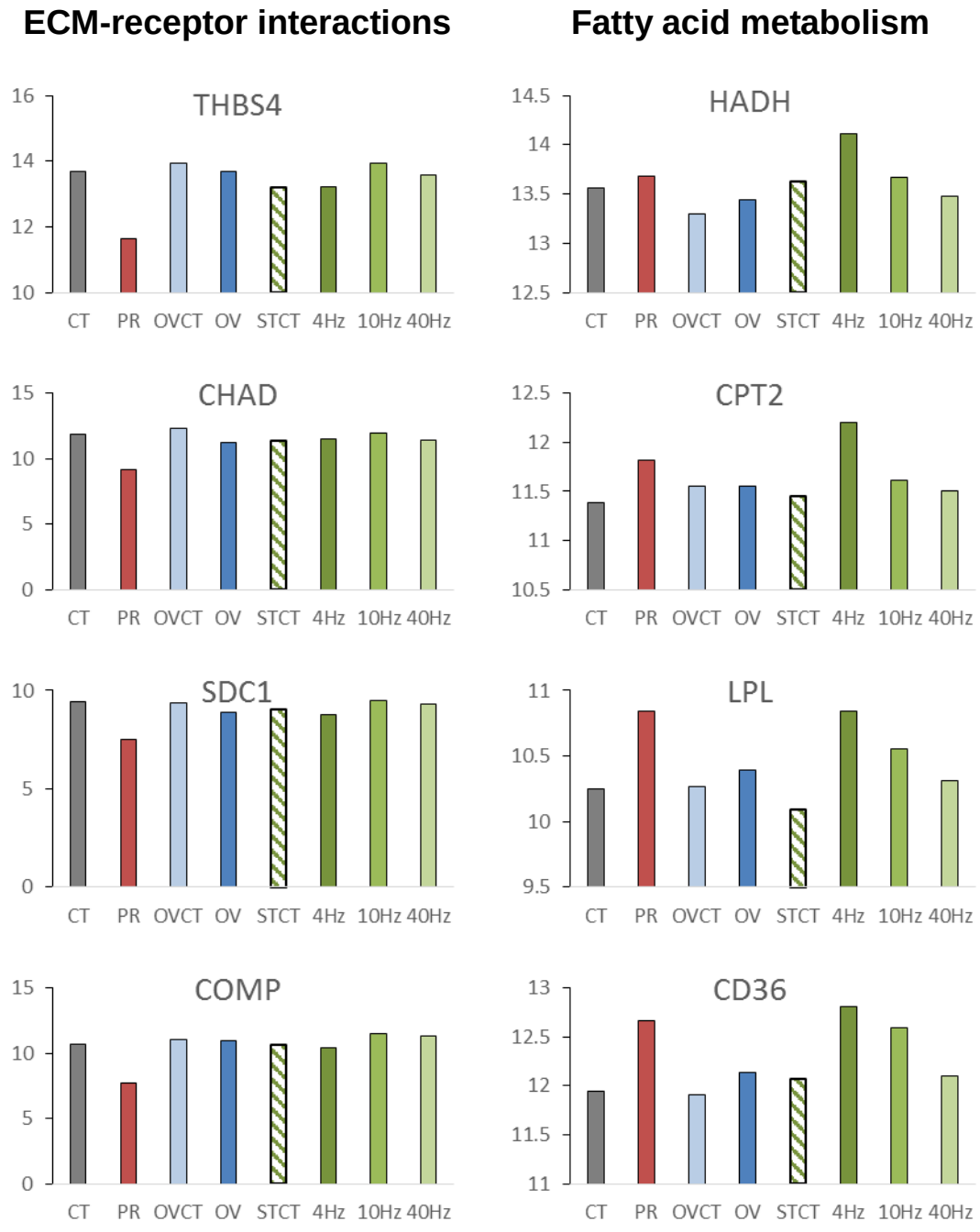

Figure 6-7. Example enriched genes from KEGG pathways, presented as average signal intensity. THBS4, thrombospondin 4; CHAD, chondroadherin; SDC1, syndecan 1; COMP, thrombospondin 5; HADH, hydroxyacyl-coenzyme A dehydrogenase; CPT2, carnitine palmitoyltransferase II; LPL, lipoprotein lipase; CD36, fatty acid translocase. From EDL muscle samples after seven days of intervening (n=3, per group).

Angiogenic hub genes derived from the HERITAGE data set were compared across the various animal models. Prazosin and overload animals revealed no overlap with significantly enriched hub gene sets (Fig. 6-8), with prazosin predominantly having significantly down-regulated hub gene sets that were significantly up-regulated in overload. Comparing prazosin directly with overload highlighted a significant cohort of genes up regulated in overload (Appendix 3) while prazosin showed a non-significant up-regulation of HIF1AN (FWER, *P*=0.062) and HDAC5 (FWER, *P*=0.056).

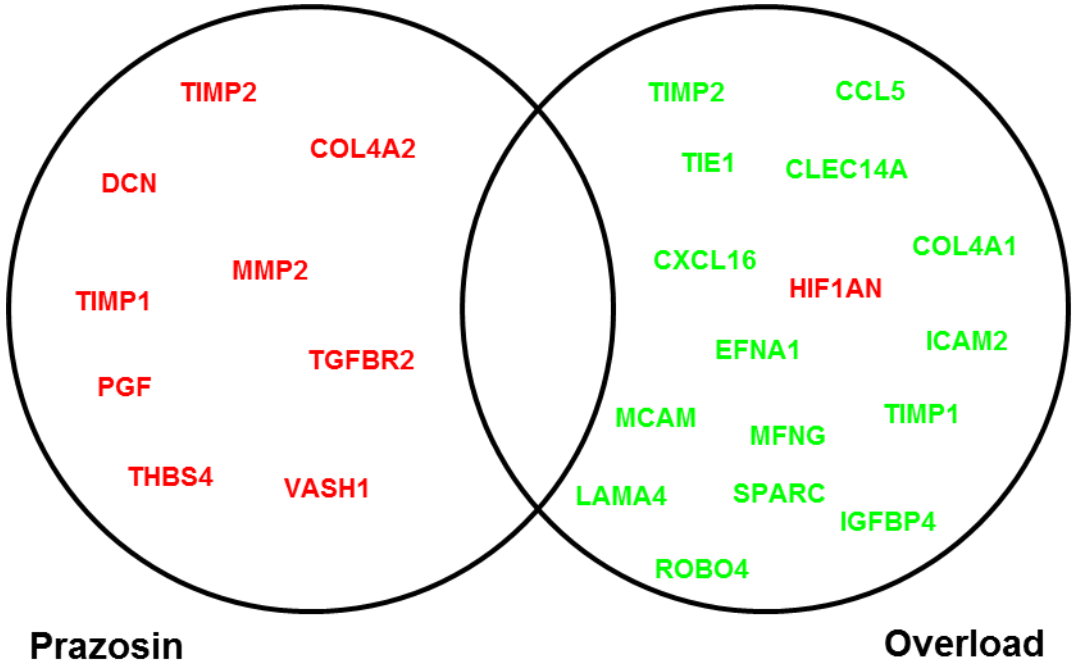

Figure 6-8. Significantly altered HERITAGE derived hub gene sets following prazosin and overload. Green up-regulated genes *vs.* comparative control (FWER, *P*<0.05), Red down-regulated genes *vs.* comparative control (FWER, *P*<0.05). Note, there are no overlapping (*i.e.* common) gene sets.

All stimulation groups showed a large proportion of overlapping genes sets that were significantly up-regulated (Fig. 6-9), however, a selection of differentially regulated genes were evident. 4Hz significantly up-regulated KDR (FWER, *P*=0.039) while 10Hz and 40Hz did not (FWER, *P*=0.233 and

P=0.804, respectively). 4Hz also had an overlapping up-regulation of the TIE1 pathway with 10Hz (FWER, *P*=0.025 and *P*=0.013, respectively), but no overlapping regulated gene sets with 40Hz alone. Likewise, 10Hz significantly up-regulated LDB2 (FWER, *P*<0.0001) and down-regulated HIF1AN (FWER, *P*=0.02) with no significant interaction in either the 4Hz or 40Hz. 10Hz stimulation also had significant commonality with 40Hz that were not apparent in 4Hz, with up-regulation of the TIMP1, TIMP2 and LAMA4 gene sets. 40Hz showed the largest differential response with significantly up-regulated MFNG (FWER, *P*=0.011) and TGFBR2 (FWER, *P*=0.032), as well as significantly down-regulating MET (FWER, *P*=0.033) and HDAC9 (FWER, *P*=0.017).

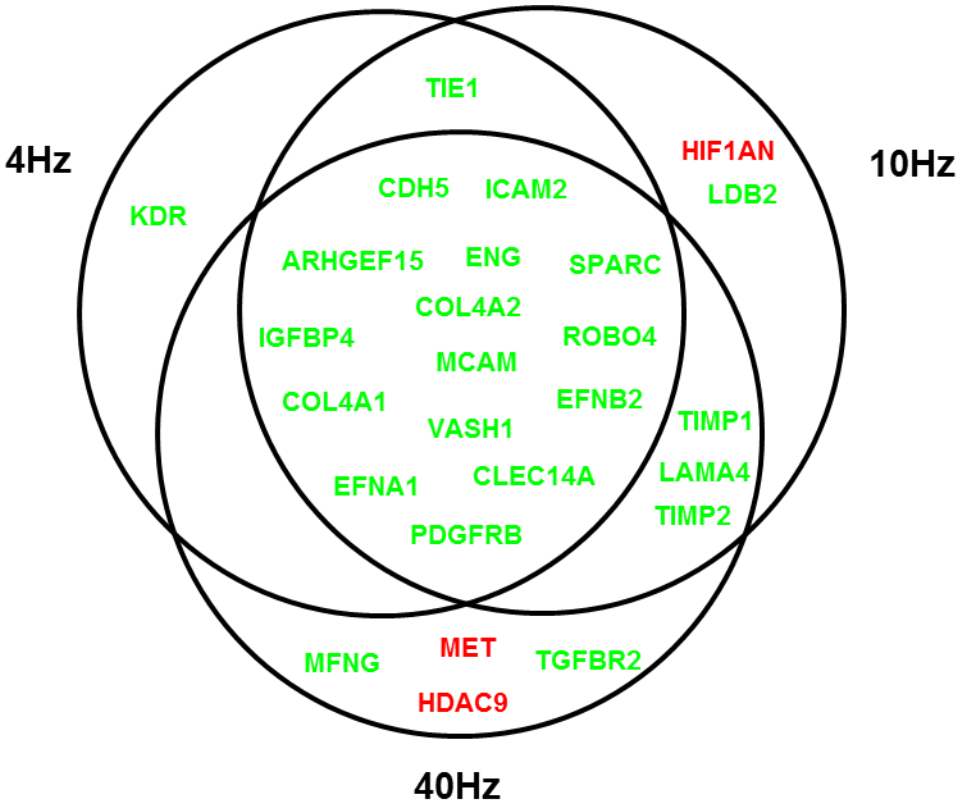

Figure 6-9. Significantly altered HERITAGE derived hub gene sets following muscle stimulation. Green up-regulated genes *vs.* STCT (FWER, *P*<0.05), Red down-regulated genes *vs.* STCT (FWER, *P*<0.05). Note, there are a large number of overlapping (*i.e.* common) gene sets, however, there are a select few that are differentially expressed at the very lowest and highest frequencies.

6.4.3 Animal models vs. human training modalities

The functional profile represented by the KEGG pathway heat map (Fig. 6-10) show a large overlap with up- and down-regulated gene ontologies between the two human training regimes. The major pathways differentially expressed were the up-regulated metabolic pathways for oxidative phosphorylation (FWER, P=0.175) and the citrate cycle (FWER, P=0.235) in the resistance trained individuals. The prazosin treated animals showed no obvious overlap with that of either human cohort, other than a significant down regulation of TGF-β signalling (FWER, P<0.001). Comparatively, up-regulation of immunological/inflammatory signalling cascades found with overload are also evident in both forms of training in the human cohorts. The various stimulation parameters largely overlapped with both the HERITAGE and DERBY data sets. 4Hz stimulated hind limb muscles showed a small overlap with the human training regimes, predominantly across the up-regulated metabolism pathways; oxidative phosphorylation (FWER, P<0.001) and citrate cycle (FWER, P<0.001). 10Hz and 40Hz had the largest overlapping global response with the predominantly up-regulated cell signalling pathways (ECM-receptor interactions, cell adhesion molecules, antigen processing and presentation and cytokine-cytokine receptor interaction).

Examining the differentially derived angiogenic hub gene pathways there are a variety of standout gene pathways, which typically have the lowest overlapping index (Fig. 6-11). Prazosin and 4Hz treated muscle showed similar levels of up-regulation in HIF1AN, HDAC5 and HDAC9, evident in the endurance trained group; these pathways were predominantly down-regulated in overload, 10Hz and 40Hz treated muscle. Conversely, MMP2, PGF, TGFBR2, PDGFRB and DCN were mostly down-regulated in the prazosin and 4Hz tissue; but up-regulated in the overload, 10Hz and 40Hz.

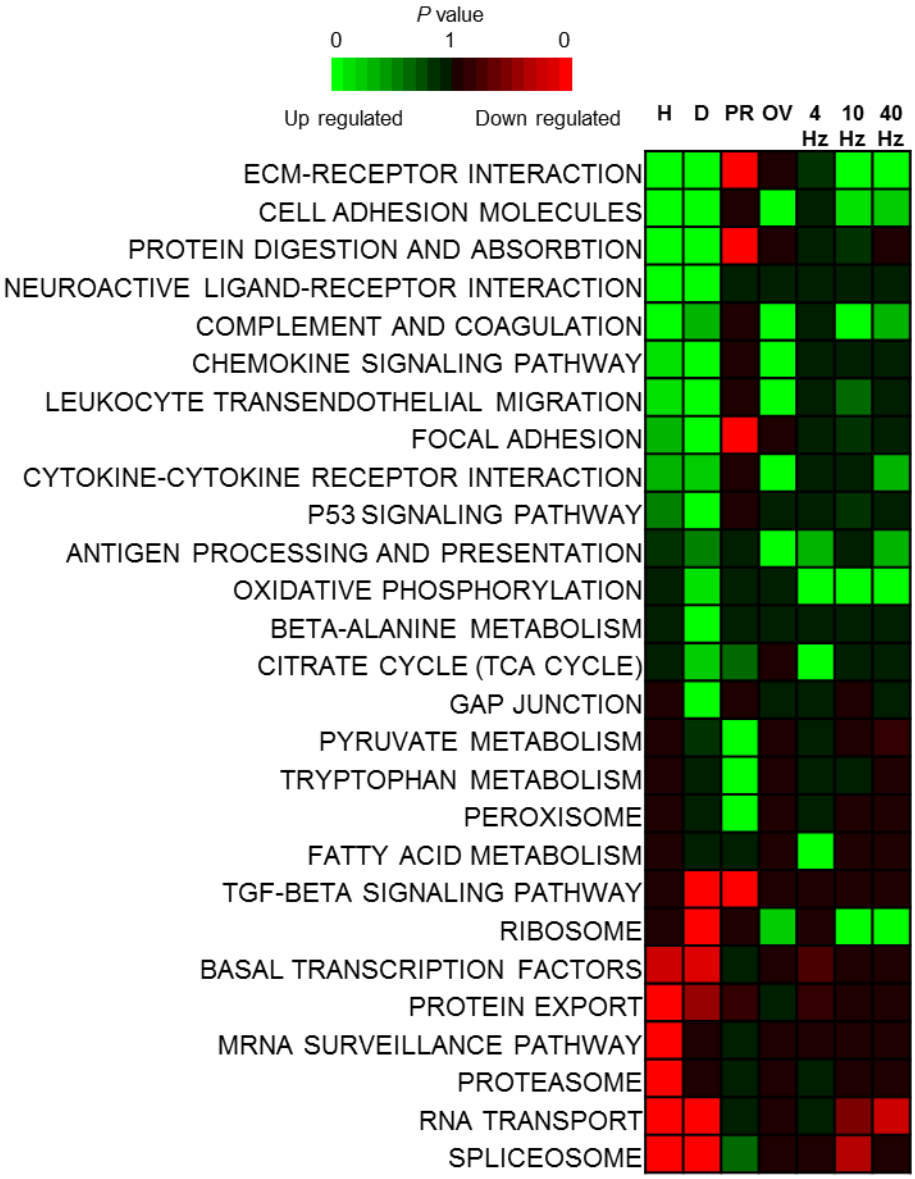

Figure 6-10. Heat map for specific KEGG pathways regulated by endurance and resistance training in comparison to animal models. The global transcriptomic response of exercise in humans following two distinct forms of exercise, compared to the various animal models of angiogenesis. H, HERITAGE data pre *vs.* post; D, DERBY data pre *vs.* post; PR, prazosin data PR *vs.* CT; OV, overload data OV *vs.* OVCT; 4Hz, 4Hz stimulation data 4Hz *vs.* STCT; 10Hz stimulation data 10Hz *vs.* STCT; 40Hz stimulation data 40Hz *vs.* STCT.

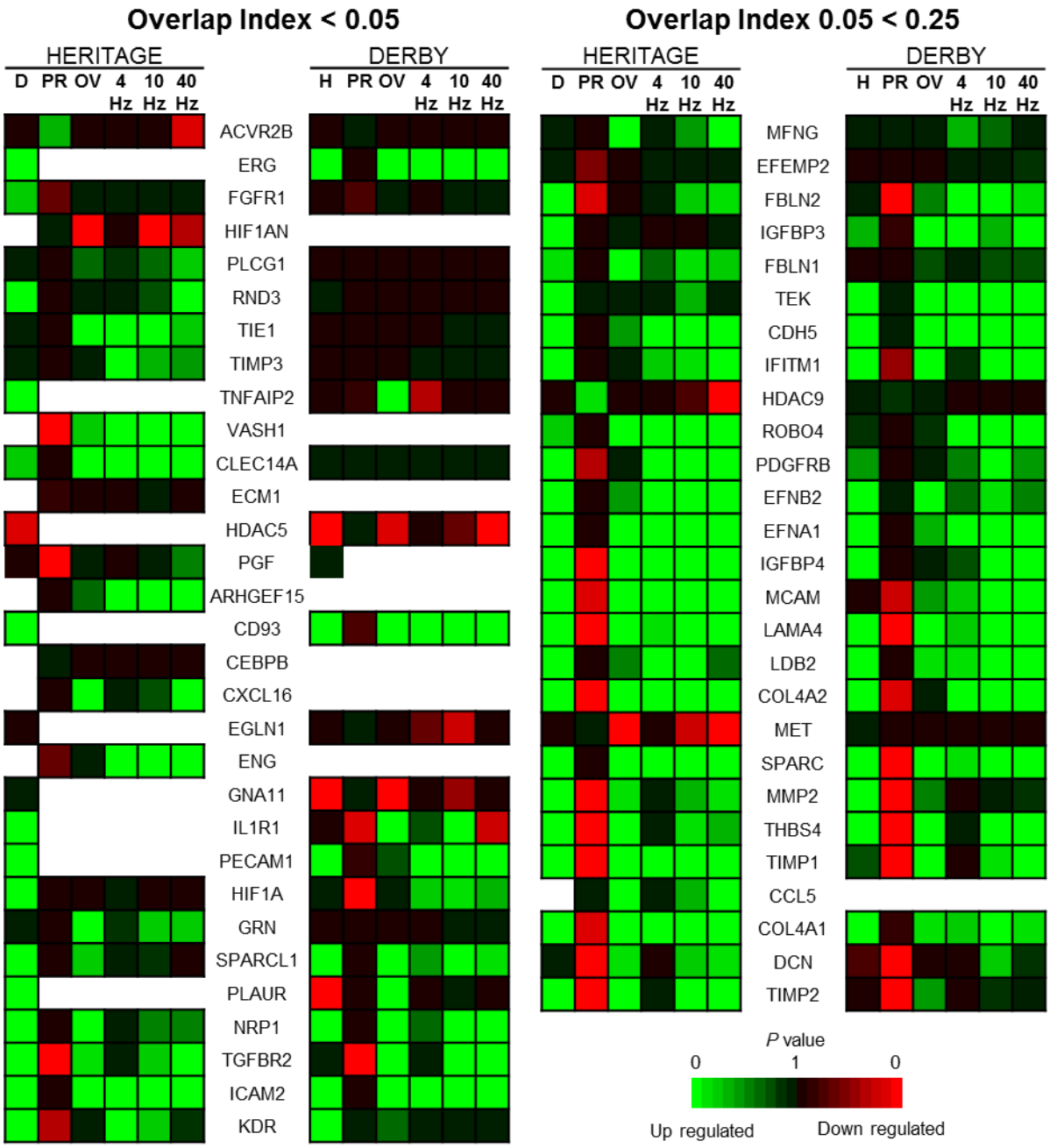

Figure 6-11. Regulation heat map, categorised in order of overlap index for hub gene sets generated using the HERITAGE or DERBY data set, in comparison to animal models. H, HERITAGE data pre *vs.* post; D, DERBY data pre *vs.* post; PR, prazosin data PR *vs.* CT; OV, overload data OV *vs.* OVCT; 4Hz, 4Hz stimulation data 4Hz *vs.* STCT; 10Hz stimulation data 10Hz *vs.* STCT; 40Hz stimulation data 40Hz *vs.* STCT.

6.5 Discussion

In this chapter we have utilised a systems biology approach to investigate the angiogenic pathways activated through chronic endurance and resistance exercise training, in an attempt to identify differential signalling pathways that may be important in functional adaptation. Subsequently, we have generated angiogenic pathways from these two exercise regimes, to test the translatability of the various animal models with known angiogenic potential. The data was analysed in a hierarchical manner, looking initially at the global functional signature, with KEGG ('general' pathways representing molecular interactions) (Fig. 6-12a) and GOBP pathways (describing more functionally specific gene ontologies, e.g. sprouting angiogenesis) (Fig. 6-12b). Deriving angiogenic networks based on known key-angiogenic factors (Fig. 6-12c) allows a more detailed differential response to be investigated, including likely interaction among functionally connected genes, and hence potential key regulatory genes to be proposed.

Figure 6-12. Conceptual overview of hierarchical analysis of activity-induced angiogenesis. KEGG, Kyoto encyclopedia of genes and genomes, are a collection of manually drawn pathway maps describing interactions of genes at a relatively global level, *e.g* .metabolic pathways, cellular processes, and human diseases (a). GOBP, gene ontology biological process, describe a molecular function/event that has a defined beginning and end *e.g.* sprouting angiogenesis, regulation of smooth muscle cell proliferation, and lamellipodium organisation (b). Hub gene sets are generated using the nearest neighbour approach, which collates the nearest associated/interacting gene to that of the user defined 'hub'. This allows comparison across independent variables to assess any changes in interactions with the defined hubs (c). It may be possible to identify/hypothesise key regulators/interacting genes with those of the hub for further investigating. Ultimately, this feed-forward control of gene function needs to be understood in the context of feed-back regulation of genes at a higher trophic level, and also the influence of the proteins transcribed.

6.5.1 The transcriptome signature of angiogenesis following chronic endurance and resistance training

It is well established that endurance exercise is a potent stimulator of increased aerobic capacity, through adaptive changes centrally and peripherally, with the latter involving changes in fuel transport, improved microvascular supply and oxygen utilisation (Gustafsson et al., 1999, Laughlin, 1999, Green et al., 1999, Prior et al., 2003, Saltin and Rowell, 1980, Saltin and Gollnick, 1983). The potential for resistance training to improve oxidative capacity and alter microvascular content is often overlooked, however a small body of work has shown that resistance training can increase the transcriptional response of mitochondrial biogenesis and a variety of angiogenic growth factors (Wang et al., 2011, Gavin et al., 2007).

Following 20 weeks of endurance or resistance exercise training there is an evident up-regulation of fundamental genes involved in mechanotransductive sensing and signalling in the ECM receptor interactions and cell adhesion molecules KEGG pathways; JAM2, PECAM1, CDH5, COL4A1, COL4A2 and VCAM1 to name a few (Cao et al., 2002, Fleming et al., 2005, Frenette and Wagner, 1996, Koch et al., 1995, Egginton, 2011).

There is a large body of cytokines up-regulated in the resistance-trained individuals that were not evident with endurance training, including CCL2 (chemokine ligand 2 or monocyte chemoattractant protein 1) and CXCL10 (chemokine 10 or interferon gamma-induced protein 10). CCL2 is typically reported as a marker for muscle damage, evident following resistance exercise, eccentric exercise and ultra-exercise events (Hubal et al., 2010, Harmon et al., 2010, Catoire and Kersten, 2015). It does, however, possess great angiogenic potential and may be important in resistance training-induced proliferation and migration of endothelial cells (Conti and Rollins, 2004, Steiner and Murphy, 2011, Soria and Ben-Baruch, 2008). Conversely, there was evidence of CCL5 (RANTES, regulated upon activation, normal T-

cell expressed and secreted) up-regulation in endurance-trained individuals, which has also been described to be a potent pro-angiogenic chemokine (Soria and Ben-Baruch, 2008, Suffee et al., 2011, Egginton and Bicknell, 2011, Lansford et al., 2016). Both these cytokines are negatively controlled by the P53 signalling pathway, (Levine et al., 2006, Tang and Amar, 2015, Soria and Ben-Baruch, 2008), which is up-regulated in the resistance- and moderately so in the endurance-trained groups. However, the P53 signalling cascade has been associated with positive regulatory effects on mitochondrial biogenesis and aerobic enzyme up-regulation, which is evident in the resistant trained cohort (Matoba et al., 2006, Wang et al., 2012, Bartlett et al., 2013, Saleem and Hood, 2013).

Resistance exercise is not thought of as a potent angiogenic form of exercise, however when we look at the global transcriptional response compared to endurance exercise, they are largely the same. They have a large portion of equally up-regulated remodelling pathways, with similar changes at the individual gene level. This may reflect a limited transcriptional repertoire available to the myocytes (genes from other cell types are likely to be diluted), and suggests a common 'exercise' phenotype that presents limited opportunity for modality-specific responses.

6.5.2 Animal models of activity-induced angiogenesis

The differential transcriptomic response of the mechanotransductive models of angiogenesis (prazosin-induced shear stress and overload-stimulated abluminal stretch) have been characterised to a greater extent in this chapter than previously. It is well established that shear stress-induced angiogenesis is dependent on NO availability and that VEGF is required for successful formation of neovasculature (Williams et al., 2006c, Williams et al., 2006a, Williams et al., 2006b), while abluminal stretch driven microvascular expansion requires VEGF and the successful breakdown of ECM proteins (Haas et al., 2000, Williams et al., 2006c, Williams et al., 2006a, Williams et

al., 2006b) (Chapter 1, 4). These are just single elements of a larger integrated response, some of which are discussed below.

Following seven days of prazosin treatment there is an evident down-regulation of ECM-remodelling pathways that are up-regulated following overload. The global overview derived from the KEGG and GOBP pathways are consistent with previous data discussing the necessary proteolysis of ECM proteins in order for angiogenesis to take place during overload (i.e. abluminal sprouting and endothelial migration) that is not required in shear stress-induced angiogenesis (i.e. intra-luminal endothelial lamellipodia formation) (Haas et al., 2000, Williams et al., 2006a, Egginton et al., 2001). This pattern is exemplified by the altered regulation of a variety of key ECM remodelling hub gene sets, specifically the down-regulation TIMP1, TIMP2, LAMA4, COL4A2, and MMP2, which are all up-regulated in the overload treated muscle (individual genes are presented in Appendix 2). Thus, prazosin invokes a widespread depression of pathways associated with the canonical, sprouting form of angiogenesis, suggesting that the distinct angiotype resulting from high shear stress activation may be reliant on a less extensive network of interacting genes.

The high mitotic and anabolic activity of the overload model is further supported by our data suggesting marked up-regulation of numerous pro-inflammatory signalling cascades and insulin growth factor binding proteins hub genes, integral in satellite cell proliferation and hypertrophic and angiogenic remodelling (Adams, 2002, Moss and Leblond, 1971, Salleo et al., 1983, Tatsumi et al., 2006, Christov et al., 2007). HIF has been shown to be an integral up-regulated transcription factor for stretch-induced angiogenesis, but not following elevated shear stress (Williams et al., 2006a, Milkiewicz et al., 2007). We have supportive data of this, as well as evidence of down-regulation of the HIF-1α-inhibitor (HIF1AN gene, also referred to as FIH-1; factor inhibiting HIF-1α) interaction pathway in overloaded muscle, which

appears to be an up-regulation in those treated with prazosin. The down-regulation of HIF1AN pathway is likely to prevent asparaginyl hydroxylation of HIF-1α and retaining its transcriptional activity in the overload muscle (Milkiewicz et al., 2007). Interestingly, this contrasts with the more common role of HIF in hypoxia-induced angiogenesis, where its activity involves post-transcriptional regulation (Pugh and Ratcliffe, 2003). Thus, overload invokes a widespread activation of ECM regulatory, inflammation, and metabolism networks consistent with a pronounced anabolic response.

An example of how this more extensive analysis can expose unexpected avenues is that prazosin treatment had an up-regulating effect on a variety of metabolic pathways, possibly a result of increased insulin sensitivity (Pollare et al., 1988), and the subsequent amplification of downstream regulation of metabolism (Saltiel and Kahn, 2001). Consistent with the chronic increased perfusion of capillaries, and decreased transient time of fuel sources in the vessel lumen, there was evidence for up-regulated fatty acid transporters (CPT2 and CD36) in skeletal muscle (Bongrazio et al., 2005). Coupling the up-regulated fatty acid transporting capacity and oxidative/glycolytic enzymes might suggest a driving potential for improved oxidative capacity of the prazosin-treated muscle. However, as there is little evidence for any change in muscle phenotype (and hence any adjustment in metabolic profile has not been predicted) this elevated microvascular supply has been assumed to result in ‘luxury’ perfusion (Baum et al., 2013), i.e. supra-normal capillarity. As elevated shear stress associated with functional hyperaemia evoked during endurance training clearly recruits an angiogenic response commensurate with the increased metabolic demand, this strongly indicates the absence of necessary feedback control elements in prazosin treatment.

Indirect electrical stimulation of the EDL showed a varying global angiogenic response across the different frequencies, with the majority of the up-regulated global pathways following 4Hz stimulation relating to energy

metabolism, compared to 40Hz that showed largely inflammatory and ECM remodelling pathways up-regulated. 10Hz stimulation had an intermediate profile between the two responses, with an up-regulation of some metabolism pathways and ECM remodelling.

The angio-hub regulatory response is largely similar across the three stimulation frequencies, up-regulating a number of key pathways (e.g. ICAM2, MCAM, COL4A1 and CLEC14A). Looking at individual genes within these up-regulated gene sets there are a large number of commonly enriched genes which suggest a generic response to indirect electrical stimulation, but with a slight variation on a theme, *i.e.* with different frequencies it is possible to identify a cohort of differentially enriched pathways. 4Hz showed an up-regulation of the KDR gene list (suggestive of enhanced VRGF signalling), that 10Hz and 40Hz did not, but shared a commonly enriched TIE1 pathway with 10Hz (indicating a role for the angiopoietins). The enriched genes within these up-regulated pathways include a variety of genes important in the RAS/MAPK signalling cascade (CAV1, caveolin 1; CDH5, vascular endothelial cadherin; SH2D3C, SH2 domain containing 3C; NOTCH4, Neurogenic locus notch homolog 4 and CCM2L, cerebral cavernous malformations-like CCM2). CDH5 and CCM2L are important proteins in the process of elongating endothelial cells and the promotion of vascular integrity (Whitehead et al., 2009, Sauteur et al., 2014). While CAV1 and NOTCH exhibit anti-angiogenic regulation through inhibition of VEGF and eNOS (Bucci et al., 2000, Bauer et al., 2005) and promotion of integrin adhesion to the ECM (Leong et al., 2002). These contrasting regulatory processes suggest a tightly controlled angiogenic response, and that the angiogenic signal may be attenuated with an up-regulation of proteins important in vascular integrity. A similar pattern exists within the 10Hz and 40Hz samples, with the up-regulated LAMA4 gene set containing a variety of basement membrane proteins (COL4A1, collagen IV-α1; JAM3, junction adhesion molecule C; NID2, nidogen-2) integral in vessel formation and stabilisation

(Rabquer et al., 2010), and the TIMP1/2 gene sets with their enriched genes (THBS4, thrombospondin 4; LOXL1, lysyl oxidase homolog 1 and GRK5, G protein-coupled receptor kinase-5) important in signalling and initiation of collagen crosslinking (Raghuwanshi et al., 2013, Bignon et al., 2011).

The two models hypothesised to comprise of predominantly shear stress-driven angiogenesis (prazosin and 4Hz stimulation) had overlapping regulatory effects on metabolism pathways (and equivalent up-regulation of fatty acid transporters CD36 and CPT2), with neither showing a large ECM remodelling influence compared to the relevant controls (FIG. 6-13). However, a direct comparison of 4Hz with prazosin identified 22 hub gene lists up-regulated in 4Hz *vs.* prazosin, while only one was up-regulated in prazosin alone, HDAC9 (Appendix. 5). The histone deacetylases 5 and 9 (HDAC5/9) gene sets are more up-regulated in the shear stress driven angiogenic models (prazosin and 4Hz) and largely down-regulated in the luminal stretch models (overload and 40Hz). These hub sets are rich with genes involved in transcriptional regulation and having pro- and anti-angiogenic functions (NR1D1, Rev-ErbA alpha; NR1D2, Rev-ErbA beta; HLF, Hepatic leukemia factor; MET, hepatocyte growth factor receptor; PDZRN3, PDZ domain-containing RING finger protein 3 and TLE1, Transducin-like enhancer protein 1). This selection has been suggested as potential therapeutic targets for suppression of tumor angiogenesis (Seo et al., 2011, Ma et al., 2003, Christensen et al., 2005, Kourtidis et al., 2010, Keller et al., 2011).

One mechanical transduction stimulus we utilised is that of longitudinal stretch (through synergist muscle ablation, overload) and we hypothesised a large overlap in gene response with the indirect stimulation frequency of 40Hz (chapter four, Fig. 4-1). These two experimental protocols showed large inflammatory and immunological pathway responses, with examples of cytokine-cytokine receptor interaction (KEGG) and the angiogenic hub

TGFBR2 enriched genes in Figure 6-13. There was no evidence of these particular pathways enriched in the prazosin treated animals, and the comparable readings across the control, overload-contralateral and stimulation contralateral muscle suggest that it is not a response to invasive recovery surgery but a driving signal for adaptive remodelling.

6.5.3 Are animal models representative models of human exercise training?

There are a number of commonly enriched, up- and down-regulated KEGG and GOBP pathways following chronic endurance and resistance training. A large proportion of which are mirrored in the overload and electrical stimulation models of angiogenesis. The standout angiogenic group were the prazosin treated animals, with very few up-regulated pathways, and minimal overlap with either exercise training regime. There is evidently an important role for muscle activation and altered levels of muscle strain in exercise induced adaptation that cannot simply be simulated by pharmacological means. The derivation of angiogenic hub gene sets from both the HERITAGE and DERBY data set highlighted the importance of a subset of angiogenic hub gene sets (KDR, EFNB2, IFITM1, TEK, CLEC14A, IGFBP3, SPARCL1 and HIF1A). These gene sets showed varying levels of overlap with the animal models dependent on the exercise regime they were derived from, for example the KDR gene set, generated from the HERITAGE data set shows a large overlap with the lower frequency stimulation regimes (4 and 10Hz) and little with 40Hz and overload. Conversely, the KDR derived gene set from the DERBY data shows a large overlap with that of overloaded muscle, and not stimulation.

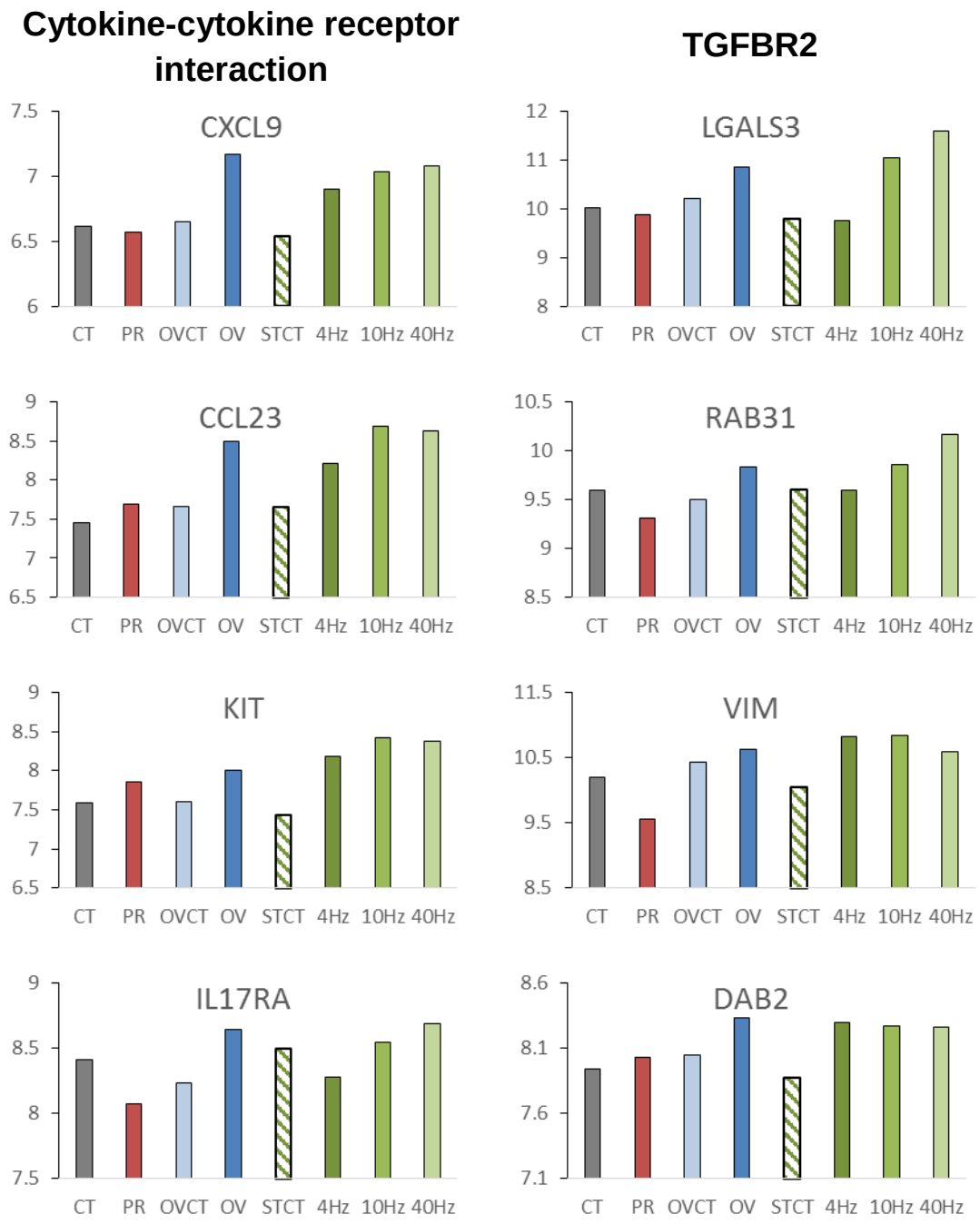

Figure 6-13. Average intensity plot for some enriched genes from the cytokine-cytokine receptor interactions (KEGG) pathway and the HERITAGE derived gene set for TGFBR2. CXCL9, chemokine ligand 9; CCL23, chemokine ligand 23; KIT, tyrosine-protein kinase kit or mast/stem cell growth factory receptor; IL17RA, interleukin 17 receptor A; LGALS3, galectin-3; RAB31, Ras-related protein RAB-31; VIM, vimentin; DAB2, disabled homolog 2. From EDL muscle samples after seven days of intervening (n=3, per group).

6.5.4 Future perspective and concluding remarks

We have successfully generated a signalling pipeline for the angiogenic remodelling cascades following endurance and resistance exercise training. Moving away from the reductionist approach which attempts to vindicate a physiological/pathological genotype to a single genetic response/mutation, which in the most part isn't true. We have begun unearthing interesting interconnected pathways in the human data that may play an important role in the temporal adaptive remodelling of the microvasculature and the sequential adaptation of oxidative enzyme content and activity. There are a multitude of secondary signalling cascades following initiation of P53 activation, and the fine control of the anti-angiogenic and pro-mitochondrial biogenesis suggest an interesting dynamic for exercise-induced adaptation that likely will provide improved understanding of the regulatory control on further examination, and possibly reveal novel targets for therapeutic interventions in angiotherapies. Furthermore, we have progressed our understanding of the phenotypically distinct models of angiogenesis (pharmacologically increased shear stress and surgically increased abluminal stretch) that suggest there is an increasingly important role for HIF-1α in stretch induced angiogenic sprouting and that the angiogenic response to luminal shear stress is in-fact driven by reduced angiogenic 'breaks'. One possible pathway is that involving HDAC's negative-regulation of the receptor tyrosine kinase for hepatocyte growth factor (MET). Finally, there appears to be a common 'exercise' phenotype between endurance and resistance exercise that is also apparent within the electrically stimulated muscles,

The transcriptomic data and angiogenic-derived networks are only the first step in the modelling of the physiological response of angiogenesis. To progress in the field and to identify key signatures of exercise induced angiogenesis there requires a multilevel informatics approach, with the incorporation of physiological measures to correlate responsiveness of training with the genetic signature. This is the most logical progressive step in

understanding the driving regulators and interactive pathways of exercise induced adaptation, given the most recent evidence of heterogeneous adaptive responses in humans to identical training regimes (Boulé et al., 2005, Keller et al., 2011, Raue et al., 2012). A transcriptomic analysis of endurance training, with identified high- and low- level responders has associated approximately 100 genes that were differentially expressed in high-responders compared to low, of which a small portion have since aligned with angiogenic gene hubs derived in our work (COL4A1, COL4A2, SPARC, LAMA4, CD93, KDR, NRP1, CAV2, ICAM2, IFI16, CD36 and ITGB1) (Keller et al., 2011). In order to further understand and generate testable hypothesis the individual genetic and adaptive response must be considered.

7 General discussion

The aim of this thesis was to characterise the angiogenic response to a variety of altered muscle activity patterns and mechanotransductive signals to elucidate their therapeutic potential. We have subsequently developed an immunohistochemical protocol that has allowed for the simultaneous identification of major fibre phenotypes and capillary location within human and rodent striated muscle. This protocol has been built around a high throughput data pipeline that allows for the quantification of local capillary indices and modelling of oxygen tension, which up until now had been a laborious and infrequently used technique. This methodological development and implementation may help in characterisation of the functional capacity of capillary supply, and aid the development of effective therapeutic interventions. This more detailed analysis of capillary remodelling has been applied to a variety of altered muscle activity patterns and a locomotory challenged disease state (spinal cord injury), which has identified new and novel data previously unreported. Finally, we have begun to unpick the angiogenic signalling response to exercise training in humans that has facilitated comparison across typically utilised angiogenic animal models. The results and importance of which will be discussed below.

7.1 Heterogeneities within skeletal muscle (Chapter 2 & 3, 4)

The heterogeneity of skeletal muscle fibre type composition and capillary distribution has been discussed in a variety of skeletal muscles across humans, rat, mice and hamsters (Henriksson-Larsén et al., 1983, Deveci and Egginton, 2002a, Egginton, 1990a). However, until now little research has been conducted into the functional capacity within compartments of skeletal muscle. Using our new histological approach we have characterised the heterogeneous fibre type distribution in EDL, increasing in oxidative capacity moving medially across the muscle (Fig. 7-1), and utilising the distal multi-tendon arrangement we have been able to distinguish the functional capacity

of two distinct elements; that of the oxidative medial and the glycolytic lateral compartment. Our data have shown that within the same muscle it is possible to have differential functional capacities and optimum working conditions, which are likely to be driven by functional demand. These data highlight the need to understand the functionality of a muscle for the development of effective targetted rehabilitation and therapeutic regimes.

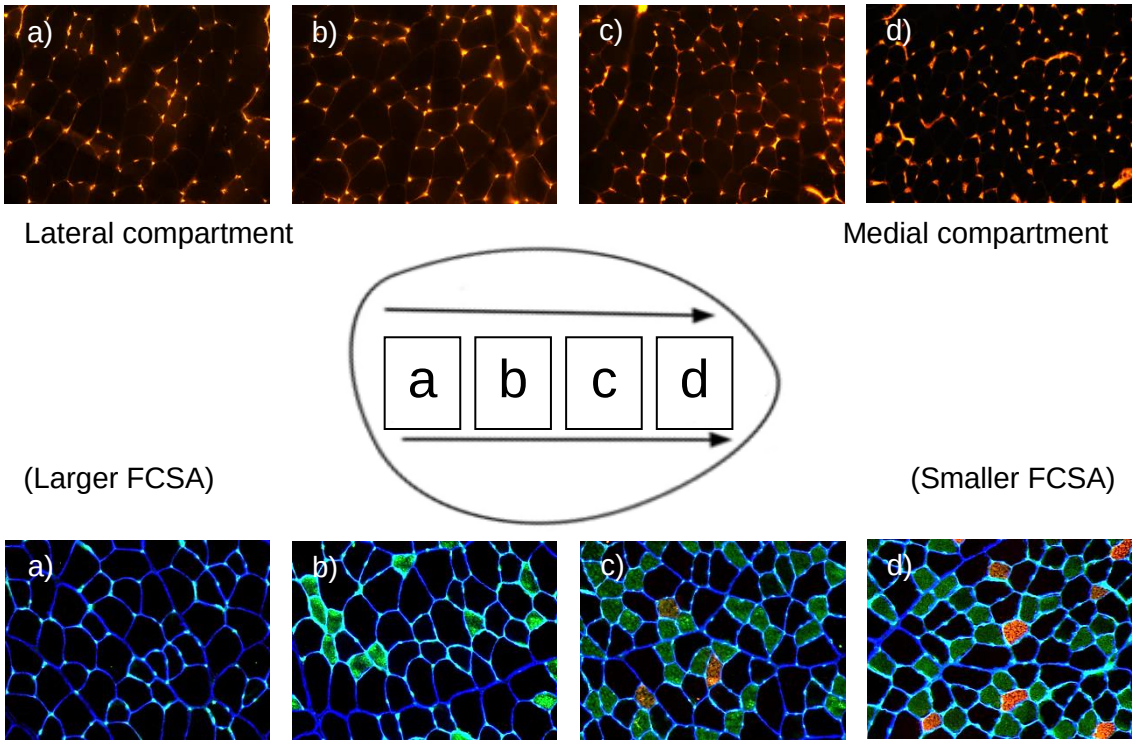

Figure 7-1. Heterogeneity of the EDL. The heterogeneous oxygen supply capacity of the EDL is demonstrated by the rhodamine labelled capillaries (histology top row, a-d). The increased oxidative supply medially across the EDL is matched by an increasing oxidative demand, in the form of increasing oxidative fibre phenotype (histology bottom row, a-d).

This thesis has re-emphasised the importance of sampling regimes and morphometric indices used to analyse histological samples and understanding their rationale. The data in Chapter 4 for the two mechanotransductive driven forms of angiogenesis (prazosin and overload) both showed similar increases in C:F, and hence a similar global response. However, looking at the regional specific changes in C:F, prazosin displayed

a relatively uniform increase across the four regions, while overload had region-specific changes. The local capillary distribution established that shear stress driven angiogenesis was primarily a stochastic response, compared to the targetted angiogenic response of the overload treated animals. This level of progressive analysis is now a feasible approach in exercise and disease physiology laboratories with our high throughput data pipeline.

The take home message from these chapters may be summarised as follows: an increasing realisation that even previously assumed 'homogeneous' muscles in fact contain functionally and structurally distinct regions demands a reappraisal of both the analytical approach when handling biopsies, and interpretation of the resulting data. This will allow improved understanding of the local factors that drive tissue remodelling, and help deliver more effective interventions that offer the equivalent of 'personalised medicine' for individual tissues and conditions.

7.2 Physiological angiogenesis (Chapters 4, 5 & 6)

Exercise, in all forms (endurance, interval or resistance training) is a powerful stimulus for adaptive remodelling. These various exercise modalities represent a compound of mechanical and chemical changes that represent large driving stimuli for adaptive remodelling (Egan and Zierath, 2013). Utilising a reductionist approach of isolating various components of exercise (*i.e.* mechanical or chemical signals that occur during exercise) to understand their importance in the phenotypic response of training has been of great interest for the last 20 years, and we are now beginning to build a more thorough understanding of exercise-specific stimuli driving adaptation (see reviews on the holistic overview of exercise adaptation (Egan and Zierath, 2013), with specific focus on human (Hoier and Hellsten, 2014) and rodent (Egginton, 2009, Egginton and Bicknell, 2011) models and mechanisms of angiogenesis). This work is crucial for the development of targetted exercise therapies and training regimes (Egginton, 2009). This thesis has concentrated

on the physiological adaptive remodelling of the microvasculature, and has expanded our current understanding of mechanotransductive angiogenic stimuli and their potential importance in exercise remodelling.

7.2.1 Chronic endurance and resistance training in humans

Our data has shown that the global response to chronic endurance (a largely aerobic, oxidative metabolism supported form of exercise) and resistance exercise (an anaerobic, anabolic form of training) have a broadly similar adaptive phenotype. The KEGG and GOBP overview of the endurance and resistance trained individuals identified few noticeable differences, other than that of up-regulated oxidative as well as glycolytic metabolic pathways in the resistance trained individuals. This would seem contrary to the idea that endurance exercise is the best way to increase oxidative capacity, and as such we need to consider the temporal response involved. There is evidence to show various oxidative and mitochondrial genes (PCG-1α, citrate synthase and β-HAD) are up-regulated as early as 2-4 hours post exercise (Perry et al., 2010), and remain elevated after 18-24 hours (CPT1, PCG-1α and 3-hydroxyacyl-CoA-dehydrogenase) (Leick et al., 2010). An improved oxidative capacity has been apparent as early as after four training sessions (Fig. 7-2a), and after six weeks there are major increases in mitochondrial content, oxidative enzymes and fuel transport proteins (Holloszy and Coyle, 1984). This adaptive response is the fundamental underpinning of improved aerobic capacity, but is not thought to be of great importance in resistance exercise. Therefore, the up-regulated metabolism pathways we see in the resistance trained individuals may be a secondary response supporting anabolism leading to muscle hypertrophy by increasing myofibril growth, following recruitment of anaerobic capacity and altered calcium handling needed to support acute activity. After successful adaptation and an improved capacity to generate power and perform work, the resistance training is likely driving key processes involved in sustaining exercise load, like those of energy metabolism.

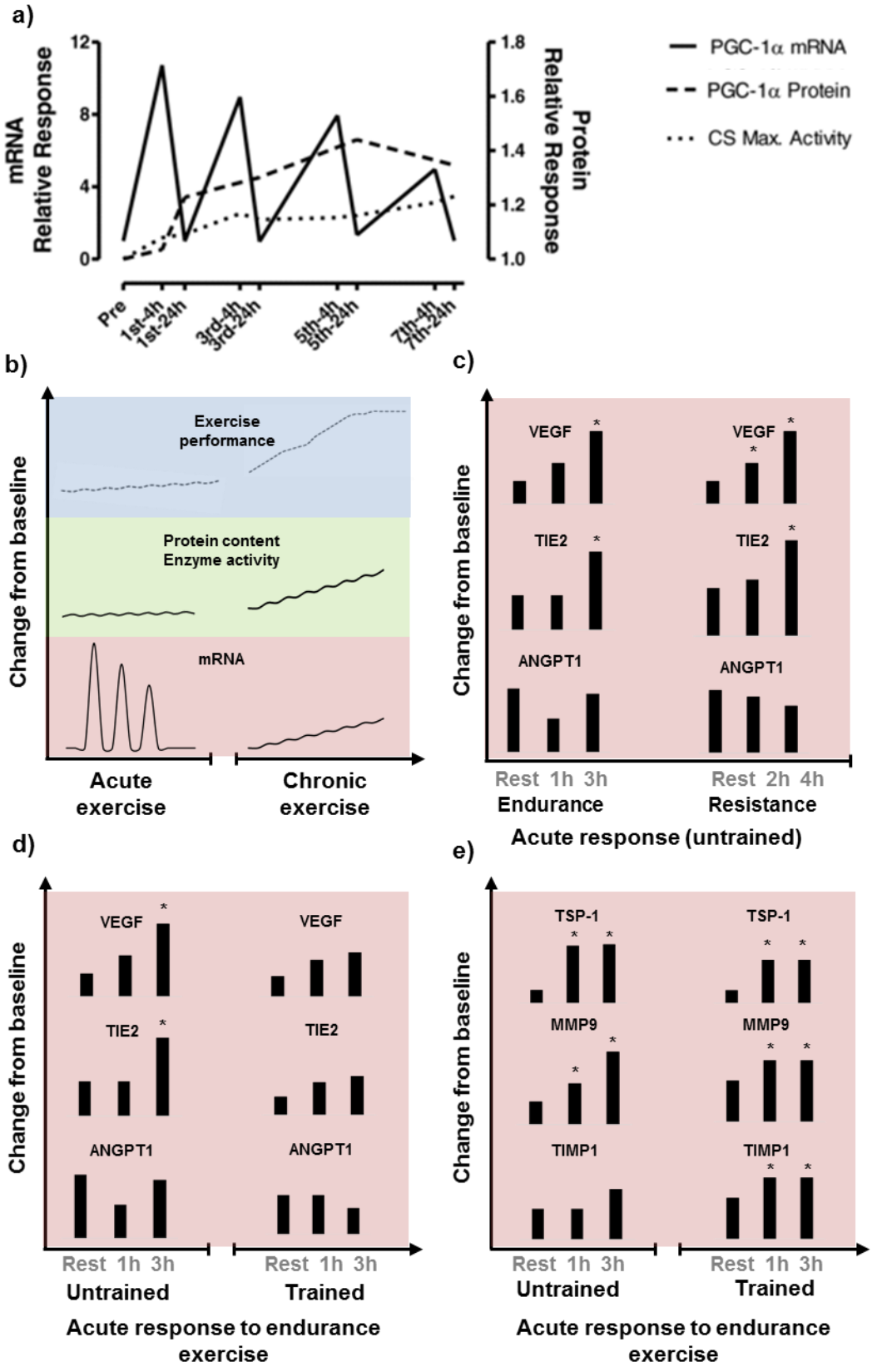
a)
mRNA Relative Response
Protein Relative Response
PGC-1α mRNA
PGC-1α Protein
CS Max. Activity
Pre
1st-4h
1st-24h
3rd-4h
3rd-24h
5th-4h
5th-24h
7th-4h
7th-24h
b)
Change from baseline
Exercise performance
Protein content
Enzyme activity
mRNA
Acute exercise
Chronic exercise
c)
Change from baseline
VEGF
TIE2
ANGPT1
Rest 1h 3h
Endurance
Rest 2h 4h
Resistance
Acute response (untrained)
d)
Change from baseline
VEGF
TIE2
ANGPT1
Rest 1h 3h
Untrained
Trained
Acute response to endurance exercise
e)
Change from baseline
TSP-1
MMP9
TIMP1
Rest 1h 3h
Untrained
Trained
Acute response to endurance exercise

Figure 7-2. Temporal response to exercise. Temporal response of PGC-1 α mRNA, protein content and citrate synthase activity (a) from Perry et al., (2010). An overview of the acute and chronic changes in mRNA, protein content/enzyme activity and exercise performance with training (b). The time course response of three angiogenic markers following an acute bout of endurance or resistance training (c). The time course response of VEGF, TIE2, and ANGPT1 (d) and TSP-1, MMP9 and TIMP1 (e) following an acute bout of endurance exercise in the untrained and trained state. Adapted from (Egan and Zierath, 2013), with data inserted from (Gavin et al., 2004) and (Hoier et al., 2012).

The acute response of both endurance and resistance exercise result in similar increases in key-angiogenic proteins and receptors (Fig. 7-2c), but show no clear differential response. Following four weeks of endurance training there is evidence of decreased mRNA content of various angiogenic proteins (VEGF and TIE2) while some increased from baseline (MMP9 and TIMP1) (Fig.7-2d,e). The equivalent data for resistance trained individuals is not currently available, and unpicking the importance of these individual genes within the complex process of angiogenesis is difficult.

We have begun to uncover interesting interconnected pathways in the human data that may play an important role in the temporal adaptive remodelling of the microvasculature, and the sequential adaptation of oxidative enzyme content and activity. As introduced in Chapter 6 the P53 pathway has a large number of down-stream activated pathways including: inhibition of angiogenesis, inhibition of mTOR/IGF-a pathway, cellular senescence, apoptosis, and mitochondrial biogenesis, and unpicking the fine control of the anti-angiogenic, anti-anabolic and pro-mitochondrial biogenesis response would be a logical next step in the analysis of these data.

7.2.2 Animal models of exercise induced angiogenesis

The differential angiogenic response of the mechanotransductive models of angiogenesis - prazosin induced shear stress and overload stimulated

abluminal stretch - were initially explored by the University of Birmingham Angiogenesis Research Group (Zhou et al., 1998a, Haas et al., 2000, Egginton et al., 2001, Rivilis et al., 2002, Williams et al., 2006c, Williams et al., 2006a, Williams et al., 2006b). The major findings of these studies were the differential growth process leading to distinct structural angiotypes, accompanied by marked differences in the gene/protein responses involved in angiogenic regulation (Fig. 7-3).

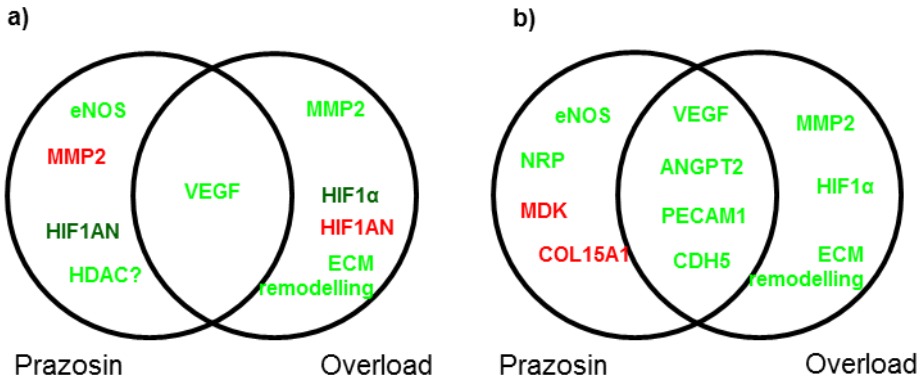

Figure 7-3. Cross-species comparison of mechanotransductive driven angiogenesis. The major up- and down-regulated individual genes/pathways with prazosin and overload driven angiogenesis in the rat (a; Chapter. 6) and mouse (b; adapted from (Williams et al., 2006a). Note there are common and specific elements associated with distinct forms of capillary growth.

We have now shown that the angiogenic response to pharmacologically induced shear stress results in no measureable change in the distribution of capillary supply area, while overload improves the overall capacity of the to deliver oxygen through reduced capillary supply areas. The stochastic response of prazosin points towards a lack of local tissue feedback stimulus that is evident in the overload model. The lack of localised angiogenic and low EC mitotic response of prazosin (Egginton et al., 2001) appears to be driven by a reduction in anti-angiogenic factors, rather than a large up-regulation of pro-angiogenic markers evident in the whole genome wide

array completed in Chapter 6. Conversely, the overloaded skeletal muscle showed a large up-regulation of ECM remodelling pathways and correlated highly with the global responses seen in both endurance and resistance trained humans.

There have also been data to further support the cross-species translational work, implementing the vasoactive pharmacological model of increased shear stress in humans. Pilot work was conducted by the Swiss anatomy group of Prof Hoppeler using prazosin (Wragg et al., 2014), with a full study by the Danish exercise science group of Prof Hellsten (University of Copenhagen, unpublished) who supplemented individuals for four weeks with terazosin (a prazosin-like vasoactive α_1 antagonist). This showed an angiogenic response in the *vastus lateralis m*uscle (12.5% increase in C:F and 24% increase in CD), with no event change in capillary domain distribution or capillary heterogeneity (Fig. 7-4a), suggesting the shear stress driven response is not responding to tissue metabolic demand, as seen in exercise (Fig. 7-4b).

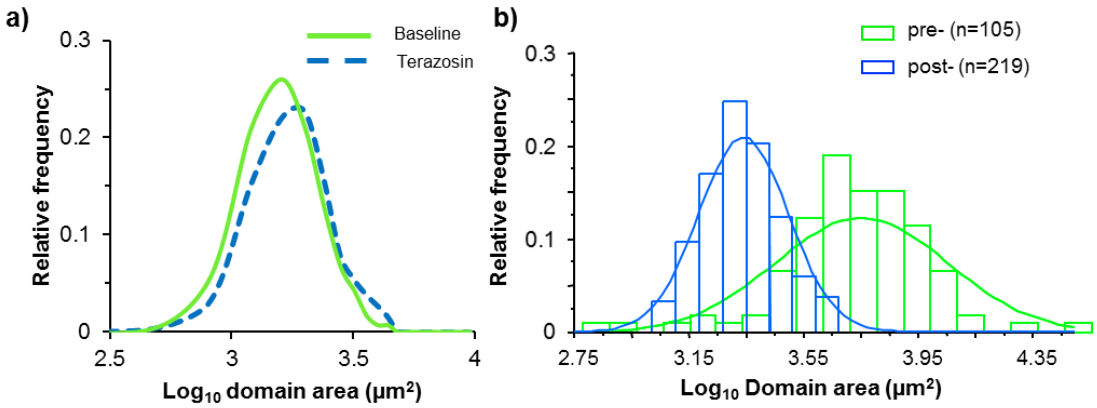

Figure 7-4. Capillary domain distributions for human angiogenic models. Human supplementation with terazosin (an α_1 antagonist, like prazosin) for four weeks (Mortensen, et al. unpublished) (a). Percutaneous needle biopsies from the lateral quadriceps muscle, pre- and post- isokinetic training at 60% maximum voluntary contraction using a Cybex Orthotron KT2 (Egginton, unpublished) (b). Both training regimes resulting in significant increases in C:F, however the capillary domain area distribution differ greatly. The terazosin data is consistent with findings in the rat and mouse models.

Indirect electrical stimulation has shown to be a potent angiogenic stimulus in skeletal muscle using stimulation frequencies similar to those recorded in slow muscles (10Hz, typically found in motor nerves supplying oxidative and highly vascularized tissues) (Brown et al., 1976, Hudlicka et al., 1994, Egginton and Hudlicka, 2000). We used varying electrical stimulation frequencies to manipulate the physiological stimuli we know to be present during exercise, to explore their concomitant effect on microvascular expansion. Based on previous work by Hudlická (1988) it was suggested that higher stimulation frequencies resulted in improved fatigue resistance through improved oxidative enzyme activity and content rather than increased microvasculature. Our data contradicts these findings, as we have shown a 20-30% increase in capillary content following indirect electrical stimulation at a range of different frequencies (Chapter 4). Physiological measures of blood flow and tension generation would suggest very different stimuli for remodelling, however whether considering structural changes (increased capillarity and homogeneous distribution) or the subsequent gene profiling it is difficult to identify any dramatic differences (as seen between endurance and resistance exercise). There is evidence for similarities between the shear stress driven angiogenic response of prazosin and the low frequency 4Hz stimulation, and similarly the overload induced muscle stretch and 40Hz. These data require more time to unpick the interconnected pathways driving shear stress and altered muscle stretch in angiogenesis, but offer a potential avenue to explore in order to provide a mechanistic basis for targetted angiotherapy.

7.2.3 Spinal cord injury

In order to validate basic research, it is helpful to determine if the principles established are applicable in other conditions. Very little research exists on the effect of spinal cord injury and subsequent rehabilitation programs on skeletal muscle oxygen delivery capacity (functional supply area of capillaries and the heterogeneity of this supply region). We have shown that following a

sever contusion injury that capillary rarefaction is evident within functionally distinct regions of the tibialis anterior, possibly contributing to reduced functional capacity of locomotory muscle. However, through the combination of load-bearing exercise and epidural electrical stimulation it is possible to ameliorate the capillary loss and phenotypic change of skeletal muscle. Chapter 5 has recapitulated the importance of the use of fine-scale local indices in the quantification of angiogenesis and microvascular remodelling. Taking the global angiogenic readouts alone would suggest very different conclusions to those made with the local indices. These data suggest an important role for weight bearing locomotor training in maintaining oxidative fibre composition and potentially important in the signalling of targetting angiogenesis.

7.3 Overview of exercise induced angiogenesis

The plastic capillary bed is able to be modified through a variety of chemical and mechanical stimuli. This thesis has sought to assess how these various physiological signals interact, through differential signal cascades for angiogenesis, and how the subsequent growth (or rarefaction) impacts the distribution of capillary supply areas and the subsequent effects on oxygen diffusion kinetics. Figure 7-5 gives an overview of important physiological signalling events that result in changes in genetic signalling and subsequent remodelling.

The outstanding stimulus appears to be that of altered muscle length in the driving of targetted angiogenesis evident in indirect stimulation, overload and spinal cord injury locomotor training (and passive movement, not discussed in this thesis (Hoier et al., 2013)). This would explain why restricted movement (through bed rest or limb immobilisation) is such a potent driver of capillary rarefaction and muscle atrophy (Harper and Lyles, 1988, Berg et al., 1997, Topp et al., 2002, Gallagher et al., 2005). The use of pharmacological intervention (*e.g.* induced shear stress) to maintain capillary supply may be

useful in an immobilised limb or bed rest situation, where repetitive movement is not feasible. It may be possible to mimic muscle signalling seen during locomotion pharmacologically that would provide the local-signal to direct angiogenesis of shear-stress induced microvascular expansion. The use of the AMPK activator AICAR has been shown to drive a large number of exercise-related signalling cascades, including expansion of oxidative fibre type content, increased oxidative enzyme activity and improved insulin-signalling (Zhang et al., 2009). However, AICAR supplementation has shown not to have any angiogenic response (Putman et al., 2003), and as such the combination of AICAR with an α_1 antagonist may provide an effective pharmacological alternative to exercise.

7.4 Future directions

There is a wealth of research to suggest that exercise adaptation differs greatly among individuals who receive the same activity stimulus. This may be underpinned by differential molecular responses (Keller et al., 2007, Timmons et al., 2010, Keller et al., 2011), but surprisingly is not accounted for by genetic variation (Bouchard and Rankinen, 2001). To build upon the angiogenic network described here, and successfully identify critical genes in the angiogenic adaptive response, we require simultaneous analysis of the transcriptional response and physiological adaptation (*i.e.* the incorporation of physiological measures like C:F, CD and VO_{2MAX}). This will provide a molecular profile of genes critical for physiological angiogenesis, which may then be tested within animal models such as those described in this thesis. We have completed a selection of the angiogenic models in mice (overload, prazosin and 10Hz stimulation) which have begun to show has the same transcriptional response as that of rat (inserted data below). Having successfully identified the molecular phenotype of the various animal models of angiogenesis, we now have the capacity to test hypotheses generated by such physiologically informed transcriptional analysis.

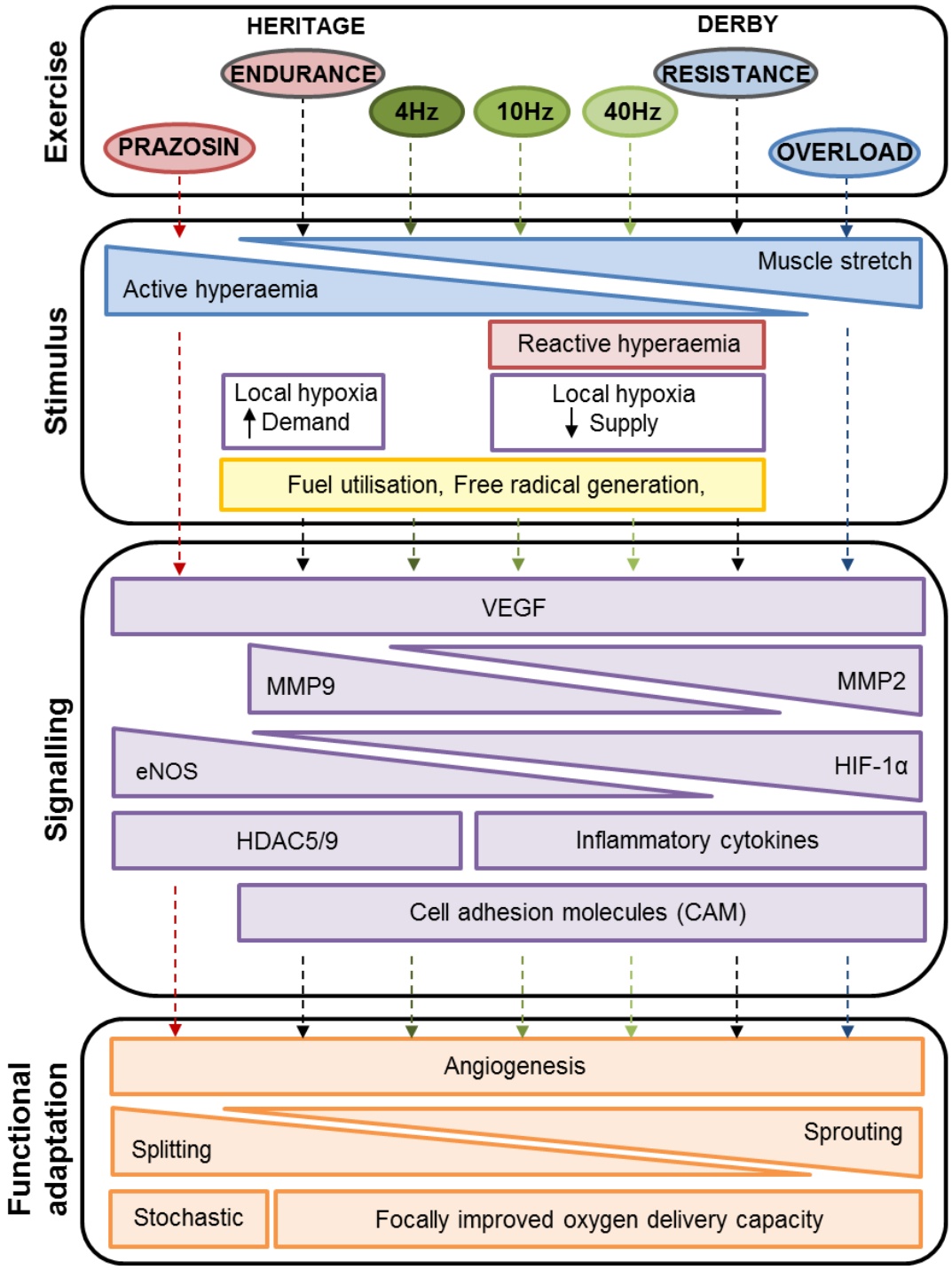

Figure 7-5. Overview schematic. Overview of the various exercise regimes and muscle activity patterns and their likely physiological stimulus, integral signalling cascades and their functional outcome.

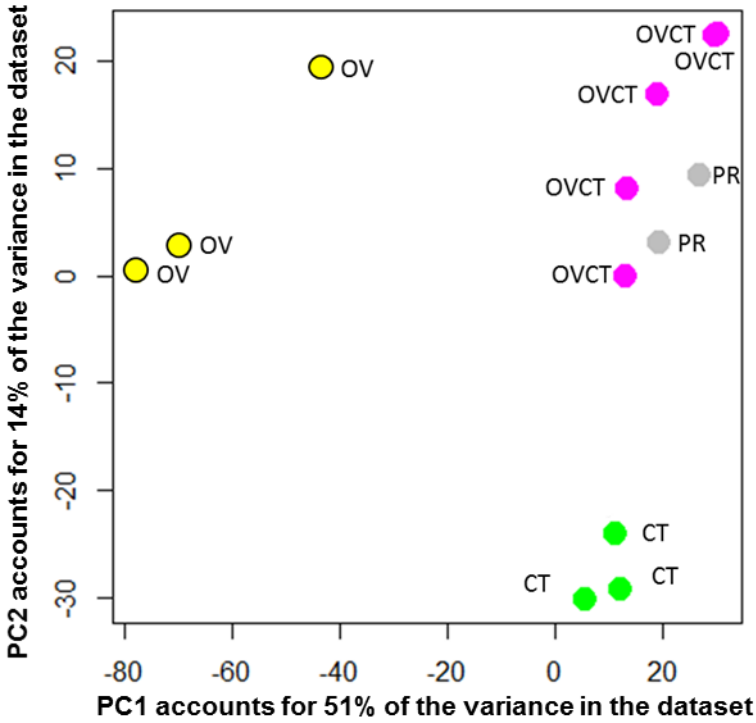

Figure 7-6. Principal component analysis for mouse angiogenic models. Global transcriptional response across each group (*CT, n=3; PR, n=2; OVCT, n=5 and OV, n=3)*. Principal component 1 (x-axis) accounts for 51% of the variation seen among the groups, while principal component 2 (y-axis) accounts for 14%. The global transcriptional response for the overload and prazosin treated mice is similar to that of the equivalent treated rats (Chapter 6, Fig. 6-6)

Table 7-1. Differential changes in KEGG and GOBP pathways between mouse models

Category	Term	Comparison	Up-regulated	Adjusted P-Value
GOBP	Response to purine-containing compound	Praz vs Con	Praz	0.09109583
KEGG	Metabolism of xenobiotics by cytochrome P450	Praz vs Con	Praz	0.04332054
GOBP	Extracellular matrix	Praz vs Con	Con	0.01883248
GOBP	Blood vessel morphogenesis	Praz vs Con	Con	0.000141343
GOBP	Regulation of cell differentiation	Praz vs Con	Con	0.000159436
GOBP	Muscle structure development	Praz vs Con	Con	0.000827001
GOBP	Extracellular matrix organization	OV vs CT	OV	2.2485E-08
GOBP	Focal adhesion	OV vs CT	OV	2.55183E-11
GOBP	Extracellular matrix disassembly	OV vs CT	OV	0.09418277
GOBP	Lymphocyte mediated immunity	OV vs CT	OV	0.006106963
GOBP	Immunoglobulin mediated immune response	OV vs CT	OV	0.005105668
GOBP	Inflammatory response	OV vs CT	OV	4.9145E-08
GOBP	Blood vessel development	OV vs CT	OV	1.30676E-06
GOBP	Mitochondrion	OV vs CT	CT	5.06914E-40
KEGG	Citrate cycle (TCA cycle)	OV vs CT	CT	4.90439E-09
KEGG	Oxidative phosphorylation	OV vs CT	CT	3.84962E-08
GOBP	Fatty acid catabolic process	OV vs CT	CT	8.75744E-07

Alternate shading to differentiate pairwise interactions in the order: PR *vs.* CT, OV *vs.* CT.

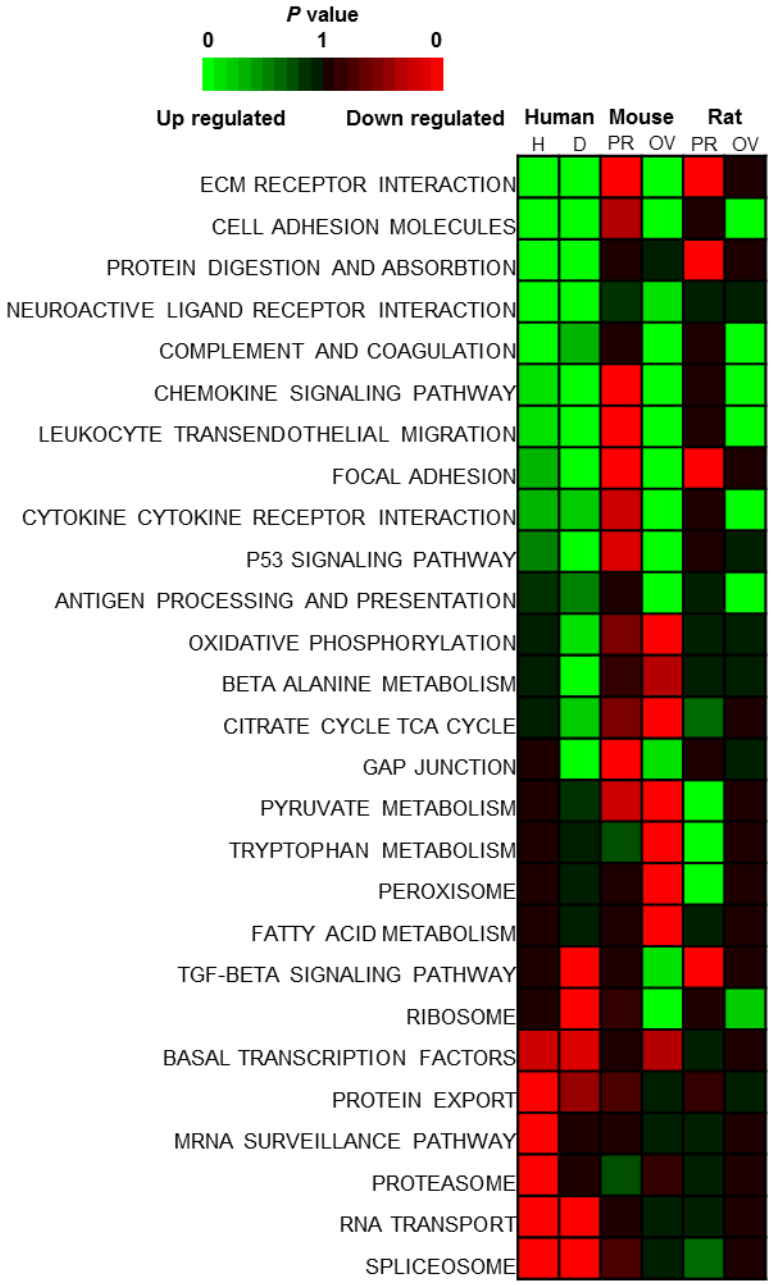

Figure 7-7. Heat map for specific KEGG pathways regulated in prazosin and overload animals across rats and mice. The global transcriptomic response of exercise in humans following two distinct forms of exercise, compared to the global transcriptomic response of seven days of prazosin and overload across rat and mouse models. H, HERITAGE data pre *vs.* post; D, DERBY data pre *vs.* post; PR, prazosin data PR *vs.* CT and OV, overload data OV *vs.* OVCT. There is a consistent overlap between the rat and mice model of overload and the two forms of exercise, with a further supporting link for cytokine driven angiogenesis in overload.

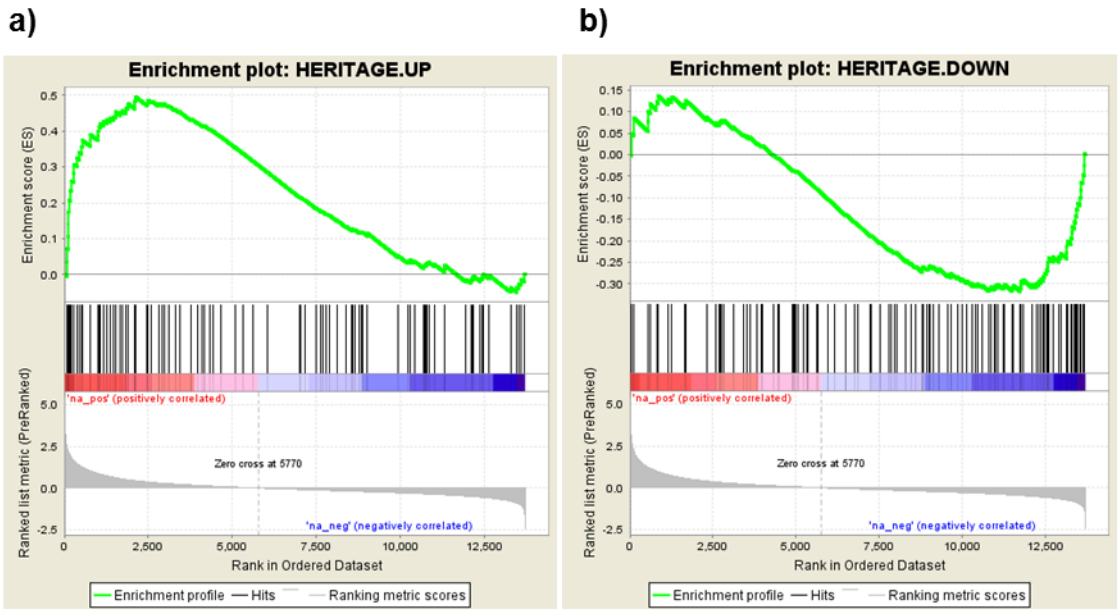

Figure 7-8. Enrichment plot for overload treated mice against the HERITAGE data set. The global transcriptomic response of seven days of overload (*i.e.* OV *vs.* OVCT) was compared to the global transcriptomic response of the endurance trained HERITAGE cohort (pre *vs.* post). There is a significant overlap in the genes up- and down-regulated in the overload trained animals to that of the endurance trained humans.

Table 7-2. Comparison in key gene up- and down-regulated in overload and endurance trained humans

Comparison	Genes	Functional Terms
Genes **up**-regulated in both the Overload vs CT comparison and after training in the HERITAGE study	ASPN, CCL5, GMFG, PRND, LCP1, SCN5A, PLEK, ARHGAP9, RBP1, CHRND, ALDH3B1, CDT1, SPARC, LYN, TYRO3, CRTAP, ELK3, NLGN2, WAS, THBS4, XAF1, ST6GALNAC1, RAB5C, TACC1, TUSC3, S1PR2, MBOAT2, PDZD11, PCDH17, C3AR1, PIK3R3, CD3E, RPL31, MYEF2, PTK7, COL4A1, ADAP1	Cell-cell adhesion (10), regulation of chemotaxis (4), cell migration (8), blood vessel development (6), KEGG-Chemokine signalling pathway (4)
Genes **down**-regulated in both the Overload vs CT comparison and after training in the HERITAGE study	MAVS, PPP1R14A, HK2, FOXO6, DNLZ, BDH1, P2RY2, ATP6AP1, CREB5, ANKRD37, MAP2K3, ACTA2, RRS1, MYOM2, NCOR2, ALPK3, MAST2, MYADML2, EIF4G1, MAN2A2, MAFK, HSPA1A, CNBP, KCNA5, NFIX, TRIM54, SLC2A4, RBM20, MYH7B, NFIL3, ARFGAP2, MED25, CFD, TCEA2, ARNTL, CTH, PLIN5, ASB2, GLUL, TUBA4A, PLIN4, MICAL2	positive regulation of gene expression (15), contractile fibre (5), regulation of blood vessel size (3)

Notable genes up-regulated discussed in this thesis are CCL5, SPARC and COL4A1

Appendix

Appendix 1: Fibre type composition protocol

Solutions:

Block solution (PBSH_2O & 1% BSA)

a) 0.01g of BSA into labelled eppendorf
b) 1ml of PBSH_2O using pipette into eppendorf
c) vortex for a 10-20 seconds

Fix solution (PBS H_2O & formaldehyde)

a) Make a 2% PFA solution – dilute 500µl of 8% stock solution in 1500µl of PBS
b) vortex for a 5-10 seconds

Solution 1: BA-D5 (1:1000) & Laminin (1:250)
Solution 2: Anti-Mouse 555 [RED] (1:1000) & Biotinylated - Anti-Rabbit (1:250)
Solution 3: SC-71(1:500) & Pacific Blue (1:250)
Solution 4: Anti-Mouse 488 [GREEN] (1:1000) & Griffonia simplicifolia Lectin (1:200)

Protocol

Fix and block:

Apply fix solution to wells.

a) Roughly 100-150µl per well
b) Leave for 2 minutes
c) Vacuum fix off
d) Wash 5-10 times (one drop = one wash) with wash PBS using vacuum to remove solution

Apply block solution to wells.

a) Roughly 100-150µl per well
b) Leave for 10 minutes
c) Vacuum off

Antibody incubation:

a) Incubate each solution for 1 hour covered
b) After 1 hour suction off antibody solution and wash 5-10 times with wash PBS
c) Apply next antibody solution using and repeat throughout solutions #1-4
d) After final solution incubation 5-10 times with distilled H_2O
e) Wash and suction off all moisture

Mount:
Mount with Vectasheild

Appendix 2. Angiogenic hub genes

ACVR2B	CCL3	CXCR2	EPHA3	FLT4	IL12RB1	MMRN1	ROBO4
ADAMTS1	CCL5	CXCR3	EPHA4	FOXO4	IL12RB2	MST1	SERPINC1
AGGF1	CCNA2	CXCR7	EPHA5	GDNF	IL15	MTOR	SERPINE1
AGT	CCR1	CYR61	EPHA7	GNA11	IL15RA	NOS1	SERPINE1
AMOT	CCR3	DCN	EPHB2	GRN	IL16	NOS3	SERPINF1
ANG	CD34	DPP4	EPHB3	HBEGF	IL17B	NRP1	SPARC
ANGPT1	CD93	ECM1	EPHB4	HDAC5	IL1A	NRP2	SPARCL1
ANGPT2	CDH5	ECM1	EPHB6	HDAC7	IL1B	PAK2	SPHK1
ANGPT4	CHRNA7	EDG1	EREG	HDAC9	IL1R1	PDGFA	TEK
ANGPTL3	CLEC14A	EDN1	ERG	HGF	IL1R2	PDGFB	TGFA
ANGPTL4	COL4A1	EFEMP1	ERN1	HIF1A	IL33	PDGFC	TGFB1
ANPEP	COL4A2	EFEMP2	ESM1	HIF1AN	IL6	PDGFD	TGFB3
ANXA3	COL4A3	EFNA1	FABP4	HOXA5	IL6R	PDGFRA	TGFBR1
APOH	COL4A4	EFNA2	FASLG	ICAM2	IL8	PDGFRB	TGFBR2
AREG	CRP2	EFNA3	FBLN1	IFITM1	ITGAV	PECAM1	TGFBR3
ARHGAP24	CSF2	EFNA4	FBLN2	IFNA1	ITGB3	PF4	THBS2
ARHGEF15	CSF3	EFNA5	FBLN5	IFNG	KDR	PF4V1	THBS4
ARNT	CTGF	EFNB1	FGF1	IGF1	KITLG	PGF	THBS1
ARTN	CTGF	EFNB2	FGF13	IGF1R	LAMA4	PIGF	TIE1
BAI1	CXCL1	EFNB3	FGF18	IGF2	LDB2	PLAT	TIMP1
BMP1	CXCL10	EGF	FGF2	IGF2R	LECT1	PLAU	TIMP2
BMP2	CXCL11	EGFR	FGF3	IGFBP1	LPHN1	PLAUR	TIMP3
BMX	CXCL12	EGLN1	FGF4	IGFBP2	MCAM	PLCG1	TIMP4
BTG1	CXCL13	EGLN2	FGF7	IGFBP3	MCF2L	PML	TNF
CALCRL	CXCL14	EGLN3	FGFR1	IGFBP4	MDK	PPARGC1A	TNFAIP2
CCL14	CXCL16	ELTD1	FGFR2	IL10	MET	PPBP	VASH1
CCL2	CXCL3	EMCN	FGFR3	IL10RA	MFNG	PTN	VEGFA
CCL2	CXCL5	ENG	FGFR4	IL10RB	MMP1	PTPRM	VEGFB
CCL20	CXCL6	EPHA1	FIGF	IL12A	MMP2	PTX3	VEGFC
CCL21	CXCR1	EPHA2	FLT1	IL12B	MMP9	RND3	WNT5A

240 identified genes in physiological and pathological angiogenesis

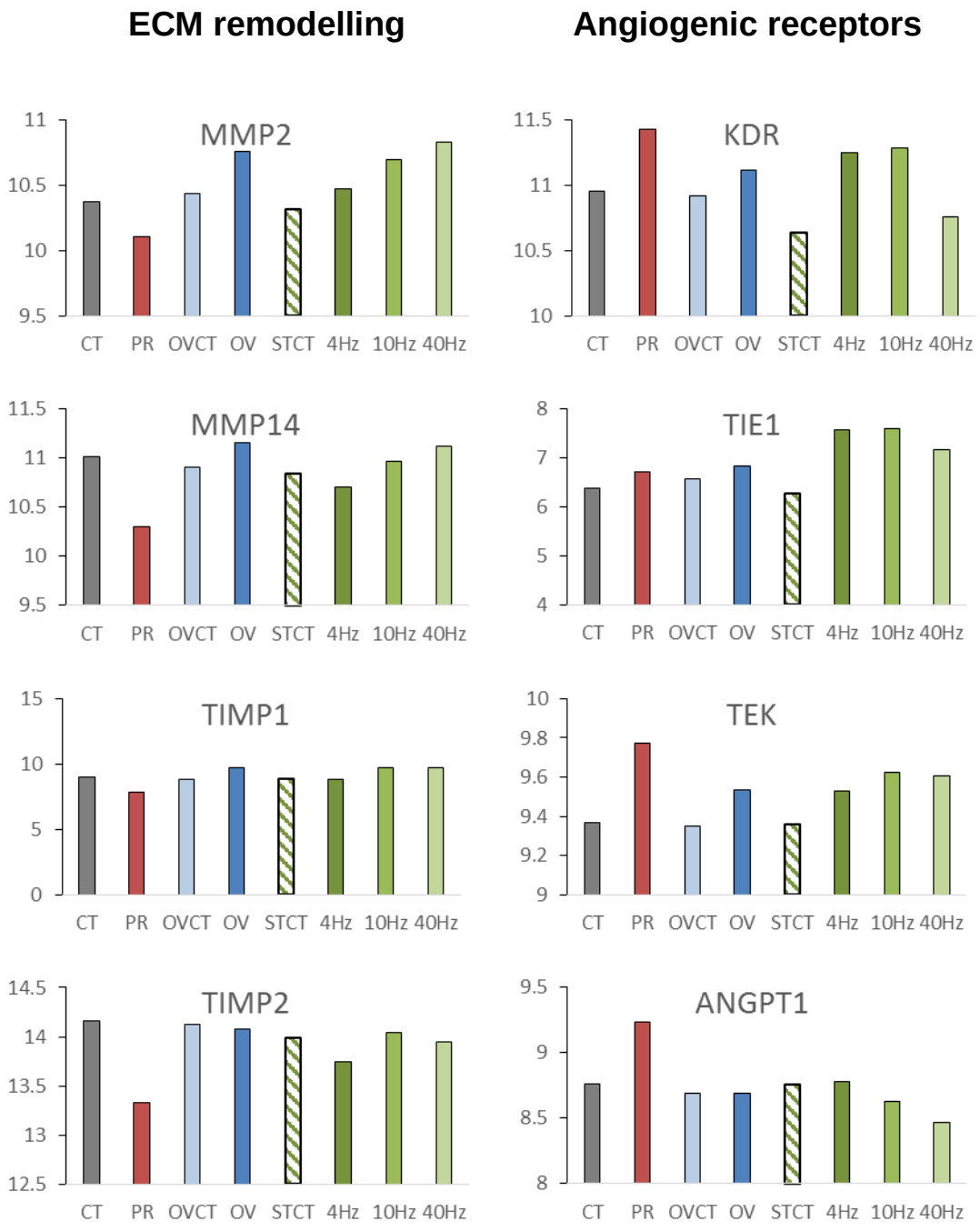

Appendix 3. Average intensity plot for key ECM remodelling genes and a variety of tyrosine kinase receptors. MMP2, Matrix metalloproteinase 2; MMP14, Matrix metalloproteinase 14; TIMP1, Tissue inhibitor of metalloproteinases 1; TIMP2, Tissue inhibitor of metalloproteinases; KDR, Kinase insert domain receptor or VEGFR2; TIE1, Tyrosine kinase with immunoglobulin-like or EGF-like domains 1; TEK, Angiopoietin-1 receptor; ANGPT1, Angiopoietin 1.

Appendix 4. Comparative hub gene pathway enrichment for overload *vs.* prazosin, across HERITAGE and DERBY derived pathways

Generated pathway	Hub gene	Interaction	Up-regulated	FWER (*P*-val)
HERITAGE	HIF1AN	OV vs. PR	PR	0.062
HERITAGE	MET	OV vs. PR	PR	0.208
DERBY	HDAC5	OV vs. PR	PR	0.056
DERBY	GNA11	OV vs. PR	PR	0.732
HERITAGE	TIMP2	OV vs. PR	OV	0
HERITAGE	COL4A2	OV vs. PR	OV	0
HERITAGE	IGFBP4	OV vs. PR	OV	0
HERITAGE	TGFBR2	OV vs. PR	OV	0
HERITAGE	VASH1	OV vs. PR	OV	0
HERITAGE	LAMA4	OV vs. PR	OV	0
HERITAGE	DCN	OV vs. PR	OV	0
HERITAGE	COL4A1	OV vs. PR	OV	0
HERITAGE	THBS4	OV vs. PR	OV	0
HERITAGE	TIMP1	OV vs. PR	OV	0
HERITAGE	PGF	OV vs. PR	OV	0.001
HERITAGE	SPARC	OV vs. PR	OV	0.001
HERITAGE	CLEC14A	OV vs. PR	OV	0.0035
HERITAGE	GRN	OV vs. PR	OV	0.005
HERITAGE	MCAM	OV vs. PR	OV	0.005
HERITAGE	PDGFRB	OV vs. PR	OV	0.0085
HERITAGE	CCL5	OV vs. PR	OV	0.0095
HERITAGE	FBLN1	OV vs. PR	OV	0.0275
HERITAGE	CXCL16	OV vs. PR	OV	0.031
HERITAGE	ROBO4	OV vs. PR	OV	0.032
HERITAGE	MMP2	OV vs. PR	OV	0.048
HERITAGE	ICAM2	OV vs. PR	OV	0.063
DERBY	PDGFD	OV vs. PR	OV	0
DERBY	TIMP1	OV vs. PR	OV	0
DERBY	TGFBR2	OV vs. PR	OV	0
DERBY	LAMA4	OV vs. PR	OV	0
DERBY	TIMP2	OV vs. PR	OV	0
DERBY	CD93	OV vs. PR	OV	0
DERBY	DCN	OV vs. PR	OV	0
DERBY	IFITM1	OV vs. PR	OV	0
DERBY	FBLN2	OV vs. PR	OV	0
DERBY	EFEMP1	OV vs. PR	OV	0
DERBY	SPARC	OV vs. PR	OV	0

DERBY	IL1R1	OV vs. PR	OV	0
DERBY	EMCN	OV vs. PR	OV	0
DERBY	THBS4	OV vs. PR	OV	0
DERBY	MMP2	OV vs. PR	OV	0
DERBY	THBS1	OV vs. PR	OV	5.00E-04
DERBY	CDH5	OV vs. PR	OV	5.00E-04
DERBY	SPARCL1	OV vs. PR	OV	5.00E-04
DERBY	PECAM1	OV vs. PR	OV	0.001
DERBY	ICAM2	OV vs. PR	OV	0.002
DERBY	ERG	OV vs. PR	OV	0.002
DERBY	PLAUR	OV vs. PR	OV	0.0065
DERBY	LDB2	OV vs. PR	OV	0.007
DERBY	NRP1	OV vs. PR	OV	0.008
DERBY	TNFAIP2	OV vs. PR	OV	0.0095
DERBY	FABP4	OV vs. PR	OV	0.0115
DERBY	COL4A1	OV vs. PR	OV	0.0115
DERBY	HIF1A	OV vs. PR	OV	0.0235
DERBY	MCAM	OV vs. PR	OV	0.034
DERBY	COL4A2	OV vs. PR	OV	0.0435
DERBY	PLAU	OV vs. PR	OV	0.0505
DERBY	PDGFRB	OV vs. PR	OV	0.0515
DERBY	CD34	OV vs. PR	OV	0.067
DERBY	THBS2	OV vs. PR	OV	0.11

Tables organized by: up-regulated pathway, in order of their FWER (*P*-val) and finally the data set the hub genes were derived from (HERITAGE or DERBY).

Appendix 5. Comparative hub gene pathway enrichment for 4Hz *vs.* 40Hz, across HERITAGE and DERBY derived pathways

Generated pathway	**Hub gene**	**Interaction**	**Up-regulated**	**FWER (*P*-val)**
HERITAGE	EFNB2	4Hz vs. 40Hz	4Hz	0.79
DERBY	HDAC5	4Hz vs. 40Hz	4Hz	0.887
HERITAGE	TIMP2	4Hz vs. 40Hz	40Hz	0
HERITAGE	PGF	4Hz vs. 40Hz	40Hz	0.008
HERITAGE	IGFBP3	4Hz vs. 40Hz	40Hz	0.065
HERITAGE	EFEMP1	4Hz vs. 40Hz	40Hz	0.068
HERITAGE	TGFBR2	4Hz vs. 40Hz	40Hz	0.068
HERITAGE	CXCL16	4Hz vs. 40Hz	40Hz	0.08
HERITAGE	DCN	4Hz vs. 40Hz	40Hz	0.088
DERBY	TIMP1	4Hz vs. 40Hz	40Hz	0.005

DERBY	MMP2	4Hz vs. 40Hz	40Hz	0.005
DERBY	DCN	4Hz vs. 40Hz	40Hz	0.049
DERBY	PDGFRA	4Hz vs. 40Hz	40Hz	0.088

Tables organized by: up-regulated pathway, in order of their FWER (*P*-val) and finally the data set the hub genes were derived from (HERITAGE or DERBY).

Appendix 6. Comparative hub gene pathway enrichment for 4Hz *vs.* prazosin, across HERITAGE and DERBY derived pathways

Generated pathway	**Hub gene**	**Interaction**	**Up-regulated**	**FWER (*P*-val)**
HERITAGE	HDAC9	4Hz *vs.* PR	PR	0.006
HERITAGE	ACVR2B	4Hz *vs.* PR	PR	0.195
DERBY	EGLN1	4Hz *vs.* PR	PR	0.6
HERITAGE	COL4A2	4Hz *vs.* PR	4Hz	0
HERITAGE	ICAM2	4Hz *vs.* PR	4Hz	0
HERITAGE	TIMP1	4Hz *vs.* PR	4Hz	0
HERITAGE	ENG	4Hz *vs.* PR	4Hz	0
HERITAGE	TIMP2	4Hz *vs.* PR	4Hz	0
HERITAGE	MCAM	4Hz *vs.* PR	4Hz	0
HERITAGE	VASH1	4Hz *vs.* PR	4Hz	0
HERITAGE	IGFBP4	4Hz *vs.* PR	4Hz	0
HERITAGE	PDGFRB	4Hz *vs.* PR	4Hz	5.00E-04
HERITAGE	ROBO4	4Hz *vs.* PR	4Hz	5.00E-04
HERITAGE	CDH5	4Hz *vs.* PR	4Hz	0.0015
HERITAGE	LAMA4	4Hz *vs.* PR	4Hz	0.002
HERITAGE	COL4A1	4Hz *vs.* PR	4Hz	0.002
HERITAGE	ARHGEF15	4Hz *vs.* PR	4Hz	0.004
HERITAGE	SPARC	4Hz *vs.* PR	4Hz	0.0095
HERITAGE	THBS4	4Hz *vs.* PR	4Hz	0.012
HERITAGE	FBLN2	4Hz *vs.* PR	4Hz	0.018
HERITAGE	CLEC14A	4Hz *vs.* PR	4Hz	0.0235
HERITAGE	EFNA1	4Hz *vs.* PR	4Hz	0.0265
HERITAGE	TIMP3	4Hz *vs.* PR	4Hz	0.0305
HERITAGE	LDB2	4Hz *vs.* PR	4Hz	0.032
HERITAGE	PGF	4Hz *vs.* PR	4Hz	0.04
HERITAGE	FBLN1	4Hz *vs.* PR	4Hz	0.044
HERITAGE	MMP2	4Hz *vs.* PR	4Hz	0.087
HERITAGE	TIE1	4Hz *vs.* PR	4Hz	0.0985
DERBY	CD93	4Hz *vs.* PR	4Hz	0
DERBY	PDGFD	4Hz *vs.* PR	4Hz	0

DERBY	COL4A2	4Hz *vs.* PR	4Hz	0
DERBY	FBLN2	4Hz *vs.* PR	4Hz	0
DERBY	LAMA4	4Hz *vs.* PR	4Hz	0
DERBY	TIMP1	4Hz *vs.* PR	4Hz	0
DERBY	PECAM1	4Hz *vs.* PR	4Hz	0
DERBY	HIF1A	4Hz *vs.* PR	4Hz	0
DERBY	ICAM2	4Hz *vs.* PR	4Hz	0.0035
DERBY	CDH5	4Hz *vs.* PR	4Hz	0.0055
DERBY	MCAM	4Hz *vs.* PR	4Hz	0.0055
DERBY	EMCN	4Hz *vs.* PR	4Hz	0.0055
DERBY	ERG	4Hz *vs.* PR	4Hz	0.0075
DERBY	TGFBR2	4Hz *vs.* PR	4Hz	0.009
DERBY	THBS4	4Hz *vs.* PR	4Hz	0.011
DERBY	IL1R1	4Hz *vs.* PR	4Hz	0.0125
DERBY	LDB2	4Hz *vs.* PR	4Hz	0.014
DERBY	TIMP2	4Hz *vs.* PR	4Hz	0.014
DERBY	EFNA1	4Hz *vs.* PR	4Hz	0.034
DERBY	PDGFRB	4Hz *vs.* PR	4Hz	0.049
DERBY	SPARC	4Hz *vs.* PR	4Hz	0.0525
DERBY	IGFBP3	4Hz *vs.* PR	4Hz	0.0625

Tables organized by: up-regulated pathway, in order of their FWER (*P*-val) and finally the data set the hub genes were derived from (HERITAGE or DERBY).

Appendix 7. Comparative hub gene pathway enrichment for 40Hz *vs.* overload, across HERITAGE and DERBY derived pathways

Generated pathway	**Hub gene**	**Interaction**	**Up-regulated**	**FWER (*P*-val)**
HERITAGE	AMOT	40Hz *vs.* OV	40Hz	0.0465
HERITAGE	EFEMP2	40Hz *vs.* OV	40Hz	0.101
DERBY	PLAUR	40Hz *vs.* OV	40Hz	0.5115
HERITAGE	CCL5	40Hz *vs.* OV	OV	0.162
HERITAGE	AGGF1	40Hz *vs.* OV	OV	0.162
HERITAGE	CXCL12	40Hz *vs.* OV	OV	0.5425
DERBY	ROBO4	40Hz *vs.* OV	OV	0.024
DERBY	MCAM	40Hz *vs.* OV	OV	0.2995

Tables organized by: up-regulated pathway, in order of their FWER (*P*-val) and finally the data set the hub genes were derived from (HERITAGE or DERBY).

References

AAGAARD, P., SUETTA, C., CASEROTTI, P., MAGNUSSON, S. P. & KJÆR, M. 2010. Role of the nervous system in sarcopenia and muscle atrophy with aging: strength training as a countermeasure. *Scandinavian journal of medicine & science in sports,* 20**,** 49-64.

ABRAHAM, L. & LOEB, G. 1985. The distal hindlimb musculature of the cat. *Experimental brain research,* 58**,** 580-593.

ADAMS, G. R. 2002. Invited Review: Autocrine/paracrine IGF-I and skeletal muscle adaptation. *Journal of Applied Physiology,* 93**,** 1159-1167.

AHMED, S., EGGINTON, S., JAKEMAN, P., MANNION, A. & ROSS, H. 1997. Is human skeletal muscle capillary supply modelled according to fibre size or fibre type? *Experimental physiology,* 82**,** 231-234.

AHN, A. N. 2012. How muscles function–the work loop technique. *Journal of Experimental Biology,* 215**,** 1051-1052.

AL-SHAMMARI, A., GAFFNEY, E. & EGGINTON, S. 2012. Re-evaluating the use of voronoi tessellations in the assessment of oxygen supply from capillaries in muscle. *Bulletin of mathematical biology,* 74**,** 2204-2231.

AL-SHAMMARI, A., GAFFNEY, E. & EGGINTON, S. 2014a. Modelling Oxygen Capillary Supply to Striated Muscle Tissues. *Advances in Applied Mathematics.* Springer.

AL-SHAMMARI, A. A. 2014. *Mathematical modelling of oxygen transport in skeletal and cardiac muscles.* University of Oxford.

AL-SHAMMARI, A. A., GAFFNEY, E. A. & EGGINTON, S. 2014b. Modelling capillary oxygen supply capacity in mixed muscles: Capillary domains revisited. *Journal of theoretical biology,* 356**,** 47-61.

ALLEN, D. G., LAMB, G. D. & WESTERBLAD, H. 2008. Impaired calcium release during fatigue. *Journal of Applied Physiology,* 104**,** 296-305.

ALLEN, D. L., HARRISON, B. C., MAASS, A., BELL, M. L., BYRNES, W. C. & LEINWAND, L. A. 2001. Cardiac and skeletal muscle adaptations to voluntary wheel running in the mouse. *Journal of Applied Physiology,* 90**,** 1900-1908.

ALWAY, S., GONYEA, W. & DAVIS, M. 1990. Muscle fiber formation and fiber hypertrophy during the onset of stretch-overload. *American Journal of Physiology-Cell Physiology,* 259**,** C92-C102.

AMARAL, S. L., LINDERMAN, J. R., MORSE, M. M. & GREENE, A. S. 2001. Angiogenesis induced by electrical stimulation is mediated by angiotensin II and VEGF. *Microcirculation,* 8**,** 57-67.

AMELN, H., GUSTAFSSON, T., SUNDBERG, C. J., OKAMOTO, K., JANSSON, E., POELLINGER, L. & MAKINO, Y. 2005. Physiological activation of hypoxia inducible factor-1 in human skeletal muscle. *The FASEB journal,* 19**,** 1009-1011.

ANDERSEN, P. & HENRIKSSON, J. 1977. Capillary supply of the quadriceps femoris muscle of man: adaptive response to exercise. *The Journal of physiology,* 270**,** 677.

ANDERSEN, T., SCHMIDT, J., THOMASSEN, M., HORNSTRUP, T., FRANDSEN, U., RANDERS, M., HANSEN, P., KRUSTRUP, P. &

BANGSBO, J. 2014. A preliminary study: Effects of football training on glucose control, body composition, and performance in men with type 2 diabetes. *Scandinavian journal of medicine & science in sports*.

ANGELI, C. A., EDGERTON, V. R., GERASIMENKO, Y. P. & HARKEMA, S. J. 2014. Altering spinal cord excitability enables voluntary movements after chronic complete paralysis in humans. *Brain,* 137**,** 1394-1409.

APPELL, H.-J. 1990. Muscular atrophy following immobilisation. *Sports Medicine,* 10**,** 42-58.

ARMSTRONG, R. & LAUGHLIN, M. 1983. Blood flows within and among rat muscles as a function of time during high speed treadmill exercise. *The Journal of Physiology,* 344**,** 189-208.

ARMSTRONG, R., MARUM, P., SAUBERT, C., SEEHERMAN, H. & TAYLOR, C. 1977. Muscle fiber activity as a function of speed and gait. *Journal of Applied Physiology,* 43**,** 672-677.

ARMSTRONG, R. B. 1988. Distribution of blood flow in the muscles of conscious animals during exercise. *The American journal of cardiology,* 62**,** 9E-14E.

ASKEW, G. N. & MARSH, R. L. 1997. The effects of length trajectory on the mechanical power output of mouse skeletal muscles. *Journal of Experimental Biology,* 200**,** 3119-3131.

ASKEW, G. N. & MARSH, R. L. 2001. The mechanical power output of the pectoralis muscle of blue-breasted quail (Coturnix chinensis): the in vivo length cycle and its implications for muscle performance. *Journal of Experimental Biology,* 204**,** 3587-3600.

ASKEW, G. N., YOUNG, I. S. & ALTRINGHAM, J. D. 1997. Fatigue of mouse soleus muscle, using the work loop technique. *Journal of Experimental Biology,* 200**,** 2907-2912.

BALDWIN, K., VALDEZ, V., SCHRADER, L. & HERRICK, R. 1981. Effect of functional overload on substrate oxidation capacity of skeletal muscle. *Journal of applied physiology: respiratory, environmental and exercise physiology,* 50**,** 1272-1276.

BALICE-GORDON, R. & THOMPSON, W. 1988. The organization and development of compartmentalized innervation in rat extensor digitorum longus muscle. *The Journal of Physiology,* 398**,** 211-231.

BAMFORD, J., PUTMAN, C. & MUSHAHWAR, V. 2005. Intraspinal microstimulation preferentially recruits fatigue-resistant muscle fibres and generates gradual force in rat. *The Journal of Physiology,* 569**,** 873-884.

BARCLAY, C. 1996. Mechanical efficiency and fatigue of fast and slow muscles of the mouse. *The Journal of Physiology,* 497**,** 781-794.

BARTLETT, J. D., LOUHELAINEN, J., IQBAL, Z., COCHRAN, A. J., GIBALA, M. J., GREGSON, W., CLOSE, G. L., DRUST, B. & MORTON, J. P. 2013. Reduced carbohydrate availability enhances exercise-induced p53 signaling in human skeletal muscle: implications for mitochondrial biogenesis. *American Journal of Physiology-Regulatory, Integrative and Comparative Physiology,* 304**,** R450-R458.

BAUER, P. M., YU, J., CHEN, Y., HICKEY, R., BERNATCHEZ, P. N., LOOFT-WILSON, R., HUANG, Y., GIORDANO, F., STAN, R. V. & SESSA, W. C. 2005. Endothelial-specific expression of caveolin-1 impairs microvascular permeability and angiogenesis. *Proceedings of the National Academy of Sciences of the United States of America,* 102**,** 204-209.

BAUM, O., SUTER, F., GERBER, B., TSCHANZ, S. A., BUERGY, R., BLANK, F., HLUSHCHUK, R. & DJONOV, V. 2010. VEGF-A Promotes Intussusceptive Angiogenesis in the Developing Chicken Chorioallantoic Membrane. *Microcirculation,* 17**,** 447-457.

BAUM, O., VIEREGGE, M., KOCH, P., GÜL, S., HAHN, S., HUBER-ABEL, F. A., PRIES, A. R. & HOPPELER, H. 2013. Phenotype of capillaries in skeletal muscle of nNOS-knockout mice. *American journal of physiology-regulatory, integrative and comparative physiology,* 304**,** R1175-R1182.

BAYLOR, S. M. & HOLLINGWORTH, S. 2012. Intracellular calcium movements during excitation–contraction coupling in mammalian slow-twitch and fast-twitch muscle fibers. *The Journal of general physiology,* 139**,** 261-272.

BEIN, K. & SIMONS, M. 2000. Thrombospondin Type 1 Repeats Interact with Matrix Metalloproteinase 2 REGULATION OF METALLOPROTEINASE ACTIVITY. *Journal of Biological Chemistry,* 275**,** 32167-32173.

BERG, H., LARSSON, L. & TESCH, P. 1997. Lower limb skeletal muscle function after 6 wk of bed rest. *Journal of Applied Physiology,* 82**,** 182-188.

BERGERON, M., YU, A. Y., SOLWAY, K. E., SEMENZA, G. L. & SHARP, F. R. 1999. Induction of hypoxia-inducible factor-1 (HIF-1) and its target genes following focal ischaemia in rat brain. *European Journal of Neuroscience,* 11**,** 4159-4170.

BIERING-SØRENSEN, B., KRISTENSEN, I. B., KJAER, M. & BIERING-SØRENSEN, F. 2009. Muscle after spinal cord injury. *Muscle & nerve,* 40**,** 499-519.

BIGNON, M., PICHOL-THIEVEND, C., HARDOUIN, J., MALBOUYRES, M., BRÉCHOT, N., NASCIUTTI, L., BARRET, A., TEILLON, J., GUILLON, E. & ETIENNE, E. 2011. Lysyl oxidase-like protein-2 regulates sprouting angiogenesis and type IV collagen assembly in the endothelial basement membrane. *Blood,* 118**,** 3979-3989.

BLOEMBERG, D. & QUADRILATERO, J. 2012. Rapid determination of myosin heavy chain expression in rat, mouse, and human skeletal muscle using multicolor immunofluorescence analysis. *PloS one,* 7**,** e35273.

BOESEN, A. P., DIDERIKSEN, K., COUPPÉ, C., MAGNUSSON, S., SCHJERLING, P., BOESEN, M., KJÆR, M. & LANGBERG, H. 2013. Tendon and skeletal muscle matrix gene expression and functional responses to immobilisation and rehabilitation in young males: effect of

growth hormone administration. *The Journal of physiology,* 591**,** 6039-6052.

BOLSTAD, B. M., IRIZARRY, R. A., ÅSTRAND, M. & SPEED, T. P. 2003. A comparison of normalization methods for high density oligonucleotide array data based on variance and bias. *Bioinformatics,* 19**,** 185-193.

BONGRAZIO, M., DA SILVA-AZEVEDO, L., BERGMANN, E., BAUM, O., HINZ, B., PRIES, A. & ZAKRZEWICZ, A. 2005. Shear stress modulates the expression of thrombospondin-1 and CD36 in endothelial cells in vitro and during shear stress-induced angiogenesis in vivo. *International journal of immunopathology and pharmacology,* 19**,** 35-48.

BOOTH, F. & KELSO, J. 1973. Effect of hind-limb immobilization on contractile and histochemical properties of skeletal muscle. *Pfluegers Archiv,* 342**,** 231-238.

BORISOV, A. B., HUANG, S. K. & CARLSON, B. M. 2000. Remodeling of the vascular bed and progressive loss of capillaries in denervated skeletal muscle. *The Anatomical Record,* 258**,** 292-304.

BOSUTTI, A., EGGINTON, S., BARNOUIN, Y., GANSE, B., RITTWEGER, J. & DEGENS, H. 2015. Local capillary supply in muscle is not determined by local oxidative capacity. *Journal of Experimental Biology,* 218**,** 3377-3380.

BOTTINELLI, R., CANEPARI, M., PELLEGRINO, M. & REGGIANI, C. 1996. Force-velocity properties of human skeletal muscle fibres: myosin heavy chain isoform and temperature dependence. *The Journal of physiology,* 495**,** 573-586.

BOTTINELLI, R., SCHIAFFINO, S. & REGGIANI, C. 1991. Force-velocity relations and myosin heavy chain isoform compositions of skinned fibres from rat skeletal muscle. *The Journal of Physiology,* 437**,** 655.

BOUCHARD, C., LEON, A. S., RAO, D., SKINNER, J. S., WILMORE, J. H. & GAGNON, J. 1995. The HERITAGE family study. Aims, design, and measurement protocol. *Medicine and Science in Sports and Exercise,* 27**,** 721-729.

BOUCHARD, C. & RANKINEN, T. 2001. Individual differences in response to regular physical activity. *Medicine and science in sports and exercise,* 33**,** S446-51; discussion S452-3.

BOULÉ, N. G., WEISNAGEL, S. J., LAKKA, T. A., TREMBLAY, A., BERGMAN, R. N., RANKINEN, T., LEON, A. S., SKINNER, J. S., WILMORE, J. H. & RAO, D. 2005. Effects of exercise training on glucose homeostasis. *Diabetes care,* 28**,** 108-114.

BROWN, M. 1995. Metabolic control of blood flow with reference to heart, skeletal muscle and brain. *Cardiovascular Regulation, Portland Press, London, UK***,** 113-126.

BROWN, M. D., COTTER, M. A., HUDLICKÁ, O. & VRBOVÁ, G. 1976. The effects of different patterns of muscle activity on capillary density, mechanical properties and structure of slow and fast rabbit muscles. *Pflügers Archiv,* 361**,** 241-250.

BUCCI, M., GRATTON, J.-P., RUDIC, R. D., ACEVEDO, L., ROVIEZZO, F., CIRINO, G. & SESSA, W. C. 2000. In vivo delivery of the caveolin-1 scaffolding domain inhibits nitric oxide synthesis and reduces inflammation. *Nature medicine,* 6**,** 1362-1367.

BUFFELLI, M., PASINO, E. & CANGIANO, A. 1997. Paralysis of rat skeletal muscle equally affects contractile properties as does permanent denervation. *Journal of Muscle Research & Cell Motility,* 18**,** 683-695.

BUNGE, R. P., PUCKETT, W., BECERRA, J., MARCILLO, A. & QUENCER, R. 1993. Observations on the pathology of human spinal cord injury. A review and classification of 22 new cases with details from a case of chronic cord compression with extensive focal demyelination. *Advances in neurology,* 59**,** 75.

BURRI, P. H., HLUSHCHUK, R. & DJONOV, V. 2004. Intussusceptive angiogenesis: its emergence, its characteristics, and its significance. *Developmental Dynamics,* 231**,** 474-488.

BURTON, R. F. 1975. *Ringer solutions and physiological salines*, Wright-Scientechnica.

CADY, E., JONES, D., LYNN, J. & NEWHAM, D. 1989. Changes in force and intracellular metabolites during fatigue of human skeletal muscle. *The Journal of Physiology,* 418**,** 311.

CAMPOS, G. E., LUECKE, T. J., WENDELN, H. K., TOMA, K., HAGERMAN, F. C., MURRAY, T. F., RAGG, K. E., RATAMESS, N. A., KRAEMER, W. J. & STARON, R. S. 2002. Muscular adaptations in response to three different resistance-training regimens: specificity of repetition maximum training zones. *European journal of applied physiology,* 88**,** 50-60.

CAO, G., O'BRIEN, C. D., ZHOU, Z., SANDERS, S. M., GREENBAUM, J. N., MAKRIGIANNAKIS, A. & DELISSER, H. M. 2002. Involvement of human PECAM-1 in angiogenesis and in vitro endothelial cell migration. *American Journal of Physiology-Cell Physiology,* 282**,** C1181-C1190.

CARMELIET, P., DE SMET, F., LOGES, S. & MAZZONE, M. 2009. Branching morphogenesis and antiangiogenesis candidates: tip cells lead the way. *Nature Reviews Clinical Oncology,* 6**,** 315-326.

CARMELIET, P., DOR, Y., HERBERT, J.-M., FUKUMURA, D., BRUSSELMANS, K., DEWERCHIN, M., NEEMAN, M., BONO, F., ABRAMOVITCH, R. & MAXWELL, P. 1998. Role of HIF-1α in hypoxia-mediated apoptosis, cell proliferation and tumour angiogenesis. *Nature,* 394**,** 485-490.

CARMELIET, P., FERREIRA, V., BREIER, G., POLLEFEYT, S., KIECKENS, L., GERTSENSTEIN, M., FAHRIG, M., VANDENHOECK, A., HARPAL, K. & EBERHARDT, C. 1996. Abnormal blood vessel development and lethality in embryos lacking a single VEGF allele. *Nature,* 380**,** 435-439.

CARMELIET, P. & JAIN, R. K. 2000. Angiogenesis in cancer and other diseases. *nature,* 407**,** 249-257.

CARMELIET, P. & JAIN, R. K. 2011. Molecular mechanisms and clinical applications of angiogenesis. *Nature,* 473**,** 298-307.

CARMELIET, P., NG, Y.-S., NUYENS, D., THEILMEIER, G., BRUSSELMANS, K., CORNELISSEN, I., EHLER, E., KAKKAR, V. V., STALMANS, I. & MATTOT, V. 1999. Impaired myocardial angiogenesis and ischemic cardiomyopathy in mice lacking the vascular endothelial growth factor isoforms VEGF164 and VEGF188. *Nature medicine,* 5**,** 495.

CASTRO, M. J., APPLE JR, D. F., HILLEGASS, E. A. & DUDLEY, G. A. 1999. Influence of complete spinal cord injury on skeletal muscle cross-sectional area within the first 6 months of injury. *European Journal of Applied Physiology and Occupational Physiology,* 80**,** 373-378.

CATOIRE, M. & KERSTEN, S. 2015. The search for exercise factors in humans. *The FASEB Journal,* 29**,** 1615-1628.

CEGLIA, L., NIRAMITMAHAPANYA, S., PRICE, L. L., HARRIS, S. S., FIELDING, R. A. & DAWSON-HUGHES, B. 2013. An evaluation of the reliability of muscle fiber cross-sectional area and fiber number measurements in rat skeletal muscle. *Biological procedures online,* 15**,** 1.

CHANG, H., BAO-WEI, W., PEILIANG, K. & KOU-GI, S. 2003. Cyclical mechanical stretch enhances angiopoietin-2 and Tie2 receptor expression in cultured human umbilical vein endothelial cells. *Clinical Science,* 104**,** 421-428.

CHIQUET, M. 1999. Regulation of extracellular matrix gene expression by mechanical stress. *Matrix biology,* 18**,** 417-426.

CHRISTENSEN, J. G., BURROWS, J. & SALGIA, R. 2005. c-Met as a target for human cancer and characterization of inhibitors for therapeutic intervention. *Cancer letters,* 225**,** 1-26.

CHRISTOV, C., CHRÉTIEN, F., ABOU-KHALIL, R., BASSEZ, G., VALLET, G., AUTHIER, F.-J., BASSAGLIA, Y., SHININ, V., TAJBAKHSH, S. & CHAZAUD, B. 2007. Muscle satellite cells and endothelial cells: close neighbors and privileged partners. *Molecular biology of the cell,* 18**,** 1397-1409.

CLOSE, R. 1964. Dynamic properties of fast and slow skeletal muscles of the rat during development. *The Journal of Physiology,* 173**,** 74-95.

CLOSE, R. 1967. Properties of motor units in fast and slow skeletal muscles of the rat. *The Journal of Physiology,* 193**,** 45-55.

CONTI, I. & ROLLINS, B. J. CCL2 (monocyte chemoattractant protein-1) and cancer. Seminars in cancer biology, 2004. Elsevier, 149-154.

CRAMERI, R., WESTON, A., CLIMSTEIN, M., DAVIS, G. & SUTTON, J. 2002. Effects of electrical stimulation-induced leg training on skeletal muscle adaptability in spinal cord injury. *Scandinavian journal of medicine & science in sports,* 12**,** 316-322.

CURTIN, N. & EDMAN, K. 1994. Force-velocity relation for frog muscle fibres: effects of moderate fatigue and of intracellular acidification. *The Journal of physiology,* 475**,** 483-494.

DAWSON, J. M. & HUDLICKA, O. 1989. The effects of long term administration of prazosin on the microcirculation in skeletal muscles. *Cardiovascular research,* 23**,** 913-920.

DEGENS, H., DEVECI, D., BOTTO-VAN BEMDEN, A., HOOFD, L. J. & EGGINTON, S. 2006. Maintenance of heterogeneity of capillary spacing is essential for adequate oxygenation in the soleus muscle of the growing rat. *Microcirculation,* 13**,** 467-476.

DEGENS, H., TUREK, Z., HOOFD, L., VAN'T HOF, M. & BINKHORST, R. 1992. The relationship between capillarisation and fibre types during compensatory hypertrophy of the plantaris muscle in the rat. *Journal of anatomy,* 180**,** 455.

DEGENS, H., VEERKAMP, J. H., VAN MOERKERK, H. T., TUREK, Z., HOOFD, L. J. & BINKHORST, R. A. 1993. Metabolic capacity, fibre type area and capillarization of rat plantaris muscle. Effects of age, overload and training and relationship with fatigue resistance. *International journal of biochemistry,* 25**,** 1141-1148.

DENNIS, R. A., PRZYBYLA, B., GURLEY, C., KORTEBEIN, P. M., SIMPSON, P., SULLIVAN, D. H. & PETERSON, C. A. 2008. Aging alters gene expression of growth and remodeling factors in human skeletal muscle both at rest and in response to acute resistance exercise. *Physiological genomics,* 32**,** 393-400.

DEVECI, D. & EGGINTON, S. 2002a. Differing mechanisms of cold-induced changes in capillary supply in m. tibialis anterior of rats and hamsters. *Journal of Experimental Biology,* 205**,** 829-840.

DEVECI, D. & EGGINTON, S. 2002b. Muscle ischaemia in rats may be relieved by overload-induced angiogenesis. *Experimental physiology,* 87**,** 479-488.

DEVECI, D., MARSHALL, J. M. & EGGINTON, S. 2001. Relationship between capillary angiogenesis, fiber type, and fiber size in chronic systemic hypoxia. *American Journal of Physiology-Heart and Circulatory Physiology,* 281**,** H241-H252.

DJONOV, V., BAUM, O. & BURRI, P. H. 2003. Vascular remodeling by intussusceptive angiogenesis. *Cell and tissue research,* 314**,** 107-117.

DUDLEY, G. A., ABRAHAM, W. M. & TERJUNG, R. L. 1982. Influence of exercise intensity and duration on biochemical adaptations in skeletal muscle. *Journal of Applied Physiology,* 53**,** 844-850.

DUPONT-VERSTEEGDEN, E. E., MURPHY, R. J., HOULÉ, J. D., GURLEY, C. M. & PETERSON, C. A. 2000. Mechanisms leading to restoration of muscle size with exercise and transplantation after spinal cord injury. *American Journal of Physiology-Cell Physiology,* 279**,** C1677-C1684.

DUROZARD, D., GABRIELLE, C. & BAVEREL, G. 2000. Metabolism of rat skeletal muscle after spinal cord transection. *Muscle & nerve,* 23**,** 1561-1568.

EBINA, T., HOSHI, N., KOBAYASHI, M., KAWAMURA, K., NANJO, H., SUGITA, A., SUGIYAMA, T., MASUDA, H. & XU, C. 2002. Physiological angiogenesis in electrically stimulated skeletal muscle in

rabbits: Characterization of capillary sprouting by ultrastructural 3-D reconstruction study. *Pathology international,* 52**,** 702-712.
ECCLES, J. C., ECCLES, R. M. & LUNDBERG, A. 1958. The action potentials of the alpha motoneurones supplying fast and slow muscles. *The Journal of Physiology,* 142**,** 275.
EDMAN, K. & MATTIAZZI, A. R. 1981. Effects of fatigue and altered pH on isometric force and velocity of shortening at zero load in frog muscle fibres. *Journal of Muscle Research & Cell Motility,* 2**,** 321-334.
EELEN, G., CRUYS, B., WELTI, J., DE BOCK, K. & CARMELIET, P. 2013. Control of vessel sprouting by genetic and metabolic determinants. *Trends in Endocrinology & Metabolism*.
EGAN, B. & ZIERATH, J. R. 2013. Exercise metabolism and the molecular regulation of skeletal muscle adaptation. *Cell metabolism,* 17**,** 162-184.
EGGINTON, S. 1990a. Morphometric analysis of tissue capillary supply. *Vertebrate Gas Exchange.* Springer.
EGGINTON, S. 1990b. Numerical and areal density estimates of fibre type composition in a skeletal muscle (rat extensor digitorum longus). *Journal of anatomy,* 168**,** 73.
EGGINTON, S. 1998. Anatomical adaptations for peripheral oxygen transport at high and low temperatures. *South African Journal of Zoology,* 33**,** 119-128.
EGGINTON, S. 2009. Invited review: activity-induced angiogenesis. *Pflügers Archiv-European Journal of Physiology,* 457**,** 963-977.
EGGINTON, S. 2011. In vivo shear stress response. *Biochemical Society Transactions,* 39**,** 1633.
EGGINTON, S., BADR, I., WILLIAMS, J., HAUTON, D., BAAN, G. C. & JASPERS, R. T. 2011. Physiological angiogenesis is a graded, not threshold, response. *The Journal of Physiology,* 589**,** 195-206.
EGGINTON, S. & BICKNELL, R. 2011. Advances in the Cellular and Molecular Biology of Angiogenesis. *Biochemical Society Transactions,* 39**,** 1551.
EGGINTON, S. & GAFFNEY, E. 2010. Experimental Physiology–Review Article: Tissue capillary supply–it's quality not quantity that counts! *Experimental physiology,* 95**,** 971-979.
EGGINTON, S. & HUDLICKA, O. 1999. Early changes in performance, blood flow and capillary fine structure in rat fast muscles induced by electrical stimulation. *The Journal of Physiology,* 515**,** 265-275.
EGGINTON, S. & HUDLICKA, O. 2000. Selective long-term electrical stimulation of fast glycolytic fibres increases capillary supply but not oxidative enzyme activity in rat skeletal muscles. *Experimental physiology,* 85**,** 567-573.
EGGINTON, S., HUDLICKA, O., BROWN, M., WALTER, H., WEISS, J. & BATE, A. 1998. Capillary growth in relation to blood flow and performance in overloaded rat skeletal muscle. *Journal of Applied Physiology,* 85**,** 2025-2032.
EGGINTON, S., HUSSAIN, A., HALL-JONES, J., CHAUDHRY, B., SYEDA, F. & GLEN, K. E. 2016. Shear stress-induced angiogenesis in mouse

muscle is independent of the vasodilator mechanism and quickly reversible. *Acta Physiologica*.

EGGINTON, S. & JOHNSTON, I. 1983. An estimate of capillary anisotropy and determination of surface and volume densities of capillaries in skeletal muscles of the conger eel (Conger conger L.). *QJ exp. Physiol,* 68**,** 603-617.

EGGINTON, S. & ROSS, H. 1989. Influence of muscle phenotype on local capillary supply. *Oxygen Transport to Tissue XI.* Springer.

EGGINTON, S. & ROSS, H. Planar analysis of tissue capillary supply. SEMINAR SERIES-SOCIETY FOR EXPERIMENTAL BIOLOGY, 1992. Cambridge University Press, 165-165.

EGGINTON, S., TUREK, Z. & HOOFD, L. 1988. Differing patterns of capillary distribution in fish and mammalian skeletal muscle. *Respiration physiology,* 74**,** 383-396.

EGGINTON, S., ZHOU, A.-L., BROWN, M. & HUDLICKA, O. 2001. Unorthodox angiogenesis in skeletal muscle. *Cardiovascular research,* 49**,** 634-646.

EIKELBOOM, R. & MILLS, R. 1988. A microanalysis of wheel running in male and female rats. *Physiology & behavior,* 43**,** 625-630.

EMMERT-STREIB, F. & GLAZKO, G. V. 2011. Pathway analysis of expression data: deciphering functional building blocks of complex diseases. *PLoS Comput Biol,* 7**,** e1002053.

FERRARA, N., CARVER MOORE, K., CHEN, H., DOWD, M., LU, L., O'SHEA, K. S., POWELL BRAXTON, L., HILLAN, K. J. & MOORE, M. W. 1996. Heterozygous embryonic lethality induced by targeted inactivation of the VEGF gene.

FERRARA, N., GERBER, H.-P. & LECOUTER, J. 2003. The biology of VEGF and its receptors. *Nature medicine,* 9**,** 669-676.

FERREIRA, J. C., BACURAU, A. V., BUENO, C. R., CUNHA, T. C., TANAKA, L. Y., JARDIM, M. A., RAMIRES, P. R. & BRUM, P. C. 2010. Aerobic exercise training improves Ca2+ handling and redox status of skeletal muscle in mice. *Experimental Biology and Medicine,* 235**,** 497-505.

FLEMING, I., FISSLTHALER, B., DIXIT, M. & BUSSE, R. 2005. Role of PECAM-1 in the shear-stress-induced activation of Akt and the endothelial nitric oxide synthase (eNOS) in endothelial cells. *Journal of cell science,* 118**,** 4103-4111.

FOLKMAN, J. 1971. Tumor angiogenesis: therapeutic implications. *New england journal of medicine,* 285**,** 1182-1186.

FOLKMAN, J. 1995. Angiogenesis in cancer, vascular, rheumatoid and other disease. *Nature medicine,* 1**,** 27-30.

FORSYTHE, J. A., JIANG, B.-H., IYER, N. V., AGANI, F., LEUNG, S. W., KOOS, R. D. & SEMENZA, G. L. 1996. Activation of vascular endothelial growth factor gene transcription by hypoxia-inducible factor 1. *Molecular and cellular biology,* 16**,** 4604-4613.

FRENETTE, P. S. & WAGNER, D. D. 1996. Adhesion molecules. *New England Journal of Medicine,* 334**,** 1526-1529.

FRISCHKNECHT, R. & VRBOVÁ, G. 1991. Adaptation of rat extensor digitorum longus to overload and increased activity. *Pflügers Archiv,* 419**,** 319-326.

FULGENZI, G., GRACIOTTI, L., COLLIS, M. & HUDLICKA, O. 1998. The effect of alpha< sub> 1</sub> adrenoceptor antagonist prazosin on capillary supply, blood flow and performance in a rat model of chronic muscle ischaemia. *European journal of vascular and endovascular surgery,* 16**,** 71-77.

GALE, N. W. & YANCOPOULOS, G. D. 1999. Growth factors acting via endothelial cell-specific receptor tyrosine kinases: VEGFs, angiopoietins, and ephrins in vascular development. *Genes & development,* 13**,** 1055-1066.

GALLAGHER, P., TRAPPE, S., HARBER, M., CREER, A., MAZZETTI, S., TRAPPE, T., ALKNER, B. & TESCH, P. 2005. Effects of 84-days of bedrest and resistance training on single muscle fibre myosin heavy chain distribution in human vastus lateralis and soleus muscles. *Acta physiologica scandinavica,* 185**,** 61-69.

GAVIN, T., DREW, J., KUBIK, C., POFAHL, W. & HICKNER, R. 2007. Acute resistance exercise increases skeletal muscle angiogenic growth factor expression. *Acta physiologica,* 191**,** 139-146.

GAVIN, T. P., ROBINSON, C. B., YEAGER, R. C., ENGLAND, J. A., NIFONG, L. W. & HICKNER, R. C. 2004. Angiogenic growth factor response to acute systemic exercise in human skeletal muscle. *Journal of applied physiology,* 96**,** 19-24.

GEORGE, D. 2012. *Are angiogenic stimuli additive? A study in the rat correlating structure and function.* University of Birmingham.

GERASIMENKO, Y. P., AVELEV, V., NIKITIN, O. & LAVROV, I. 2003. Initiation of locomotor activity in spinal cats by epidural stimulation of the spinal cord. *Neuroscience and behavioral physiology,* 33**,** 247-254.

GERHARDT, H. & BETSHOLTZ, C. 2003. Endothelial-pericyte interactions in angiogenesis. *Cell and tissue research,* 314**,** 15-23.

GIANGREGORIO, L. M., WEBBER, C. E., PHILLIPS, S. M., HICKS, A. L., CRAVEN, B. C., BUGARESTI, J. M. & MCCARTNEY, N. 2006. Can body weight supported treadmill training increase bone mass and reverse muscle atrophy in individuals with chronic incomplete spinal cord injury? *Applied physiology, nutrition, and metabolism,* 31**,** 283-291.

GOLDMAN, D., BATEMAN, R. M. & ELLIS, C. G. 2006. Effect of decreased O2 supply on skeletal muscle oxygenation and O2 consumption during sepsis: role of heterogeneous capillary spacing and blood flow. *American Journal of Physiology-Heart and Circulatory Physiology,* 290**,** H2277-H2285.

GOSLOW, G., CAMERON, W. & STUART, D. 1977. Ankle flexor muscles in the cat: Length-active tension and muscle unit properties as related to locomotion. *Journal of morphology,* 153**,** 23-37.

GOSLOW, G. E., REINKING, R. M. & STUART, D. G. 1973. The cat step cycle: hind limb joint angles and muscle lengths during unrestrained locomotion. *Journal of morphology,* 141**,** 1-41.

GRAY, S. D. & RENKIN, E. M. 1978. Microvascular supply in relation to fiber metabolic type in mixed skeletal muscles of rabbits. *Microvascular research,* 16**,** 406-425.

GREEN, H., GOREHAM, C., OUYANG, J., BALL-BURNETT, M. & RANNEY, D. 1999. Regulation of fiber size, oxidative potential, and capillarization in human muscle by resistance exercise. *American Journal of Physiology-Regulatory, Integrative and Comparative Physiology,* 276**,** R591-R596.

GREGOREVIC, P., MEZNARICH, N. A., BLANKINSHIP, M. J., CRAWFORD, R. W. & CHAMBERLAIN, J. S. 2008. Fluorophore-labeled myosin-specific antibodies simplify muscle-fiber phenotyping. *Muscle & nerve,* 37**,** 104-106.

GRUNER, J., ALTMAN, J. & SPIVACK, N. 1980. Effects of arrested cerebellar development on locomotion in the rat. *Experimental brain research,* 40**,** 361-373.

GU, J.-W., GADONSKI, G., WANG, J., MAKEY, I. & ADAIR, T. H. 2004. Exercise increases endostatin in circulation of healthy volunteers. *BMC physiology,* 4**,** 1.

GUSTAFSSON, T., AMELN, H., FISCHER, H., SUNDBERG, C., TIMMONS, J. & JANSSON, E. 2005. VEGF-A splice variants and related receptor expression in human skeletal muscle following submaximal exercise. *Journal of Applied Physiology,* 98**,** 2137-2146.

GUSTAFSSON, T., PUNTSCHART, A., KAIJSER, L., JANSSON, E. & SUNDBERG, C. J. 1999. Exercise-induced expression of angiogenesis-related transcription and growth factors in human skeletal muscle. *American Journal of Physiology-Heart and Circulatory Physiology,* 276**,** H679-H685.

GUTE, D., LAUGHLIN, M. H. & AMANN, J. F. 1994. Regional changes in capillary supply in skeletal muscle of interval-sprint and low-intensity, endurance-trained rats. *Microcirculation,* 1**,** 183-193.

HAAS, T., MILKIEWICZ, M., DAVIS, S., ZHOU, A., EGGINTON, S., BROWN, M., MADRI, J. & HUDLICKA, O. 2000. Matrix metalloproteinase activity is required for activity-induced angiogenesis in rat skeletal muscle. *American Journal of Physiology-Heart and Circulatory Physiology,* 279**,** H1540-H1547.

HANAHAN, D. 1997. Signaling vascular morphogenesis and maintenance. *Science,* 277**,** 48-50.

HANG, J., KONG, L., GU, J. & ADAIR, T. 1995. VEGF gene expression is upregulated in electrically stimulated rat skeletal muscle. *American Journal of Physiology-Heart and Circulatory Physiology,* 269**,** H1827-H1831.

HANSEN-SMITH, F. M., HUDLICKA, O. & EGGINTON, S. 1996. In vivo angiogenesis in adult rat skeletal muscle: early changes in capillary

network architecture and ultrastructure. *Cell and tissue research,* 286**,** 123-136.

HARMON, B. T., ORKUNOGLU-SUER, E. F., ADHAM, K., LARKIN, J. S., GORDISH-DRESSMAN, H., CLARKSON, P. M., THOMPSON, P. D., ANGELOPOULOS, T. J., GORDON, P. M. & MOYNA, N. M. 2010. CCL2 and CCR2 variants are associated with skeletal muscle strength and change in strength with resistance training. *Journal of applied physiology*.

HARPER, C. M. & LYLES, Y. M. 1988. Physiology and complications of bed rest. *Journal of the American Geriatrics Society,* 36**,** 1047-1054.

HAWKER, M. & EGGINTON, S. 1999. The effect of stimulation frequency on blood flow in rat fast skeletal muscles. *Experimental physiology,* 84**,** 941-946.

HELLSTEN, Y. & HOIER, B. 2014. Capillary growth in human skeletal muscle: physiological factors and the balance between pro-angiogenic and angiostatic factors. *Biochemical Society Transactions,* 42**,** 1616-1622.

HELLSTEN, Y., RUFENER, N., NIELSEN, J. J., HØIER, B., KRUSTRUP, P. & BANGSBO, J. 2008. Passive leg movement enhances interstitial VEGF protein, endothelial cell proliferation, and eNOS mRNA content in human skeletal muscle. *American Journal of Physiology-Regulatory, Integrative and Comparative Physiology,* 294**,** R975-R982.

HENRIKSSON-LARSÉN, K. B., LEXELL, J. & SJÖSTRÖM, M. 1983. Distribution of different fibre types in human skeletal muscles. I. Method for the preparation and analysis of cross-sections of whole tibialis anterior. *The Histochemical journal,* 15**,** 167-178.

HIRAIZUMI, Y., FUJIMAKI, E. & TACHIKAWA, T. 1990. Long-term morphology of spastic or flaccid muscles in spinal cord-transected rabbits. *Clinical orthopaedics and related research,* 260**,** 287-296.

HODSON-TOLE, E. & WAKELING, J. 2007. Variations in motor unit recruitment patterns occur within and between muscles in the running rat (Rattus norvegicus). *Journal of Experimental Biology,* 210**,** 2333-2345.

HOIER, B. & HELLSTEN, Y. 2014. Exercise-Induced Capillary Growth in Human Skeletal Muscle and the Dynamics of VEGF. *Microcirculation,* 21**,** 301-314.

HOIER, B., NORDSBORG, N., ANDERSEN, S., JENSEN, L., NYBO, L., BANGSBO, J. & HELLSTEN, Y. 2012. Pro-and anti-angiogenic factors in human skeletal muscle in response to acute exercise and training. *The Journal of physiology,* 590**,** 595-606.

HOIER, B., WALKER, M., PASSOS, M., WALKER, P. J., GREEN, A., BANGSBO, J., ASKEW, C. D. & HELLSTEN, Y. 2013. Angiogenic response to passive movement and active exercise in individuals with peripheral arterial disease. *Journal of applied physiology,* 115**,** 1777-1787.

HOLLOSZY, J. O. & COYLE, E. F. 1984. Adaptations of skeletal muscle to endurance exercise and their metabolic consequences. *Journal of applied physiology,* 56**,** 831-838.

HOLLOSZY, J. O. & LARSSON, L. 1995. Motor units: remodeling in aged animals. *The Journals of Gerontology Series A: Biological Sciences and Medical Sciences,* 50**,** 91-95.

HOLLOWAY, G., GREEN, H. & TUPLING, A. 2006. Differential effects of repetitive activity on sarcoplasmic reticulum responses in rat muscles of different oxidative potential. *American Journal of Physiology-Regulatory, Integrative and Comparative Physiology,* 290**,** R393-R404.

HOOFD, L., TUREK, Z., KUBAT, K., RINGNALDA, B. & KAZDA, S. 1985. Variability of intercapillary distance estimated on histological sections of rat heart. *Oxygen transport to tissue VII.* Springer.

HORTOBÁGYI, T., DEMPSEY, L., FRASER, D., ZHENG, D., HAMILTON, G., LAMBERT, J. & DOHM, L. 2000. Changes in muscle strength, muscle fibre size and myofibrillar gene expression after immobilization and retraining in humans. *The Journal of physiology,* 524**,** 293-304.

HUBAL, M. J., DEVANEY, J. M., HOFFMAN, E. P., ZAMBRASKI, E. J., GORDISH-DRESSMAN, H., KEARNS, A. K., LARKIN, J. S., ADHAM, K., PATEL, R. R. & CLARKSON, P. M. 2010. CCL2 and CCR2 polymorphisms are associated with markers of exercise-induced skeletal muscle damage. *Journal of applied physiology,* 108**,** 1651-1658.

HUDLICKA, O., BROWN, M., COTTER, M., SMITH, M. & VRBOVA, G. 1977. The effect of long-term stimulation of fast muscles on their blood flow, metabolism and ability to withstand fatigue. *Pflügers Archiv,* 369**,** 141-149.

HUDLICKA, O., BROWN, M., EGGINTON, S. & DAWSON, J. 1994. Effect of long-term electrical stimulation on vascular supply and fatigue in chronically ischemic muscles. *Journal of Applied Physiology,* 77**,** 1317-1324.

HUDLICKA, O., DODD, L., RENKIN, E. & GRAY, S. 1982. Early changes in fiber profile and capillary density in long-term stimulated muscles. *American Journal of Physiology-Heart and Circulatory Physiology,* 243**,** H528-H535.

HUDLICKÁ, O., TYLER, K. & AITMAN, T. 1980. The effect of long-term electrical stimulation on fuel uptake and performance in fast skeletal muscles. *Plasticity of muscle. Walter de Gruyter, Berlin New York***,** 401-408.

HUEY, K. A., ROY, R. R., BALDWIN, K. M. & EDGERTON, V. R. 2001. Temporal effects of inactivty on myosin heavy chain gene expression in rat slow muscle. *Muscle & nerve,* 24**,** 517-526.

HUTCHINSON, K. J., LINDERMAN, J. K. & BASSO, D. M. 2001. Skeletal muscle adaptations following spinal cord contusion injury in rat and the relationship to locomotor function: a time course study. *Journal of neurotrauma,* 18**,** 1075-1089.

HUTTENHOWER, C., FLAMHOLZ, A. I., LANDIS, J. N., SAHI, S., MYERS, C. L., OLSZEWSKI, K. L., HIBBS, M. A., SIEMERS, N. O., TROYANSKAYA, O. G. & COLLER, H. A. 2007. Nearest Neighbor Networks: clustering expression data based on gene neighborhoods. *Bmc Bioinformatics,* 8**,** 1.

ICHIYAMA, R., GERASIMENKO, Y. P., ZHONG, H., ROY, R. & EDGERTON, V. 2005. Hindlimb stepping movements in complete spinal rats induced by epidural spinal cord stimulation. *Neuroscience letters,* 383**,** 339-344.

ICHIYAMA, R. M., COURTINE, G., GERASIMENKO, Y. P., YANG, G. J., VAN DEN BRAND, R., LAVROV, I. A., ZHONG, H., ROY, R. R. & EDGERTON, V. R. 2008a. Step training reinforces specific spinal locomotor circuitry in adult spinal rats. *The Journal of Neuroscience,* 28**,** 7370-7375.

ICHIYAMA, R. M., GERASIMENKO, Y., JINDRICH, D. L., ZHONG, H., ROY, R. R. & EDGERTON, V. R. 2008b. Dose dependence of the 5-HT agonist quipazine in facilitating spinal stepping in the rat with epidural stimulation. *Neuroscience letters,* 438**,** 281-285.

INGJER, F. 1979a. Capillary supply and mitochondrial content of different skeletal muscle fiber types in untrained and endurance-trained men. A histochemical and ultrastructural study. *European Journal of Applied Physiology and Occupational Physiology,* 40**,** 197-209.

INGJER, F. 1979b. Effects of endurance training on muscle fibre ATP-ase activity, capillary supply and mitochondrial content in man. *The Journal of Physiology,* 294**,** 419-432.

IRRCHER, I., ADHIHETTY, P. J., JOSEPH, A.-M., LJUBICIC, V. & HOOD, D. A. 2003. Regulation of mitochondrial biogenesis in muscle by endurance exercise. *Sports Medicine,* 33**,** 783-793.

IWAHARA, T., ATSUTA, Y., GARCIA-RILL, E. & SKINNER, R. 1991. Locomotion induced by spinal cord stimulation in the neonate rat in vitro. *Somatosensory & motor research,* 8**,** 281-287.

JAKUBIEC-PUKA, A., SŁAWIŃSKA, U., RĘDOWICZ, M. J., BIRAL, D., ŁAPIŃSKA, I., CHOMONTOWSKA, H., KARCZEWSKA, E., KRAWCZYK, K., BILSKI, H. & PLISZKA, B. 2008. Influence of locomotor training on the structure and myosin heavy chains of the denervated rat soleus muscle. *Neurological research,* 30**,** 170-178.

JAMES, R., ALTRINGHAM, J. D. & GOLDSPINK, D. F. 1995. The mechanical properties of fast and slow skeletal muscles of the mouse in relation to their locomotory function. *The Journal of experimental biology,* 198**,** 491-502.

JAMES, R., COX, V., YOUNG, I., ALTRINGHAM, J. & GOLDSPINK, D. 1997. Mechanical properties of rabbit latissimus dorsi muscle after stretch and/or electrical stimulation. *Journal of Applied Physiology,* 83**,** 398-406.

JANSSON, E., SYLVEN, C., ARVIDSSON, I. & ERIKSSON, E. 1988. Increase in myoglobin content and decrease in oxidative enzyme activities by leg muscle immobilization in man. *Acta physiologica scandinavica,* 132**,** 515-517.

JELTSCH, M., KAIPAINEN, A., JOUKOV, V., MENG, X., LAKSO, M., RAUVALA, H., SWARTZ, M., FUKUMURA, D., JAIN, R. K. & ALITALO, K. 1997. Hyperplasia of lymphatic vessels in VEGF-C transgenic mice. *Science,* 276**,** 1423-1425.

JENSEN, L., BANGSBO, J. & HELLSTEN, Y. 2004. Effect of high intensity training on capillarization and presence of angiogenic factors in human skeletal muscle. *The Journal of physiology,* 557**,** 571-582.

JOSEPHSON, R. & EDMAN, K. 1988. The consequences of fibre heterogeneity on the force-velocity relation of skeletal muscle. *Acta physiologica scandinavica,* 132**,** 341-352.

JOSEPHSON, R. K. 1985. Mechanical power output from striated muscle during cyclic contraction. *Journal of Experimental Biology,* 114**,** 493-512.

KANO, Y., SHIMEGI, S., MASUDA, K., SAKATO, H., OHMORI, H. & KATSUTA, S. 1997. Effects of different intensity endurance training on the capillary network in rat skeletal muscle. *Journal of Vascular Research,* 17**,** 93-96.

KELLER, P., VOLLAARD, N., BABRAJ, J., BALL, D., SEWELL, D. & TIMMONS, J. 2007. Using systems biology to define the essential biological networks responsible for adaptation to endurance exercise training. *Biochemical Society Transactions,* 35**,** 1306-1309.

KELLER, P., VOLLAARD, N. B., GUSTAFSSON, T., GALLAGHER, I. J., SUNDBERG, C. J., RANKINEN, T., BRITTON, S. L., BOUCHARD, C., KOCH, L. G. & TIMMONS, J. A. 2011. A transcriptional map of the impact of endurance exercise training on skeletal muscle phenotype. *Journal of applied physiology,* 110**,** 46-59.

KEMI, O. J., LOENNECHEN, J. P., WISLØFF, U. & ELLINGSEN, Ø. 2002. Intensity-controlled treadmill running in mice: cardiac and skeletal muscle hypertrophy. *Journal of Applied Physiology,* 93**,** 1301-1309.

KIM, K. J., LI, B., WINER, J., ARMANINI, M., GILLETT, N., PHILLIPS, H. S. & FERRARA, N. 1993. Inhibition of vascular endothelial growth factor-induced angiogenesis suppresses tumour growth in vivo.

KJELLMER, I. 1964. The effect of exercise on the vascular bed of skeletal muscle. *Acta physiologica scandinavica,* 62**,** 18-30.

KLAUSEN, K., ANDERSEN, L. B. & PELLE, I. 1981. Adaptive changes in work capacity, skeletal muscle capillarization and enzyme levels during training and detraining. *Acta physiologica Scandinavica,* 113**,** 9-16.

KLINGMULLER, G. 1958. [Demonstration of alkaline phosphatase in the capillaries.]. *Der Hautarzt; Zeitschrift fur Dermatologie, Venerologie, und verwandte Gebiete,* 9**,** 84-88.

KOCH, A. E., HALLORAN, M. M., HASKELL, C. J., SHAH, M. R. & POLVERINI, P. J. 1995. Angiogenesis mediated by soluble forms of E-selectin and vascular cell-adhesion molecule-1.

KOURTIDIS, A., JAIN, R., CARKNER, R. D., EIFERT, C., BROSNAN, M. J. & CONKLIN, D. S. 2010. An RNA interference screen identifies metabolic regulators NR1D1 and PBP as novel survival factors for

breast cancer cells with the ERBB2 signature. *Cancer research,* 70**,** 1783-1792.

KREUZER, F. 1982. Oxygen supply to tissues: the Krogh model and its assumptions. *Experientia,* 38**,** 1415-1426.

KRILLEKE, D., NG, Y.-S. & SHIMA, D. 2009. The heparin-binding domain confers diverse functions of VEGF-A in development and disease: a structure-function study. *Biochemical Society Transactions,* 37**,** 1201.

KRISHNAN, J., KIRKIN, V., STEFFEN, A., HEGEN, M., WEIH, D., TOMAREV, S., WILTING, J. & SLEEMAN, J. P. 2003. Differential in vivo and in vitro expression of vascular endothelial growth factor (VEGF)-C and VEGF-D in tumors and its relationship to lymphatic metastasis in immunocompetent rats. *Cancer research,* 63**,** 713-722.

KROGH, A. 1919. The number and distribution of capillaries in muscles with calculations of the oxygen pressure head necessary for supplying the tissue. *The Journal of Physiology,* 52**,** 409-415.

KURZ, H., BURRI, P. H. & DJONOV, V. G. 2003. Angiogenesis and vascular remodeling by intussusception: from form to function. *Physiology,* 18**,** 65-70.

LANDRY, E., FRENETTE, J. & GUERTIN, P. A. 2004. Body weight, limb size, and muscular properties of early paraplegic mice. *Journal of neurotrauma,* 21**,** 1008-1016.

LÄNNERGREN, J. & WESTERBLAD, H. 1991. Force decline due to fatigue and intracellular acidification in isolated fibres from mouse skeletal muscle. *The Journal of Physiology,* 434**,** 307.

LANSFORD, K. A., SHILL, D. D., DICKS, A. B., MARSHBURN, M. P., SOUTHERN, W. M. & JENKINS, N. T. 2016. Effect of acute exercise on circulating angiogenic cell and microparticle populations. *Experimental physiology,* 101**,** 155-167.

LAUGHLIN, M. H. 1999. Cardiovascular response to exercise. *Am J Physiol,* 277**,** S244-S259.

LAWLER, J. 2000. The functions of thrombospondin-1 and-2. *Current opinion in cell biology,* 12**,** 634-640.

LEE, S. H., WOLF, P. L., ESCUDERO, R., DEUTSCH, R., JAMIESON, S. W. & THISTLETHWAITE, P. A. 2000. Early expression of angiogenesis factors in acute myocardial ischemia and infarction. *New England Journal of Medicine,* 342**,** 626-633.

LEICK, L., PLOMGAARD, P., GRØNLØKKE, L., AL-ABAIJI, F., WOJTASZEWSKI, J. & PILEGAARD, H. 2010. Endurance exercise induces mRNA expression of oxidative enzymes in human skeletal muscle late in recovery. *Scandinavian journal of medicine & science in sports,* 20**,** 593-599.

LEONG, K. G., HU, X., LI, L., NOSEDA, M., LARRIVÉE, B., HULL, C., HOOD, L., WONG, F. & KARSAN, A. 2002. Activated Notch4 inhibits angiogenesis: role of β1-integrin activation. *Molecular and Cellular Biology,* 22**,** 2830-2841.

LEVINE, A., HU, W. & FENG, Z. 2006. The P53 pathway: what questions remain to be explored? *Cell Death & Differentiation,* 13**,** 1027-1036.

LINDERMAN, J. R., KLOEHN, M. R. & GREENE, A. S. 2000. Development of an implantable muscle stimulator: measurement of stimulated angiogenesis and poststimulus vessel regression. *Microcirculation,* 7**,** 119-128.

LLOYD, P. G., PRIOR, B. M., YANG, H. T. & TERJUNG, R. L. 2003. Angiogenic growth factor expression in rat skeletal muscle in response to exercise training. *American Journal of Physiology-Heart and Circulatory Physiology,* 284**,** H1668-H1678.

LOTTA, S., SCELSI, R., ALFONSI, E., SAITTA, A., NICOLOTTI, D., EPIFANI, P. & CARRARO, U. 1991. Morphometric and neurophysiological analysis of skeletal muscle in paraplegic patients with traumatic cord lesion. *Spinal Cord,* 29**,** 247-252.

LUFF, A. 1981. Dynamic properties of the inferior rectus, extensor digitorum longus, diaphragm and soleus muscles of the mouse. *The Journal of Physiology,* 313**,** 161.

LUNDBY, C., GASSMANN, M. & PILEGAARD, H. 2006. Regular endurance training reduces the exercise induced HIF-1α and HIF-2α mRNA expression in human skeletal muscle in normoxic conditions. *European journal of applied physiology,* 96**,** 363-369.

MA, P. C., MAULIK, G., CHRISTENSEN, J. & SALGIA, R. 2003. c-Met: structure, functions and potential for therapeutic inhibition. *Cancer and Metastasis Reviews,* 22**,** 309-325.

MAKANYA, A. N., STAUFFER, D., RIBATTI, D., BURRI, P. H. & DJONOV, V. 2005. Microvascular growth, development, and remodeling in the embryonic avian kidney: the interplay between sprouting and intussusceptive angiogenic mechanisms. *Microscopy research and technique,* 66**,** 275-288.

MARSH, R. L. & BENNETT, A. 1986. Thermal dependence of contractile properties of skeletal muscle from the lizard Sceloporus occidentalis with comments on methods for fitting and comparing force-velocity curves. *Journal of Experimental Biology,* 126**,** 63-77.

MARSH, R. L., ELLERBY, D. J., CARR, J. A., HENRY, H. T. & BUCHANAN, C. I. 2004. Partitioning the energetics of walking and running: swinging the limbs is expensive. *Science,* 303**,** 80-83.

MATOBA, S., KANG, J.-G., PATINO, W. D., WRAGG, A., BOEHM, M., GAVRILOVA, O., HURLEY, P. J., BUNZ, F. & HWANG, P. M. 2006. p53 regulates mitochondrial respiration. *Science,* 312**,** 1650-1653.

MCCALL, G., BYRNES, W., DICKINSON, A., PATTANY, P. & FLECK, S. 1996. Muscle fiber hypertrophy, hyperplasia, and capillary density in college men after resistance training. *Journal of applied physiology,* 81**,** 2004-2012.

MCFARLANE, L., ALTRINGHAM, J. D. & ASKEW, G. N. 2016. Intra-specific variation in wing morphology and its impact on take-off performance in blue tits (Cyanistes caeruleus) during escape flights. *Journal of Experimental Biology,* 219**,** 1369-1377.

MIAZAKI, M., VIANA, M. P., YANG, Z., COMIN, C. H., WANG, Y., DA F COSTA, L. & XU, X. 2015. Automated high-content morphological

analysis of muscle fiber histology. *Computers in biology and medicine,* 63**,** 28-35.

MILKIEWICZ, M., BROWN, M., EGGINTON, S. & HUDLICKA, O. 2001. Association between shear stress, angiogenesis, and VEGF in skeletal muscles in vivo. *Microcirculation,* 8**,** 229-241.

MILKIEWICZ, M., DOYLE, J. L., FUDALEWSKI, T., ISPANOVIC, E., AGHASI, M. & HAAS, T. L. 2007. HIF-1α and HIF-2α play a central role in stretch-induced but not shear-stress-induced angiogenesis in rat skeletal muscle. *The Journal of physiology,* 583**,** 753-766.

MINASSIAN, K., JILGE, B., RATTAY, F., PINTER, M., BINDER, H., GERSTENBRAND, F. & DIMITRIJEVIC, M. R. 2004. Stepping-like movements in humans with complete spinal cord injury induced by epidural stimulation of the lumbar cord: electromyographic study of compound muscle action potentials. *Spinal Cord,* 42**,** 401-416.

MOLÉ, P. A., CHUNG, Y., TRAN, T. K., SAILASUTA, N., HURD, R. & JUE, T. 1999. Myoglobin desaturation with exercise intensity in human gastrocnemius muscle. *American Journal of Physiology-Regulatory, Integrative and Comparative Physiology,* 277**,** R173-R180.

MONDON, C. E., DOLKAS, C. B., SIMS, C. & REAVEN, G. M. 1985. Spontaneous running activity in male rats: effect of age. *Journal of Applied Physiology,* 58**,** 1553-1557.

MORLEY, J. E., BAUMGARTNER, R. N., ROUBENOFF, R., MAYER, J. & NAIR, K. S. 2001. Sarcopenia. *Journal of Laboratory and Clinical Medicine,* 137**,** 231-243.

MORTENSEN, S. P., ASKEW, C. D., WALKER, M., NYBERG, M. & HELLSTEN, Y. 2012. The hyperaemic response to passive leg movement is dependent on nitric oxide: a new tool to evaluate endothelial nitric oxide function. *The Journal of physiology,* 590**,** 4391-4400.

MOSS, F. & LEBLOND, C. 1971. Satellite cells as the source of nuclei in muscles of growing rats. *The Anatomical Record,* 170**,** 421-435.

MULA, J., LEE, J. D., LIU, F., YANG, L. & PETERSON, C. A. 2013. Automated image analysis of skeletal muscle fiber cross-sectional area. *Journal of Applied Physiology,* 114**,** 148-155.

NICOLOPOULOS-STOURNARAS, S. & ILES, J. 1984. Hindlimb muscle activity during locomotion in the rat (Rattus norvegicus)(Rodentia: Muridae). *Journal of Zoology,* 203**,** 427-440.

NORENBERG, M. D., SMITH, J. & MARCILLO, A. 2004. The pathology of human spinal cord injury: defining the problems. *Journal of neurotrauma,* 21**,** 429-440.

O'REILLY, M. S., BOEHM, T., SHING, Y., FUKAI, N., VASIOS, G., LANE, W. S., FLYNN, E., BIRKHEAD, J. R., OLSEN, B. R. & FOLKMAN, J. 1997. Endostatin: an endogenous inhibitor of angiogenesis and tumor growth. *cell,* 88**,** 277-285.

OLENICH, S. A., GUTIERREZ-REED, N., AUDET, G. N. & OLFERT, I. M. 2013. Temporal response of positive and negative regulators in

response to acute and chronic exercise training in mice. *The Journal of physiology,* 591**,** 5157-5169.

OLFERT, I. M., BREEN, E. C., GAVIN, T. P. & WAGNER, P. D. 2006. Temporal thrombospondin-1 mRNA response in skeletal muscle exposed to acute and chronic exercise. *Growth Factors,* 24**,** 253-259.

OLOFSSON, B., JELTSCH, M., ERIKSSON, U. & ALITALO, K. 1999. Current biology of Vegf-B and Vegf-C. *Current opinion in biotechnology,* 10**,** 528-538.

OTIS, J. S., ROY, R. R., EDGERTON, V. R. & TALMADGE, R. J. 2004. Adaptations in metabolic capacity of rat soleus after paralysis. *Journal of Applied Physiology,* 96**,** 584-596.

OZAKI, H., YU, A., DELLA, N., OZAKI, K., LUNA, J., YAMADA, H., HACKETT, S., OKAMOTO, N., ZACK, D. & SEMENZA, G. 1999. Hypoxia inducible factor-1alpha is increased in ischemic retina: temporal and spatial correlation with VEGF expression. *Investigative ophthalmology & visual science,* 40**,** 182-189.

PARK, J. E., KELLER, G.-A. & FERRARA, N. 1993. The vascular endothelial growth factor (VEGF) isoforms: differential deposition into the subepithelial extracellular matrix and bioactivity of extracellular matrix-bound VEGF. *Molecular Biology of the Cell,* 4**,** 1317.

PARTRIDGE, J. S., HARARI, D. & DHESI, J. K. 2012. Frailty in the older surgical patient: a review. *Age and ageing,* 41**,** 142-147.

PERRET, C. & CABELGUEN, J.-M. 1980. Main characteristics of the hindlimb locomotor cycle in the decorticate cat with special reference to bifunctional muscles. *Brain research,* 187**,** 333-352.

PERRY, C. G., LALLY, J., HOLLOWAY, G. P., HEIGENHAUSER, G. J., BONEN, A. & SPRIET, L. L. 2010. Repeated transient mRNA bursts precede increases in transcriptional and mitochondrial proteins during training in human skeletal muscle. *The Journal of Physiology,* 588**,** 4795-4810.

PETTE, D., SMITH, M. E., STAUDTE, H. W. & VRBOVÁ, G. 1973. Effects of long-term electrical stimulation on some contractile and metabolic characteristics of fast rabbit muscles. *Pflügers Archiv,* 338**,** 257-272.

PHILLIPS, B., WILLIAMS, J., ATHERTON, P., SMITH, K., HILDEBRANDT, W., RANKIN, D., GREENHAFF, P., MACDONALD, I. & RENNIE, M. J. 2012. Resistance exercise training improves age-related declines in leg vascular conductance and rejuvenates acute leg blood flow responses to feeding and exercise. *Journal of Applied Physiology,* 112**,** 347-353.

PHILLIPS, B. E., WILLIAMS, J. P., GUSTAFSSON, T., BOUCHARD, C., RANKINEN, T., KNUDSEN, S., SMITH, K., TIMMONS, J. A. & ATHERTON, P. J. 2013. Molecular networks of human muscle adaptation to exercise and age. *PLoS Genet,* 9**,** e1003389.

POLLARE, T., LITHELL, H., SELINUS, I. & BERNE, C. 1988. Application of prazosin is associated with an increase of insulin sensitivity in obese patients with hypertension. *Diabetologia,* 31**,** 415-420.

PRIOR, B. M., LLOYD, P. G., YANG, H. & TERJUNG, R. L. 2003. Exercise-induced vascular remodeling. *Exercise and sport sciences reviews,* 31**,** 26-33.

PRIOR, B. M., YANG, H. & TERJUNG, R. L. 2004. What makes vessels grow with exercise training? *Journal of Applied Physiology,* 97**,** 1119-1128.

PUGH, C. W. & RATCLIFFE, P. J. 2003. Regulation of angiogenesis by hypoxia: role of the HIF system. *Nature medicine,* 9**,** 677-684.

PULLEN, A. 1977. The distribution and relative sized of fibre types in the extensor digitorum longus and soleus muscles of the adult rat. *Journal of anatomy,* 123**,** 467.

PUTMAN, C. T., DIXON, W. T., PEARCEY, J. A., MACLEAN, I. M., JENDRAL, M. J., KIRICSI, M., MURDOCH, G. K. & PETTE, D. 2004. Chronic low-frequency stimulation upregulates uncoupling protein-3 in transforming rat fast-twitch skeletal muscle. *American Journal of Physiology-Regulatory, Integrative and Comparative Physiology,* 287**,** R1419-R1426.

PUTMAN, C. T., KIRICSI, M., PEARCEY, J., MACLEAN, I. M., BAMFORD, J. A., MURDOCH, G. K., DIXON, W. T. & PETTE, D. 2003. AMPK activation increases uncoupling protein-3 expression and mitochondrial enzyme activities in rat muscle without fibre type transitions. *The Journal of physiology,* 551**,** 169-178.

RABQUER, B. J., AMIN, M. A., TEEGALA, N., SHAHEEN, M. K., TSOU, P.-S., RUTH, J. H., LESCH, C. A., IMHOF, B. A. & KOCH, A. E. 2010. Junctional adhesion molecule-C is a soluble mediator of angiogenesis. *The Journal of Immunology,* 185**,** 1777-1785.

RAGHUWANSHI, S. K., SMITH, N., RIVERS, E. J., THOMAS, A. J., SUTTON, N., HU, Y., MUKHOPADHYAY, S., CHEN, X. L., LEUNG, T. & RICHARDSON, R. M. 2013. G Protein–Coupled Receptor Kinase 6 Deficiency Promotes Angiogenesis, Tumor Progression, and Metastasis. *The Journal of Immunology,* 190**,** 5329-5336.

RANATUNGA, K. 1984. The force-velocity relation of rat fast-and slow-twitch muscles examined at different temperatures. *The Journal of Physiology,* 351**,** 517.

RAUE, U., TRAPPE, T. A., ESTREM, S. T., QIAN, H.-R., HELVERING, L. M., SMITH, R. C. & TRAPPE, S. 2012. Transcriptome signature of resistance exercise adaptations: mixed muscle and fiber type specific profiles in young and old adults. *Journal of applied physiology,* 112**,** 1625-1636.

RAY, C. J. & MARSHALL, J. M. 2009. Elucidation in the rat of the role of adenosine and A2A-receptors in the hyperaemia of twitch and tetanic contractions. *The Journal of physiology,* 587**,** 1565-1578.

RISAU, W. 1997. Mechanisms of angiogenesis. *Nature,* 386**,** 671-674.

RIVILIS, I., MILKIEWICZ, M., BOYD, P., GOLDSTEIN, J., BROWN, M. D., EGGINTON, S., HANSEN, F. M., HUDLICKA, O. & HAAS, T. L. 2002. Differential involvement of MMP-2 and VEGF during muscle stretch- versus shear stress-induced angiogenesis. *American Journal of Physiology-Heart and Circulatory Physiology,* 283**,** H1430-H1438.

ROCHESTER, L., BARRON, M., CHANDLER, C., SUTTON, R., MILLER, S. & JOHNSON, M. 1995. Influence of electrical stimulation of the tibialis anterior muscle in paraplegic subjects. 2. Morphological and histochemical properties. *Spinal Cord,* 33**,** 514-522.

RODNICK, K., REAVEN, G., HASKELL, W., SIMS, C. & MONDON, C. 1989. Variations in running activity and enzymatic adaptations in voluntary running rats. *Journal of Applied Physiology,* 66**,** 1250-1257.

ROSENBLATT, J. D. & PARRY, D. J. 1993. Adaptation of rat extensor digitorum longus muscle to gamma irradiation and overload. *Pflügers Archiv,* 423**,** 255-264.

ROUND, J. M., BARR, F. M., MOFFAT, B. & JONES, D. A. 1993. Fibre areas and histochemical fibre types in the quadriceps muscle of paraplegic subjects. *Journal of the neurological sciences,* 116**,** 207-211.

ROY, R. R., TALMADGE, R. J., HODGSON, J. A., OISHI, Y., BALDWIN, K. M. & EDGERTON, V. R. 1999. Differential response of fast hindlimb extensor and flexor muscles to exercise in adult spinalized cats. *Muscle & nerve,* 22**,** 230-241.

ROY, R. R., TALMADGE, R. J., HODGSON, J. A., ZHONG, H., BALDWIN, K. M. & EDGERTON, V. R. 1998. Training effects on soleus of cats spinal cord transected (T12–13) as adults. *Muscle & nerve,* 21**,** 63-71.

RUHRBERG, C., GERHARDT, H., GOLDING, M., WATSON, R., IOANNIDOU, S., FUJISAWA, H., BETSHOLTZ, C. & SHIMA, D. T. 2002. Spatially restricted patterning cues provided by heparin-binding VEGF-A control blood vessel branching morphogenesis. *Genes & development,* 16**,** 2684-2698.

SALEEM, A. & HOOD, D. A. 2013. Acute exercise induces tumour suppressor protein p53 translocation to the mitochondria and promotes a p53–Tfam–mitochondrial DNA complex in skeletal muscle. *The Journal of physiology,* 591**,** 3625-3636.

SALLEO, A., LA SPADA, G., FALZEA, G., DENARO, M. & CICCIARELLO, R. 1983. Response of satellite cells and muscle fibers to long-term compensatory hypertrophy. *Journal of submicroscopic cytology,* 15**,** 929-940.

SALTIEL, A. R. & KAHN, C. R. 2001. Insulin signalling and the regulation of glucose and lipid metabolism. *Nature,* 414**,** 799-806.

SALTIN, B. & GOLLNICK, P. D. 1983. Skeletal muscle adaptability: significance for metabolism and performance. *Comprehensive Physiology*.

SALTIN, B. & ROWELL, L. Functional adaptations to physical activity and inactivity. Federation proceedings, 1980. 1506-1513.

SAUTEUR, L., KRUDEWIG, A., HERWIG, L., EHRENFEUCHTER, N., LENARD, A., AFFOLTER, M. & BELTING, H.-G. 2014. Cdh5/VE-cadherin promotes endothelial cell interface elongation via cortical actin polymerization during angiogenic sprouting. *Cell reports,* 9**,** 504-513.

SCHEFF, S. W., RABCHEVSKY, A. G., FUGACCIA, I., MAIN, J. A. & LUMPP JR, J. E. 2003. Experimental modeling of spinal cord injury:

characterization of a force-defined injury device. *Journal of neurotrauma,* 20**,** 179-193.

SCHIAFFINO, S., HANZLÍKOVÁ, V. & PIEROBON, S. 1970. Relations between structure and function in rat skeletal muscle fibers. *The Journal of cell biology,* 47**,** 107-119.

SCHLATTER, P., KÖNIG, M., KARLSSON, L. & BURRI, P. 1997. Quantitative study of intussusceptive capillary growth in the chorioallantoic membrane (CAM) of the chicken embryo. *Microvascular research,* 54**,** 65-73.

SELSBY, J. T., MORINE, K. J., PENDRAK, K., BARTON, E. R. & SWEENEY, H. L. 2012. Rescue of dystrophic skeletal muscle by PGC-1α involves a fast to slow fiber type shift in the mdx mouse. *PloS one,* 7**,** e30063.

SEO, D.-W., LI, H., GUEDEZ, L., WINGFIELD, P. T., DIAZ, T., SALLOUM, R., WEI, B.-Y. & STETLER-STEVENSON, W. G. 2003. TIMP-2 mediated inhibition of angiogenesis: an MMP-independent mechanism. *Cell,* 114**,** 171-180.

SEO, S. W., LEE, H., LEE, H. I. & KIM, H. S. 2011. The role of TLE1 in synovial sarcoma. *Journal of Orthopaedic Research,* 29**,** 1131-1136.

SHERWIN, C. 1998. Voluntary wheel running: a review and novel interpretation. *Animal Behaviour,* 56**,** 11-27.

SHIMA, D. T., KUROKI, M., DEUTSCH, U., NG, Y.-S., ADAMIS, A. P. & D'AMORE, P. A. 1996. The Mouse Gene for Vascular Endothelial Growth Factor GENOMIC STRUCTURE, DEFINITION OF THE TRANSCRIPTIONAL UNIT, AND CHARACTERIZATION OF TRANSCRIPTIONAL AND POST-TRANSCRIPTIONAL REGULATORY SEQUENCES. *Journal of Biological Chemistry,* 271**,** 3877-3883.

SIMONEAU, J., KAUFMANN, M. & PETTE, D. 1993. Asynchronous increases in oxidative capacity and resistance to fatigue of electrostimulated muscles of rat and rabbit. *The Journal of Physiology,* 460**,** 573-580.

SINGH, H., TAHIR, T. A., ALAWO, D. O., ISSA, E. & BRINDLE, N. P. 2011. Molecular control of angiopoietin signalling. *Biochemical Society Transactions,* 39**,** 1592.

SKINNER, J. S., JASKÓLSKI, A., JASKÓLSKA, A., KRASNOFF, J., GAGNON, J., LEON, A. S., RAO, D., WILMORE, J. H. & BOUCHARD, C. 2001. Age, sex, race, initial fitness, and response to training: the HERITAGE Family Study. *Journal of applied physiology,* 90**,** 1770-1776.

SMERDU, V. & SOUKUP, T. 2009. Demonstration of myosin heavy chain isoforms in rat and humans: the specificity of seven available monoclonal antibodies used in immunohistochemical and immunoblotting methods. *European Journal of Histochemistry,* 52**,** 179-190.

SMITH, J. L., EDGERTON, V. R., BETTS, B. & COLLATOS, T. 1977. EMG of slow and fast ankle extensors of cat during posture, locomotion, and jumping. *Journal of Neurophysiology,* 40**,** 503-513.

SMITH, L. R. & BARTON, E. R. 2014. SMASH–semi-automatic muscle analysis using segmentation of histology: a MATLAB application. *Skeletal muscle,* 4**,** 1.

SORIA, G. & BEN-BARUCH, A. 2008. The inflammatory chemokines CCL2 and CCL5 in breast cancer. *Cancer letters,* 267**,** 271-285.

SOUKUP, T., ZACHAŘOVÁ, G. & SMERDU, V. 2002. Fibre type composition of soleus and extensor digitorum longus muscles in normal female inbred Lewis rats. *Acta histochemica,* 104**,** 399-405.

STEINER, J. L. & MURPHY, E. A. 2011. Importance of chemokine (CC-motif) ligand 2 in breast cancer. *The International journal of biological markers,* 27**,** e179-85.

STETLER-STEVENSON, W. G. 1999. Matrix metalloproteinases in angiogenesis: a moving target for therapeutic intervention. *The Journal of clinical investigation,* 103**,** 1237-1241.

STETLER-STEVENSON, W. G. & SEO, D.-W. 2005. TIMP-2: an endogenous inhibitor of angiogenesis. *Trends in molecular medicine,* 11**,** 97-103.

SUBRAMANIAN, A., TAMAYO, P., MOOTHA, V. K., MUKHERJEE, S., EBERT, B. L., GILLETTE, M. A., PAULOVICH, A., POMEROY, S. L., GOLUB, T. R. & LANDER, E. S. 2005. Gene set enrichment analysis: a knowledge-based approach for interpreting genome-wide expression profiles. *Proceedings of the National Academy of Sciences,* 102**,** 15545-15550.

SUETTA, C., FRANDSEN, U., MACKEY, A. L., JENSEN, L., HVID, L. G., BAYER, M., PETERSSON, S. J., SCHRØDER, H. D., ANDERSEN, J. L. & AAGAARD, P. 2013. Ageing is associated with diminished muscle re-growth and myogenic precursor cell expansion early after immobility-induced atrophy in human skeletal muscle. *The Journal of physiology,* 591**,** 3789-3804.

SUFFEE, N., RICHARD, B., HLAWATY, H., OUDAR, O., CHARNAUX, N. & SUTTON, A. 2011. Angiogenic properties of the chemokine RANTES/CCL5. Portland Press Limited.

SULLIVAN, T. & ARMSTRONG, R. 1978. Rat locomotory muscle fiber activity during trotting and galloping. *Journal of Applied Physiology,* 44**,** 358-363.

TANG, X. & AMAR, S. 2015. p53 suppresses CCL2-induced subcutaneous tumor xenograft. *Tumor Biology,* 36**,** 2801-2808.

TATSUMI, R., LIU, X., PULIDO, A., MORALES, M., SAKATA, T., DIAL, S., HATTORI, A., IKEUCHI, Y. & ALLEN, R. E. 2006. Satellite cell activation in stretched skeletal muscle and the role of nitric oxide and hepatocyte growth factor. *American Journal of Physiology-Cell Physiology,* 290**,** C1487-C1494.

THOTA, A. K., WATSON, S. C., KNAPP, E., THOMPSON, B. & JUNG, R. 2005. Neuromechanical control of locomotion in the rat. *Journal of neurotrauma,* 22**,** 442-465.

TIMMONS, J. A., KNUDSEN, S., RANKINEN, T., KOCH, L. G., SARZYNSKI, M., JENSEN, T., KELLER, P., SCHEELE, C., VOLLAARD, N. B. & NIELSEN, S. 2010. Using molecular classification to predict gains in

maximal aerobic capacity following endurance exercise training in humans. *Journal of applied physiology,* 108**,** 1487-1496.

TISCHER, E., MITCHELL, R., HARTMAN, T., SILVA, M., GOSPODAROWICZ, D., FIDDES, J. & ABRAHAM, J. 1991. The human gene for vascular endothelial growth factor. Multiple protein forms are encoded through alternative exon splicing. *Journal of Biological Chemistry,* 266**,** 11947-11954.

TOKURIKI, M. 1973a. Electromyographic and joint-mechanical studies in quadrupedal locomotion. I. Walk. *Nihon juigaku zasshi. The Japanese journal of veterinary science,* 35**,** 433.

TOKURIKI, M. 1973b. Electromyographic and joint-mechanical studies in quadrupedal locomotion. II. Trot. *Nihon juigaku zasshi. The Japanese journal of veterinary science,* 35**,** 525-533.

TOMANEK, R. J. & LUND, D. D. 1974. Degeneration of different types of skeletal muscle fibres. II. Immobilization. *Journal of anatomy,* 118**,** 531.

TOPP, R., DITMYER, M., KING, K., DOHERTY, K. & HORNYAK III, J. 2002. The effect of bed rest and potential of prehabilitation on patients in the intensive care unit. *AACN Advanced Critical Care,* 13**,** 263-276.

TORVINEN, S., SILVENNOINEN, M., PIITULAINEN, H., NÄRVÄINEN, J., TUUNANEN, P., GRÖHN, O., KOCH, L. G., BRITTON, S. L. & KAINULAINEN, H. 2012. Rats Bred for Low Aerobic Capacity Become Promptly Fatigued and Have Slow Metabolic Recovery after Stimulated, Maximal Muscle Contractions. *PloS one,* 7**,** e48345.

TSUTAKI, A., OGASAWARA, R., KOBAYASHI, K., LEE, K., KOUZAKI, K. & NAKAZATO, K. 2013. Effect of Intermittent Low-Frequency Electrical Stimulation on the Rat Gastrocnemius Muscle. *BioMed research international,* 2013.

URBICH, C., WALTER, D. H., ZEIHER, A. M. & DIMMELER, S. 2000. Laminar shear stress upregulates integrin expression. *Circulation Research,* 87**,** 683-689.

VISSE, R. & NAGASE, H. 2003. Matrix metalloproteinases and tissue inhibitors of metalloproteinases structure, function, and biochemistry. *Circulation research,* 92**,** 827-839.

WAGNER, P. D. 2001. Skeletal muscle angiogenesis. *Hypoxia.* Springer.

WAKELING, J. M., UEHLI, K. & ROZITIS, A. I. 2006. Muscle fibre recruitment can respond to the mechanics of the muscle contraction. *Journal of The Royal Society Interface,* 3**,** 533-544.

WANG, L., MASCHER, H., PSILANDER, N., BLOMSTRAND, E. & SAHLIN, K. 2011. Resistance exercise enhances the molecular signaling of mitochondrial biogenesis induced by endurance exercise in human skeletal muscle. *Journal of applied physiology,* 111**,** 1335-1344.

WANG, P.-Y., ZHUANG, J. & HWANG, P. M. 2012. p53: exercise capacity and metabolism. *Current opinion in oncology,* 24**,** 76.

WATERS, R. E., ROTEVATN, S., LI, P., ANNEX, B. H. & YAN, Z. 2004. Voluntary running induces fiber type-specific angiogenesis in mouse skeletal muscle. *American Journal of Physiology-Cell Physiology,* 287**,** C1342-C1348.

WESTERBLAD, H., ALLEN, D., BRUTON, J., ANDRADE, F. & LÄNNERGREN, J. 1998. Mechanisms underlying the reduction of isometric force in skeletal muscle fatigue. *Acta physiologica Scandinavica,* 162**,** 253-260.

WHITEHEAD, K. J., CHAN, A. C., NAVANKASATTUSAS, S., KOH, W., LONDON, N. R., LING, J., MAYO, A. H., DRAKOS, S. G., JONES, C. A. & ZHU, W. 2009. The cerebral cavernous malformation signaling pathway promotes vascular integrity via Rho GTPases. *Nature medicine,* 15**,** 177-184.

WILLIAMS, J., WEICHERT, A., ZAKRZEWICZ, A., PRIES, A., BAUM, O. & EGGINTON, S. 2006a. Differential gene and protein expression in abluminal sprouting and intraluminal splitting forms of angiogenesis. *Clinical Science,* 110**,** 587-595.

WILLIAMS, J. L. 2005. *Cellular and molecular mechanisms of angiogenesis in mouse skeletal muscle.* University of Birmingham.

WILLIAMS, J. L., CARTLAND, D., HUSSAIN, A. & EGGINTON, S. 2006b. A differential role for nitric oxide in two forms of physiological angiogenesis in mouse. *The Journal of Physiology,* 570**,** 445-454.

WILLIAMS, J. L., CARTLAND, D., RUDGE, J. S. & EGGINTON, S. 2006c. VEGF Trap Abolishes Shear Stress-and Overload-Dependent Angiogenesis in Skeletal Muscle. *Microcirculation,* 13**,** 499-509.

WILSON, D., CHILDERS, M., COOKE, D. & SMITH, B. 1997. Kinematic changes following botulinum toxin injection after traumatic brain injury. *Brain injury,* 11**,** 157-168.

WINDISCH, A., GUNDERSEN, K., SZABOLCS, M., GRUBER, H. & LØMO, T. 1998. Fast to slow transformation of denervated and electrically stimulated rat muscle. *The Journal of Physiology,* 510**,** 623-632.

WISLØFF, U., NAJJAR, S. M., ELLINGSEN, Ø., HARAM, P. M., SWOAP, S., AL-SHARE, Q., FERNSTRÖM, M., REZAEI, K., LEE, S. J. & KOCH, L. G. 2005. Cardiovascular risk factors emerge after artificial selection for low aerobic capacity. *Science,* 307**,** 418-420.

WRAGG, J. W., DURANT, S., MCGETTRICK, H. M., SAMPLE, K. M., EGGINTON, S. & BICKNELL, R. 2014. Shear stress regulated gene expression and angiogenesis in vascular endothelium. *Microcirculation,* 21**,** 290-300.

YAMAGUCHI, S., YAMAGUCHI, M., YATSUYANAGI, E., YUN, S.-S., NAKAJIMA, N., MADRI, J. A. & SUMPIO, B. E. 2002. Cyclic strain stimulates early growth response gene product 1–mediated expression of membrane type 1 matrix metalloproteinase in endothelium. *Laboratory Investigation,* 82**,** 949-956.

YEGHIAZARYAN, M., ŻYBURA-BRODA, K., CABAJ, A., WŁODARCZYK, J., SŁAWIŃSKA, U., RYLSKI, M. & WILCZYŃSKI, G. M. 2012. Fine-structural distribution of MMP-2 and MMP-9 activities in the rat skeletal muscle upon training: a study by high-resolution in situ zymography. *Histochemistry and cell biology,* 138**,** 75-87.

ZHANG, B. B., ZHOU, G. & LI, C. 2009. AMPK: an emerging drug target for diabetes and the metabolic syndrome. *Cell metabolism,* 9**,** 407-416.

ZHENG, W., SEFTOR, E. A., MEININGER, C. J., HENDRIX, M. J. & TOMANEK, R. J. 2001. Mechanisms of coronary angiogenesis in response to stretch: role of VEGF and TGF-β. *American Journal of Physiology-Heart and Circulatory Physiology,* 280**,** H909-H917.

ZHOU, A.-L., EGGINTON, S., HUDLICKA, O. & BROWN, M. 1998a. Internal division of capillaries in rat skeletal muscle in response to chronic vasodilator treatment with α1-antagonist prazosin. *Cell and tissue research,* 293**,** 293-303.

ZHOU, A. L., EGGINTON, S., BROWN, M. & HUDLICKA, O. 1998b. Capillary growth in overloaded, hypertrophic adult rat skeletal muscle: an ultrastructural study. *The Anatomical Record,* 252**,** 49-63.

ZIADA, A., HUDLICKA, O. & TYLER, K. 1989. The effect of long-term administration of α1-blocker prazosin on capillary density in cardiac and skeletal muscle. *Pflügers Archiv,* 415**,** 355-360.